UNIVERSITÄT
LEIPZIG

Consciousness Level Assessment in Completely Locked-in Syndrome Patients using Soft Clustering

Von der Fakultät für Mathematik und Informatik der Universität Leipzig

angenommene

D I S S E R T A T I O N

zur Erlangung des akademisches Grades

DOKTOR-INGENIEUR

im Fachgebiet Informatik

vorgelegt

von Dipl.-Ing. Volafidy Sophie ADAMA
von Diégo-Suarez, Madagaskar

Die Annahme der Dissertation wurde empfohlen von:

1. Prof. Dr. Martin Bogdan (Universität Leipzig)
2. Dr. Ander Ramos-Murguialday (Universität Tübingen)

Die Verleihung des akademischen Grades erfolgt mit Bestehen der Verteidigung am **18.03.2022** mit dem Gesamtprädikat ***magna cum laude***.

À mes parents.

"Ny hazo no vanon-ko lakana, ny tany naniriany no tsara. "

-– Ohabolana malagasy

Abstract

Consciousness Level Assessment in Completely Locked-in Syndrome Patients using Soft Clustering

Brain-computer interfaces (BCIs) are very convenient tools to assess locked-in (LIS) and completely locked-in state (CLIS) patients' hidden states of consciousness. For the time being, there is no ground-truth data in respect to these states for above-mentioned patients. This lack of gold standard makes this problem particularly challenging. In addition to consciousness assessment, BCIs also provide them with a communication device that does not require the presence of motor responses, which they are lacking. Communication plays an important role in the patients' quality of life and prognosis. Significant progress have been made to provide them with EEG-based BCIs in particular. Nonetheless, the majority of existing studies directly dive into the communication part without assessing if the patient is even conscious. Additionally, the few studies that do essentially use evoked brain potentials, mostly the P300, that necessitates the patient's voluntary and active participation to be elicited. Patients are easily fatigued, and would consequently be less successful during the main communication task. Furthermore, when the consciousness states are determined using resting state data, only one or two features were used.

In this thesis, different sets of EEG features are used to assess the consciousness level of CLIS patients using resting-state data. This is done as a preliminary step that needed to be succeeded in order to engage to the next step, communication with the patient. In other words, the "conversation" is initiated only if the patient is sufficiently conscious. This variety of EEG features is utilised to increase the probability of correctly estimating the patients' consciousness states. Indeed, each of them captures a particular signal attribute, and combining them would allow the collection of different hidden characteristics that could have not been obtained from a single feature. Furthermore, the proposed method should allow to determine if communication shall be initiated at a specific time with the patient.

The EEG features used are frequency-based, complexity related and connectivity metrics. Besides, instead of analysing results from individual channels or specific brain regions, the global activity of the brain is assessed. The estimated consciousness levels are then obtained by applying two different soft-clustering analysis methods, namely Fuzzy c-means (FCM) and Gaussian Mixture Models (GMM), to the individual features and ensembling their results using their average or their product. The proposed approach is first applied to EEG data recorded from patients with unresponsive wakefulness syndrome (UWS) and minimally conscious state (MCS) (patients with disorders of consciousness (DoC)) to evaluate its performance. It is subsequently applied to data from one CLIS patient that is unique in its kind because it contains a time frame during which the experimenters affirmed that he was conscious. Finally, it is used to estimate the levels of consciousness of nine other CLIS patients. The obtained results revealed that the presented approach was able to take into account the variations of the different features and deduce a unique output taking into consideration the individual features contributions. Some of them performed better than others, which is not surprising

since each person is different. It was also able to draw very accurate estimations of the level of consciousness under specific conditions.

The approach presented in this thesis provides an additional tool for diagnosis to the medical staff. Furthermore, when implemented online, it would enable to determine the optimal time to engage in communication with CLIS patients. Moreover, it could possibly be used to predict patients' cognitive decline and/or death.

Acknowledgement

Avant tout, je tiens particulièrement à remercier mes parents, mes sœurs et mon oncle Charles pour leurs continuels et intarissables supports et leurs fois en mes capacités. Je n'oublie pas non plus mes ami.e.s pour leurs encouragements incessants durant l'accomplissement de cette thèse.

I am grateful to Prof. Dr. Martin Bogdan for giving me the opportunity and for all his guidance during the accomplishment of this thesis, and for also leading such a friendly workplace.

This thesis would have not been possible without the data of CLIS patients graciously provided by Prof. Dr. Dr. hc. mult. Niels Bierbaumer and Dr. Ujwal Chaudhary from the Institute for Medical Psychology and Behavioural Neurobiology, University of Tübingen; and the EEG recordings of patients with disorders of consciousness kindly provided by Dr Manuel Schabus and Malgorzata Wilowska from the Laboratory of Sleep, Cognition and Consciousness & Centre for Cognitive Neuroscience (CCNS), University of Salzburg, Austria.

Last but not least, I thank God for giving me the strength and courage to accomplish this thesis.

Leipzig, 18 March 2022

Contents

Acronyms

ACRM American Congress of Rehabilitation Medicine.

AEP Auditory Evoked Potential.

AI Artificial Intelligence.

ALS Amyotrophic Lateral Sclerosis.

ALSFRS-R ALS Functional Rating Scale–Revised.

ANN Artificial Neural Networks.

BCI Brain-Computer Interfaces.

CCNS Centre for Cognitive Neuroscience.

CLIS Completely Locked-in Syndrome.

CNS Central Nervous System.

CRS-R Coma Recovery Scale - Revised.

CVA Cerebrovascular accident.

DoC Disorders of Consciousness.

ECoG Electrocorticogram.

EEG Electroencephalogram.

EKG Electroccardiogram.

EM Expectation-Maximization algorithm.

eMCS Emergence from Minimally Conscious State.

EMG Electromyogram.

EOG Electrooculogram.

EP Evoked Potential.

ERP Event-Related Potential.

ERR Ellipsoid Radius Ratio.

FCM Fuzzy c-means clustering.

fMRI functional Magnetic Resonance Imaging.

fNRIS functional Near Infra-Red Spectroscopy.

FUS Fused in Sarcoma.

GCS Glasgow Coma Scale.

GMM Gaussian Mixture Model.

iCOH Imaginary part of Coherency.

IFSECN International Federation of Societies for Electroencephalography and Clinical Neurophysiology.

LDA Latent Discriminant Analysis.

LIS Locked-in Syndrome.

LZC Lempel-Ziv Complexity.

MATLAB MATrix LABoratory.

MCS Minimally Conscious State.

MEG Magnetoencephalography.

MI Motor Imagery.

MMN Mismatched Negativity.

MND Motor Neuron Disease.

Nessi Neural signal surfing interface.

NIRS Near Infra-Red Spectroscopy.

PCI Perturbational Complexity Index.

PET Positron Emission Tomography.

PSD Power Spectral Density.

PSG Polysomnography.

QoL Quality of Life.

REM Rapid Eye Movement.

RG Riemannian geometry.

RSVP Rapid Serial Visual Presentation.

SCP Slow Cortical Potentials.

SD Standard Deviation.

sdn Subject's Derived Name.

SEF Spectral Edge Frequency.

SMA Supplementary Motor Area.

SMR Sensorimotor rhythms.

SOF Subject's Own Face.

SON Subject's Own Name.

SPECT Single Photon Emission Computed Tomography.

SSPE Subacute Sclerosing Panencephalitis.

SSVEP Steady-State Visual Evoked Potentials.

SVM Support Vector Machines.

SWS Slow Wave Sleep.

TBI Traumatic Brain Injury.

TMS Transcranial Magnetic Stimulation.

TTD Thought Translation Device.

UNP Utrecht NeuroProsthesis.

UWS Unresponsive Wakefulness Syndrome.

VEP Visual Evoked Potential.

VS Vegetative State.

WHO World Health Organisation.

wSMI weighted Symbolic Mutual Information.

List of Figures

List of Tables

1 Introduction

> The beginning is the most important part of the work.
>
> *Plato*

We wake up every morning and go to sleep every night. During the time we are up, we experience things: we can see, hear, smell, taste or sense things that are around us, we can feel hungry or thirsty. We can also be actively engaging in a task such as reading a book, or passively listening to some music. *Consciousness* comprises all these experiences and also the awareness that we are doing something (reading the book, for example). A relatively simple definition of what consciousness means is given by Posner and Plum in [Pos+07]: "Consciousness is the state of full awareness of the self and one's relationship to the environment". In normal circumstances, it begins in the morning when we wake up and lasts until we fall asleep again, in which case we become *unconscious* [Koc04].

According to [Gos+11], consciousness is characterised by two components: *arousal*, which is the level of consciousness, and *awareness* representing the content of the conscious experience. It originates from the brain and is usually demonstrated by motor activity [Koc04; GIM18]. The ancient Greeks already recognised that an intact brain is indispensable for a normal consciousness [Pos+07]. Therefore, a traumatic brain injury[1] (TBI) generates altered states of consciousness on one hand, but on the other hand it can also induce covert conscious states in which no purposeful movement from a subject can be observed although consciousness is present [LCERDM02; GIM18; Lau+05]. Typically, arousal and awareness are positively correlated with one another. When this relationship is disrupted, an altered state of consciousness also known as *disorder of consciousness* (DoC) occurs [Gos+11]. There are different types of disorders of consciousness: coma, Unresponsive Wakefulness Syndrome (UWS), and Minimally Conscious State (MCS). No arousal nor awareness indicate that a person is in a coma [Bau05]. It cannot then be awakened and does not respond even to intense stimulation [Pos+07]. UWS are described by non-existent signs of awareness in response to sensory stimuli, but the presence of signs of arousal recovery demonstrated by periods of eyes opening [GM08; Pos+07]. MCS patients on the other hand have preserved arousal level, but alternating signs of awareness [Gos+11; Pos+07]. The characteristics of the disorders of consciousness are described in more details in Section 2.1.1.

A TBI can also lead to a state called Locked-In Syndrome (LIS). Nevertheless, LIS can also arise as a transition from Amyotrophic Lateral Sclerosis (ALS). This condition, also known

[1] TBI is generally caused by a violent blow to the head or body, causing damages to the brain.

as Lou Gehrig's disease, is a neurodegenerative disease that progressively causes the loss of motor neurons that handle voluntary muscle movements. It is the most common motor neuron disease [BCP16]. LIS patients are fully conscious, with unaltered cognitive functions, but are unable to produce speech or perform any muscle movements [KN05; Pos+07]. Patients in this state are generally able to move their eyes and are, thus, able to communicate using eye movements and blinking [Gos+09; Bau05; Gos+11]. This limited communication mechanism becomes impossible when patients enter a total or complete locked-in state (CLIS) and lose control of voluntary muscle movements altogether. It is nonetheless thought that cognitive functions and consciousness are still maintained during this state that develops some months or years after LIS [Gos+09; Roh+17]. This covert state of consciousness is further discussed in Section 2.1.2.

1.1 Motivation and problem statement

Although the LIS is not a disorder of consciousness, it is frequently misdiagnosed as one. One such case was a patient who was considered in an UWS for 20 years [Van+18]. A complementary assessment of the patient's state was requested by the family after they were under the impression that he was conscious. This was done by evaluating the patient's behavioural responses using neuroimaging techniques. After a series of tests, it was established that the patient was not in UWS anymore, and has emerged to MCS instead. Furthermore, the patient was able to communicate by giving *yes* or *no* answers to questions asked to him. Consequently, his diagnosis was revised to incomplete LIS. Another case involved a patient with a brain tumour that lost consciousness in 1991, and spent the following 14 years without any kind of rehabilitation because he was thought to be at a terminal stage [LMT10]. The patient's state started improving after introducing exercises in 2005, so that in 2007 he was quadriplegic but conscious.

The difficulty to establish a diagnosis for such patients is probably due to the apparent similarity of the condition with VS, which exhibit motor immobility and eyes opening, but without signs of awareness [Sch+09]. Such diagnosis error denies the patients appropriate medical care and a chance at rehabilitation and a better quality of life [Bru+11]. It can also have dreadful consequences especially regarding end-of-life decisions. It is without a doubt awful hearing others deciding their fate but not being able to agree nor object. In any case, this type of conversation should include the patients, not be about them [Pos+07], especially since the majority of LIS patients have no desire to end their life [KN05].

As communication is an important part of being human, it is particularly crucial for these patients. Several studies revealed that the ability to communicate with their relatives increases CLIS patients' quality of life [Bir+00; K‡01]. Since they are unfortunately unable to overtly communicate their states of consciousness [G‡21], and that a brain-computer interface (BCIs) can provide a direct pathway between the brain and an external device [SM10], this latter has been employed to attempt to establish communication with such patients. Electroencephalography (EEG)- or electrocorticography (ECoG)-based BCIs in particular have been successfully

used by LIS patients to communicate [K‡01; Bir+99; Van+16]. Despite initial doubts, it has been later demonstrated that it was also possible for CLIS patients to communicate using their brain signals, in particular their EEGs [KB08; Gug+17; Han+19]. Likewise, it has also been established that being able to communicate with their relatives improved LIS patients' mood, reducing any desire to end their life [Bir+00; K‡01; KN05; Rou+15].

For such communication to be successful, it is important to determine the appropriate time to initiate it. Otherwise, all attempts would fail. This may be the case for patient GR described in Section 5.1.2 for instance, for which there was only one successful communication out of 170 attempts. However, most studies do not consider this step and directly begin the experiment without determining if the patient is in a state to do so. It is after all difficult to determine the patients' state, if they are conscious or not at any given time considering their condition. Moreover, there are no existing ground-truth distinguishing these states at the moment. Consequently, it is not possible to determine with absolute certainty the "true" level of consciousness as CLIS patients are unable to express their will or answer in any manner [K‡20].

1.2 Goal of the research

One of the factors leading to misdiagnosis of LIS patients is the use of behavioural tests such as the Coma Recovery Scale - Revised (CRS-R) or the Glasgow Coma Scale (GCS) [Sat+15; Pos+07]. CRS-R in particular consists of auditory, visual, motor, oromotor and verbal functions, as well as arousal. Basically, these methods assess the extent of the brain injury by rating each function. The higher the score, the lesser the extent of the injury. In the case of GCS for example, a total score of 13 or higher is considered a mild brain injury, a value between 9 and 12 is considered a moderate brain injury, while a value of 8 or less is regarded as a severe brain injury [Pos+07]. In the case of CRS-R, the scores range is from 0 to 23 [Sat+15]. This type of evaluation is not sufficient since it only accounts for the patients' behavioural response. Therefore, a direct recording of the brain activity without the intervention of behavioural responses makes more sense since it does not rely on external motor responses [Van+18]). In addition, the use of neuroimaging techniques has the potential to show hidden cognitive states. BCIs, in particular, can provide an alternate way to detect consciousness in paralysed patients by circumventing the motor pathway. Furthermore, misdiagnosis heavily impairs patients' treatment by giving them inadequate medicine. Also, when they are believed to be unconscious, no attempt at communicating with them will ever be done, which will deteriorate their condition faster [Sec+21].

The goal of this thesis is not to differentiate LIS/CLIS patients from those with DoC as it is the case in most of the existing literature. The aim is rather to assess if the patient is conscious or not. More specifically, a consciousness level assessment method is proposed as a step prior to any communication attempt with the patients. This is because the hypothesis in this work is that communication with LIS or CLIS patients fail because the experiment was carried out at times when they were not fit to do it (in a sleep state, for example) or simply did not want to. On that account, the patient's consciousness level is first determined and

communication is only established once indications that he/she is conscious enough to do so are observed. Each subject being different, distinctive features comprising spectral, complexity and connectivity characteristics are extracted from the EEG signals and assessed in order to do so. A soft-clustering analysis is thus employed using the computed features as input to produce a value between 0 (*unconscious*) and 1 (*conscious*) characterising the patient's level of consciousness. An overview of how the proposed approach operates is given in Chapter 4. The set of features used in this context are reported in Section 5.2, and the data analysis as well as the details of the consciousness level assessment are developed in Section 5.2.4.

1.3 Dissertation organisation

The present work is organised in 7 chapters. After establishing the topic and motivating the work in this chapter, some basics and foundations regarding consciousness, brain signals and machine learning as well as brain-computer interfaces are introduced in Chapter 2. Chapter 3 deals with the current state-of-the-art of consciousness assessments and attempts made to establish communication with LIS and CLIS patients using BCIs. It is subsequently followed by Chapter 4, which outlines the adopted *modus operandi* after introducing the problem and the aim of the thesis. The presented method is first applied to data from patients with DoC to validate it. Afterwards, it is applied to data from CLIS patients to evaluate their levels of consciousness. The different groups of patients are recounted in Chapter 5. The results and discussion part are presented in Chapter 6 afterwards before concluding this thesis with Chapter 7 by giving a summary of the work and presenting potential future works.

2 Basics

Je pense, donc je suis.

René Descartes

This chapter presents basic information associated to consciousness and the brain. It starts by introducing the concept of consciousness and how it relates to the brain. This is followed by some foundations on brain signals sources, acquisition, processing and applications. It concludes with an overview of pattern recognition and machine learning methods that are commonly used with biomedical signals. These notions are important to understand the fundamental parts of this thesis.

2.1 What is consciousness?

It is difficult to define the term **consciousness**. Along the years, a lot of philosophers, neurologists, and neuroscientists have tried to define it, but so far no concise definition have been agreed upon. The term comes from the Latin *conscientia*, which is composed of *cum*, meaning "with" or "together" and *scire* that means "to know" [Koco4]. It is related to visual and sensory perception and is also closely related to attention i.e. our ability to concentrate on one thing and ignore other things [BCP16]. In [Koco4], the following definition of the term is given: "Consciousness consists of those states of sentience, or feeling, or awareness, which begin in the morning when we are awake from a dreamless sleep and continue throughout the day until we fall into a coma or die or fall asleep again or otherwise become unconscious." In *Neural models of consciousness*, John G. Taylor asserts that: "Consciousness is synonymous with awareness or conscious awareness [...]. The content of consciousness encompass all that we are conscious of, aware of, or experience." [Tayo2]

However, the psychologist Stuart Sutherland explains the term as "The having of perceptions, thoughts, and feelings; awareness. The term is impossible to define except in terms that are unintelligible without a grasp of what consciousness means. Many fall into the trap of equating consciousness with self-consciousness[2] - to be conscious it is only necessary to be aware of the external world. Consciousness is a fascinating but elusive phenomenon: it is impossible to specify what it is, what it does, or why it evolved. Nothing worth reading has been written on it." [GIM18].

[2]Self-consciousness is the ability to think about ourselves as individuals [Gaz99; Gos+11].

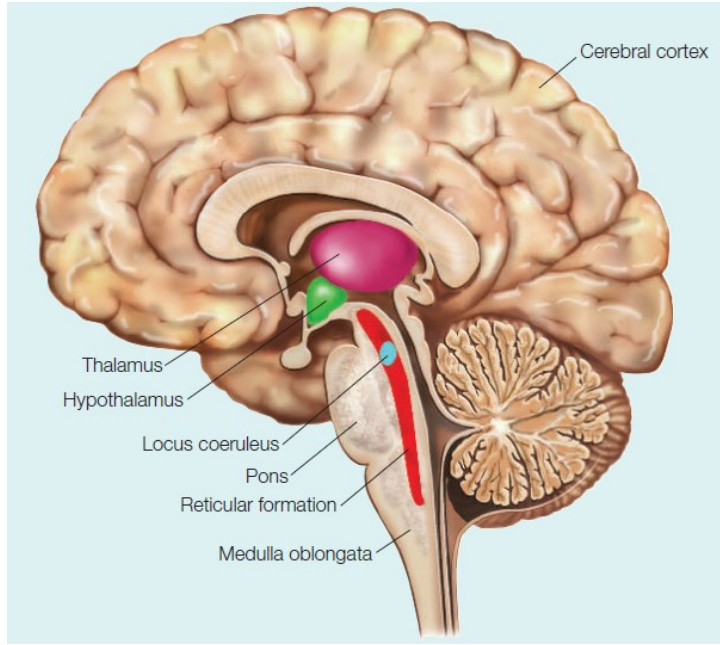

Figure 2.1: Brain anatomy of consciousness. The cerebral cortex, thalamus, brain stem, and hypothalamus play important roles in consciousness generation. From [GIM18]. Copyright © 2014, 2009, 2002, 1998 by Michael S. Gazzaniga, Richard B. Ivry, and George R. Mangun. Used with permission of W.W. Norton & Company, Inc.

According to [Gos+11], two components characterises consciousness: **awareness** and **arousal**. Awareness represents conscious perception or the content of consciousness. It encompasses cognition, past and present experiences, and intentions. Clinically, it is assessed by command following such as "close/open your eyes". It is supported by the cerebral cortex. Arousal also known as *level of consciousness* or *wakefulness*, on the other hand, is reinforced by the brainstem and the thalamus. More precisely, it is the degree to which a person is conscious [Ton+16]. It is synonymous to vigilance or alertness, and is evaluated by the presence of eye opening. For any substantial response to occur, a basic wakefulness is essential. Consciousness is subjected to the interaction between the activity of the cerebral cortex, the brainstem and the thalamus (cf. Fig. 2.1). It is composed by the correlation between awareness and arousal, in other words, by the relationship between the cerebral cortex and the brainstem and thalamus. These two components as well as their levels for each state of consciousness are illustrated in Fig. 2.2.

2.1.1 Disorders of consciousness

As stated in Section 2.1, consciousness depends on the interaction between the activity of the thalamus, the brainstem and the cerebral cortex. Damages in one of these systems will result in an impairment of consciousness. In other words, a disruption of the relationship between

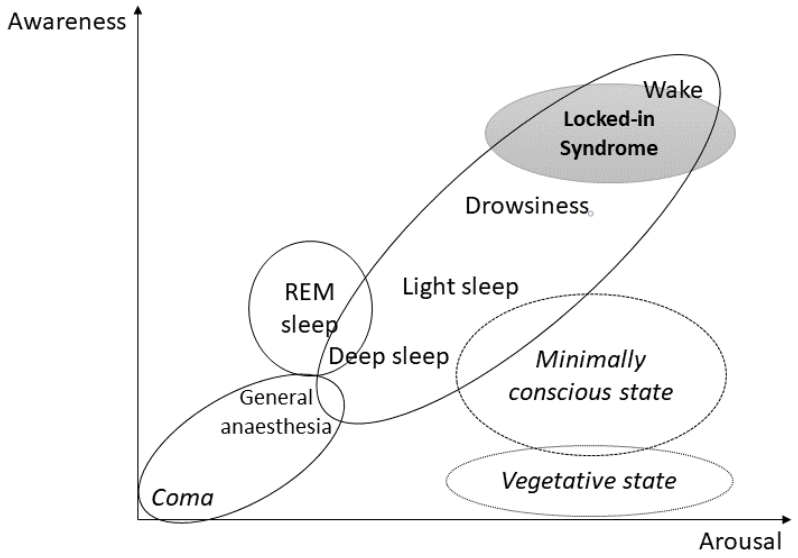

Figure 2.2: Major components of consciousness: **Arousal**: level of consciousness or wakefulness and **Awareness**: content of consciousness. The level and content of consciousness are positively correlated in normal states and in coma. Consciousness occurs when both arousal and awareness levels are high, and vice versa. Adapted from [Gos+11].

arousal and awareness will lead to a condition called disorder of consciousness [Gos+11]. Table 2.1 summarises the characteristics behaviours of patients in different conditions.

After a brain injury, behavioural assessments are administered to the patients to determine their consciousness levels and establish a diagnosis. The CRS-R is usually the most used measure to do so. It is a standardised evaluation used to establish prognosis in addition to the diagnosis. Moreover, this assessment also allows to monitor patients' recovery rate and to determine adequate treatment [Sat+15]. Table 2.2 shows the different elements of the assessment. The numbers on the left are scores attributed to each item, and general score vary from 0 to 23. High scores reflect cognitive behaviour, while low scores represent reflexive activity [Sat+15].

2.1.1.1 Coma

In [Bau05], a coma state is described as an "unarousable unconsciousness". It is defined by the absence of spontaneous eyes opening as well as reflexive or voluntary muscle movements [Les+15]. This state can last from two to four weeks [Les+15; Pos+07]. It can be provoked by an acute brain injury and is characterised by an absence of arousal and awareness [Gos+11] (see Fig. 2.2). This unarousability distinguished it from sleep, which is a physiological loss of consciousness. Coma may result in different outcomes, namely, LIS described in Section 2.1.2, VS, chronic coma in some rare cases, and eventually in brain death[3] as illustrated in Fig. 2.3.

[3] irreversible loss of all function of the entire brain [Pos+07].

Table 2.1: Consciousness and motor behaviour characteristics in patients with disorders of consciousness and locked-in syndrome [MLO10].

Condition	Sleep-wake cycles	Awareness	Motor behaviour characteristics
Coma	no	no	No purposeful behaviour
UWS[a]/ VS[b]	yes	no	No purposeful behaviour
MCS[c]	yes	Partial, fluctuating	Inconsistent but reproducible purposeful behaviour
LIS[d]	yes	yes	Yes, limited to eye movements (depending on lesion)

[a] Unresponsive Wakefulness Syndrome
[b] Vegetative State
[c] Minimally Conscious State
[d] Locked-In Syndrome

2.1.1.2 Vegetative state (VS)

Patients in the VS[4], currently known as UWS patients, present no sign of awareness in response to visual, auditory, or tactile stimuli, indicating an absence of signs of cortical function [GM08]. Patients develop alternating periods of sleep and wakefulness that manifest by periodic eye opening, which suggest a recovery of arousal [Bau05; Gos+11], and show no purposeful motor behaviour (cf. Table 2.1 and Fig. 2.2). A reduction of head, limbs and eyes movements are also observed [GM08]. The condition may develop suddenly, for example after a brain injury, or gradually as a result of a neurodegenerative disorder, such as Alzheimer's disease [MLO10]. A patient is diagnosed as in a VS when the CRS-R is between 0 and 9; more precisely, when the scores for the individual items in Table 2.2 are: Auditory ≤ 2, Visual ≤ 1, Motor ≤ 2, Oromotor/Verbal ≤ 2, Communication $= 0$, and Arousal ≤ 2 [Sat+15]. After some time, VS can turn into MCS or permanent VS, and eventually to death (cf. Fig. 2.3). VS is considered permanent or persistent when it lasts longer than a month [Pos+07].

2.1.1.3 Minimally Conscious State (MCS)

The MCS is portrayed by a preserved arousal level and fluctuating signs of awareness [Gos+11] as illustrated in Fig. 2.2. Indeed, sleep-wake cycles could be observed as well as inconsistent but reproducible motor behaviours. Patients with MCS can follow simple command and produce intelligible speech (high-level behavioural response), and some are able to show behaviours that are not attributable to reflexive activity like visual pursuit or appropriate smiling or crying to emotional stimuli (low-level behavioural response) [GM08]. Those who are displaying high-level responses are categorised as MCS+, while those who exhibit low-level behavioural responses are classified as MCS- [Bru+11]. A patient is usually diagnosed as in a MCS when the

[4] also called *coma vigil* or *apallic state* [Pos+07]

Table 2.2: Coma Recovery Scale-Revised. Adapted from http://www.tbims.org/combi/crs/CRS_Syllabus.pdf

Auditory function scale	
4	Consistent movement to command[a]
3	Reproducible movement to command[a]
2	Localisation to sound
1	Auditory startle
0	None
Visual function scale	
5	Object recognition[a]
4	Object localisation: Reaching[b]
3	Visual pursuit[b]
2	Fixation[b]
1	Visual startle
0	None
Motor function scale	
6	Function object use[c]
5	Automatic motor response[b]
4	Object manipulation[b]
3	Localisation to noxious stimulation[b]
2	Flexion withdrawal
1	Abnormal posturing
0	None
Oromotor/Verbal function scale	
3	Intelligible verbalisation[a]
2	Vocalisation / Oral movement
1	Oral reflexive movement
0	None
Communication scale	
2	Functional: Accurate[c]
1	Non-functional: Intentional[a]
0	None
Arousal scale	
3	Attention
2	Eye opening without stimulation
1	Eye opening with stimulation
0	Unarousable

[a] Denotes Minimally Conscious State Plus (MCS+)

[b] Denotes Minimally Conscious State Minus (MCS-)

[c] Denotes emergence from Minimally Conscious State (eMCS)

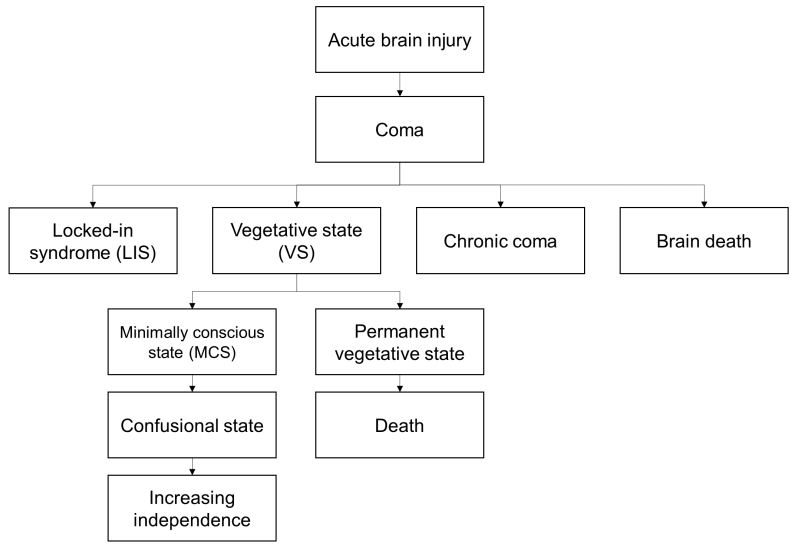

Figure 2.3: Different states of consciousness that may arise after a coma. If the state of the patient improves, they transition to a vegetative state, and in some rare cases in locked-in syndrome after a short period [Les+15]. The worse cases result in chronic coma and eventually in brain death. Vegetative state in turn evolves to a minimally conscious state (best case scenario) or into a permanent vegetative state that can result in death (worst case scenario). Normally, the minimally conscious state ameliorate and in time, the patient becomes progressively independent. Figure adapted from [MLO10].

CRS-R is from 9 to 21. The detailed score for each item is: Auditory $= 3$ *to* 4, Visual $= 2$ *to* 5, Motor $= 3$ *to* 5, Oromotor/Verbal $= 3$, Communication $= 1$. Nevertheless, when the scores are between 7 to 9 included, the patient can be either VS or MCS [Sat+15]. Moreover, a motor score equal to 6 and a communication score equal to 2 denote an emergence from MCS (eMCS) (cf. Table 2.2). eMCS develops when the patient is able to communicate accurately and/or practically use objects and is therefore not considered a DoC [Gos+14a]. MCS can develop from a vegetative state, and may also transition to a confusional state,[5] which in turn can eventually lead to an increasing independence (see Fig. 2.3).

2.1.2 Covert states of consciousness: Locked-in syndrome

A level of wakefulness is fundamental for consciousness, which can also manifest by action [GIM18]. This latter is however not necessary for consciousness [Koco4]. One such state is the LIS, which is described below.

Locked-in syndrome (LIS) is a neurodegenerative disorder, in particular a motor neuron disease (MND) that causes a patient to be completely paralysed, thus leaving her/him unable to perform any voluntary movement except for the muscles that control vertical eye movements

[5] condition wherein consciousness is maintained but with no intellectual understandability and orientation to time, area, and sometimes the self.

[Pos+07; Les+15]. According to the American Congress of Rehabilitation Medicine (ACRM), LIS is characterised by the presence of sustained eye opening, aphonia[6] or severe hypophonia[7], quadriplegia[8] or quadriparesis[9], preserved cognitive functioning, and a primary and elementary code of communication using vertical eye movements or blinking [Sch+09]. LIS patients also have normal sleep-wake cycles [GIM18], but as their condition evolves, increasing signs of insomnia are observed [Soe+13; Pos+07]. The condition is very rare and affects approximately 1 out of 20,000 persons. There is no cure nor standard course of treatment at the moment, but medication like *riluzole*[10] can slow the disease down by a few months [BCP16; PP04].

On one hand, the LIS (also known as *de-efferented state* or *pseudo-coma*) may arise after a traumatic brain injury (TBI) as illustrated in Fig. 2.3, a disease of the circulatory system, or even from medication overdose. Brain lesions can be located in the ventral part of the pons in the brainstem or in rare cases, in the midbrain and bilateral internal capsules [GIM18; PP04; Lau+05]. TBI constitutes the most common cause of the condition [K̈20]. On the other hand, it may also result as an evolution of neurological diseases such as ALS or Guillain-Barré syndrome. ALS, which is the most frequent neurodegenerative cause of LIS [K̈01], was first described in 1869 by the French neurologist Jean-Martin Charcot. The initial signs of the condition are muscle weakness and atrophy, probably resulting from a motor neuron disease among other causes, most of them unknown. Excitotoxicity[11] constitutes another cause of ALS. The patient loses all voluntary movement such as walking, speaking, swallowing and breathing over the course of one to five years. This will eventually lead to death due to failure of the respiratory muscles [Mur+11]. Fig. 2.4 illustrates the different causes of paralysis in ALS and stroke.

Depending on the extent of motor impairment, the state can be separated into different categories: *classical LIS* consists of total immobility except for vertical eye movements or blinking; *incomplete LIS* during which some remnants of voluntary motion still remains; and *total LIS* during which no voluntary muscle movement are possible [Lau+05]. Total LIS develop after a transition from ALS-LIS, but it can also arise following a coma or disorders of consciousness such as VS in which case, the inability to move is due to extensive brain damage [KB08]. A study of this transition in one CLIS patient showed that eye movements were the very last muscle group that becomes uncontrolled. It is preceded by facial muscle activity and external anal sphincter [Mur+11].

Locked-in syndrome is not a disorder of consciousness but is more than often diagnosed as one [Lau+05; BPL08]. It is characterised by high levels of both arousal and awareness (see Fig. 2.2). Therefore, the patient presents no alteration of consciousness and can think and reason. Communication is generally possible via blinking [Gos+11; Bau05; Gos+09]. One inspiring story of a patient in the locked-in state after a severe stroke is that of Jean-Dominique Bauby, editor

[6] inability to produce voiced sound
[7] soft speech
[8] also known as *tetraplegia*: partial or total loss of use of all the limbs and torso due to illness
[9] temporary or permanent weakness in all four limbs
[10] an oral medication that is presumed to lessen damages to motor neurons by reducing levels of glutamate, which carries messages between nerve cells and motor neurons [NIN13].
[11] deterioration or death of nerve cells due to an unhealthy increase of the levels of some neurotransmitters, resulting in too much stimulation for the receptors.

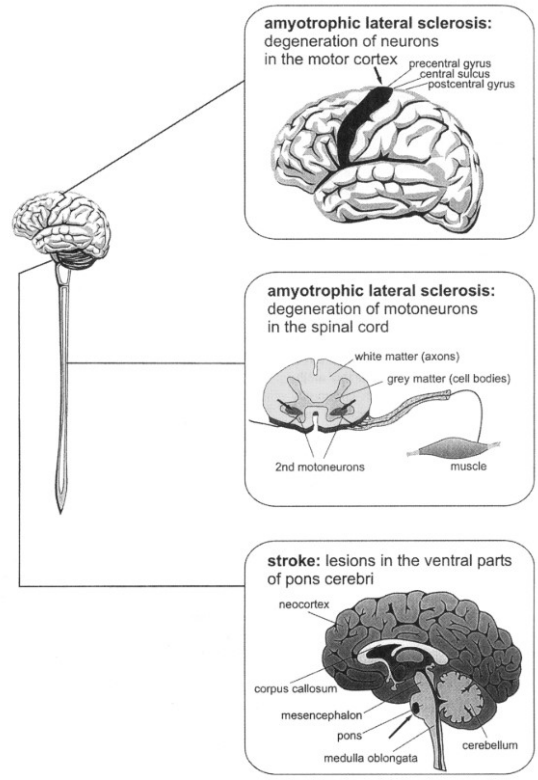

Figure 2.4: Causes of paralysis in ALS and stroke. ALS can be caused by either the degeneration of neurons in the motor cortex, or the degeneration of the first and second motoneurons in the spinal cord. Stroke, on the other hand, is caused by an haemorrhage in the ventral parts of the pons. From [K+01]. Copyright © 2001 by American Psychological Association. Reproduced with permission of the copyright owner.

of ELLE magazine,[12] who wrote a book titled "*Le scaphandre et le papillon*" in 1997 using only eye movements [Koc04]. Table 2.3 showcases some books written by other LIS patients.

2.2 Brain signals

Consciousness is subjected to the interaction between the activity of several brain areas [Gos+11; Koc04]. Consequently, using brain signals can provide an objective assessment of a subject's consciousness level. This section gives a brief overview of human brain signal acquisition and processing, and introduces brain-computer interfaces.

The brain is the most complex organ in the human body. It is responsible for different processes such as perception, reasoning, self-awareness, language or imagination. It is composed of the *cerebrum*, the *cerebellum* and the *brain stem*. The cerebrum is composed of several lobes: the

[12] `https://www.elle.com`

Table 2.3: Some books written by LIS patients [BPL08]

Author	Year	Title	Publisher
Jean-Dominique Bauby	1998	The Diving Bell and the Butterfly: A Memoir of Life and Death	Vintage
Julia Tavaro	1997	Look Up for Yes	Kodansa (NY)
Karl-Heinz Pankte	1999	Locked-in. Gefangen im eigenen Körper (Taschenbuch)	Mabuse-Verlag
Philippe and Stéphane Vigand	2000	Only the Eyes say Yes (original title: Putain de silence)	LGF - Livre de Poche
Philippe Vigand	2002	Promenade immobiles	Le Livre de Poche
Roland Boulengier	2002	Solitaire, dans le silence	Imprimerie - Editions Demol
Vincent Humbert	2003	Je vous demande le droit de mourir	Michel Lafon
Laetitia Bohn-Derrien	2005	Je parle: l'extraordinaire retour à la vie d'un Locked-In Syndrome	J.-C- Lattès

frontal lobe, the parietal lobe, the temporal lobe and the occipital lobe as can be seen in Fig. 2.5. The Sylvian fissure divides the frontal lobe from the temporal lobe, and the central sulcus separates the frontal lobe from the parietal lobe. Each of the brain areas have specific functions. For example, the frontal lobe is responsible for motor control, speech and problem solving among other things. Facial recognition and hearing functions are located in the temporal love. The cerebellum is responsible for coordination as the occipital lobe is in charge of vision. Touch, taste and body awareness are functions of the parietal lobe [BCP16].

Cognitive neuroscience enables the analysis of brain signals in order to attempt to understand these different mechanisms. The term comes from *cognition*, which is the process of knowing and *neuroscience*, which is the study of the functions and organisations of the nervous system [GIM18; BCP16].

2.2.1 Brain signal acquisition

2.2.1.1 Types of brain recordings

Several methods have been developed to measure brain activity, depending on the temporal and spatial resolution needed, and the type of signals to be recorded (electrical activity, magnetic fields, etc.) [GIM18; Sub19]. Fig. 2.7 illustrates the most common brain recording techniques, and Fig. 2.6 shows different brain imaging techniques relative to their temporal and spatial resolutions.

- *Electroencephalography* (EEG): measures the electrical activity of the brain, be it spontaneous or evoked (cf. Fig. 2.7a).

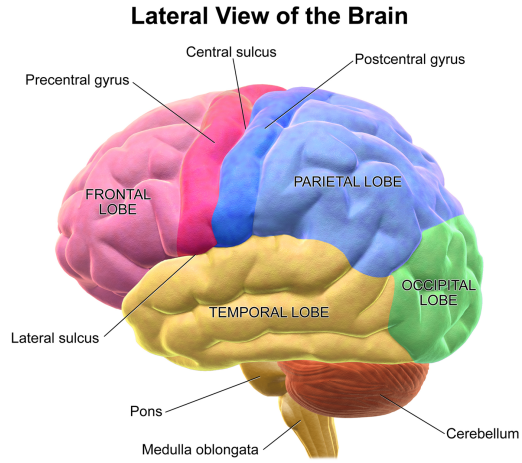

Figure 2.5: Different lobes of the cerebral cortex. Important landmarks separate them: the frontal and the parietal lobes by the *central sulcus*, the temporal lobe from the other lobes by the *lateral sulcus* or Sylvian fissure. From Wikipedia (CC BY 3.0).

- *Functional Near Infrared Spectroscopy* (fNRIS): measures the cortical haemodynamic activity that occurs in response to neural activity by the means of near-infrared. A typical setup for measuring fNRIS is shown in Fig. 2.7b.
- *Magnetoencephalography* (MEG): allows the localisation of the sources of the brain's neural activity, especially those deep below the surface. It measures magnetic fields produced by the brain's electrical activity (cf. Fig. 2.7c).
- *Functional Magnetic Resonance Imaging* (fMRI): determines the metabolic changes in blood flow correlated with neural activity in the brain. Fig. 2.7d illustrates an fMRI machine.
- *Positron Emission Tomography* (PET): measures local variations in the cerebral blood flow that correlate with mental activity using radioactive-labelled compounds.
- *Single Photon Emission Computed Tomography* (SPECT): scan used to identify altered blood flow in the brain.

This research is limited only to EEG and ECoG recording techniques, consequently only those will be further described.

Electroencephalography EEG is a non-invasive measurement of the electrical activity of the brain from the surface of the scalp by means of electrodes. This activity is generated by the excitation of the dendrites of several groups of pyramidal neurons in the cerebral cortex [SC13]. The first human EEG recording was performed by German psychiatrist Hans Berger in 1929 [BCP16]. EEG allow an overview of the generalised activity of the underlying brain region. It is possible to record the brain's electrical potential at the scalp because tissues of the brain, skull, and scalp

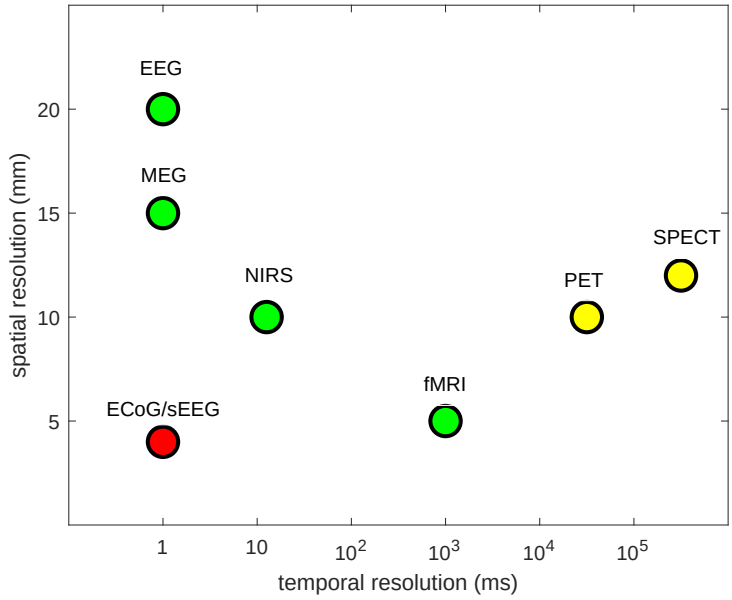

Figure 2.6: Spatial and temporal resolutions of different brain imaging techniques. Adapted from [Hit15]. In red: strong invasiveness, in yellow: medium invasiveness, in green: non invasive.

passively conduct the electrical currents produced by the synaptic activity. In general, EEG scalp amplitude range varies between 10 and 100 μV [Nie05; SM10]. EEG provides an excellent time resolution, but a limited spatial resolution (cf. Fig. 2.6) [KSD09]. The maximal number of electrodes in any EEG recording is currently limited to 256 [GIM18].

To generate an EEG signal big enough to be seen, it necessitates the activation of many thousands of underlying neurons. The number and synchronicity of these neurons contribute to the amplitude of the obtained EEG signal. Fig. 2.8 illustrates the generation of an EEG signal. Synchronous activity of neurons underneath an electrode generate large EEG signals, while asynchronous cell responses produce small EEG amplitudes [BCP16].

To allow reproducibility and comparison between different experiments, a standardised EEG location system called the **10-20 system** has been developed. It uses anatomic landmarks of the brain such as F (*frontal*), C (*central*), P (*parietal*), and O (*occipital*). In addition, EEG channels located in the left side of the brain are identified by odd numbers while those located on the right side are represented by even numbers, and channels located in the midline are represented by *z* (*midline sagittal*). For example, Fz is located in the midline of the frontal area. Along with channel Cz commonly used as reference, it is often used as ground [Rei05; Jas58; BCP16; Sub19]. Referencing can also be performed using contralateral channels located in the left and right mastoids A1 and A2 (A as in *auricle* (ear)), since their potentials are close to zero [NS06]. The 10 and 20 in *10-20 system* represent the distance as the percentage of the total distance between the *nasion* and the *inion* (cf. Fig. 2.9). The later developed 10/10 system is an extension of the 10/20 system that includes more channels [Nuw+98].

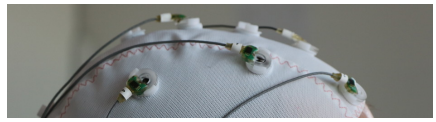

(a) EEG (self-recorded).

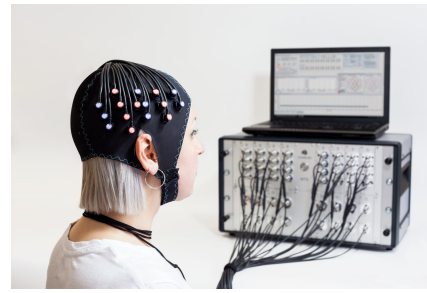

(b) fNIRS. From Wikipedia (CC BY-SA 4.0)

(c) MEG. From Wikipedia (Public domain)

(d) fMRI. From Source

Figure 2.7: Most common brain recording techniques used to regulate a BCI.

Electrocorticography (ECoG) ECoG or *intraoperative cortical electroencephalogram* is an invasive method of brain recording. Hans Berger introduced it in the 1940s to map the location and extent of epileptogenic brain tissue before surgically removing it to treat partial epilepsy [QN05]. ECoG electrodes measure electrical signals before they pass through the scalp and skull. The only difference between EEG and ECoG recordings is that, for the latter, the electrodes are placed directly on the surface of the brain, either outside the *dura* or beneath it (cf. Fig 2.8). There is consequently far less signal distortion compared with EEG [GIM18]. ECoG also has a much higher spatial resolution than EEG (millimetres vs. centimetres), a higher characteristic amplitude (50-100 μV vs 10-20 μV), and is less vulnerable to artefacts [SM10]. The recordings are usually performed using strip and grid electrodes. One disadvantage of this type of recording is that these strips and grids tend to curve and pull slightly away from the cortex, resulting

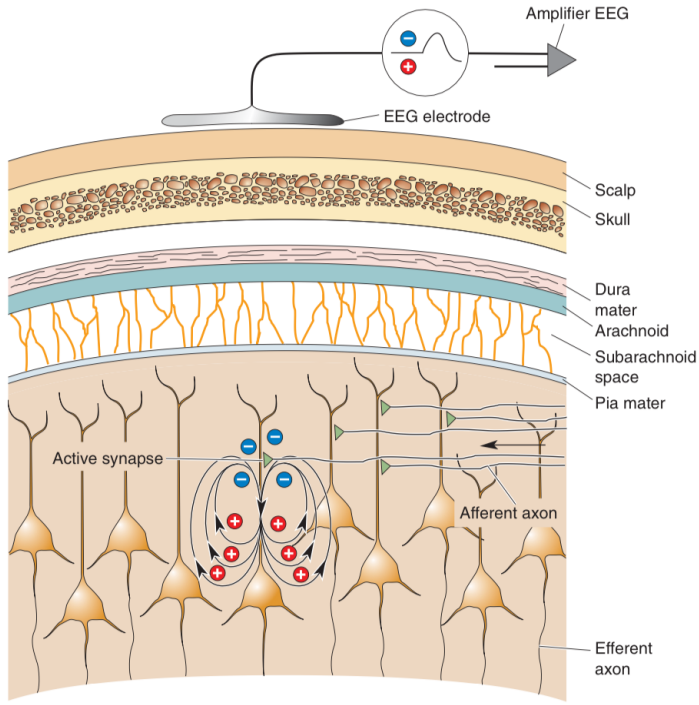

Figure 2.8: EEG signal generation. The EEG electrodes measures the averaged activity of a large population of neurons through different tissue layers. The signal will only be detected if the pyramidal neurons are firing synchronously. From [BCP16]. Copyright © 2016 by Wolters Kluwer. Used with permission from the copyright owner.

in weak contact connection to some contacts [QN05]. Fig. 2.10 shows the implanted ECoG electrodes of one of the CLIS patients in this work.

2.2.1.2 Modalities of recordings

Brain electrical activity can be categorised into two groups: *spontaneous EEG* and *Evoked Potentials* (EPs) or *Event-Related Potentials* (ERPs).

Spontaneous brain recordings Spontaneous EEG is obtained when there are no specific sensory stimulus [NS06]. Brain recordings oscillate at different frequencies that are named after different Greek letters and indicate the state of the brain [GIM18]. Typically, high frequencies manifest themselves during alertness, waking states, but also during dreaming state of sleep (Rapid Eye Movement (REM) sleep). On the other hand, low frequencies are dominant during non-dreaming stages of sleep and the pathological state of coma [BCP16]. Fig. 2.11 displays four canonical frequency bands of a healthy subject extracted from an EEG signal $x(t)$. No tasks were performed during the recording.

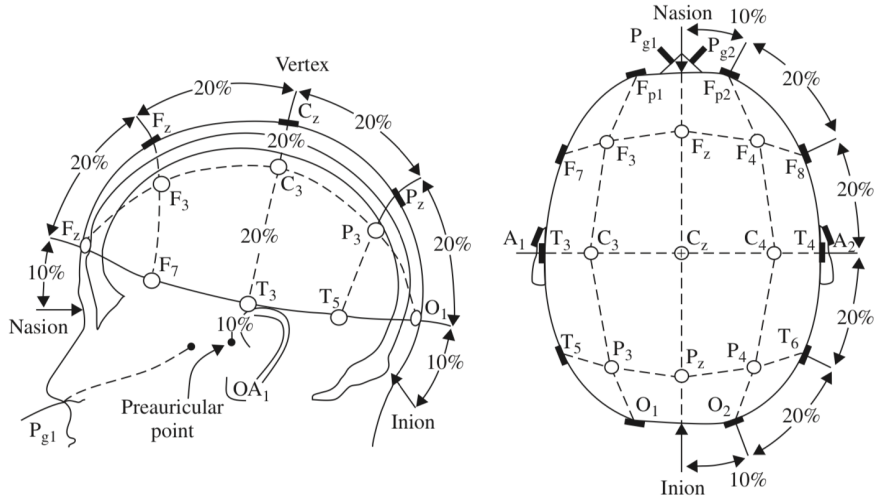

Figure 2.9: 10-20 system for EEG signal recording. The figure shows the spacing between the different recording channels. If d represents the distance from the nasion to the inion, channel Fpz at the forefront is located at 10%d. Fz, in turn is located at 20%d of Fpz, and so on (transversal channels). The same goes for the lateral electrodes (right figure). From [SC13]. Copyright © 2013. Reprint with permission from John Wiley & Sons.

Alpha rhythm α rhythms were first introduced by Hans Berger in 1929. They are associated with quiet but waking states, i.e. when the subject is awake but do not perform any task [SC13]. They were best obtained with eyes closed and attenuates with high degree of alertness. Fig. 2.11b illustrates such a frequency band. The International Federation of Societies for Electroencephalography and Clinical Neurophysiology (IFSECN) defines it as a:

"Rhythm at 8-13 Hz occurring during wakefulness over the posterior regions of the head, generally with higher voltage over the occipital areas. Amplitude is variable but is mostly below 50 μV in adults. Best seen with eyes closed and under conditions of physical relaxation and relative mental inactivity. Blocked by attenuated attention, especially visual, and mental effort." [aut74].

μ rhythms are similar in frequency to the α rhythms, except that they are larger over the motor and sensorimotor areas. Mu rhythms are greatly related to functions of the motor cortex, involving mostly the channels C3 and C4. It is reduced with movement or imagination of movement of the opposite upper limb, also referred as *de-synchronisation* [Nie05; BCP16; GIM18].

Beta rhythm β rhythms (Fig. 2.11e) were also introduced by Hans Berger and indicate an activated cortex. Its frequencies lie between 13 and 30 Hz [BCP16]. When the brain is engaged in information processing, the cortical neurons are highly activated and relatively asynchronous. This low synchrony in turn produces EEG with low amplitudes [GIM18; Nie05]. Beta activity is usually observed in the frontal and central areas, with an amplitude of 30 μV at most [SC13].

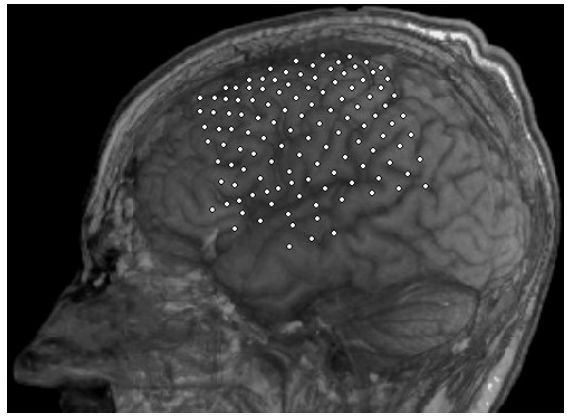

Figure 2.10: ECoG electrodes surgically implanted in a CLIS patient. The grid contains 128 channels in total, but only 64 of them were effectively usable. Image courtesy of the Universitätsklinikum of the University of Tübingen, Germany.

Theta rhythm θ rhythms (Fig. 2.11c) were introduced by Walter and Dovey in 1944 and denote frequency ranges between 4 and 8 Hz [BCP16]. The name comes from the belief that these waves originate in the thalamic region. They appear during deep sleep, during which cortical neurons are not involved in any information processing. Many of them are phasically excited by a common, slow, rhythmic input leading to a high synchrony. This will then result in high EEG amplitude. θ waves can also occur during waking states, for example during mental activity such as problem solving, and are larger over the frontal midline region in this case [GIM18; Nie05].

Delta rhythm δ rhythms (Fig. 2.11b) are slow rhythms with frequencies below 4 Hz [BCP16]. They occur mostly during deep sleep states and are characterised by large amplitudes. Theta waves are related to the level of arousal and represent the boundary between consciousness and drowsiness [SC13]. They were introduced by Walter in 1936, and designated at first all frequency below the α frequencies. Later however, Walter also introduced the previously described θ rhythms [GIM18; Nie05].

Other brain rhythms Gamma rhythms (γ) are high frequencies oscillating between 30 and 70 Hz. Other EEG frequency components also exist but are rarely used. For example, ω waves with frequency between 60 and 120 Hz that have retinal origin, or ρ waves that are around 250 Hz [Dro06].

Evoked and Event-related potentials As opposed to spontaneous potentials, an evoked potential is a brain potential obtained as a direct response to some external stimulus. This can be an auditory tone or a flashing light for example. Evoked-potentials have very low amplitudes that are difficult to detect from a single trial. They are embedded in the ongoing EEG signal. Thus, a large number of single trials needs to be averaged to extract the signal related to the

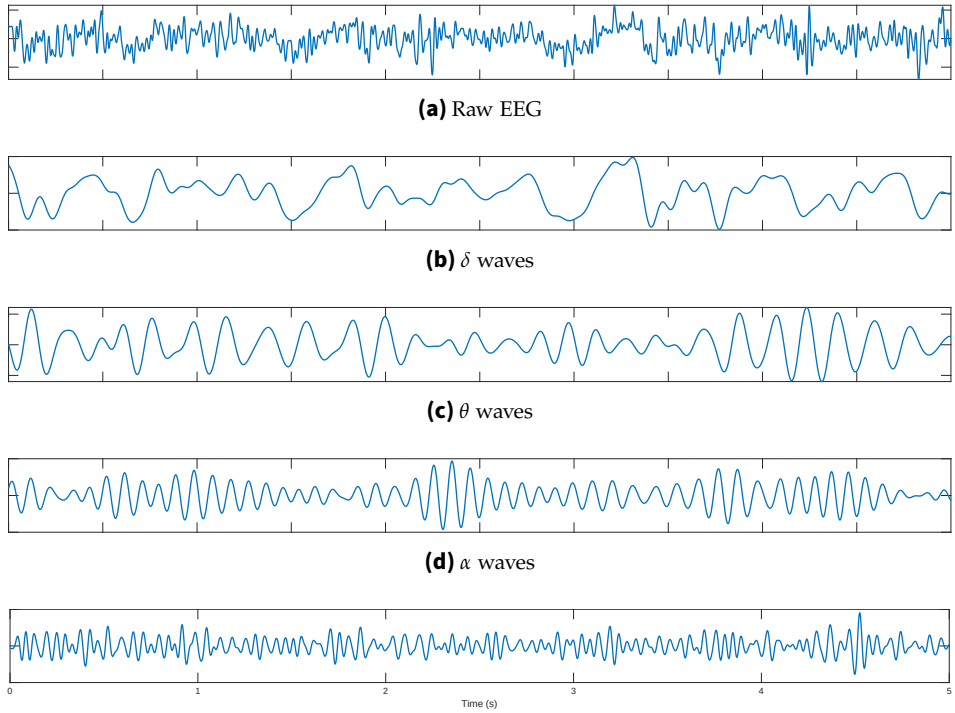

(a) Raw EEG

(b) δ waves

(c) θ waves

(d) α waves

(e) β waves

Figure 2.11: Normal EEG brain waves at location FP2 recorded from one healthy person (myself). **(a)** raw data, **(b)** $\delta : 0.5 - 4$ Hz, **(c)** $\theta : 4 - 8$ Hz, **(d)** $\alpha : 8 - 12$ Hz, and **(e)** $\beta : 12 - 30$ Hz. Waveform with time on the x-axis and voltage expressed in μV on the y-axis. It oscillates between a positive and a negative voltage. Usually an increase in the θ band indicates that the subject is engaged in a cognitively demanding task. On the other hand, an increase of α marks a reduced state of attention.

event that evoked it. Evoked potentials that occur after an auditory stimulus are called *Auditory Evoked Potentials* (AEPs), while those who appear after a visual stimulus are called *Visual Evoked Potentials* (VEPs). They are mostly studied to detect abnormalities in the auditory and visual systems [GIM18; NS06]. In particular, in a *Steady-State Visual Evoked Potential* (SSVEP) experiment, the stimulus consists of a continuous sinusoidal modulated signal delivered through a computer screen. Its effects in the brain are measured by analysing the signals in the stimulus frequency. ERPs have been used as a diagnosis tool in neurology and psychiatry, and have been also widely employed in BCIs [SC13].

Event-related potentials (ERPs) are also evoked by external stimulus, but additionally they are also linked to endogenous brain states. Furthermore, they occur at a relatively much longer latency. The ERP components are named after the combination of the polarity (Positive (P) or Negative (N)) of the waveform and the time of appearance of the waveform after the stimulus onset. For example, P300 is a positive wave that appears around 300 ms after a stimulus. Many ERPs are linked to specific psychological processes. Sensory processing usually occurs 50 to 100 ms after the stimulus onset. Attentional states normally produce potentials after 100 ms of the stimulus onset. N100 and P100 are examples of potentials related to selective attention. A

typical latency of 150-250 ms is observed after the onset of an unexpected auditory stimulus in the N200 or Mismatched Negativity (MMN) [GIM18].

2.2.2 EEG signal pre-processing

During an EEG recording, the signal is exposed to other noises or *artefacts* coming from physiologic or non-physiologic sources. Physiologic sources can be electrooculagraphic (EOG), electromyographic (EMG), electrocardigraphic (EKG) or movement executed by the patient for example. As non-physiologic sources, noises caused by the environment, the instruments or the electrodes can be named [DHI05; SC13]. Some pre-processing steps are then necessary in order to remove or reduce them before analysing the signal.

Artefacts caused by muscle movement can be reduced or rejected by using a band-pass filter with cut-off frequencies between 1 and 20 Hz, since muscle movements cover the spectral range of around 20 to 300 Hz [DHI05; Mut13]. Another method would be to simultaneously record the signals potentially inducing these noises, such as EKG or EOG, and then subtraction them from the EEG signal [DHI05]. Low frequency noise such as breathing can be reduced by using a high-pass filter with a cut-off frequency of 0.5 Hz or less. Noises generated by the power supply can be attenuated using a Notch filter with a null frequency of 50 Hz [SC13].

It is also common to perform a baseline correction, i.e. demeaning the signal, before further analysis to remove linear trends [Dro06]. Depending on the application, the EEG signal could also be filtered into frequency bands of interest (cf. Fig. 2.11). Some analysis methods require that the data is stationary, which is not the case of EEG signals. To ensure this stationarity, the signal is divided into smaller segments of a few seconds.

To analyse ERP, an averaging of several trials is necessary to remove the background EEG and only retain the signal of interest [Dro06].

2.2.3 Brain-computer interfaces

A Brain-Computer Interface (BCI) is a system that uses brain activity to operate a computer-controlled device [PN05; SM10]. It has the potential to particularly improve the lives of people with conditions that affect their ability to move voluntarily [GIM18]. BCI has also been implemented to assist LIS patients in communicating with their relatives, offering them a better quality of life with greater autonomy [Sub19].

There are several types of BCIs. A BCI that uses brain activity that is directly and consciously controlled by the user is called *active* BCI. When the brain activity arises as a result of an external stimulation, it is called *reactive* BCI. *Passive* BCI on the other hand does not necessitate any voluntary control from the user and make use only of the spontaneous brain signal [ZK11].

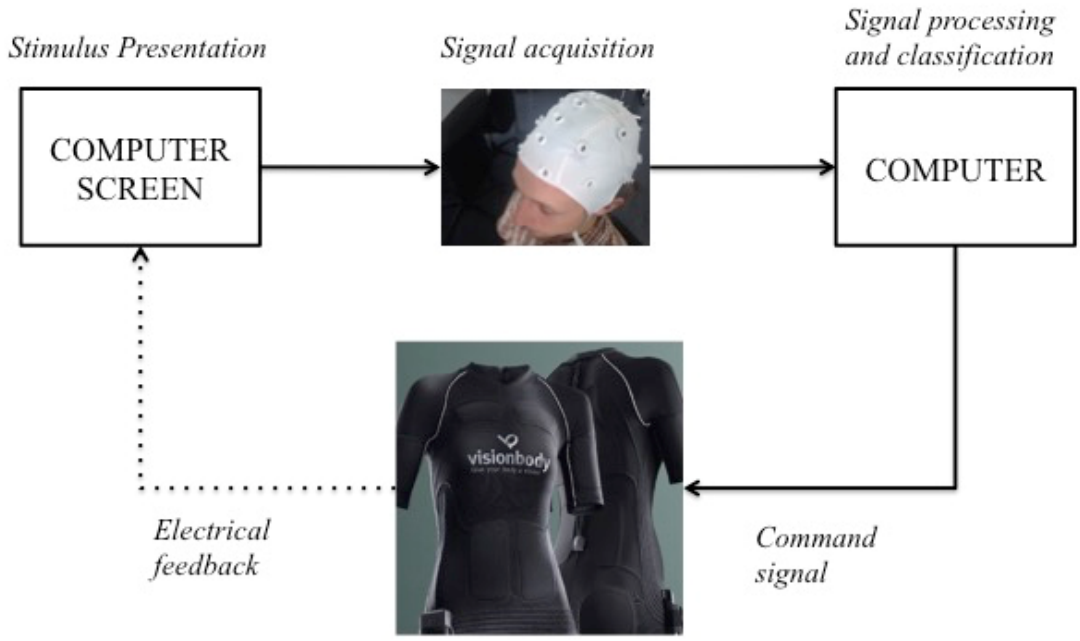

Figure 2.12: EEG-based Brain-Computer Interface designed for motor rehabilitation in stroke and Parkinson disease patients. Slow Cortical Potentials (SCPs: electrical brain activity usually oscillating at less than 1 Hz [HMB03]) are extracted from the recorded EEG signal to detect the subject's intention to move. Once a movement intention is detected or a tremor predicted, the targeted muscle is electrically stimulated to help the subject produce the movement, or to counter the effect of the tremor [AB18].

A BCI system is composed of four components: a signal acquisition unit, a signal processing unit, an output device and an operating protocol [PN05; SM10]. The acquired brain signals or features extracted from it are processed and translated into device commands [ZK11]. The output devices can be a spelling device, a robotic arm or other systems that need to be controlled, which makes BCI a very convenient tool for patients who have highly compromised motor functions. The operating protocol guides all operations by regulating their onsets, offsets and timing [SM10]. Fig. 2.12 illustrates a BCI system designed for motor rehabilitation of stroke and Parkinson's disease patients. The EEG signals were acquired when stimuli were presented on the computer screen using a g.tec gUSBamp amplifier[13] and BCI2000.[14] The stimuli directed the subjects to perform imaginary left or right hand movements. The features extracted from the data would then be used to trigger a VisionBody suit[15] to deliver an electrical stimulation in the chosen hand and help the production of hand movement [AB18]. In this particular instance, motor imagery was used. However, the control of the BCI can also be done using self-regulated SCPs [Bir+99; Bir+00]. Furthermore, the command signal can be obtained after the features of interest are elicited by a mental task (e.g. motor imagery, mental arithmetic, etc.)

[13] https://www.gtec.at/product/gusbamp-research/
[14] The BCI2000 project aims at providing researchers with a software that facilitates the development of BCI applications that necessitate real-time data acquisition, processing and feedback [SM10]. It can be downloaded at https://www.bci2000.org/mediawiki/index.php/Main_Page
[15] https://www.vision-body.com/en/start

or after presentation of a visual or auditory stimulus [KN05]. Different brain responses such as event-related potentials and sensorimotor rhythms (SMR) also known as μ rhythms are also frequently used [K+01].

Apart from enabling patients with spinal cord injury to control a neuroprosthesis, one of the most important applications of BCI is certainly the establishment of communication with LIS patients [PN05]. In this context, BCI has been successfully employed to communicate with the patients. They were able for example to control a cursor or use a speller to communicate using EEG or ECoG signals [KN05; Fre+19]. Later on, it has also been proven that BCI could also be used to communicate with some CLIS patients [Sch+09; Gug+17]. Applications of BCI for communication with LIS and CLIS patients are more thoroughly discussed in Section 3.1.

2.3 Machine learning

Machine learning is a branch of Artificial Intelligence (AI), which is "the science and engineering of making intelligent machines, especially intelligent computer programs" [McC04]. As illustrated in Fig. 2.13, machine learning can be classified into three categories: **supervised**, **unsupervised** and **reinforcement learning**.

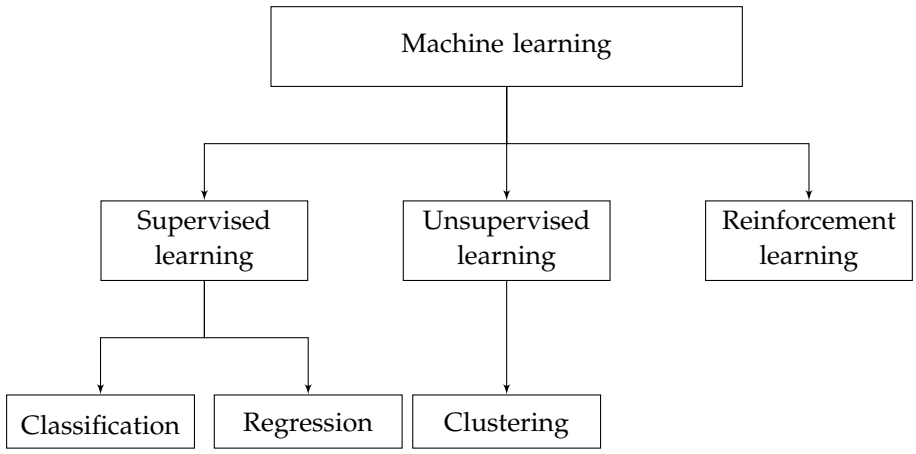

Figure 2.13: Types of Machine Learning. Machine learning can be partitioned into three categories: supervised learning, unsupervised learning and reinforcement learning. Supervised learning in turn can be broken down into two sub-categories: classification and regression, while unsupervised learning deals with clustering. In a classification task, the classes are predefined, while during clustering, the clusters are determined according to the similarities of the data points. Reinforcement learning is about learning the optimal behaviour of a system that maximises a reward signal.

Supervised learning Given a data set X with p features $X_1, X_2, ..., X_p$ measured on n observations, there is an associated response vector Y for each of the n observations. The goal is to train an algorithm that provides the best predictions of Y using X. In other words, the intention is to

fit a model that relates Y to X in order to correctly predict the response for future data in case of a *prediction*, or to understand the relationship between the predictors and the response vector in case of an *inference* [NS05; Jam+13]. There are two types of supervised learning algorithms. Typically, when the response vector Y is quantitative, i.e. has numerical values, it is referred to as a *regression* problem while if Y is qualitative or categorical, it is designated as a *classification* problem [Jam+13; Bis06].

Unsupervised learning No response vector associated with the data set X is available to the learning algorithm. In this case, the purpose is to discover hidden patterns in the data. The data points are grouped into *clusters* depending on how similar they are in what is called *cluster analysis* [Bis06; Jam+13]. As opposed to a classification problem, in which the number of clusters are known *a priori* and is used to predict new data, clusters represent the partition of the data into natural groups [Wit+17]. Their numbers can either be fixed or determined.

Reinforcement learning In this case, the goal is to determine what actions should be taken in a given situation so that a reward signal is maximised [SB18]. Similar to unsupervised learning, no response vector is provided to the learning algorithm that must determine it by a process of trials and errors instead [Bis06]. Consequently, the output of such system is a sequence of actions that yields the most reward [Alp09; SB18]. The learning algorithm gathers information by interacting with its environment, and for each action, receives an immediate reward. Nonetheless, the environment does not provide long term feedback. Thus, the learning algorithm faces an *exploration* (gain more information to see how effective each action is) versus *exploitation* (use already gathered information to obtain a high reward) dilemma [Bis06].

The work in this thesis makes use of clusters analysis, which is the focus of the next section, to evaluate the levels of consciousness of several patients with DoC and CLIS.

2.3.1 Clusters analysis

Clustering is a method that consists of discovering unknown subgroups in a data. These subgroups can be determined using either a *hierarchical* or a *partitive* cluster analysis [SS12].

A hierarchical clustering can be executed using one of two approaches: an agglomerative or a divisive one. The agglomerative method is the most used of the two. It starts with n clusters, each cluster containing one point. The clusters are combined, one at a time, based on distinct similarities, until all points are contained within a single cluster [SS12]. Fig. 2.14 illustrates a *dendrogram* representing the results of a hierarchical analysis performed on the Iris dataset.[16]

The most popular partitive clustering method, especially in biomedical signal analysis, is K-means clustering [NS05]. The algorithm attempts to establish a set of rules to group the data

[16] Fisher's Iris data set, data set containing 3 classes of Iris plants, introduced by the British statistician, eugenicist, and biologist Ronald Fisher in 1936 [Fis36].

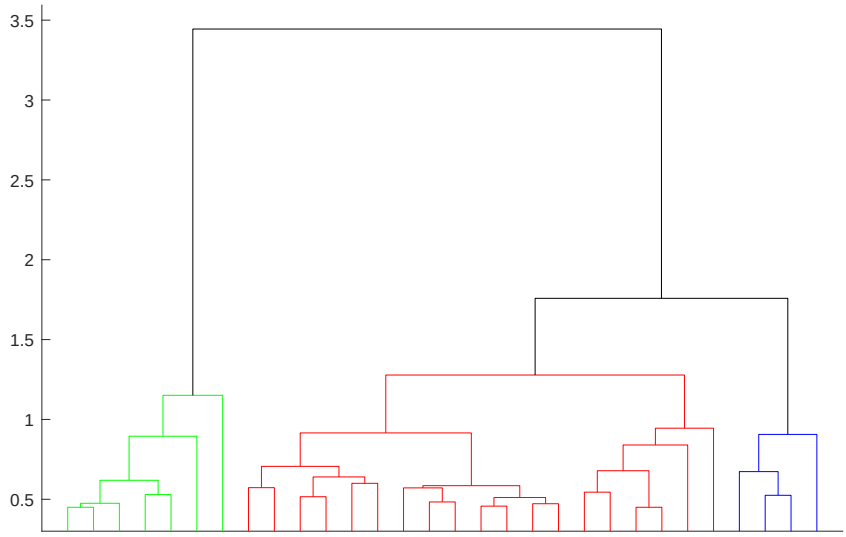

Figure 2.14: Dendrogram representing clustering of Fisher's Iris dataset. A much higher root node compared to the remaining nodes is observed. The figure also shows that there are two distinct groups of observations. When smaller distances are considered, different levels of groups emerge.

without the help of examples, by partitioning it into K distinct and non-overlapping clusters (*hard clustering*, see Fig. 2.16a). It is therefore imperative to provide the number of clusters. The general algorithmic structure of a partitive clustering is summarised in Algorithm 2.1. The details of the needed parameters and the computation of new clusters centres for each clustering method used in this work will be developed in Section 2.3.2.

Algorithm 2.1: Partitive clustering.

Initialisation:;
Set number of clusters K and further parameters where applicable;
Assign the objects to the K clusters;
Iteration:;
1. Compute new cluster centres;
2. Assign the objects to the new clusters.;
3. Converged? Yes: stop / No: goto 1;

In order to assign a specific cluster to the observations, K-means clustering algorithm randomly assign a number, from 1 to K, to each of them first. These act as initial cluster assignments for the observations. The objective is to minimise the distance between the observations and the centres of these clusters (*objective function*). New cluster centres are computed using that objective function, and each object is assigned to the cluster whose centroid is the closest (defined using Euclidean distance). This is repeated until its convergence [Pet+13].

Fig. 2.15b illustrates the results of a K-means clustering applied to Fisher's Iris dataset represented in Fig. 2.15a. When comparing these results to the actual classes, it can be concluded that the algorithm clearly separates the Setosa (characterised by smaller petal lengths and

widths) from the other two groups. There are some overlapping in terms of petal lengths and widths between Versicolor and Virginica, leading to a few incorrect grouping by the algorithm (circled points in Fig 2.15b). Hence, the algorithm correctly identified all Setosa types, 96% of the Versicolor and 88% of the Virginica.

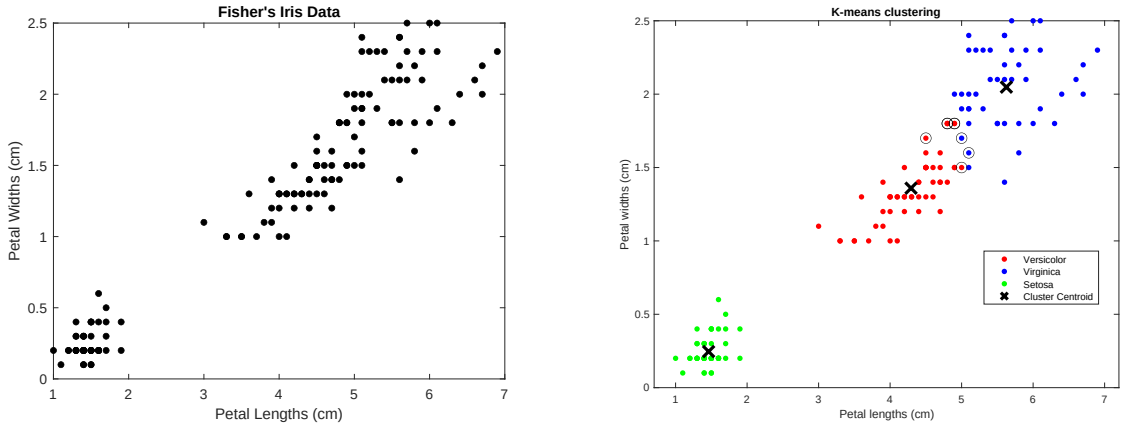

Figure 2.15: Grouping objects in clusters using *K*-means. Given the Fisher's Iris data in **(a)**, the algorithm partitions the data into *K*=3 clusters relative to their position and distance from each other. The clusters are mutually exclusive and are characterised by their respective centre point or *centroids*, represented by black crosses in **(b)**. Data points belonging to each cluster are shown in different colours. There is an overlapping between Versicolor and Virginica from the *K*-means clustering. The circled points in **(b)** are the ones misclassified by the clustering analysis.

It can also happen that the membership degrees are not bivalent, in which case the cluster analysis is known as *soft clustering* [Pet+13]. This approach is elaborated in the following section.

2.3.2 Soft-clustering

Two soft clustering approaches are used in this work, namely **fuzzy c-means** (FCM) and **Gaussian Mixture Models** (GMM).

2.3.2.1 FCM clustering

FCM is a soft-clustering approach that allows each data point to belong to multiple clusters with varying degrees of membership. In other words, as opposed to hard-clustering approach such as *K*-means in which the membership degrees are bivalent, a data point is assigned a membership grade ranging from 0 to 1 for each cluster as can be observed in Fig. 2.16b. On one hand, a data point which membership degree to a cluster equals 1 represents that cluster perfectly; on the other hand, a membership degree of 0 means that it is not "representative" of

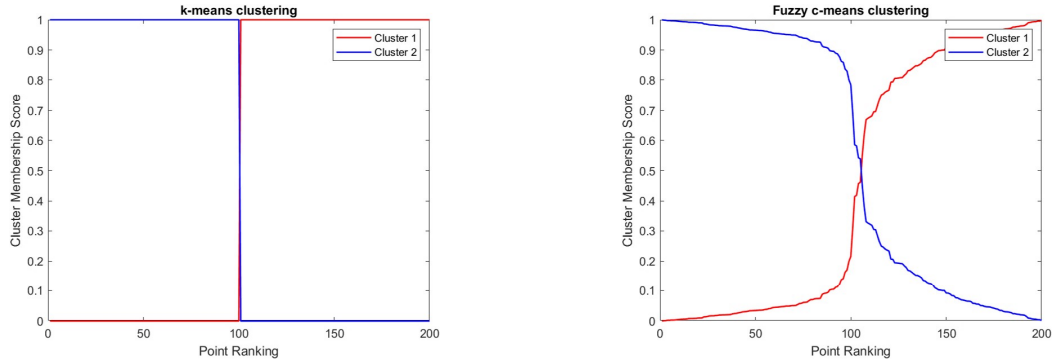

(a) Hard clustering

(b) Soft clustering

Figure 2.16: Cluster membership for hard and soft clustering. **(a)** Hard membership, obtained using *K*-means. Each data point belongs to only one cluster. **(b)** Soft clustering, using fuzzy c-means. Each data point belongs to a cluster to a certain degree. The sum of cluster membership equals 1.

the cluster at all [Chi94; Pet+13]. This technique was first introduced in [Bez81] with the goal to improve earlier clustering methods, and has been well established since.

Similarly to hard-clustering, the goal in soft-clustering is also to minimise an objective function:

$$J_m = \sum_{i=1}^{D} \sum_{j=1}^{N} \mu_{ij}^m ||x_i - c_j||^2 \tag{2.1}$$

where D represents the number of data points and N the number of clusters. m, $(m > 1)$, is a fuzzy partition matrix that defines the cluster's fuzziness. In other words, it determines the number of data points that have significant membership in more than one cluster. Larger values indicate a higher degree of overlap. $m = 1$ corresponds to a hard-clustering analysis. c_j designates the centre of the j-th cluster and is obtained by applying Eq. 2.2:

$$c_{ij} = \frac{\sum_{i=1}^{D} \mu_{ij}^m x_i}{\sum_{i=1}^{D} \mu_{ij}^m} \tag{2.2}$$

where x_i is the i-th data point. The degree of membership of x_i in the j-th cluster is given by μ_{ij} in Eq. 2.3, and the sum of the membership values for all clusters is 1 [Pet+13]. To measure the dissimilarity between data points and the cluster centre, the algorithm uses the squared Euclidean distance [Bis06].

$$\mu_{ij} = \frac{1}{\sum_{k=1}^{N} \left(\frac{||x_i - c_j||}{||x_i - c_k||} \right)^{\frac{2}{m-1}}} \tag{2.3}$$

For any given data point, the objective function expresses the distance to a cluster centre weighted by that data point's membership grade. The fuzzy c-means algorithm is implemented as follows [Bez81; Chi94; Pet+13]:

1. First, the number of clusters is specified and the cluster membership values μ_{ij} is randomly initialised.
2. Then, the cluster centres are computed using Eq. 2.2.
3. The cluster membership values μ_{ij} are subsequently updated according to Eq. 2.3.
4. Finally, the objective function J_m is calculated using Eq. 2.1.
5. The steps 2-4 are repeated until the objective function improves by less than a specified minimum threshold or until a given maximum number of iterations is achieved.

Fig. 2.17 illustrates the results of a FCM clustering applied to the Fisher's Iris dataset introduced in Fig. 2.15a. The colorbar on the right of the figure represents the degree of membership of the objects to the Versicolor group. The previously reported K-means clustering results showed that it was able to perfectly cluster the Setosa group. So, unsurprisingly, the degree of membership of this group is quasi null. As the boundary between Versicolor and Virginica is unclear, the degree of membership of the latter to the former decreases as the values of the petal lengths and width increases.

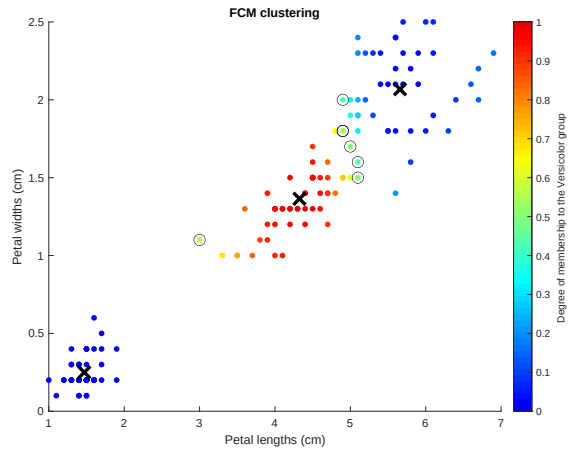

Figure 2.17: Soft-clustering of the Iris dataset using FCM. The colorbar represents the degree of membership of each data point to the Versicolor group (in red). Data points belonging to the Virginica group have great degree of membership to the Versicolor group, illustrating the overlapping mentioned earlier, as opposed to those from the Setosa group that are clearly separated (degree of membership ≈ 0). The circled points have degrees of membership between 0.4 and 0.6 (have relatively strong affinity to both groups).

2.3.2.2 Gaussian Mixture Model

A GMM is a model-based cluster analysis approach that uses a Gaussian mixture distribution $f\left(\mathrm{x}_i|z_{ig}=1,\theta_g\right) \sim \mathcal{N}\left(\mu_g,\Sigma_g\right)$ as a model. The assumption is that the data is generated by a random statistical model that the clustering method attempts to recover [FG20]. Simply put, a Gaussian mixture model is a simple linear superposition of several Gaussian components (Eq. 2.4) that gives a richer class of density models than a single component [Biso6]. Given $\mathrm{x}=(\mathrm{x}_1,\mathrm{x}_2,...,\mathrm{x}_\mathrm{n}) \in \mathbb{R}^p$, the random vector x_i is assumed to arise from a finite mixture of probability density functions:

$$f\left(\mathrm{x}_i,\Theta\right)=\sum_{g=1}^{K}\pi_g\Phi\left(\mathrm{x}_i|\mu_g,\Sigma_g\right) \tag{2.4}$$

where:

- K: number of components (clusters);
- $\pi_g > 0, (g=1,...,K)$ and $\sum g = 1^K \pi_g = 1$: mixing proportions;
- $\Phi=(\pi_1,...\pi_{g-1},\mu_1,...\mu_g,\Sigma_1,...,\Sigma_g)$: parameter vector;
- $\Phi\left(\mathrm{x}_i|\mu_g,\Sigma_g\right)$: underlying component-specific density function with parameters $\mu_g,\sigma_g,g=1,...,K$.

Each mixture component density is associated to a specific parametric class and represents a cluster. The parameters in Φ are estimated by the maximum likelihood optimisation, more precisely by using the iterative *Expectation-Maximization (EM) algorithm* [FG20]. K-means is a particular non-probabilistic limit of EM applied to mixtures of Gaussian [Biso6]. The model in Eq. 2.4 generates ellipsoidal clusters centred at the mean vector μ_g, and σ_g controls the other geometrical properties of each cluster. Difference of means in the different component models suggest that the model distinguishes among the K classes [MP00].

The EM algorithm consists of two steps:

1. The **E-step**, during which the algorithm calculates posterior probabilities[17] of cluster memberships. The result can be thought as an n-by-k matrix, where element (i,j) contains the posterior probability that observation i is from cluster j.
2. The **M-step**, during which it estimates the cluster parameters by applying maximum likelihood and using the cluster-membership posterior probabilities as weights.

The EM algorithm iterates over these steps until convergence to a local optimum. Once it reaches it, the soft partition is obtained by assigning each data point to the cluster with the highest posterior probability. This local optimum depends on the initial conditions which can be chosen randomly or selected using the k-means++ algorithm (see Appendix A).

[17] conditional probability that is assigned after the relevant evidence is taken into account

Fig. 2.18 represents the results of GMM clustering applied to the Fisher's Iris dataset introduced in Fig. 2.15a. The colobar on the right of the figure illustrates the degree of membership of the objects to the Versicolor group. Same as for FCM clustering, the degree of membership of all Setosa to Versicolor is very close to zero, and for Virginica the value decrease as the values of the petal lengths and width increases. In addition, the results obtained in this case differ from those from FCM in that there are less intermediate values of the membership degree (circled points in the figure).

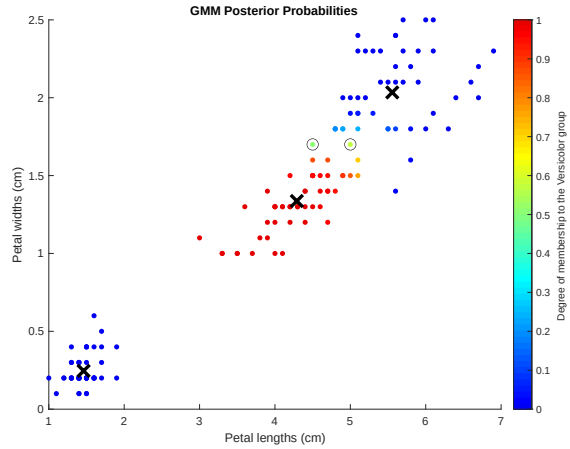

Figure 2.18: Soft-clustering of the Iris dataset using GMM. The colorbar on the right side of the figure represents the degree of membership of each data point to the Versicolor group (in red). Data points belonging to the Virginica group have high degree of membership to the Versicolor group, but decreases as one move away from its centroid. The Setosa group is clearly separated from the other two groups. The circled points have degrees of membership between 0.4 and 0.6 (have relatively strong affinity to both groups).

2.4 Summary

This chapter introduced a few principles necessary for the understanding of the contents of the following chapters. It started by defining what consciousness is, at least in the context of this thesis. In particular, it dived into states known as disorders of consciousness. The main group of interest of this thesis is however completely locked-in syndrome patients. It then provided the foundations of brain signals and the recording process as well as brain-computer interfaces. The chapter ends with some notions of machine learning, especially of clustering analysis that will be specifically used to infer the patients' consciousness levels. The details of how it goes about is presented in Chapter 5.

3 State-of-the-art

After a brain injury, the state of the patient is usually evaluated using standardised neurobehavioural assessment measures such as the Coma Recovery Scale - Revised (CRS-R) presented in the previous chapter in Table 2.2. These assessments evaluate the patient's eye, motor and verbal responses [Pos+07]. The behavioural assessments are however not appropriate for LIS and CLIS patients since they cannot move and that the tests mostly rely on motor response [Hei+18]. This often causes misdiagnosing them as DoC patients. Generally, the first diagnosis is made several months after the injury, normally around 2.5 months after onset. But for a lot of them, it was only detected after several years [LCERDM02; KN05]. An extreme case being a patient that was believed to be in an UWS/VS for 20 years. It was later discovered, after a series of behavioural and neuroimaging assessments, that the patient was in an incomplete LIS state instead [Van+18]. The misdiagnosis of LIS as a DoC may be due to the fact that outwardly, LIS patients look like patients in VS or in MCS [KN05; Pos+07]. In addition, in the way to recovery, patients go through a *functional LIS* state which combines motor dysfunction and preserved higher cortical functions that can only be detected using functional imaging techniques [FDC13]. Anyhow, the patient's conscious state is usually discovered by family members [Pos+07]. Fig. 3.1 illustrates the rate of discovery of the patients' conscious states in [LCERDM02], where more than half the time a family member notices that the patient is conscious. This state is discovered by the physician in only 22.7% of the cases.

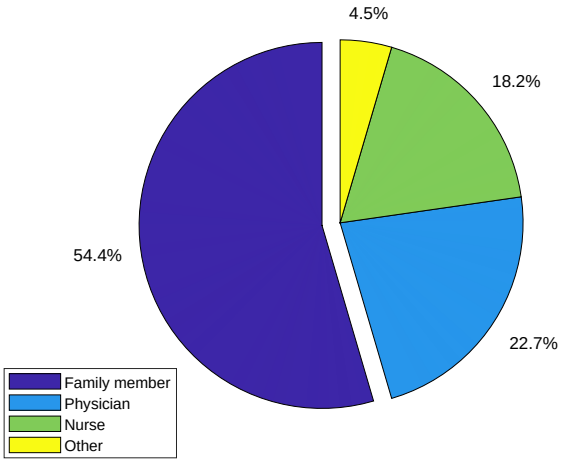

Figure 3.1: LIS patient's awareness discovery. Most of the time, family member are the first to observe signs of awareness from the patient [LCERDM02].

Living in a state of LIS appears to be a very challenging situation. Patients that experienced pharmacologically induced LIS during anaesthesia reported an anxious desire to move and speak while being unable to do so [Gos+09]. Moreover, a glimpse at the life of LIS patients can be imagined by reading some books written by such patients. A few examples of these books can be found in Table 2.3. Surprisingly, most patients report a rather fulfilling life, especially when they have the ability to communicate with their family or somewhat interact with their surroundings. The survey in [LCERDM02] also reported that 73.2% of the patients enjoyed going out, and 81% of them actually meet their friends at least two times monthly. Most of the time, communication are performed using lateral or vertical eye movements, or blinking [Lau+05]. In addition to that, a 6-year longitudinal study of the quality of life[18] of patients with LIS also revealed that the majority of them were relatively satisfied with their quality of life and still enjoyed social interaction [Rou+15]. For this reason, patients' desire to end their life is relatively rare [KN05]. It is therefore crucial that the patients have someone to communicate with since their quality of life heavily depends on that [Bir+00; K‡01]. Besides, it also appears that the ability for CLIS patients to communicate and interact with others are highly correlated with a positive state of mind [Rou+15]. Misdiagnosis of such patients could therefore lead to wrongful termination of their life, which is tragic given that most LIS patients lead meaningful life despite their state. Furthermore, it delays every opportunity for the patients and their family to communicate and accordingly decreases their mood and quality of life.

On one hand, BCIs offer the potential to reveal hidden brain signal patterns that indicate conscious states, independently of external motor functions responses. On the other hand, they provide a direct connection between the brain and a computer, allowing the control of other devices. This in turn permit people, especially those with no motor control, to communicate using only their brain signals. This chapter gives an overview of the state of current researches in communication in the completely locked-in state using EEG or ECoG signals before reporting on those involving consciousness detection in such patients.

3.1 BCI-based communication for CLIS patients

The first speller for LIS patients with ALS was developed by Birbaumer et al. in the late 90s, and uses self-regulated SCPs to command a speller device. Comparable to healthy subjects, two patients were able to learn to regulate their brain responses in order to operate the device, allowing them to select letters of the alphabet using a cursor on a video screen [Bir+99; HMB03]. The speller has been expanded into a Thought Translation Device (TTD), providing the patients with a system in which they can also select words and pictograms in addition to letters [HMB03]. The system was tested with five LIS patients and demonstrated the usefulness of such system to communicate with completely paralysed patients [Bir+00]. These communication systems were further improved granting the patients with an adapted web browser and an e-mail

[18] World Health organisation (WHO) defines quality of life (QoL) as "an individual's perception of their position in life in the context of the culture and value systems in which they live and in relation to their goals, expectations, standards and concerns" [WHO12].

interface [Ben+07]. The system was called Nessi (Neural signal surfing interface) and allowed patients to chose any selectable item on the web page using their brain signals, SCPs in particular, and to read and write e-mails using a virtual German keyboard.

This represents an encouraging development in the quest of developing communication systems for such patients. Nonetheless, BCIs using SCPs (and also SMR) are relatively slow given that the brain responses can take around 5 seconds [Ben+07]. In addition, training can be rather time-consuming since the patients need to go through a sophisticated learning procedure to be able to regulate their SCPs [K‡01], inducing patients' fatigue. This prompted the investigation of other faster brain responses such as the ERPs, in particular the P300.

Relatively fast BCIs are based on VEPs, which are less demanding for patients than SCPs. In [Oke+14], a rapid serial visual presentation (RSVP) paradigm was implemented to control a keyboard part of a system that incorporates a statistical language model for letter prediction using machine learning. The system was tested with nine LIS patients along with nine healthy controls and the experiment consisted of five levels of difficulty of different spelling tasks. The experiment resulted in all of the patients being able to use the spelling at level 1, but only one of them was able to complete level 5 compared to six participants from the healthy control group. Another study used SSVEP-based BCI to provide a binary communication device to six patients in locked-in state after a stroke or a TBI. To answer *yes*, the patients were instructed to focus on yellow flashes (at frequency 10 Hz), and to answer *no*, they were asked to concentrate in red flashes (with frequency 14 Hz) [Les+14]. Latent Discriminant Analysis (LDA) was used afterwards to classify *yes* and *no* answers using spectral features extracted from the brain signal. A comparison of spellers using visual P300 and those employing SSVEPs to communicate with seven patients showed that SSVEP induced less mental workload compared to P300, thus is more advantageous in terms of patients' fatigue. It is also faster, exhibiting a transfer rate of 25 bits/min as opposed to 9 bits/min for the P300 ERP [Com+13]. A major drawback of such systems is that it is not practical for subjects that have no gaze control. Moreover, patients reported fatigue after a prolonged use.

Due to the progressive visual impairment of LIS patients as the condition develops, auditory P300-based BCI were developed to continue communication with them. The achievability of such enterprise was investigated in [K‡09] with four LIS/CLIS patients. A 5x5 spelling matrix with all letters of the alphabet except Z were presented on a monitor to the patients, which could select a letter by attending to number words presented in an audible manner. Each character's position in the matrix was coded by two numbers representing the row (1 to 5) and the column (6 to 10). The patients were able to achieve accuracy above 70% and even 90% using a visual P300-based speller, but reliable communication could not be achieved using an auditory speller for the same task. Healthy control also performed slightly better in the visual ERP BCI compared to the auditory one.

Most of the time, non-invasive BCIs are used, but in certain cases, the patients can also be implanted with ECoG. The LIS patient with ALS in [Van+16] was implanted with electrode strips in the left motor cortex and left prefrontal region to investigate the usability of an independent communication system for home use. The system uses motor imagery of the right hand to allow the patient to control a pointer. She completed two training sessions weekly,

and was able after some time to achieve a 89% (±6%) accuracy for spelling, with an increasing speed as she became more familiar with the system (the spelling speed of 52 seconds at the beginning improved to 33 seconds later). The motivation as well as the patient's mood were evaluated, and the results showed that she was always highly motivated except in days with health-related issues, her mood improved as her capacity to communicate developed. This study was part of a larger one, the Utrecht NeuroProsthesis (UNP) study that also included another LIS patient in locked-in state caused by stem stroke and other subjects that are able-bodied used as controls [Fre+19]. Differences in the power spectral responses were observed between both LIS patients, suggesting that patient's aetiology should be taken into account during the development of BCI-based communication system.

All of these research only involve LIS patients and attempts to communicate with CLIS patients using their EEG signals have failed at first, begging the question whether the brain control learned during LIS could be transferred to CLIS [KB08]. Nonetheless, several research have since then reported successful communication with such patients. In [Gug+17], vibro-tactile P300 and motor imagery were tested with nine LIS and three CLIS patients with ALS. Vibratory stimulation of the hands or the foot with two (VT2) or three (VT3) stimulators were employed to elicit a P300 response. Additionally, motor imagery (MI) of left or right hand movement, along with the P300, were also investigated to permit a binary communication with these patients. One one hand, nine out of the twelve patients were able to successfully use the vibro-tactile P300, with an average of 8 out of 10 correct answers. On the other hand, three of them were able to communicate using MI. Only one CLIS patient was unable to communicate using VT3, and the successful two were able to achieve 90% and 70% accuracy respectively. This research constitutes the first study that reports a successful communication of CLIS patients using EEG-based BCI. It is also the first that achieved such high accuracy. After 5 to 20 min of MI training, it takes around 8 seconds to answer each question with a *yes* or a *no*. Furthermore, this constitutes one of the rare researches that evaluates the patient's consciousness level before initiating communication.

A few years later, an EEG-based endogenous BCI was developed to communicate with a totally locked-in patient with ALS [Han+19]. The patient presented no remaining muscle movement, her ALS Functional Rating Scale-Revisited (ALSFRS-R) was zero, but her hearing and cognitive functions were preserved. To distinguish between *yes* and *no* answers from the patient, a combination of motor imagery and mental subtraction was used, and brain responses were classified using Riemannian geometry (RG), LDA and Support Vector Machines (SVM). The patient was able to achieve an average offline accuracy of 95% with RG, 87.5% with LDA, and 85% with SVM. RG gave the best offline accuracy, it was therefore used for the online classification of the *yes* and *no* answers. The patient was able to achieve an online average accuracy of 87.5%. Unfortunately, due to patient's health state, no follow-up experiments were performed. But when the experiments were resumed several months later, no signs of consciousness were found. This underlines the importance of maintaining a regular schedule of experiments and communication with the patients. It was found to delay cognitive decline [Sec+21].

Another study reported the case of a CLIS patient in his early thirties suffering from a clinical variant of non-bulbar ALS. To communicate with the patient, his family developed a custom-made speller on paper in which the patient could select letters with eyes movements:

any visible eye movement represents a *yes* while none means *no* [Cha+20]. As it became more difficult for the patient to move his eyes, his ability to communicate decreased. He and his family were then looking for other means of communication. Two intra-cortical microelectrode arrays were implanted into his primary motor cortex areas and in the supplementary motor area (SMA), 8x8 electrodes each. The same custom-made spelling system as before was used, and the patient was able to form sentences by modulating his neural firing rates by the means of an auditory-guided neurofeedback-based strategy to select the letters.

Almost none of these studies performs a preliminary assessment of the patients' consciousness before performing the tasks. Agreed that the capability of following commands in itself can be considered as proof of consciousness [Les+15], however it seems more logical to first determine if the patient is in fact apt to complete the tasks. Studies assessing LIS/CLIS patients' consciousness levels are reported in the following section.

3.2 Patients' consciousness assessment

The previous sections demonstrate the importance of a correct diagnosis to allow an optimal medical care for the patients, especially to offer them the opportunity to communicate with their relatives despite the state they are in. This section gather some important research dealing with the assessment of patients' conscious states. Most of the literature assessing consciousness after a TBI involve MCS and UWS/VS patients. Only a handful of them include LIS patients, and still, in a very limited number (usually only one per study). This low number of researches is certainly due to the rarity of the disease. According to OrphaNet,[19] the prevalence of LIS is below 1/1000000. Furthermore, the goal of these studies was not to evaluate if the patient is conscious per se, rather to differentiate between MCS, VS and/or healthy subjects. Only the studies comprising at least one LIS or CLIS patient will be addressed in this section. The methods normally used to assess patients' consciousness can be categorised into two groups: event-related potentials in response to some sensory stimulation, and features extracted from resting state data [JR20].

3.2.1 Assessment using brain sensory responses

Sensory-based stimuli include auditory, tactile, visual and olfactory stimulations. This type of experiment generally necessitate the patient's engagement to the task to evaluate his ability to follow commands as such capacity is seen as proof of consciousness [Les+15]. P300 is undoubtedly the most used brain potential to assess patients' consciousness, used in conjunction with auditory-based stimuli. Other than audio tones, the subject's own name (SON) is also often used in this case [Ser+17; Ann+20; Gao+19; Pan+18].

In [Per+06], a P300 auditory paradigm is used to attempt to discriminate between 5 VS, 6 MCS and 4 LIS patients. For the analysis, they were instructed to passively listen to the

[19] OrphaNet is a database for rare disease and orphan drugs. `https://www.orpha.net/`

stimuli with their eyes closed. Their results determined that P300 were elicited for all of them after SON, except for 2 VS patients. Moreover, no difference were observed by the authors between the different groups, leading them to conclude that P300 responses could be used to differentiate between them. A similar paradigm was applied to 18 DoC patients consisting of 2 coma, 9 VS and 7 MCS patients along with 2 LIS patients [Zha+17]. The SON said by a familiar voice was used as the deviant stimulus, and a 1000 Hz tone and the subject's derived name (sdn) as the standard stimulus. In both cases, intact P300 responses were observed for all LIS patients. It was also the case for all MCS and 4 of the 9 VS patients, but only with one or the other paradigm. Follow-ups were carried out 2, 6 and 12 months after recording, and it determined that patients that displayed P300 response in both paradigms woke up after 12 months. Consequently justifying the usability of P300 as a recovery predictor for DoC patients.

P300 can also be combined with SSVEP in a visual hybrid BCI. In [Pan+14], four healthy controls, four VS patients, three MCS patients, as well as one LIS patient participated in the experiment. The task consisted on focusing on one photo containing the Subject's Own Face (SOF) or another unfamiliar photo. They were flashed at 6 and 7.5 Hz respectively. The BCI should detect which photo the patient was focusing on. The goal is evidently to ascertain if the subjects are able to follow instructions, suggesting an underlying consciousness. The results showed that all controls and the LIS patient, in addition to one MCS and one UWS patients, were able to attend to the photo they were instructed to concentrate on. Moreover, the obtained accuracy for both groups of DoC patients were comparable, although the CRS-R of the UWS patients were lower (4 to 7) than those of the MCS patients (10 to 12).

Other methods not relying on eye movement control have also been investigated. The feasibility of using vibro-tactile stimulation to evoke P300 responses was examined in [Lug+14], with the participation of 6 chronic LIS patients. The experiment consisted of two tasks: a vibro-tactile oddball paradigm during which the patients are asked to count a target stimulus, and a binary communication in which patients answer *yes* by counting vibrations on their right wrist, and *no* by counting those on their left wrist. The results showed that 5 out of the 6 patients were able to elicit P300 responses, with an accuracy of 100% for 4 of them. In addition, 1 out the 6 patients obtained an accuracy of 100% during questions answering while the accuracies achieved by the other patients vary from 20 to 60%. In the end, the study proved that it was possible to evoke P300 responses in LIS patients using somatosensory stimulation. The same method was used in [Gug+17] to assess LIS and CLIS patients' consciousness before completing the binary communication (see previous section).

On the other hand, the use of motor imagery (MI) in evaluating consciousness states have also been explored. One study implicating a LIS patient and two MCS patients concluded that EEG power spectral analysis could be used as a tool to detect patients' awareness at the bedside [Gol+11]. During the experiment, the patient was instructed to imagine "swimming" (*motor imagery*) or imagine "walking through their house" (*spatial imagery*). The LIS patient and one of the MCS patients displayed consistent patterns of spectral changes depending on the task. However, these variations differ from the expected results from healthy subjects. LIS patients usually show levels of consciousness comparable to that of healthy subjects [JR20]. However this depends on what has caused the condition. In [Hei+18] for instance, two groups of LIS patients (one group as a result of stroke, and another as a transition from ALS) were

instructed to count some rare stimuli delivered to one wrist. Two stimulators called VT2 were place on their left and right wrists. Results show that higher difference in the P300 amplitude were observed with ALS patients compared to the stroke patients, reflecting the pathological mechanisms difference in each group of patients and pinpointing the reduced tactile sensitivity in patients with LIS following a stroke.

All of those researches involve LIS patients. One of the few studies involving a CLIS patient was performed with patient GR (introduced in Section 5.1.2.1) who is in late stage ALS. He was implanted with ECoG and a longitudinal analysis of his attention and cognitive processing was carried out 1, 2, 3 and 6 months after the grid electrodes were implanted [Ben+14]. Auditory stimuli consisting of standard and deviant tones were used to evoke brain responses. In addition, frequency powers of δ, θ, α, β and γ were also analysed. The patient was 40 years old at the time of the study [Soe+13]. The goal of the study was to investigate the progression of the disease and eventually find an alternative communication pathway that could be used for BCI. The results revealed that during the course of the study, N1 and P2 potentials were always detectable, implying moderately intact attention and cognitive functions. On the other hand, the P3 responses decreased until they were no longer discernable three months after the last communication with the patient. Moreover, a gradual session to session increase of the δ power along with a clear drop in γ between the penultimate and last sessions were observed, possibly indicating transition to CLIS [Ben+14].

In general, LIS patients display significant P300 brain responses to sensorimotor stimuli. However, the response of this potential decreased for the CLIS patient as his condition evolved. Nonetheless, the presence of attention-related brain responses (N1 and P2) are still noted. This indicates the usefulness of evoked brain potentials to assess LIS and CLIS patients' consciousness level. The type of tasks that elicits them usually requires the patients to engage to them. Nevertheless, in the previous section detailing researches in communication with these patients, it was pointed out that they tend to be easily fatigued. This is why resting state data is used in this thesis to assess the levels of consciousness of principally CLIS patients instead of the evoked potentials. This way, less energy is spent during the consciousness detection part of the experiment, hopefully allowing for a more efficient communication afterwards, provided the patient is conscious enough to initiate it. The following section presents studies evaluating patients' consciousness using resting state data.

3.2.2 Assessment using resting state data

Consciousness level following a brain injury can also be assessed using resting state data. This type of recording provides useful information about the patients' spontaneous neural activity, without requiring them to perform any specific task. Accordingly, features such as the power spectral analysis of δ, θ, α, and β frequency bands or complexity measures such as the Lempel-Ziv complexity or derivate metrics are employed [Mal+13; G+21; Gos+14b]. Additionally, entropy-based approaches and functional connectivity are also used [JR20].

An investigation of the presence or absence of consciousness in LIS and DoC patients along with healthy controls using Perturbational Complexity Index (PCI) is performed in [Gos+14b]. PCI is a measure derived from LZC. Higher complexity values are usually associated with conscious states. Their method combined high density EEG with Transcranial Magnetic Stimulation[20] (TMS) to discriminate MCS from VS patients. The brain activation generated by the TMS was preserved in the long-range and high values of PCI were observed during consciousness, and the opposite is detected during unconsciousness. Besides, the method was able to discriminate between MCS and VS patients. In addition, the PCI values obtained by the LIS patients were comparable to those of the healthy controls.

Another study involving 89 DoC, 11 eMCS, 4 LIS patients and 26 healthy subjects utilised spectral connectivity to determine their consciousness [Che+17]. The data consisted of a combination of high density EEG and PET. Moreover, the mean relative power over all channels, the median connectivity as well as different graph theory characteristics computed in the δ, θ and α bands. Strong brain networks connectivity were observed for patients misdiagnosed as unresponsive but later revised as being in a MCS. This finding may be used to reduce misdiagnosis rates since it was able to detect consciousness in incorrectly diagnosed patients.

Preliminary studies to detect consciousness in the same patient as in [Ben+14] were performed in [Ada+19b; Ada+21] using the imaginary part of the coherency, multi-scale entropy and Granger causality separately. Sample entropy was also applied to the same data in [WNB20]. Each method produce one possible consciousness state of the patient and sometimes the results are overlapping. Similarly, these methods were also applied to assess consciousness in the CLIS patients presented in Section 5.1.2.2 [AB21b; WB21].

There are considerably less researches that assess LIS/CLIS patients using resting state data. Different EEG signal characteristics were examined: connectivity and complexity measures as well as spectral features, each of them showing effectiveness at discriminating conscious and unconscious states to some extent. Nevertheless, in each study, only one or two features are used. Using a unique measure only brings a single facet of the signal to light. Several features are thus used in this thesis to collect as much signal characteristics related to conscious states as possible and maximise the chances of determining the correct state of the patients.

3.3 Summary

In this chapter, the relevant sources regarding consciousness assessment in patients in the locked-in state were presented. There exists a relatively extensive literature on communication with LIS/CLIS patients, considering the rarity of the condition. P300 ERP appears to be the most popular brain response used to regulate a BCI in this context and seems quite efficient. However, most of the studies get straight to the point without assessing if the patient is even conscious. On the other hand, the number of studies actually probing for consciousness are

[20] type of non-invasive brain stimulation that uses a changing magnetic field to generate electric current in a particular area of the brain through electromagnetic induction. Source: `https://en.wikipedia.org/wiki/Transcranial_magnetic_stimulation`

somewhat limited, especially those using resting state data. The usage of evoked potentials often requires some participation of the patients' part. Furthermore, each of the methods to detect consciousness in the current literature only uses a few features. On that account, this thesis aims at estimating the levels of consciousness of CLIS patients before engaging in communication with them. More precisely, this latter is to be initiated only when the patient is predisposed to do so. Moreover, a set of different EEG features is used to increase the chances of accurately determining their states of consciousness. No such research direction has ever been carried out as of yet. An overview of how the proposed approach operates is presented in the next chapter.

4 Modus operandi

4.1 Aims and scope of the work

In one of the CLIS dataset studied in this work and described in Section 5.1.2.1, only one of the 170 attempts to communicate with the patient was successful. This patient was trained in using BCI since he was in the early stages of ALS. One hypothesis would be that during the unsuccessful attempts, the patient was either unconscious or not in the mood, and that the one successful experiment occurred at a time when he was actually conscious and willing to perform the tasks. It is therefore critical to determine the periods of time during which the patient's level of consciousness is high enough to allow communication. Given the importance of being able to communicate for these patients, it is vital to offer them the opportunity to do so. The goal of the present research is to introduce a system that evaluates CLIS patients' consciousness levels in order to identify the optimal time for a communication using several sets of features including frequency, complexity and connectivity characteristics. Previous researches suggest that the brain waves of locked-in syndrome patients are nearly similar to those of healthy subjects [Van+18], and that their cognitive functions are mostly intact [KB08]. For that reason, we hypothesise that CLIS patients' brain rhythms would to some extent liken that of healthy subjects'.

4.2 Design of the approach

The proposed method makes use of a set of features to assess CLIS patients' level of consciousness (defined in Section 2.1) as a preceding step before an eventual communication attempt. The features were chosen so that they comprise different characteristics extracted from the pre-processed EEG or ECoG signal. The first set of features consists of spectral features, namely the relative powers of θ and β bands, and the spectral edge frequency at 95% (SEF95). In normal circumstances, the values of the different frequency powers provide information about the brain states [GIM18]. The second set of features comprises complexity measures that evaluate the randomness of a signal. The more random the signal is, the higher its complexity. This high value symbolises an activated cortex and consequently, a higher level of consciousness. For example, Poincaré plots are a geometry-based approach frequently used to assess levels of consciousness in anaesthesia research [HMS14]. LZC is a complexity measure that uses symbolic representation of the signal, and is mostly used for data compression [LZ76]. But it has also been employed recently to analyse biomedical data such as EKG and EEG [Abo+06].

The last set of features employed involves brain functional connectivity. One fundamental characteristic of the brain is its inter-connectivity that provides information on how one brain region is connected to another. Two different measures were used in this case: the imaginary part of the coherency (iCOH), which is a linear approach and a non-linear method termed weighted Symbolic Mutual Information (wSMI). The imaginary part of the coherency has been used in conjunction with artificial neural networks (ANNs) to evaluate consciousness level of CLIS patients [Ada+19a; Ada+19b; AB21b], and both methods have also been employed with the same goal with DoC patients [KSF13; Imp+19]. As the frequency-based and the complexity measures are calculated in single electrodes, the connectivity metrics are computed between pairs of channels. Table 4.1 details all the features extracted from the EEG or ECoG signals.

Table 4.1: List of features extracted from the EEG/ECoG signals.

Feature	Type	Additional infos	Reference
Relative power (RP)	Spectral	In θ and β bands	Section 5.2.1.1
Spectral Edge Frequency (SEF)	Spectral	95%	Section 5.2.1.2
Poincaré ERR	Complexity	Time delay $\tau = 2$ samples.	Section 5.2.2.1
Lempel-Ziv Complexity (LZC)	Complexity		Section 5.2.2.2
imaginary Coherence (iCOH)	Connectivity	Absolute value in θ band	Section 5.2.3.1
weighted Symbolic Mutual Information (wSMI)	Connectivity	$\tau = 16$ ms	Section 5.2.3.2

Fig. 4.1 illustrates the signal processing and analysis pipeline of the approach proposed in this thesis. We theoretically introduced the *modus operandi* implemented here in [Ada+21]. Three different features were initially used to introduce the system: the imaginary part of the coherency, multi-scale entropy and Granger causality. More features are however used in this thesis. The idea is to maximise the chances to identifying the actual patient's consciousness level by combining them, since each of the methods extracts particular signal characteristics. Assuming that the CLIS patients' cognitive functions in this study are still intact, a *conscious state* is determined using the following hypothesis:

- **An increase of θ power combined with an increase of β power.** Relative power as a potential marker for consciousness for patients with disorders of consciousness has been investigated and results showed that θ and α in particular are among the best features that could distinguish MCS from UWS patients. Moreover, verbal and spatial memory tasks induce an increase of θ power [Bor+13] and the recovery of consciousness after anaesthesia is indicated by a global increase of the θ power and also the γ power and coherence [Pal+15].

- **A higher value of Spectral Edge Frequency at 95% (SEF95).** SEF95 is frequently used in anaesthesia research to assess the depth of anaesthesia in healthy subjects. Its value

represents the frequency below which 95% of the EEG signal power is contained. Research show that the deeper the anaesthesia level, the lower the frequency value [Ram+80]. Light anaesthesia is characterised by SEF95 higher than 15 Hz (in the β band). For moderate anaesthesia, the values lie between 8 and 13 Hz (α band). Frequencies lower than 7 Hz (in the δ and θ bands) indicate deep anaesthesia [Tou+19]. Accordingly, a larger SEF95 value indicates a higher level of consciousness.

- **A higher Ellipsoid Radius Ratio (ERR) of the Poincaré plots.** ERR is the ratio SD1/SD2 of the standard deviation of the points of the ellipse along the line of identity by that of those perpendicular to the line of identity. An increased depth of anaesthesia is symbolised by a reduced randomness of the EEG signal and the short-term variability SD1, and by extension ERR [HMS14]. A rounder shape of the ellipsoid (ERR $\approx$ 1) corresponds to randomness, thus more complex signals. Consequently, the closer to 1 the value is, the higher the consciousness level is.

- **A higher LZC value.** A normalised version of LZC, on the other hand, has only been used recently to assess consciousness levels of different types of patients compared to healthy control [LBMM15]. In principle, a higher level of consciousness is portrayed by a increase of signal complexity, and inversely [G+21; Gos+14b].

- **A higher iCOH in the θ band.** During periods of unresponsiveness in healthy subjects under anaesthesia, a decrease of δ coherence, especially across hemispheres in frontal and central electrodes, are observed [Pul+20]. In addition, global coherence is reduced for example during ketamine-induced unconsciousness, and power and coherence in high frequencies increases during recovery of consciousness [Pal+15]. Given the type of task presented to the patient and that θ band plays an important part in working memory [Bor+13], only the coherence in this frequency band will be used.

- **A higher wSMI in the θ band.** Consciousness is normally detected by the characteristics of the brain signal in the higher frequencies. Research suggest that the long-range connectivity patterns theoretically related to consciousness are most robustly and accurately assessed by the wSMI in the θ band [Eng+18]. It has been determined that higher values of this metric in that frequency band correspond to higher levels of consciousness [Bou+20]. This is why only its values in the θ band will be used.

At first, the raw EEG signal is pre-processed. This is done by filtering it into specific frequency bands. Each of the features were computed on short overlapping segments of the filtered signal. Afterwards, the results are averaged over all recording channels, leading to one value for each feature and for each segment. This is done to obtain a global estimate of each measure. For the connectivity metrics in particular, the average is computed as the mean of the lower part of the connectivity matrix representing the couplings between the pairs of channels, excluding the diagonal.

The global value of each metric is considered instead of the distinctive channels to highlight characteristics shared by the whole brain, instead of localised peculiarities. The averaged results are gathered into an n-dimensional matrix, where n denotes the number of features used, and

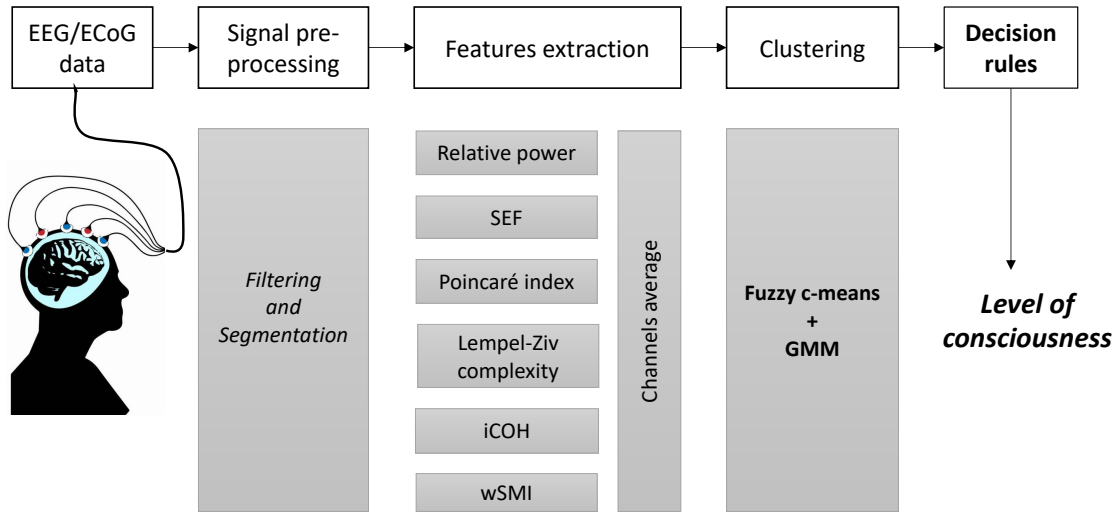

Figure 4.1: Signal processing and analysis pipeline. The recorded signal is filtered and segmented, before extracting the different features. Each feature is then averaged across all channels before performing the clustering analysis. The patient's consciousness level is subsequently determined by applying a decision rule presented in Section 4.2.

cluster analysis is performed to partition the data into two clusters: *conscious* and *unconscious*. Rather than using a hard-clustering approach, a soft-clustering analysis is preferred in that an output that expresses a degree of how likely a patient is conscious is desired. In this case, data points can belong to multiple clusters and the sum of membership to all clusters equals one [Pet+13]. The method provides a very convenient way to reach a final decision by analysing the different available variables. Two well established methods are used in this case: *fuzzy c-means* (FCM) [Bez81] and *Gaussian mixture models* (GMM) [SS12]. The cluster membership value ($[0, 1]$) corresponding to the *conscious*-cluster is then used as the estimated level of consciousness and is determined by combining the results of these two soft-clustering methods. The closer to 1 the value is, the higher the probability that the patient is conscious.

The proposed approach is initially applied to a DoC data-set containing EEG recordings of VS and MCS patients. Different scoring associated with the DoC patients' eyes states (*open* or *closed*) are available and are thus used to evaluate the approach. In the end, the approach is applied to ECoG and EEG data recorded from CLIS patients to assess their consciousness levels. The details of the computation of each measure and the parameters used to do so are reported in Chapter 5.

4.3 Thesis contributions and significance of the study

In this thesis, a new set of features is used to analyse EEG/ECoG signals recorded from CLIS patients in order to assess their levels of consciousness. The usage of different features allows

the extraction of distinctive meaningful information from the data. This in turn can reduce misdiagnosis rate and possibly allows an early diagnosis in that a consciousness signature detected by one method could be missed or ignored by another. In other words, each measure capture a different phenomena. Consequently, combining several measures maximise the chances of getting the correct state of the patient. This can subsequently be used as a supplementary diagnosis tool for the physicians. By using cluster analysis to associate all those features, an index that estimates the patient's consciousness is derived and will be used to identify the optimal time to communicate with the patient. Such information would reduce the time wasted on unsuccessful communication attempts and would be beneficial for all parties.

5 Data analysis

The previous chapters defined the problem at hand, discussed the state-of-the-art of studies in consciousness detection and communication with LIS patients and introduced the proposed approach to solve the problem. This chapter starts with introducing the different datasets that will be used, and proceeds by describing in more details the different methods employed to obtain the features that will serve as input to the clusters analysis systems. This is followed by the description of how the patients' levels of consciousness is deduced from the clustering results.

5.1 Data description

5.1.1 Disorders of consciousness data

The dataset is composed of polysomnograms[21] (PSG) obtained from the Laboratory for Sleep, Cognition and Consciousness, and Centre for Cognitive Neuroscience (CCNS) of the University of Salzburg in Austria. In addition to EEG, other physiological signals were also recorded along with scores representing the patients' eyes states: *eyes open* (O) or *eyes closed* (C). When the eyes repeatedly switched between opening and closure, the state was scored "O/C". Furthermore, the data was divided into night (period of darkness) and day (period of lightsomeness) [Wis+17].

The original dataset contains data from 11 MCS and 12 UWS patients [Wie+18]. However, six patients were excluded from the analysis performed in this thesis since the time stamps for their eyes scoring were unavailable. The demographic information of the remaining patients are presented in Table 5.1 and more information about the complete dataset can be found in [Wis+17]. For 58.82% of the patients, the condition was caused by TBI. For the rest of them, it was caused either by a cerebrovascular accident (CVA) or by anoxia[22] (17.67% each). A unique patient's state was induced by subactute sclerosing panencephalitis[23] (SSPE). The period since injury varies between 1 and 120 months, and the CRS-R between 3 and 14.

[21] Polysomnography: technique to assess sleep and its disorders by recording several physiologic attributes such as EEG, EMG, EOG and EKG.

[22] Condition characterised by an absence of oxygen supply to an organ or a tissue

[23] SSPE: progressive neurological disorder of children and young adults that affects the central nervous system (CNS). It is a slow, but persistent, viral infection caused by defective measles virus. Source: `https://www.ninds.nih.gov/Disorders/All-Disorders/Subacute-Sclerosing-Panencephalitis-Information-Page`

Table 5.1: Demographic information of patients with disorders of consciousness.

Patient	Age	Gender	Clinical Assessment	Aetiology	Period since injury (months)	CRS-R total
L1	21	M	UWS	TBI[a]	7	6
L3	16	F	UWS	TBI	1	7
L13	74	F	UWS	TBI	1	3
S12	52	M	UWS	TBI	13	4
S13	58	F	UWS	CVA[b]	28	4
S14	61	M	UWS	anoxia[c]	32	4
S16	50	F	UWS	CVA	45	4
S17	19	M	MCS/VS	SSPE[d]	24	3
L4	48	M	MCS	TBI	8	11
L7	66	M	MCS	CVA	3	10
L8	62	M	MCS	TBI	2	8
L9	61	M	MCS	anoxia	2	10
L16	43	F	MCS	TBI	6	21
S2	45	M	MCS	TBI	12	8
S5	21	M	MCS	anoxia	28	13
S6	50	F	MCS	TBI	113	14
S7	30	M	MCS	TBI	120	13

[a] TBI: Traumatic Brain Injury
[b] CVA: Cerebrovascular Accident
[c] anoxia: Condition characterised by an absence of oxygen supply to an organ or a tissue
[d] SSPE: Subacute Sclerosing Panencephalitis

The number of recording channels depends on where the patient was located: Salzburg (Austria) or Liege (Belgium). Patients from Salzburg were identified with an 'S' and those from Liege, with an 'L'. The EEG data was recorded from 18 channels (resp. 12 channels) placed according to the 10-20 system [Jas58] for the Austrian (resp. Belgian) group. Only the common channels illustrated in Fig. 5.1 are used for further analysis.

5.1.2 CLIS data

Although a locked-in state could result from a coma following a brain injury (cf. Fig. 2.3), all CLIS states in the dataset used in this work resulted from ALS. The data consists of ECoG and EEG recordings obtained from the Universtitätsklinikum of the University of Tübingen in Germany.

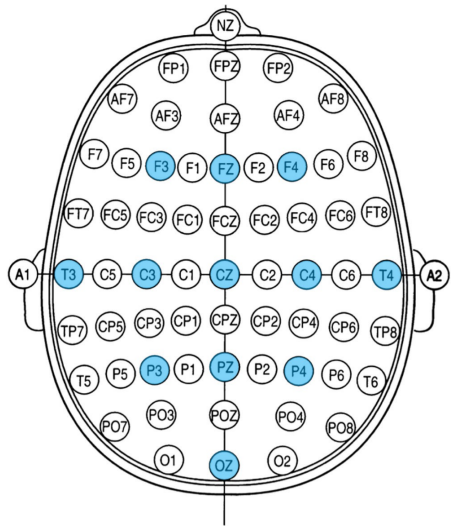

Figure 5.1: Illustration of the common recording channels for all DoC patients. The sampling rate is 500 Hz. Patients were based in Austria (Austrian group) and in Belgium (Belgian group) [Wie+18]. The 12 channels highlighted in the figure represent the common channels for both groups.

5.1.2.1 ECoG data

The 24-hour long data was obtained from a 40-year-old male in a totally locked-in state, which was first diagnosed with ALS in 1997 at age 29 and entered CLIS 11 years later [Mur+11; Soe+13]. The data was acquired with a BrainAmp amplifier from Brainproducts GmbH (Munich, Germany) at a sampling rate of 500 Hz. For this patient, an ECoG grid of 128 platinum electrodes from Ad-Tech Medical Instruments Corporation (Wisconsin, USA) was surgically placed and covered the left frontal, temporal and parietal lobes [Ben+14; Soe+13]. The specific locations of the recording channels, as well as the locations of the ground and reference electrodes, are shown in Fig. 5.2. Due to recurrent signal failures, the electrodes in the middle were not used, leaving a total of 64 usable channels [Ben+14]. These channels are shown in green in Fig. 5.2. This data recorded from 16/03/2008 00:34 to 17/03/2008 00:34 consists of the last successful communication session with this patient denoted as GR [Mur+11].

An experiment during which the patient was performing an auditory paradigm task was performed from 14:50 to 17:00. He was asked questions requiring *yes* or *no* answers. The questions are of general knowledge, or are personal questions which answers are known by the family members and/or the caregiver. The question can be for example: "*Is Paris the capital of Germany?*" or "*Are you German?*". The questions are also paired, meaning that for each question with a positive answer, there is a matching question that answers negatively. The equivalent paired questions for the previous examples would be: "*Is Berlin the capital of Germany?*" or "*Are you Dutch?*". At first, during training sessions, these paired questions with known answers are used to train a classifier. Motor imagery, specifically μ rhythms were used to distinguish between both answers. To answer *yes*, the patient has to imagine movement of his right hand, and to answer *no*, he has to imagine movement of his foot. Afterwards, the trained classifier is

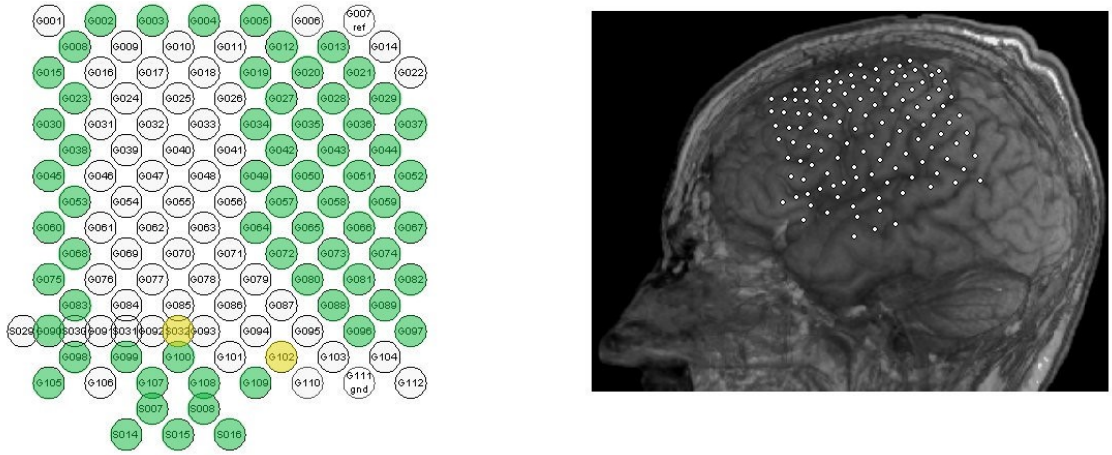

Figure 5.2: Implanted ECoG electrodes in a CLIS patient, showing the 128 channels and emphasising the 64 recording channels (in green). S032: ground, and G102: reference (in yellow). Image courtesy of the Universitätsklinikum, University of Tübingen in Germany.

used in a feedback session during which the patient is also asked paired questions with known answer, but after each question, the patient is given an assessment of his answer. An example of such feedback is illustrated in Fig. 5.4. When the classifier's accuracy is satisfying (above 70% [K+09]), it is subsequently used to classify answers to open questions. Open questions covered topics such as the patient's mood and feelings, and also his physiological status, for example: "*You feel good today?*"/"*You feel bad today?*". The questions asked during the experiment, as well as the experimenter's notes and comments are reported in Table C.2 in Appendix C.

The data from this patient is exceptional in the sense that first, the patient has been trained to use BCI since the time he was diagnosed with ALS. And secondly, to the best of our knowledge, this is the only dataset in which the experimenter confirmed that during a specific time frame, the patient was undoubtedly conscious: he was able to correctly answer all the questions that were asked to him. This was also the first successful communication out of 170 attempts for this patient.

5.1.2.2 EEG data

The EEG data were recorded from 2015 to 2019 from nine CLIS patients (mean age ($\pm$SD) = 48.1 ($\pm$21.26) years) during rest and while accomplishing the same auditory paradigm described in the previous subsection. The states of the patients reported here are as of 2019 and more information about them can be found in Table 5.2. A detailed description of each patient is also provided in Appendix D. All of them are ALS patients and no brain disease unrelated to that were discovered. In addition, all of them present almost normal sleep patterns [Mal+19]. All patients' information as well as the dates of recordings and the recording channels are summarised in Table 5.2. More information can also be found in [Mar+21; Mal+19]. It is important to note that this dataset was involved in a controversy after the legitimacy of the

results obtained by Chaudhary et al., in their now retracted publication [Cha+17] asserting a successful communication with several CLIS patients using fNRIS and EEG, were questioned in [Spu19]. The researchers were accused of scientific misconduct related to the manipulation of the data [Rij19; Fin19], which in turn were denied by the accused [Cha+18]. The validity of the raw data itself and the circumstances of its recordings were never questioned and this study make use only of the raw data of the patients.

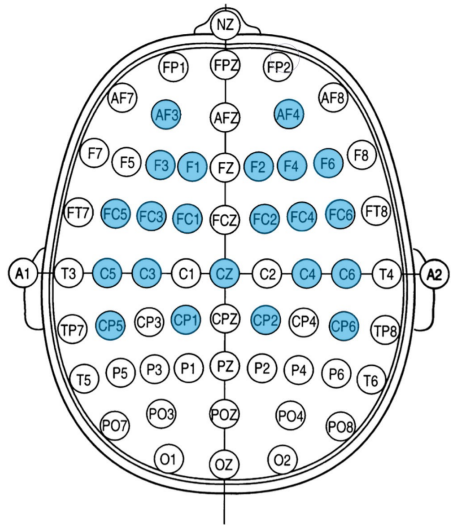

Figure 5.3: Overall list of electrodes from which the EEG signals were recorded for the CLIS patients. Electrodes were placed over the frontal lobe, the motor and sensorimotor cortices, and over the central sulcus.

The experimental setup is similar to the one reported in the previous subsection. Particularly, a binary communication is attempted using an EEG-based BCI. Fig. 5.4 illustrates the structure of the BCI system developed to communicate with the CLIS patients. They were asked a series of questions with known answers, a classifier was trained, and used afterwards to classify their answers during a feedback session. In this case, the classification results are provided to the patients.

The sampling rates and electrodes sites were different for each patient and/or session. Overall, the sampling rates used were 200, 250 and 500 Hz and the number of EEG channels varies from 4 to 8, except for patient P6 (22 channels). This inconsistency across patients, even across sessions for the same patient, is due to the difficulty to record data from CLIS patients and other external factors. Fig. 5.3 shows the overall channels positions for all patients. Each session lasted about 10 minutes, during which the patient was asked 10 pairs of questions. This means that 10 of them requires a positive answer and 10, a negative one.

Table 5.2: CLIS patients information.

Patient	Age	Gender	ALS[d]	Recording dates	Fs[a]	Labels
P1	75[b]	F	10	18/05/15	200	FC5, FC1, FC6, CP5, CP1, CP6
				20/05/15		FC5, FC1, FC6, CP5
				24/01/17		FCC5, FCC3, FCC4, FCC6, Cz
				11/04/19	500	FFC3h, FCC3H, CCP3H, Cz, FFC4h, FCC4h, CCp4h
P2	65[c]	M	4	22-26/06/15	200	FC5, FC1, FC6, CP5, CP1, CP6, AF3, AF4
P3	80	F	7	13-16/07/17	500	FC4, FC5, FC3, FC6, Cz
P4	29	F	4	18-22/01/16	200	FC5, FC1, FC2, FC6, CP5, CP1, CP2, CP6
				27-28/03/19	500	FFC3h, FCC3H, CCP3H, Cz, FFC4h, FCC4h, CCp4h
				08(-11)/07/19		AF3, F3, Cz, F4, AF4
P5	58	M	7	27-31/07/15	200	FC5, FC1, FC2, FC6, CP5, CP1, CP2, CP6
				27-28/01/16		
P6	37[c]	M	8	29/05-01/06/17	500	FC5, FC6, C5, C6, Cz, T9, T10
				02-03/06/17		FC5, FC6, C5, C6, Cz
				15-17/04/18		Cz, C1, C2
				21-25/05/18		
				26-29/05/18		C2, Cz, C1, Fz, P4, Pz, P3
				17-18/01/19		AF3, F3, F5, FC3, FC5, C5, C3, T7, CP5, CP3, CP1, C1, Fz, FCz, F4, Cz, FC4, C4, C2, CP2, CP4, CPz
				11-13/02/19		FP1, Fz, F3, F7, FT9, FC5, FC1, C3, T7, TP9, CP5, CP1, Pz, P3, P7, O1, Oz, O2, P4, P8, TP10, CP6, CP2, Cz, C4, T8, FT10, FC6, FC2, F4, F8, Fp2
P7	56[b]	F	7	14-17/11/16	250	FC3, FC4, FC5, FC6, Cz
				18,20-21/04/17	500	T9, T10, FC5, FC6, C5, C4, Cz
P9	33	F	6	12/06/17	500	F3, F4, C3, C4, Cz
				13/03/19		Cz, C3, C4, Fz, F3, F4, AF3, AF4
				14/03/19		FFC3h, FCC3H, CCP3H, Cz, FFC4h, FCC4h, CCp4h
P10	25	M	5	29-30/06/17	500	C5, C6, FC5, FC6
				09-10/07/18		Cz, C1, C2

[a] Sampling frequency in Hz.
[b] Deceased in 2019.
[c] Deceased in 2018.
[d] Years since ALS.

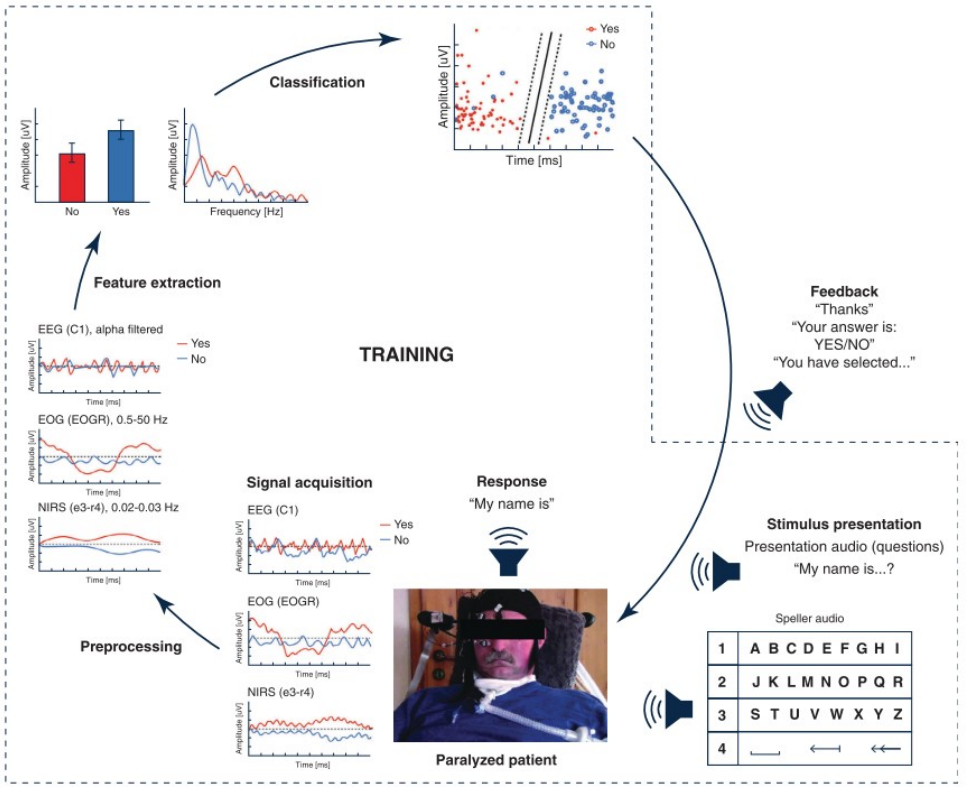

Figure 5.4: Experimental setup of the BCI-based communication with the CLIS patients. The EEG, EOG, as well as NIRS signals were acquired and pre-processed before extracting the features to classify the *yes* and *no* answers. The questions were provided in an audible manner. From [CMKB21] (CC BY 4.0).

5.2 Methods description

The following sections describe in more details the approach illustrated in Fig. 4.1. All analysis except stated otherwise were performed using MATLAB R2018b (Massachusetts, Texas, USA), the `Fieldtrip` toolbox [Oos+01] and custom written codes. Prior to any other processing and analysis, the data was re-referenced to the mean and band pass filtered at frequencies 0.5 to 45 Hz using a third order Butterworth filter using the MATLAB commands `butter` and `filtfilt` [Coh14]. The signal was subsequently partitioned into segments of 3-seconds length sliding 1-second at a time. Given the states of the patients, no artefacts removal were performed on the data.

5.2.1 Spectral analysis

A transformation of the signal from time into frequency domain can be done using Fourier transformation [Dro06]. This does not change the signal, only its representation. For a time series $x(t)$, the frequency representation is obtained by:

$$X(f) = \frac{1}{T} \sum_{t=1}^{T} x(t) e^{i2\pi f(t-1)/T} \tag{5.1}$$

where f is the set of discrete frequencies $[-\frac{T}{2}, \frac{T}{2}]$ and T is the window length [BZ11]. The Fast Fourier algorithm is usually used to analyse a signal in the frequency domain. It outputs complex values and to interpret them, it is common to employ the **power spectrum** of the signal [Nie05]. Spectral analysis is commonly used to evaluate the different frequency bands (δ, θ, α, and β) of the EEG signal [Dro06]. High-frequency contents of a signal are often interpreted as a measure of rapid variation in the signal [NS05].

5.2.1.1 Relative power

For a signal $x(t)$, the relative power of the δ (0.5-4 Hz), θ (4-8 Hz), α (8-12 Hz) and β (12-30 Hz) were calculated using Eq. 5.2 [BCP16; Wan+15].

$$RP = \frac{\sum_{f=f_1}^{f_2} S_x(f)}{\sum_{f=f_l}^{f_h} S_x(f)} \tag{5.2}$$

where: f_1 and f_2 specify respectively the lower and upper limits of the frequency band of interest. $f_l = 0$ Hz and $f_h = 45$ Hz (upper limit of the cut-off frequency during filtering) in this particular case, and $S_x(f)$ is the power spectral density of the signal $x(t)$ at the frequency f [SM05]. A commonly used method to estimate $S_x(f)$ is based on the Fourier transform of the signal $x(t)$ [BZ11]:

$$S_x(f) = \lim_{N \to \infty} X(f) X^*(f) \tag{5.3}$$

where $X(f)$ is the Fourier transform of the signal $x(t)$ obtained from Eq. 5.1. Practically, the PSD was estimated using the MATLAB function `pwelch` with a Hamming window of 1/8 size of the data segment and a 50% overlap, using the Welch method [Wel67].

5.2.1.2 Spectral edge frequency

Spectral Edge Frequency (SEF) is a commonly used feature for sleep analysis and classification. It consists of computing the r-th percentile of the total power that was obtained from the power spectral density [Nak+17]. In other words, it is the frequency below which a certain fraction of the signal power is contained. It is expressed as SEF_r where r represents the fraction of the signal power for which the edge frequency is calculated [IRV14; AMK09].

The most common r values for the SEF are 50% and 95%. SEF50 corresponds to the median frequency of the signal [IRV14; AMK09]. SEF95 is computed using Eq. 5.4, where f is the frequency, Fs represents the sampling frequency and $r = 0.95$. The obtained value was further normalised by dividing it to the upper limit of the critical frequency during filtering, which equals 45 Hz.

$$\sum_{f=0}^{SEF_r} S_x(f) = r \sum_{f=0}^{Fs/2} S_x(f) \tag{5.4}$$

5.2.2 Complexity analysis

Complexity measures quantitatively assess how sophisticated the structure of a biological system is. Signals with a certain regularity do not have a too large complexity and in contrast, irregular signals have higher complexity. An activated brain produces largely complex signals [NS05].

5.2.2.1 Poincaré plots

A Poincaré plot is a non-linear analytic method to analyse the variability of time series signals. It describes the behaviour of the signal in the phase space. For a given signal X of length N, it is constructed by plotting the signal so that the x-axis represents the EEG voltage at a specific time x_k and the y-axis represents the EEG voltage $x_{k+\tau}$ after a constant time delay τ. Specifically, the Poincaré plot is the scatter plot representing the set S of points in Eq. 5.6 [Hen+15]. This time delay τ should be carefully chosen since too small time delays may produce near-linear reconstructions with high correlations between consecutive phase space points, and too large delays might neglect any deterministic structure of the series [SC13]. An optimum value of τ is 1/5 to 1/4 of the dominant cycle period [HMS14]. For example, a time delay value of one sample is equivalent to 4 ms at a sampling rate of 256 Hz.

$$X = x_1, x_2, ..., x_N \tag{5.5}$$

$$S = (x_1, x_{1+\tau}), (x_2, x_{2+\tau}), ... (x_{N-\tau}, x_N) \tag{5.6}$$

Fig.5.5 illustrates one such plot with the descriptors SD1 and SD2 that can be used to geometrically quantify it. On one hand, SD2 represents the standard deviation (SD) of the points along the line of identity. It represents the variability over the entire recording period, namely the long term variability. On the other hand, SD1 is perpendicular to the line of identity and represents the variability from one point in the time series to the next, namely the short term variability of the signal. Both SD are computed using Eq. 5.7 and 5.8 [Gol13; HMS14].

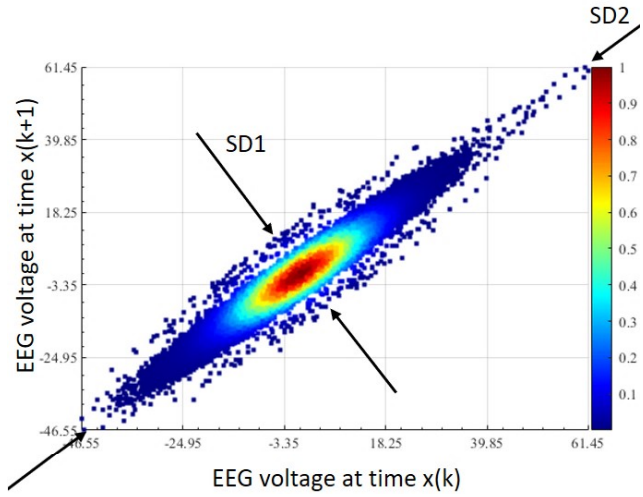

Figure 5.5: Poincaré plot showing the descriptors SD1 and SD2 with $\tau = 1$. Statistically, SD2 and SD1 represent the standard deviation of the points from the long axis (line of identity) and the short axis (perpendicular to the line of identity) respectively. A round oval pattern of the plot represents a random signal, while an elongated shape represents signals with linear features.

$$SD1 = \frac{\sqrt{2}}{2} SD(x_n - x_{n+\tau}) \tag{5.7}$$

$$SD2 = \sqrt{2SD(x_n)^2 - \frac{1}{2}(x_n - x_{n+\tau})^2} \tag{5.8}$$

The SD1/SD2 ratio also known as Ellipsoid Radius Ratio (ERR) [Eag+18] can also be used to evaluate signal randomness. A round oval pattern corresponds to a random signal, while a more elongated shape represents signal with linear features [HMS14]. The values of SD1 and SD2 for all datasets were computed using the extended Poincaré plot algorithm developed in [Sat+19].

5.2.2.2 Lempel-Ziv complexity

This complexity measure developed by Abraham Lempel and Jacob Ziv [LZ76] evaluates repetitiveness in binary sequences. Before computing the LZC, the data should be transformed into a binary sequence (see Fig. 5.6). An analytic signal is related to a real signal $x(t)$ by:

$$x_a(t) = x(t) + ix_h(t) \tag{5.9}$$

where $x_h(t)$ is the Hilbert transform of $x(t)$ [BZ11].

$$a_i(t) = |x_h(t)| \tag{5.10}$$

$$b_i(t) = \begin{cases} 0, & \text{if } a_i(t) \leq mean(a_i) \\ 1, & \text{otherwise} \end{cases} \tag{5.11}$$

A binary vector b_i : ...01010010001... is then obtained. For a given binary sequence $S = s_1 s_2 ... s_n$ of length n, LZC counts the number of distinct patterns in the data. Let $c(n)$ be the complexity counter, which value increased by one unit every time a new sequence of characters is encountered. In addition, let P and Q be two sub-sequences of S. At the beginning, $P = S(1)$ and $c(n) = 1$. Q is then set to extract all sub-strings starting from position 1 ($Q = S(2)$) until the further possible to the right. Q can be thought as a delimiter. Every encountered new word is added to a dictionary if it did not occur before ($c(n) = c(n) + 1$). During the next step, $P = S(2)$ and the same process as before is repeated. LZC is the number of different sub-strings encountered as the binary sequence is streamed from the left to the right. The greater the degree of randomness, the greater the number of different sub-sequences that will be present, thus the higher the Lempel-Ziv complexity [Sch+15; Abo+06].

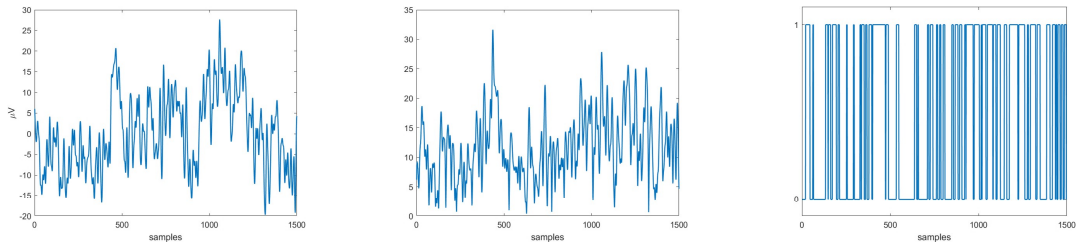

(a) Raw EEG signal $x(t)$ **(b)** abs(hilbert($x(t)$)) **(c)** Obtained binary signal

Figure 5.6: Signal binarisation for the computation of the Lempel-Ziv complexity. **(a)** Raw EEG signal. **(b)** Hilbert transformation of the signal. The binary values in **(c)** are obtained by using the mean of the absolute value of the transformation as a threshold, and assigning 1 to values higher than the threshold, and 0 to lower values.

In practice, $x_h(t)$ is extracted from the analytic signal using the MATLAB function `hilbert`. The binary sequence is obtained by taking the mean of the absolute value of the Hilbert transform of the signal as a threshold, as expressed in Eq. 5.11 [Sch+15]. LZC is then computed on each binarised EEG data segment using the MATLAB toolbox `calc_lz_complexity` [TR15; BR15].

5.2.3 Connectivity analysis

Brain connectivity assesses the interaction between two brain regions or between signals recorded from two channels. The different brain regions communicate with one another during mental tasks. Investigating this may shade some lights on the underlying brain processes. Generally, high connectivity values indicate high cooperation and more information sharing

between the two underlying brain regions or channels. The temporal coherence between the activities of different brain areas is known as *functional connectivity* [SC13]. It represents the statistical relationship between measures from both regions. Two connectivity measures were utilised in this thesis: the iCOH and the wSMI.

5.2.3.1 Coherency

Coherency is a linear method that was designed to identify the relative timing of brain activity between two regions as well as their phase consistency [KSD09; Sak+16; Nol+04; BZ11]. It is based on the Fourier analysis of the time series signal. The signal is transformed from the time domain to the frequency domain, allowing the separation of the amplitude from the phase information. The latter allows the computation of the phase delay, which can be used to determine the temporal offset between the time series. An increased functional interaction between the underlying neuronal networks leads to a higher value of coherency [Silo5]. At frequency f, the coherency C_{xy} of two signals x and y is defined as the ratio:

$$C_{xy}(f) = \frac{S_{xy}(f)}{\sqrt{S_{xx}(f) \cdot S_{yy}(f)}} \tag{5.12}$$

where $S_{xy}(f)$ is the cross power spectral density of the signals obtained using Eq. 5.13 [BZ11], and $S_{xx}(f)$ and $S_{yy}(f)$ are the auto power spectral density of x and y respectively [Pri81].

$$S_{xy}(f) = \lim_{T \to \infty} \frac{1}{T} X(f,T) Y^*(f,T) \tag{5.13}$$

where $Y^*(f)$ is the complex conjugate of $Y(f)$. $S_{xy}(f)$ is a complex value with a distinct magnitude and a distinct phase, which represents the relative phase i.e. the average phase difference between x and y [NSo6]. Consequently, the coherency C_{xy} is a complex quantity:

$$C_{xy}(f) = |C_{xy}(f)| e^{i\phi} \tag{5.14}$$

$$|C_{xy}(f)| = \sqrt{\Re(C_{xy}(f))^2 + \Im(C_{xy}(f))^2} \tag{5.15}$$

$$\phi = arg(C_{xy}) \tag{5.16}$$

$|C_{xy}(f)|^2$ is known as the *magnitude-squared coherence* or simply *coherence*. ϕ represents the phase angle between x and y. A possible determination of the direction of information flow can be inferred from the sign of the phase. Two independent EEG channels have a random phase difference, in which case, the coherency is zero [Sak+16]. A deterministic signal yields a coherence value of one, since the amplitude and phase are fixed on every signal observation [NSo6].

The electrical brain activity generated by one source spreads across the cortex. Hence, it can be measured in many channels. This is called volume conduction. Volume conduction can cause false brain interaction to be detected. It is accepted that "an observed scalp potential have no time lag to the underlying source activity". Since the imaginary part of coherency is only sensitive to two processes that are time-lagged to each other, it is not affected by volume conduction. Consequently, using only the imaginary part of coherency $\Im(C_{xy}(f))$ solve this volume conduction problem [Nol+04]. In general, a positive value of the imaginary part of the coherence between x and y implies that they are interacting and that x precedes y. This suggests that information is flowing from x to y [Sak+16; Nol+04].

Since this study is concerned with the degree of relationship between two channels and not its direction, the absolute value $|\Im(C_{xy}(f))|$ of the imaginary coherence is employed. It is then calculated between all pairs of recording channels using custom written MATLAB scripts. Thus, for each data segment, a connectivity matrix representing the coupling between all pairs of channels is obtained.

5.2.3.2 Weighted Symbolic Mutual Information (wSMI)

The wSMI is another method that evaluates the functional connectivity between signals from two channels or brain regions. It can estimate both linear and non-linear relationships by evaluating the extent to which the two signals present non-random joint fluctuations that suggest sharing of information.

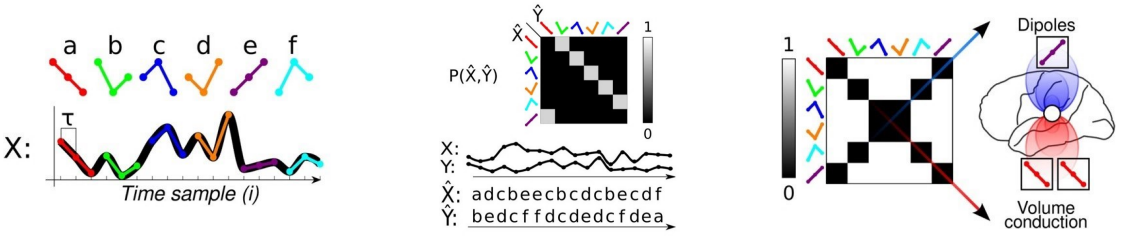

(a) Symbolic Transform **(b)** Non-linear coupling **(c)** Weights

Figure 5.7: weighted Symbolic Mutual Information. **(a)** The signal is transformed into a series of symbols. Symbol length k is equals to 3 in this case, which gives $3! = 6$ possible symbols. **(b)** Non-linear coupling identification by checking of increase or decrease in the signal. **(c)** The weights are assigned such that it is 0 for symbols that are identical or of the opposite sign. Otherwise, its value is set to 1. Adapted from [KSF13]. Copyright © 2013. Reproduced with permission from Elsevier.

First, the time series x and y are converted into sequences of discrete symbols $(\hat{x}, \hat{y})$ depending on amplitudes trends of a specific predefined number k of consecutive time points separated by a temporal separation of elements τ [LBMM15]. Using symbolisation of the data reduces the sensitivity to measurement noise and increases the efficiency of numerical computations [KSF13]. In general, the symbols are constituted of $k = 3$ elements, leading to a total of $3! = 6$ different potential symbols (a, b, c, d, e, f) [LBMM15] (cf. Fig. 5.7a). The value of τ is chosen in a way to sensitise wSMI to specific frequency ranges: wSMI is sensitive to higher frequency

bands when smaller values of τ are used [KSF13]. For instance, with $\tau = 4$ ms, the analysis captures patterns of relatively high frequency. Although, with that value, it is impossible to estimate wSMI when the sampling frequency is 250 Hz or 125 Hz. The value of τ is determined depending on the frequency of interest according to:

$$f_{max} = \frac{f_s}{k.\tau} \tag{5.17}$$

where f_{max} is the maximum resolved frequency and f_s is the sampling frequency [Imp+19; KSF13]. The wSMI value between two signals x and y is determined by computing the joint probability of each pair of symbols co-occurring in the two time series using Eq. 5.18.

$$wSMI(x,y) = \frac{1}{\log(k!)} \sum_{\hat{x}\in\hat{X}} \sum_{\hat{y}\in\hat{Y}} w(\hat{x},\hat{y}) p(\hat{x},\hat{y}) \log\left(\frac{p(\hat{x},\hat{y})}{p(\hat{x})p(\hat{y})}\right) \tag{5.18}$$

where $p(\hat{x},\hat{y})$ is the joint probability of co-occurrence of symbol $\hat{x}$ and symbol $\hat{y}$, $p(\hat{x})$ and $p(\hat{y})$ are the probabilities of those symbols in each respective signal.

The method checks symbolic patterns of increase or decrease in the signal in order to rapidly and robustly evaluates the signal entropy, which in turn estimates non-linear couplings (cf. Fig. 5.7b). Moreover, on one hand, wSMI neglects co-occurrences of identical or opposite-sign symbols, which could likely come from common-source artefacts, by setting the weights $w(\hat{x},\hat{y})$ in Eq. 5.18 to zero [KSF13]. This will eliminate volume conduction artefacts (cf. Fig. 5.7c). Furthermore, wSMI quickly decreased to zero as the distance between channels decreases given that the measure was designed to eliminate common source artefacts. On the other hand, it favours non-trivial pairs of symbols. As a result, wSMI is less susceptible to traditional EEG artefacts [KSF13].

This approach was introduced in [KSF13] as a potential consciousness signature by measuring the global information sharing across brain areas, under the hypothesis that "conscious content that we experience is defined by the global communication between distant cortical areas". Essentially used in disorders of consciousness research, it successfully distinguished between patients in UWS, MCS, and conscious healthy subjects. In the meanwhile, results from sleep research showed that significant levels of connectivity were observed in all electrodes during wakefulness and that the highest values were detected in the posterior brain areas. In addition, the connectivity values were reduced during N3-sleep [Imp+19]. In [Roh+17], wSMI was further used to correctly diagnose a trauma patient that was initially diagnosed with UWS, to be in a total locked-in state instead.

To reduce the computational cost during the analysis, the patients' data were down-sampled from 500 Hz to 200 Hz when necessary. Subsequently, wSMI was computed using custom written MATLAB scripts. Similarly to $iCOH_\theta$, a connectivity matrix is obtained for each data segment.

5.2.4 Consciousness level assessment

Based on the hypothesis presented in Section 4.2, the following features were extracted to evaluate the patient's level of consciousness: relative powers in the θ and β bands, $SEF95$, ERR, LZC, $iCOH_\theta$, and $wSMI$ in the θ band. The recordings were performed from different channels for the CLIS patients, but in general the channels were located in the central and frontal areas. Thereupon, the results obtained for each session were averaged over all channels or pairs of channels, leading to a feature vector of size $n - by - p$, where n represents the data samples and p is the dimension of the feature vector. The average for $iCOH_\theta$ and wSMI were obtained by computing the mean of the lower part of the respective connectivity matrices without the diagonal. So that each feature has equal weight during the clustering analysis, the feature vector was normalised so that the values in each dimension range from 0 to 1.

The feature vector is in turn analysed using two soft-clustering approaches, namely the *fuzzy c-mean clustering* (FCM) and *Gaussian Mixture Model* (GMM) already introduced in Section 2.3.1. Soft-clustering gives a membership degree to each cluster. In this case, the goal is to separate the features into two clusters corresponding to *conscious* and *unconscious* respectively. The consciousness level is determined as the value of the degree of membership of each data point to the cluster corresponding to a conscious state. The characteristics of this cluster are determined according to the hypothesis mentioned in Section 4.2.

On one hand, to implement the FCM clustering approach, the MATLAB function `fcm` was applied to the data with the specified parameters: $N = 2$ clusters, the fuzzifier parameter m was set to 2 as recommended by previous research [Pet+13], the maximum number of iterations was fixed at 1000 and the minimum improvement in objective function between two consecutive iterations ϵ at $1e^{-5}$. The algorithm then returns $N = 2$ clusters centres for each dimension of the feature vector. On the other hand, the MATLAB function `fitgmdist` was used to fit GMMs to the data using the EM algorithm presented in Section 2.3.2.2 and the same parameters as with the FCM clustering analysis. In addition, MATLAB `posterior` function of the Statistics and Machine Learning Toolbox was used to estimate the component-membership posterior probabilities [SS12].

From an algorithmic point of view, FCM uses Euclidean distance to evaluate the distance between the objects and the cluster centres, which is more susceptible to outliers, while GMM relies on Mahalanobis distance. Moreover, FCM assumes that the shape of the clusters are more or less spherical with approximately the same size. This corresponds to a Gaussian mixture distribution with a single covariance matrix that is shared across all components, and is a multiple of the identity matrix. Furthermore, GMM is more flexible by allowing unequal variance for the variables [Mat21].

Results obtained from both clustering methods are subsequently combined to get a consensus probability. Several methods exist to undertake such task. However, most of them are only applicable to hard clustering, and thus only produce binary results [Wan+13]. Soft-voting allows the use of different soft clustering results (also called *based clustering results*) obtained from different clustering methods or from the same method using different parameters. In

this situation, a consensus between the results obtained from FCM and GMM is desired. The final clustering result is determined by averaging the based clustering results (Eq. 5.19) or by computing their product (Eq. 5.20) [ANV20; SBL21]. Specifically, if the probability that the object i is a member of the cluster c in partition m_1 is $P(c, m_1)$, and the probability that the same object belongs to the cluster c in partition m_2 is $P(c, m_2)$, the probability that it is member of both partitions simultaneously is:

$$P_{avg}(c, m_1 m_2) = average\,(P(c, m_1), P(c, m_2)) \tag{5.19}$$

$$P_{prod}(c, m_1 m_2) = prod\,(P(c, m_1), P(c, m_2)) \tag{5.20}$$

The new degree of membership is then the value located at the same position in the matrix. For example, if $m_1 = \begin{bmatrix} 0.8 & 0.2 \\ 0.3 & 0.7 \\ 0.1 & 0.9 \end{bmatrix}$ and $m_2 = \begin{bmatrix} 0.7 & 0.3 \\ 0.1 & 0.9 \\ 0.2 & 0.8 \end{bmatrix}$ respectively, the new degree of membership for the first object would be $[0.8 * 0.7, 0.2 * 0.3] = [0.56, 0.06]$. The results need to be normalised afterwards so that the degree of membership sum up to 1 [Wan+13]. In this case, the final result would be $[0.56/(0.56 + 0.06), 0.06/(0.56 + 0.06)] = [0.903, 0.097]$.

5.2.5 Statistical analysis

All statistical tests are performed using MATLAB R2018b Statistics and Machine Learning Toolbox. A t-test (MATLAB: `ttest`) is performed on normally distributed data, which normality is assessed using `ztest`. In case the data comes from an unknown probability distribution, non-parametric tests such as Wilcoxon rank sum test (MATLAB: `ranksum`) or Friedman's test (MATLAB: `friedman`) are performed. On one hand, a Wilcoxon rank sum test checks if two independent samples come from identical continuous distributions with equal medians, against the alternative that they are not. On the other hand, a Friedman's test assesses if the column effects in a two-way layout are all the same, against the alternative that they are not [HWC14; BZ11; CF14].

5.3 Summary

This chapter introduced the different groups of patients as well as the details of the approach used to evaluate their levels of consciousness. First, the data from patients with disorders of consciousness were described followed by the data of the CLIS patients. This is then followed by the description of the different approaches used to extract the features from the EEG/ECoG signals. Selected features were afterwards analysed by the means of two clustering methods, which results were combined using an ensemble method and a consensus result is obtained.

The chapter ends with a comprehensive description of the clustering analysis as well as the parameters used to determine the clusters. The results of all analysis are presented in the following chapter.

6 Results and discussions

The goal of this thesis is to evaluate the levels of consciousness of CLIS patients using EEG. To do so, several measures based on the signal frequency power, complexity and connectivity were computed. Then the group of selected features were analysed using two cluster analysis algorithms, and an estimation of consciousness level is output. The patients and methods used to assess their levels of consciousness were introduced in Chapter 5. In this chapter, the corresponding results are presented and discussed. First, the results for the DoC patients are presented, followed by those of CLIS patient GR. After evaluating the performance of the presented approach on both datasets to show that it is working, it is finally applied to the EEG data of the remaining CLIS patients.

6.1 Patients with disorders of consciousness

The approach is initially applied and evaluated with data recorded from patients with disorders of consciousness, which results will be presented first. The hypothesis being that since their levels of consciousness are relatively lower than that of CLIS patients, and that CLIS patients brain signals are comparable to that of healthy subjects.

Results from UWS patient L1 and MCS patient S7 in particular will be showcased in the following subsection. As presented in Table 5.1, patient L1 is 21 years old and in a VS following a TBI, with a CRS-R score of 6. The injury occurred 7 months prior the data recording. This is the only patient which EEG features produced practically concurring results as will be shown in Section 6.1.1. In addition, patient L1 also possesses the most eyes scoring information (see Table B.1 in Appendix B). Patient S7, on the other hand, is a 30 years old MCS patient, which condition also results from a TBI and with a CRS-R score of 13. At the time of the recording, 120 months have passed since the injury. This is the longest time since injury across all patients in this group. Apart from that, patient S7 also exhibited the lowest centroid linkage distance[24] in the clustering results. The results for the rest of the DoC patients are presented in Appendix B.

[24]distance between two objects belonging to two different clusters, computed as the Euclidean distance.

6.1.1 Results of individual measures

6.1.1.1 Spectral features

The spectral features consisted of the relative powers of θ and β bands, as well as the SEF95. An increase of θ power can be observed during drowsiness, but also during mental task, especially when associated with an increase of β power [Nie05; BCP16; GIM18]. Consequently, conjoined increases of both frequency power suggest an increase of the consciousness level. On the other hand, a value of SEF95 above 13 Hz is considered as definitely conscious [Ram+80; Tou+19].

Patient L1 Fig. 6.1 illustrates the relative powers of the β and θ bands averaged across all channels for this patient. The shaded area between 21:26 and 07:10 represents the night time.

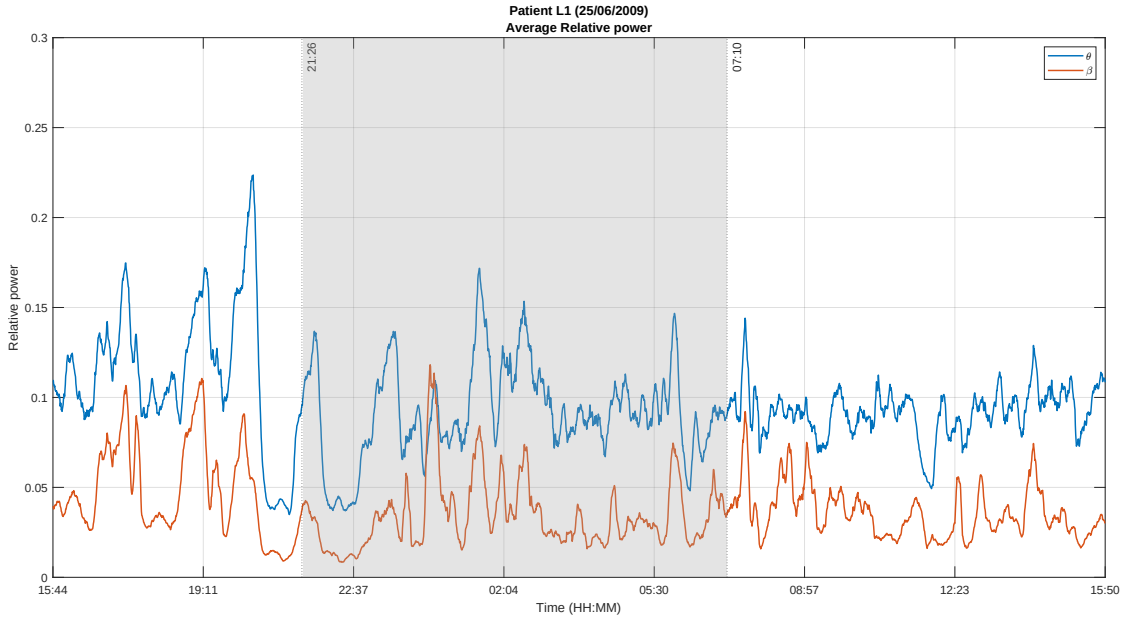

Figure 6.1: Average relative power for UWS patient L1. Only the frequency bands of interest are presented: θ in blue and β in red. A simultaneous increase of power on both frequencies indicates an increased consciousness level, and vice versa. The shaded area between 21:26 and 07:10 represents the night time.

Some variations are observed during the course of the recording. For instance, there is a particularly noticeable decrease of the powers of both θ and β between 20:15 and 21:11 (with an average value of 0.0797 and 0.0211 for θ and β respectively). This drop is more pronounced between 21:50 and 22:50 with an average value of 0.0470 and 0.0126 respectively. Besides, the average values of the relative powers in both frequency bands are slightly higher before night time, with 0.1128 and 0.0479 respectively, versus 0.092 and 0.035 after night time. These values suggest that on one hand, the patient's level of consciousness was higher before night time and decreased during the night throughout the following day. On the other hand, they also imply that it was markedly reduces particularly between 20:15 and 22:50.

Fig. 6.2 shows the average SEF95 for UWS patient L1. Similar to the relative powers, fluctuations are also observed throughout the recording. For example, SEF95 drops to less than 5 Hz between the same time frames as before: from 20:15 to 21:11 and from 21:50 to 22:50. This small value means that 95% of the total power was attained in the δ band, which is mostly the case during deep sleep states. SEF95 values are also essentially below the θ band. Since that band represents the frontier between consciousness and unconsciousness [SC13], this indicates that the patient was most likely unconscious during that time. Outside these time frames, the values are oscillating between 8 and 30 Hz, with a mean value of 18 Hz. This indicates that patient L1 was conscious most of the time but that his consciousness level was oscillating between low and high. In other words, he was most likely slipping in and out of consciousness.

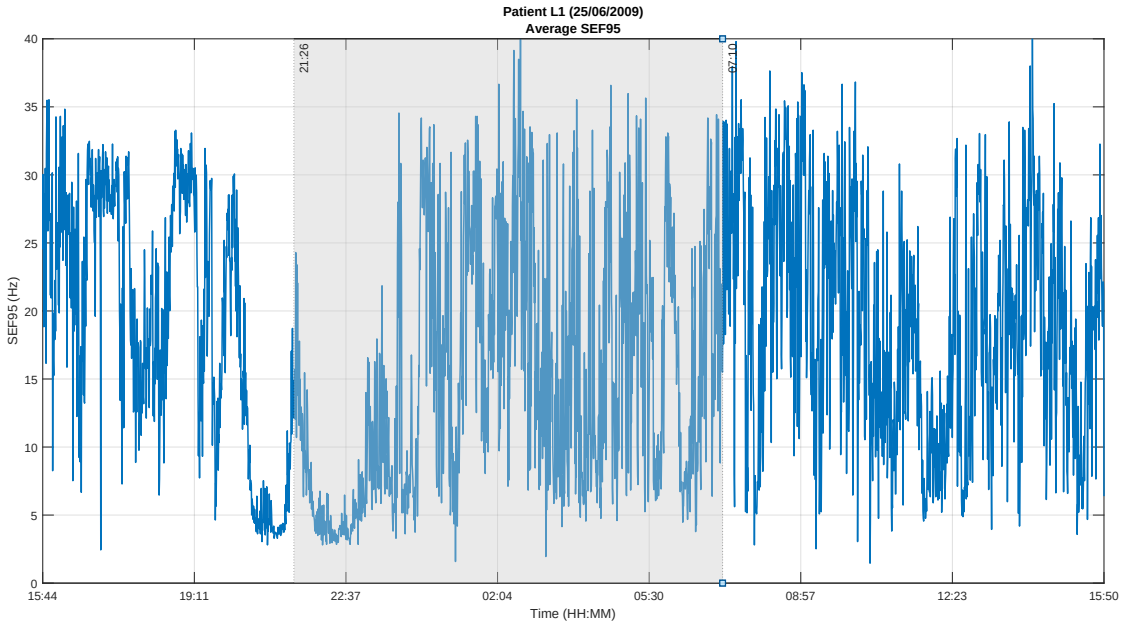

Figure 6.2: Average SEF95 for UWS patient L1. SEF95 represents the frequency below which 95% of the signal power is contained. Night time is represented by the shaded area between 21:26 and 07:10.

Generally speaking, the average values of the θ and β relative powers are higher during the day (0.0391 and 0.0977, respectively) compared to the night (0.0376 and 0.0942, respectively). A Wilcoxon rank sum test performed on the data revealed that the differences between night and day are significant at a 5% significance level for both frequency bands. Hence, the level of consciousness of the patient was significantly lower during the night. The corresponding p-values for all features can be found in Table B.18 of Appendix B. In the same manner as with the relative power, night and day values of the SEF95 also differ between night and day with a mean value of 12.42 Hz versus 19.31 Hz respectively. A Wilcoxon rank sum test indicates that these differences are also significant with a $p < 0.05$. These values imply, equally as with the relative power, that the patient was definitely conscious during daytime and that his consciousness level was lower at night.

Patient S7 The relative powers of θ and β bands for patient S7 are illustrated in Fig. 6.3. Night time started at 23:00 and ended at 05:00 (shaded area in the figure). Relative β power increases between 22:25 and 00:30 with a mean value of 0.2035 and is higher than θ ($mean = 0.1592$). The same trend is also observed right before 08:00, after 10:16, and around 17:23. This surge of β power indicates an increased brain activity, signifying an heightened consciousness level during those times. Contrarily, a simultaneous decrease of both relative powers is observed from 02:48 to 02:59 with a mean value of 0.1210 for θ and of 0.0719 for the β band. This is also the case from 03:59 until 04:15 with mean values of 0.1120 for θ and 0.0915 for β.

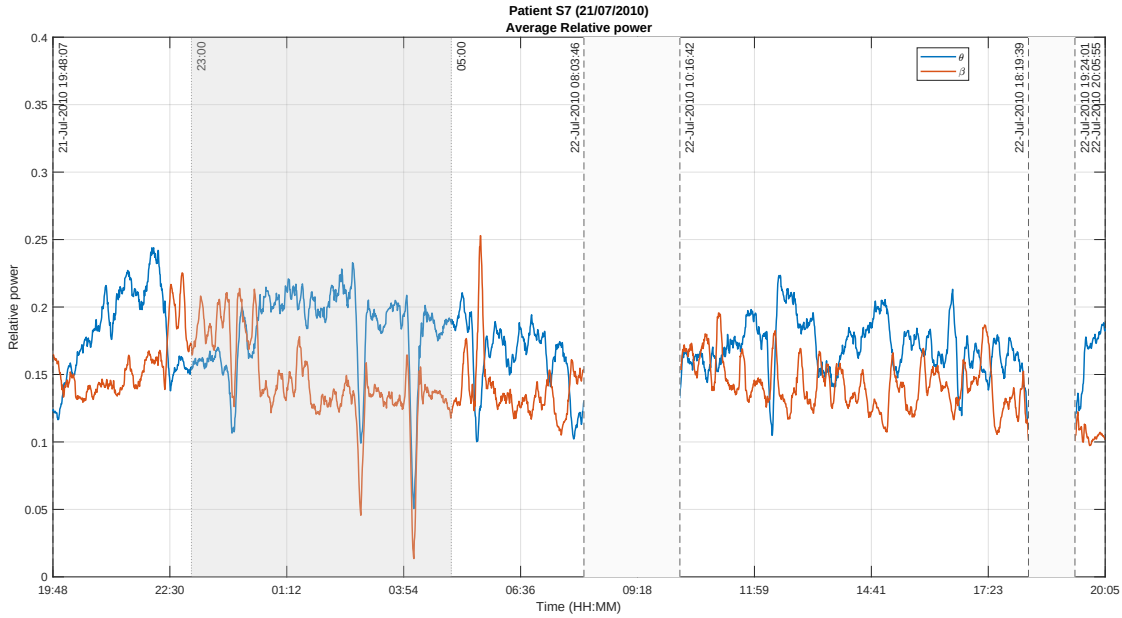

Figure 6.3: Average relative power for MCS patient S7. Only the frequencies of interest are presented: θ in blue and β in red. A simultaneous increase of power on both frequencies indicate an increased consciousness level, and vice versa. Night time is represented by the shaded area between 23:00 and 05:00. The blank areas represent times when no data were recorded.

Likewise, the overall SEF95 for patient S7 is above the β band as illustrated in Fig. 6.4. At the beginning of the recording, more precisely from 19:48 to 22:30, the value of the edge frequency is 25.15 Hz. This value further increases to an average of 30.04 Hz between 22:30 and 00:30. Thus, 95% of the EEG power was attained in the β bands. Consequently, the patient was certainly conscious during these moments. On the other hand, in some short time segments no longer than 10 minutes, the SEF95 lies in the α or θ bands. This occurs for instance between 02:52 and 02:58 with a mean value of 9.94 Hz, and between 04:03 and 04:11 with 5.92 Hz. These low values imply that the patient was surely unconscious during these time frames. These observations are analogous to the results obtained from the relative power. All of this suggests that, on one hand the patient was mostly conscious given that 95% of the signal power were only achievable above 20 Hz. On the other hand, he was definitely unconscious on short time frames, specifically between 02:52 and 02:58 as well as from 04:03 to 04:11.

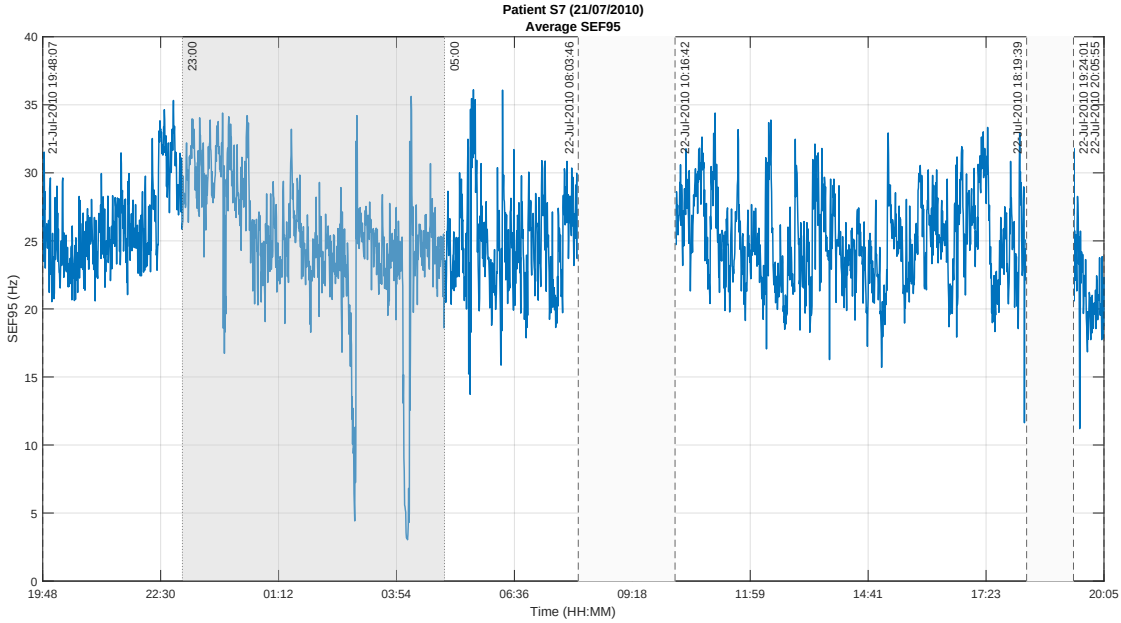

Figure 6.4: Average SEF95 for MCS patient S7. SEF95 represents the frequency below which 95% of the signal power is contained. Night time is represented by the shaded are between 23:00 and 05:00. The blank areas represent times when no data were recorded.

The relative powers of the θ and β frequency bands are generally higher during night-time as opposed to day time. The mean values are respectively 0.1833 vs 0.1715, and 0.1452 vs 0.1429. Statistical analysis performed on the relative powers to compare night/day differences using a Wilcoxon rank sum test determined that they were significant at the 5% level for the two frequency bands. This implies that the patient's consciousness level was higher during the night.

6.1.1.2 Complexity features

Geometry-based Poincaré plots and Lempel-Ziv complexity symbolic approach were used to assess the EEG signals complexity. Typically, highly complex signals are associated with an activated brain, hence a high level of consciousness [NS05; Sch+15; Abo+06]. Practically, a value of 0 corresponds to *unconsciousness*. The higher the complexity value is, the higher the level of consciousness. More specifically, a value of 1 or above indicates that the patient is definitely conscious for both methods.

Patient L1 Fig. 6.5 and Fig. 6.6 illustrate the obtained EEG complexity for patient L1 using the ERR of the Poincaré plots and the LZC respectively. On both figures, the shaded area represents night-time.

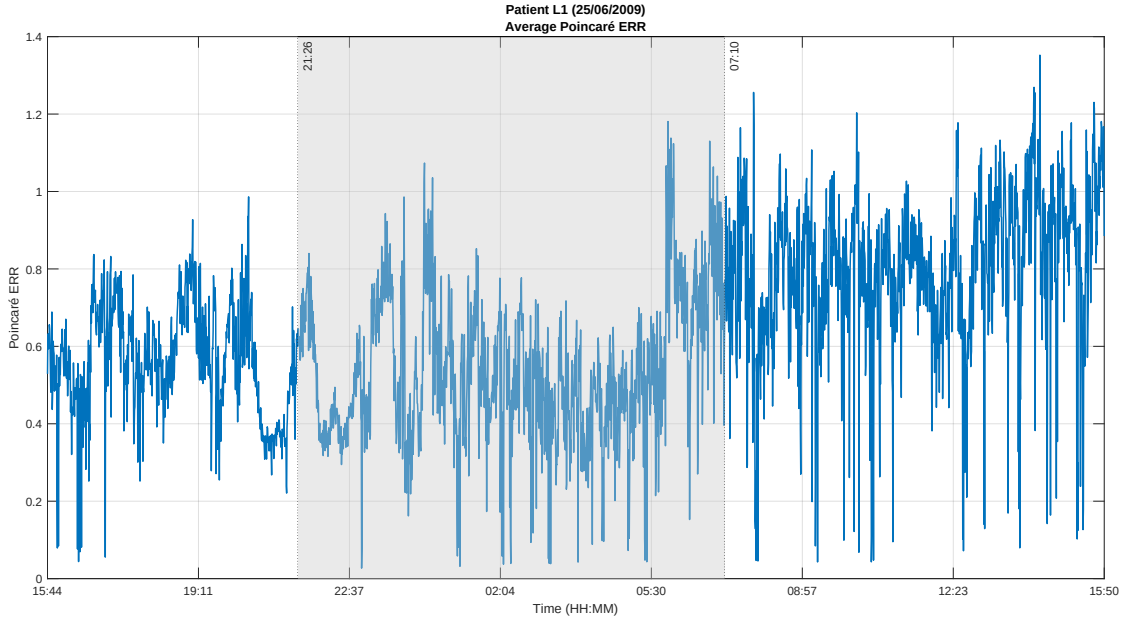

Figure 6.5: Average ERR of the Poincaré plots with $\tau = 2$ data points for UWS patient L1. A value of 0 means definitely unconscious. The larger the value, the higher the level of consciousness. Night time is represented by the shaded area between 21:26 and at 07:10.

On one hand, the values of the ERR are low, especially before 05:55, and increase afterwards with an average value of 0.7877. In addition, the persistent low values ($mean = 0.45$) between 20:20 and 21:21 as well as from 21:44 to 23:00 ($mean = 0.42$) suggest a reduced consciousness level, and fit the observations in Figs. 6.1 and 6.2 of the relative powers and the SEF95 respectively. The mean values of ERR before, during and after night time are respectively 0.5613, 0.5368 and 0.7936. The first two values are approximately equivalent but comparatively less than the mean value after night time. One may conclude then that the level of consciousness is much higher the second day of recording.

On the other hand, the highest values of the averaged Lempel-Ziv complexity were detected prior night time. Moreover, a decreasing trend is noted from the start to the end of the recording, except between 20:00 and 23:00 ($mean = 0.62$). These distinguishable drops in values are consistent with previously presented results. The mean values of LZC before, during and after night time (from 21:26 to 07:10) are respectively 1.024, 0.8699, and 0.8669. This latter is indeed low compared to the value before night time, but it is high enough to still indicate a moderate level of consciousness.

In both cases, the average EEG signal complexity of the patient during the day was higher (0.7014 for ERR and 0.9291 for LZC) than during the night (0.5368 for ERR and 0.8699 for LZC). Wilcoxon rank sum tests applied to the values of ERR and LZC during both times showed a significant difference at the 5% level for both complexity measures.

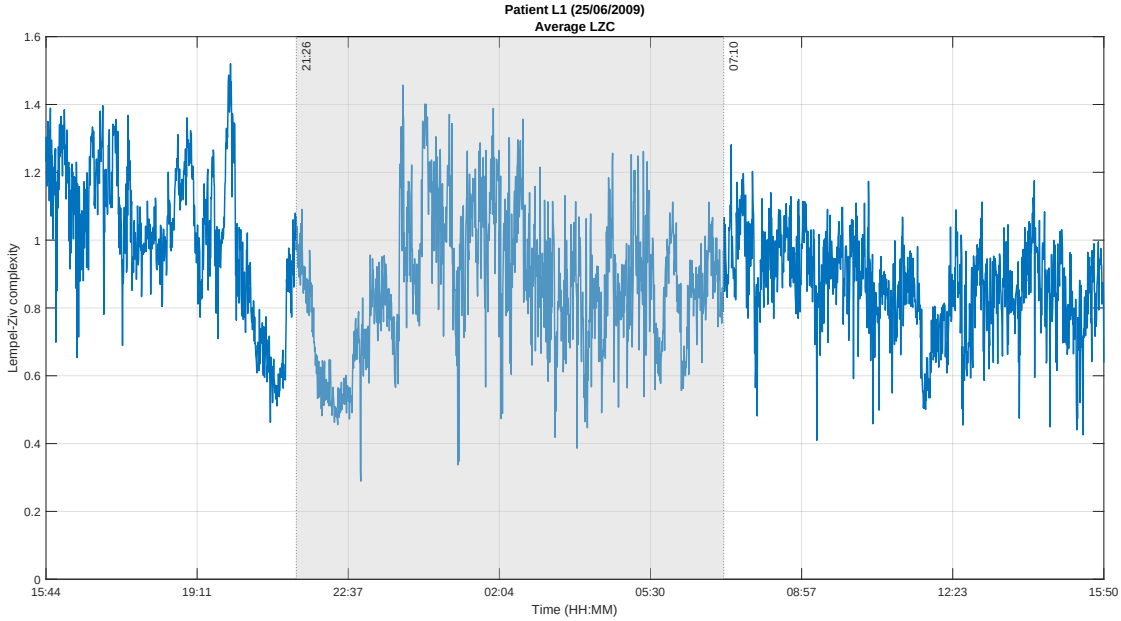

Figure 6.6: Average LZC for UWS patient L1. A value of 0 means definitely unconscious. The larger the value, the higher the level of consciousness. Night time is represented by the shaded area between 21:26 and 07:10.

Patient S7 The average ERR of the Poincaré plots for this patient is illustrated in Fig. 6.7. Three notable intervals featuring surge of the ERR values were observed, namely from 22:30 and 00:40 ($mean = 0.4752$), between 05:30 and 07:55 ($mean = 0.5638$), and from 15:08 to 16:50 ($mean = 0.6385$). Those values are considerably higher than the ERR value before 22:30, which amounts to 0.4390. From these values, it can be concluded that the patient was at least in a moderate level of consciousness during the night, but also between 10:16 and 15:08. Apart from this time frame and during the day, the values of the ERR suggest a higher consciousness level, meaning that the patient was plausibly conscious.

Fig. 6.8 illustrates the LZC during the course of the recording. The lowest values are observed at the beginning of the recording, from 19:48 to 22:30 with a mean value of 1.0183. An increasing trend is afterwards detected throughout the night until day time at around 06:12. The LZC slightly decreases starting at 10:16, but ultimately its value increases starting at 15:08. Finally, its value drops in the last part of the recording beginning at 19:24.

It was determined that in average, the values of ERR were lower during the night compared to daytime (0.6291 vs 0.6483) for patient S7. However, a Wilcoxon rank sum test indicated that these differences were not statistically significant with $p = 0.88793$. Contrarily, the values of LZC during day and night-time differ significantly, with an average value of 1.4438 and 1.264 respectively ($p < 0.05$).

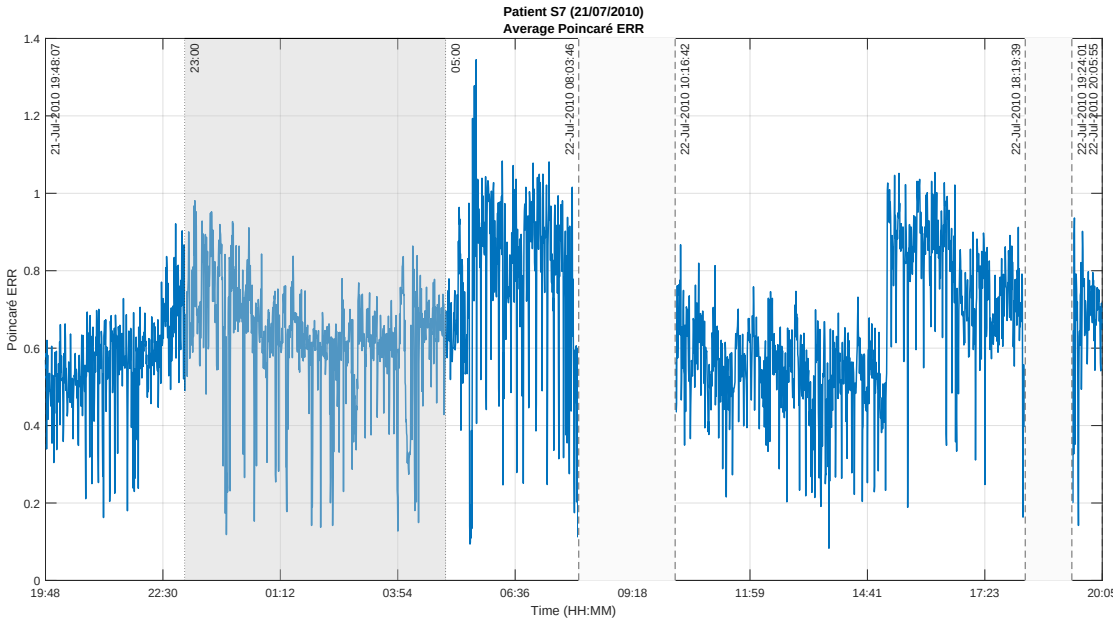

Figure 6.7: Average ERR of the Poincaré plots with $\tau = 2$ data points for MCS patient S7. A value of 0 means definitely unconscious. The larger the value, the higher the level of consciousness. The shaded are between 23:00 and 05:00 represents the night time. The blank areas represent times when no data were recorded.

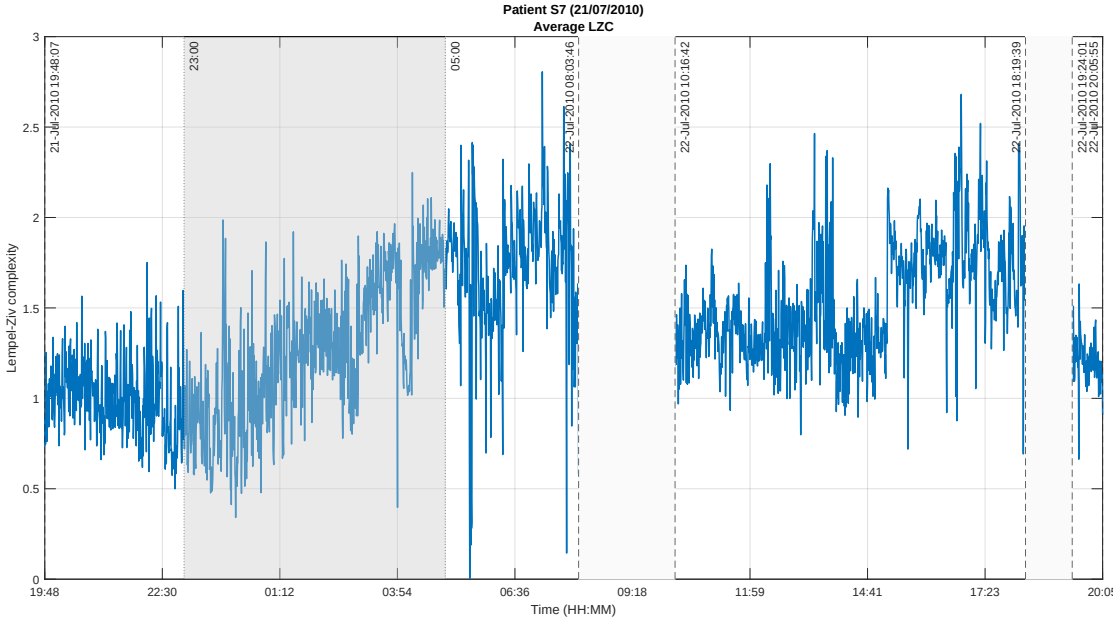

Figure 6.8: Average LZC for MCS patient S7. A value of 0 means definitely unconscious. The larger the value, the higher the level of consciousness. Night time is represented by the shaded areas between 23:00 and 05:00. The blank areas represent times when no data were recorded.

6.1.1.3 Connectivity measures

Connectivity measures determine the association between brain regions or channels [KSD09; Sak+16]. On one hand, linear connections between two entities can be determined using the iCOH. On the other hand, both linear and non-linear relationships can be identified with the wSMI measure. Both methods neglect the effects of the volume conduction in the brain, allowing the avoidance of false connectivity in the results [Nol+04]. The connectivity was computed between all pairs of channels and then averaged across all of them. Connectivity in the θ band was specifically computed with both methods given the role of this frequency band in working memory and mental task [Bor+13].

Patient L1 Looking into Fig. 6.9 that illustrates the variation of the averaged imaginary part of θ coherence for patient L1, no distinguishable variations like in the case of the previous features are observed. There is however a slight increase between 19:00 and the start of night time at 21:26 ($mean = 0.058$). The average wSMI with $\tau = 16$ ms for this patient is shown in Fig. 6.10. This temporal lag corresponds to the θ frequency band. An apparent decrease between 20:10 and 23:45 is observed, with a mean value of 0.0488. This indicates that patient L1 was probably unconscious during that time frame, comparable to the results obtained from the frequency-based features.

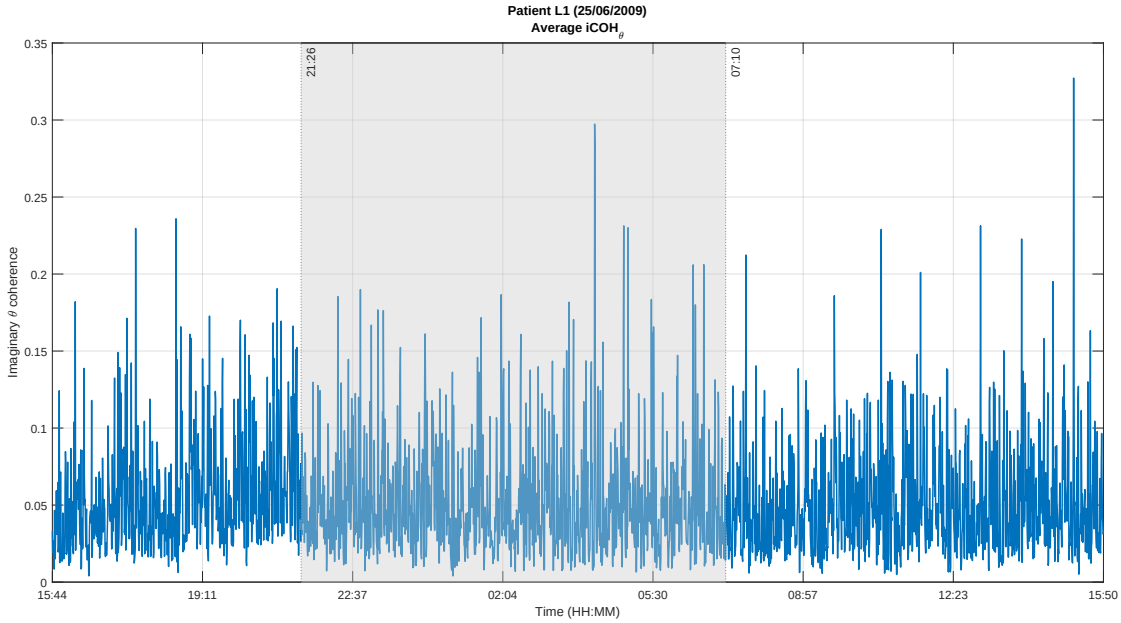

Figure 6.9: Average iCOH in the θ band for UWS patient L1. An increased iCOH value in the θ band implies a higher consciousness level, and vice versa. The shaded area between 21:26 and 07:10 represents the night time.

The two connectivity measures give conflicting results regarding the average value during the day compared to the night. On one hand, $iCOH_\theta$ values are larger during night-time with

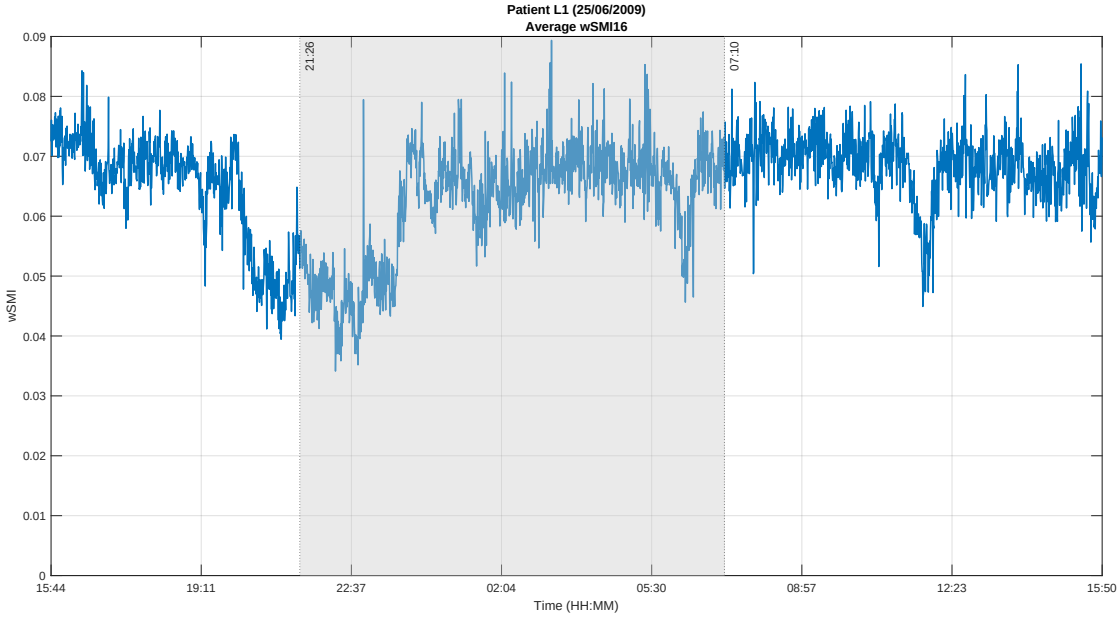

Figure 6.10: weighted Symbolic Mutual Information with $\tau = 16ms$ for patient L1 (UWS). An increased wSMI with this value of τ imply a higher consciousness level, and vice versa. The shaded are between 21:26 and 07:10 represents the night time.

a mean of 0.0577 as opposed to 0.0483 during daytime. In contrast, wSMI values are lower at night with a mean of 0.0557; its mean value during the day is 0.0682. Wilcoxon rank sum tests applied to each case determined that: first, the differences of $iCOH_\theta$ were not significant ($p = 0.5496$) and second, they were statistically significant in the case of wSMI at 5% significance level. A decrease in overall brain connectivity is considered a reduced consciousness level and vice versa.

Patient S7 Fig. 6.12 displays the wSMI averaged across all channels for MCS patient S7. Between the start of the recording and 22:20, the mean wSMI connectivity value attains 0.0395. It decreases to 0.0363 between 22:20 and 00:05, and also after 06:00 up until 08:03 droping to 0.0329. This indicates a decrease of the level of consciousness, relative to the time outside this time interval. On the other hand, the last part of the recording starting at 19:34 exhibits a larger connectivity than during 10:16-18:19, with a mean value of 0.0380, suggesting a higher consciousness level in the last part of the recording. These results are in contradiction to those found previously and illustrated in Figs. 6.3, 6.4, 6.7 and 6.8.

Night versus day connectivity values are different for this patient. No changes can be visually observed from Fig. 6.11, which shows the averaged $iCOH_\theta$ for said patient. Its mean value is 0.0614 during the night as opposed to 0.0621 during the day. An additional Wilcoxon rank sum test performed to assess the night versus day differences indicate that they were no significant variation ($p = 0.6064$) although the consciousness level of the patient was higher during the day. Mean wSMI values, on the other hand, are higher during the night with a mean value

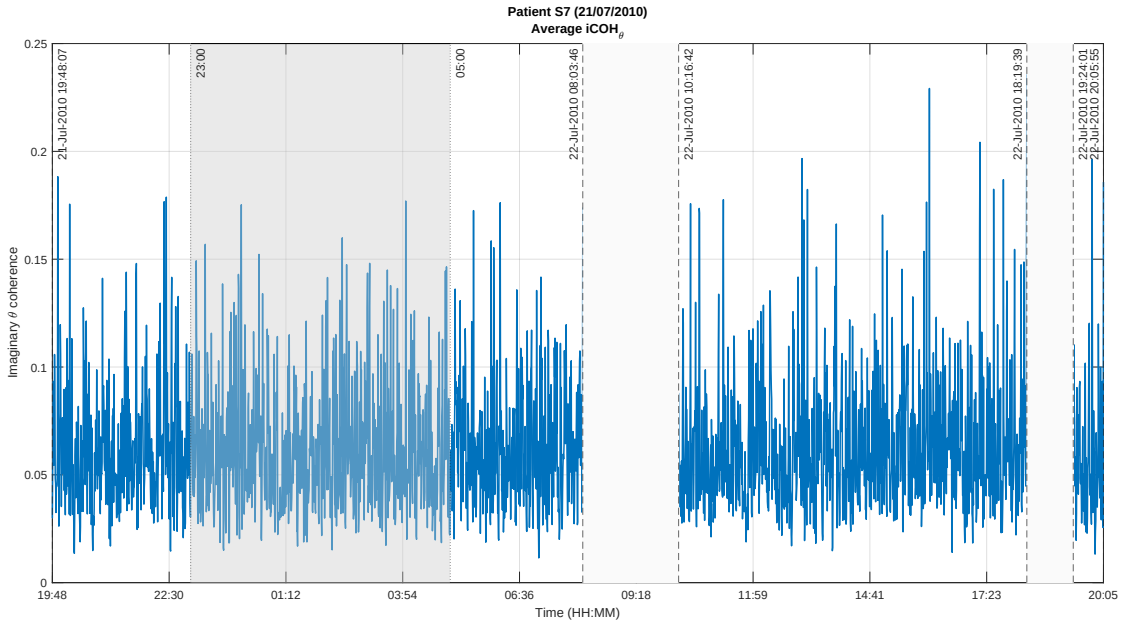

Figure 6.11: Average $iCOH_\theta$ for MCS patient S7. An increased iCOH value in the theta band implies a higher consciousness level, and vice versa. The shaded area between 23:00 and 05:00 represents the night time. The blank areas represent times when no data were recorded.

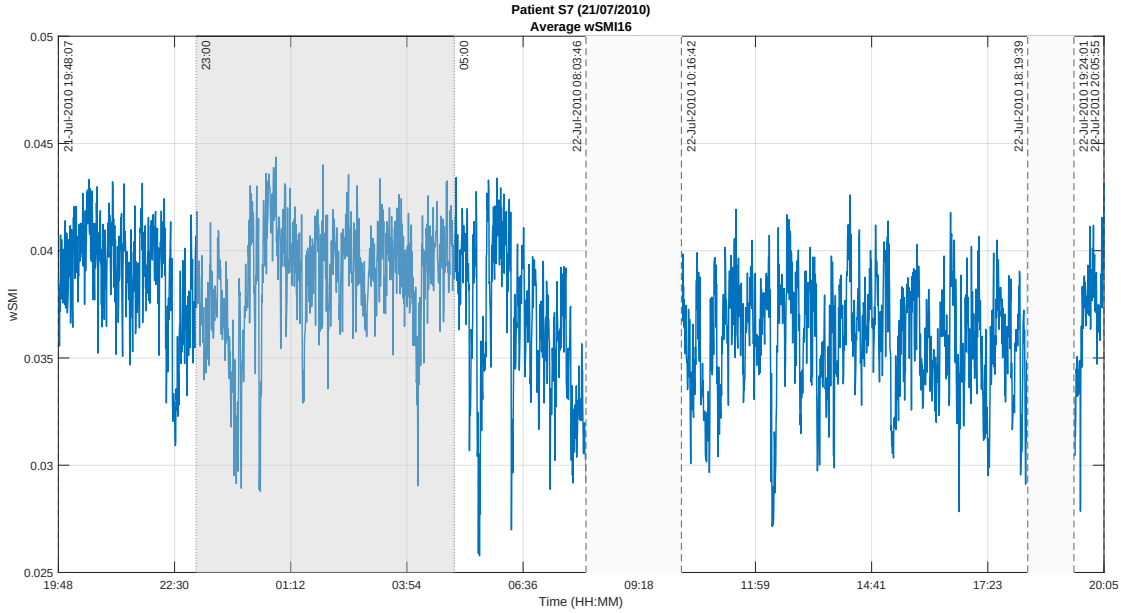

Figure 6.12: weighted Symbolic Mutual Information with $\tau = 16ms$ for MCS patient S7. An increased wSMI with this value of τ implies a higher consciousness level, and vice versa. The shaded area between 23:00 and 05:00 represents the night time. The blank areas represent times when no data were recorded.

of 0.0387. The mean value during the day amounts to 0.0368. The night/day differences are statistically significant at $p < 0.05$ according to a Wilcoxon rank sum test.

6.1.1.4 Inferences from individual features

This part recapitulates the results obtained in the previous section of the individual features for patients L1 (UWS) and S7 (MCS). Patient L1's results were among the best in terms of clustering analysis outcomes, while those of patient S7 were not so good.

Patient L1 All features gave comparable results, i.e. their values increased or decreased during roughly the same time frames. As outlined in Section 4.2, higher values of each specific feature corresponds to conscious state, and vice versa. Therefore, it can be deduced that the patient was certainly unconscious between 20:15 and 21:11 up to 23:00 given the drop observed in all features during that time interval. On the other hand, the values of the features before 20:15 and also during daytime the next day were higher than the remaining of the recording, except for ERR. Therefore, patient L1 was certainly conscious especially from 19:48 until 20:15, and after 07:10. The values of the different features during night time are varying greatly, but overall they are lower during night-time. Wilcoxon ranksum tests revealed that, except for iCOH, the difference between these two time periods are significant at the 5% significance level. This suggests that the patient's consciousness level is significantly lower during the night. This instance exemplifies the perfect case in which all results are mostly consistent with one another.

Patient S7 In most cases, the outcomes of the distinctive signal characteristics may diverge. For example, for this patient, results obtained from the spectral features and the complexity measures are similar, but are differing from those of the connectivity measures. When an increase is observed on the former group, a decrease is detected in the latter, and inversely. For example, while an increase of the θ and β relative powers, SEF95, and ERR was observed between 22:25 and 00:40, LZC and wSMI values were dropping. Applying a simple majority vote, it can be deduced that, on one hand, the consciousness levels of patient S7 heightened particularly between 22:25 and 00:30, 05:00 and 08:00, and between 15:00 and 16:00. On the other hand, values of all features except $iCOH_\theta$ and wSMI decreased between 02:48 and 03:00 as well as between 03:59 and 04:15. The low values suggest a reduction of the consciousness level to the point of unconsciousness. Overall and except for these short time intervals, the values of the features were high, implying that the patient was certainly conscious the whole time. Furthermore, daytime mean complexity values (ERR and LZC) along with $iCOH_\theta$ values were higher than during night time. However, the differences were significant only for LZC. The values were significantly smaller during the day for the other features.

6.1.2 Consciousness level assessment

Now that the results of the different features are obtained, they are analysed by the means of two different clustering approaches: *fuzzy c-means* (FCM) and *Gaussian mixture models* (GMM) that were introduced in Section 2.3.2. These soft-clustering methods are used in particular since the goal in the present work is to infer patients' states using the selected features at any given time with the maximum certainty, and these methods allow that. The membership value to the cluster corresponding to *consciousness* is considered as an assessment of the level of consciousness of the patient and is determined according to the hypothesis mentioned in Section 4.2. Afterwards, an ensemble approach is used to deduce the level of consciousness by combining results from the two clustering methods.

6.1.2.1 Patient L1

The two clusters obtained from the clustering analysis are labelled *Cluster 1* and *Cluster 2*. The values of their centres are summarised in Table 6.1. The cells in blue represent the value that identifies with the higher level of consciousness for each feature. The cluster corresponding to the *conscious* state is the one containing the most features that verifies the conditions reported in Section 4.2. Essentially, higher values correspond to higher levels of consciousness. Therefore, *Cluster 1* contains the data points corresponding to *conscious* states. Table 6.1 also reveals that results from all features correspond, i.e. all "high" values are in the same cluster (*Cluster 1*).

Table 6.1: Clusters centroids for UWS patient L1. Values displayed here are the real values reconverted from the normalised values. Cluster 1 represents the first cluster and Cluster 2 represents the second one. For each feature, the higher centroid value is highlighted in blue. The cluster corresponding to a *conscious* state is the one with the most cells in blue. So, for both cases, it is Cluster 1.

Features	FCM		GMM	
	Cluster 1	Cluster 2	Cluster 1	Cluster 2
P_{theta}	0,1107	0,0820	0,1111	0,0764
P_{beta}	0,0531	0,0236	0,0507	0,0200
SEF95	24,64	10,63	23,69	8,82
ERR	0,7331	0,5328	0,7237	0,5079
LZC	1,0226	0,7878	1,0113	0,7536
$iCOH_{theta}$	0,0504	0,0500	0,0516	0,0498
wSMI	0,0676	0,0623	0,0674	0,0616

The assessment of the centroids values indicates a high level of consciousness for *Cluster 1* compared to *Cluster 2* in both clustering cases. For instance, for FCM, the SEF95 values are centred at 24.64 Hz that is in the β band. Signal complexity were also high: the ERR is 0.7331, and LZC is above 1. The connectivity values are also significant. In *Cluster 2*, SEF95 values are centred around 10.63 Hz, right in the middle of the α band. The complexity values are low, amounting to 0.5328 and 0.7878 respectively for ERR and LZC.

Furthermore, the overall inter-clusters differences, computed on the normalised values of the features, are significant, 0.4809 for FCM and 0.5177 for GMM. Large values of inter-clusters difference suggest that the clusters are well separated, i.e. as far away from each other as possible [KC16; MP00]. Figs. 6.13 and 6.14 illustrate the inter-clusters distance between LZC and SEF95, as well as between wSMI and $iCOH_\theta$ for patient L1. In an ideal case, the lower left corner of the plot would gather the data points corresponding to unconscious states, while the upper right corner will contain those identifying conscious states. Additionally, the points in-between will have increasing values of consciousness levels.

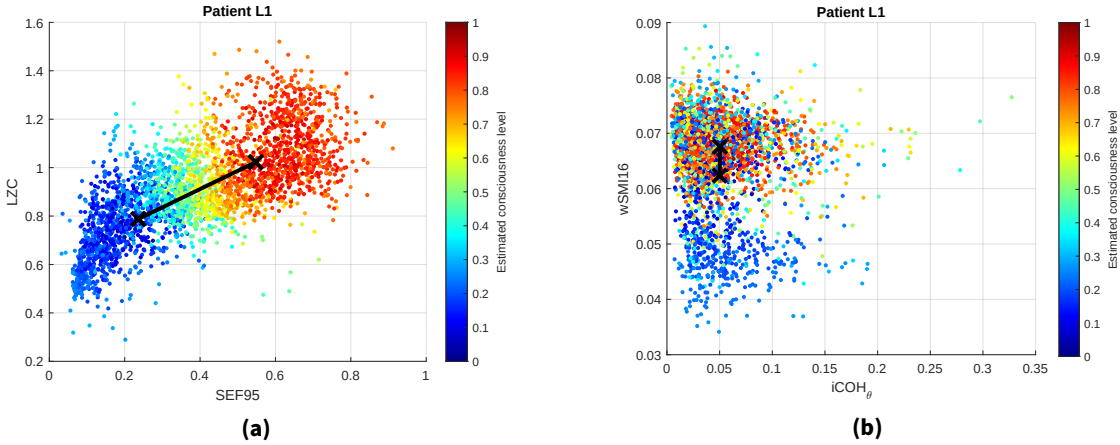

Figure 6.13: FCM clusters plots for UWS patient L1 for the pair of features displaying **(a)** the highest and **(b)** the lowest centroid linkage distance. The barplot on the right side of each figure represents the degree of membership to the *conscious* cluster. 0: unconscious, 1: conscious.

On one hand, SEF95 exhibits the largest inter-clusters distance with the other features, especially with LZC for both clustering approaches with $d_{FCM}(SEF95, LZC) = 0.4024$, and $d_{GMM}(SEF95, LZC) = 0.4302$. Figs. 6.13a and 6.14a respectively illustrate these cases. A smooth transition between unconscious and conscious states is observed, i.e. the degree of membership of the objects progresses evenly from low (in blue) to high (in red) as one moves from the bottom left to the top right of the figure. This validates the hypothesis presented in Section 2.2 regarding the values of these features relative to the level of consciousness. On the other hand, both connectivity measures show the smallest centroid linkage distance, except with SEF95 as previously stated. Figs. 6.13b and 6.14b illustrate the clustering results of wSMI and $iCOH_\theta$ that displayed the lowest inter-cluster differences: $d_{FCM}(wSMI, iCOH) = 0.095$ and $d_{GMM}(wSMI, iCOH) = 0.1060$. As opposed to the previous case, data points with different degree of membership values to the *conscious* cluster are intermingled. The lower part of the figures mostly contain objects with low degree of membership, as it should be. However, the upper part contain objects with different degrees of membership values.

From these results, it can be concluded that LZC and SEF95 constitute the best features for patient L1, while both connectivity measures, wSMI and $iCOH_\theta$, yield non-distinguishable clusters for both clustering analysis methods.

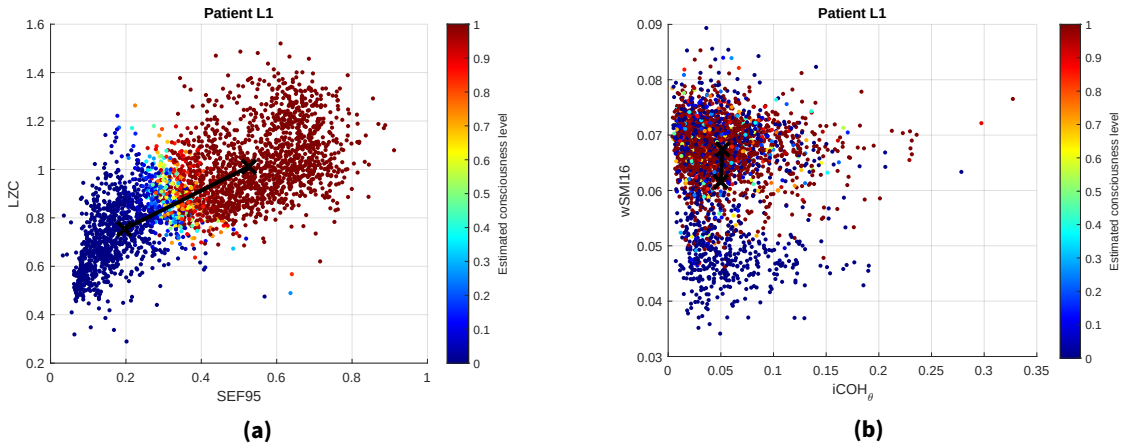

Figure 6.14: GMM clusters plots for UWS patient L1 for the pair of features displaying **(a)** the highest and **(b)** the lowest centroid linkage distance. The barplot on the right side of each figure represents the degree of membership to the *conscious* cluster. 0: unconscious, 1: conscious.

Fig. 6.15 illustrates the estimated consciousness level (alias the degree of membership to the *conscious* cluster) obtained from both clustering methods for patient L1. The values range from 0 (*unconscious*) to 1 (*conscious*). Figs. 6.15a and 6.15b display the results of FCM and GMM clustering analysis respectively. As opposed to the estimated consciousness levels obtained with GMM that covers the entire $[0, 1]$ interval, its values for FCM rarely attain the lower or the upper limit. Distinctive low values of the degree of membership are observed between 20:15 and 23:00, indicating extremely low levels of consciousness. The patient was undoubtedly unconscious in most of that time, except during the sharp increase around 21:26. In addition, the degree of membership is predominantly high before 20:15 and after 07:10, with values close to or equal to 1. This implies that the patient was certainly conscious. Additionally, intermittent phases of low consciousness level are detected after 23:00 until 07:10. These estimations are confirmed by the inferences made from the values of the individual features based on frequency, signal complexity and connectivity in Section 6.1.1.4. Definite low values are also observed between 06:00 and 06:25, and from 11:25 to 12:23. This reflects the trend observed in the same time frame of the relative powers, the SEF95, the ERR, the LZC, and more clearly with the wSMI. Results obtained from GMM appear notably drastic as opposed to that of FCM, as already mentioned previously.

Fig. 6.15e shows the eyes scoring of the patient. O represents open eyes and C denotes closed eyes. When the patient's eyes are intermittently open and closed, it was scored O/C. Some of the scoring were not available due to some technical or visibility problems and were thus labelled as NA/nv [Wie+18]. Moreover, blank areas in the figure represent times when it was unavailable. At first glance, high levels of consciousness obtained with the presented approach seem to coincide with open eyes, while eyes closed correspond to low levels of consciousness.

Table 6.2 recapitulates the results of the Spearman correlation analysis between all the features and the obtained levels of consciousness using FCM and GMM. The values of the coefficients

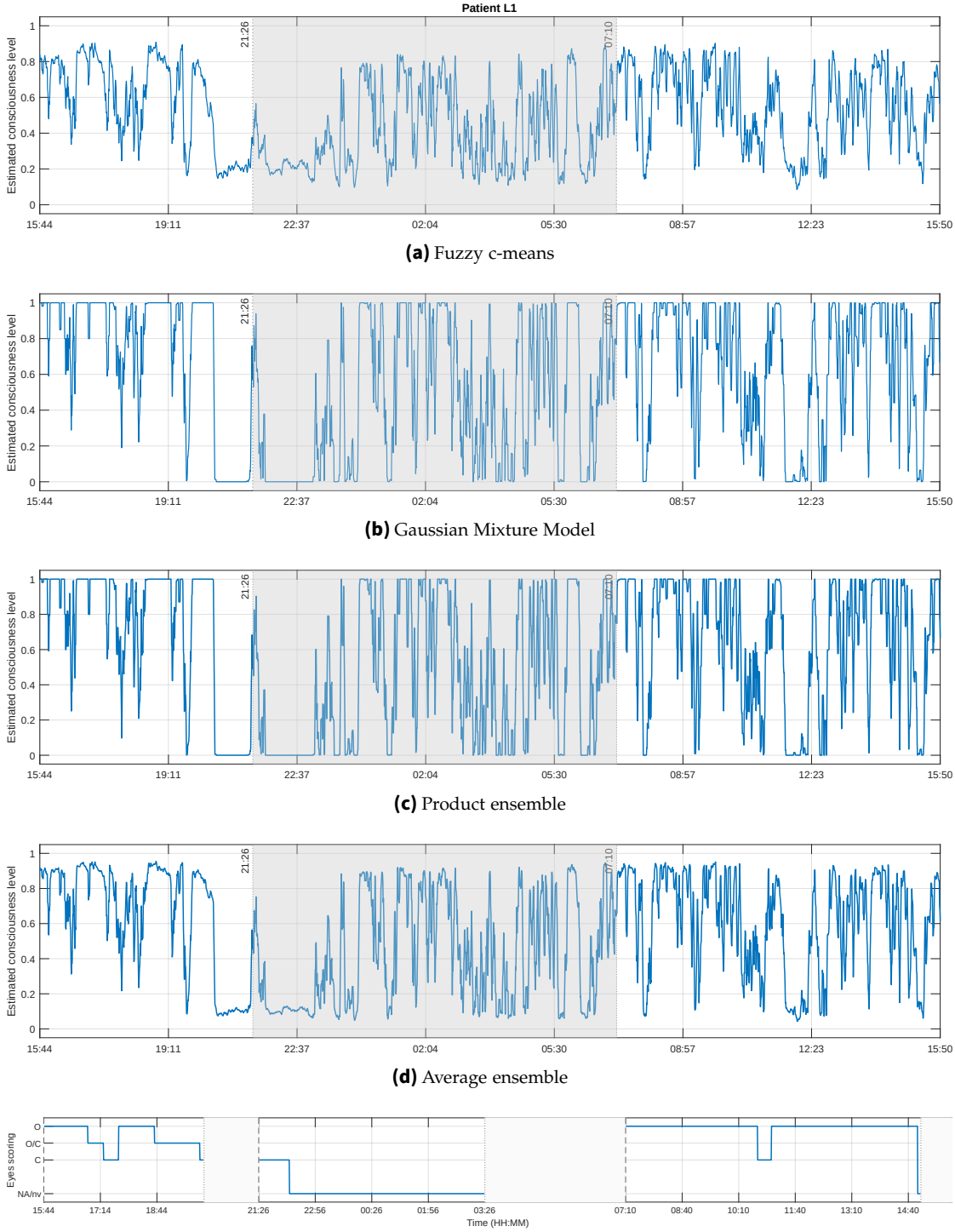

(a) Fuzzy c-means

(b) Gaussian Mixture Model

(c) Product ensemble

(d) Average ensemble

(e) Eyes scoring

Figure 6.15: Estimated consciousness level for UWS patient L1 using **(a)** FCM, **(b)** GMM, **(c)** product ensemble, and **(d)** average ensemble of FCM and GMM. The closer to 1 the curve is, the higher the probability that the patient is conscious, and inversely. The blank areas in **(e)** represent the time frames during which no eyes scoring were recorded. *O*: eyes open, *C*: eyes closed, *Na*/*nv*: scoring unavailable due to some technical problems. Shaded areas between 21:26 and 07:10 delimit the night time.

range from -1 to $+1$, with 0 meaning that no association exists [SBS18]. For this specific patient, all features are highly and positively correlated with the obtained estimations of the consciousness level, except for the $iCOH_\theta$. Consequently, its values only slightly influence the final result. The largest centroid linkage distance was obtained for the pair SEF95,and LZC, while the lowest was for wSMI and $iCOH_\theta$. The table shows that the estimated level of consciousness is more heavily determined by the former than the latter. For example, the values of the correlation coefficients for SEF95 are $Corr_{FCM}(SEF95) = 0.8928$ and $Corr_{GMM}(SEF95) = 0.9579$, compared to $Corr_{FCM}(iCOH_\theta) = 0.7254$ and $Corr_{GMM}(iCOH_\theta) = 0.8003$ for $iCOH_\theta$.

Table 6.2: Spearman correlation coefficients for UWS patient L1 between all features and estimated levels of consciousness. The cells in green represent the correlation coefficients with $p > 0.05$.

Features	Spearman correlation			
	FCM	GMM	Product ens.	Average ens.
P_{theta}	0,5016	0,6331	0,6321	0,5159
P_{beta}	0,8407	0,9449	0,9438	0,8571
SEF95	0,8928	0,9579	0,9588	0,9039
ERR	0,5391	0,5433	0,5485	0,5350
LZC	0,7254	0,8003	0,8012	0,7385
$iCOH_{theta}$	0,0062	0,0197	0,0191	0,0058
wSMI	0,2963	0,2782	0,2851	0,2888

Overall, the estimated level of consciousness of patient L1 retrieved from the clustering analysis of the different EEG features concur the outcomes of the individual features summarised in Section 6.1.1.4. In addition to correctly "translating" the increases and decreases of this level, it accurately evaluate its extent (*conscious* versus *unconscious*). Moreover, the obtained results are also consistent with the eyes scoring when it is available. This means that the estimated levels of consciousness correlate with the patient's eyes states, namely eyes open corresponding to conscious state, and vice versa. Unfortunately, the scoring was mostly unavailable during night time (designated by *NA/nv*). Figs. 6.15c and 6.15d represent the results of the product and average ensembles respectively. The average ensemble seem to produce a reasonable consensus between FCM and GMM, while the product ensemble tend to favour the outcomes of GMM.

These observations demonstrate that the proposed approach is working perfectly in this case, proving its potential. It is therefore the reason of choosing the clustering parameters of this patient for later use.

6.1.2.2 Patient S7

As mentioned previously, the clusters obtained from the clustering analysis are labelled *Cluster 1* and *Cluster 2*. Table 6.3 displays the clusters centroids for patient S7. The cells in colour represent the larger centroid centre. The column with the most blue cells corresponds to the *conscious* cluster, in this case *Cluster 1* for FCM and *Cluster 2* for GMM. As opposed to the results obtained from patient L1, the results of the different features for this patient diverge and

the highest centroid value for P_{theta} and wSMI are in *Cluster 2* for the FCM clustering method, and in *Cluster 1* for GMM. These divergence are marked by the cells in orange in the table.

Table 6.3: Clusters centroids for UWS patient S7. Values displayed here are the real values reconverted from the normalised values. Cluster 1 represents the first cluster and Cluster 2, the second one. For each feature, the higher centroid centre value is highlighted. The cluster corresponding to a *conscious* state is the one with the most cells in blue. In this case, it is Cluster 1 for FCM and Cluster 2 for GMM. The cells in orange signify that for that feature, the values contradict that of the other features (in blue).

Features	FCM		GMM	
	Cluster 1	Cluster 2	Cluster 1	Cluster 2
P_{theta}	0,1745	0,1753	0,1906	0,1435
P_{beta}	0,1439	0,1433	0,1357	0,1594
SEF95	25,11	25,02	24,07	27,06
ERR	0,6441	0,6415	0.6405	0,6474
LZC	1,3947	1,3903	1,3820	1,4136
$iCOH_{theta}$	0,0620	0,0618	0,0591	0,0674
wSMI	0,0373	0,0374	0,0386	0,0347

The values of the cluster centres obtained from FCM are very close to each other, with a global inter-cluster difference of 0.0067. GMM on the other hand exhibits a much larger value of 0.2908. The dissimilarities were computed on the normalised features. Figs. 6.16a and 6.16b represent the FCM clustering results for the features displaying the largest and lowest centroid linkage distances respectively. The clustering analysis results show that wSMI and P_{theta} have the highest inter-clusters difference with $d_{FCM}(wSMI, P_{theta}) = 0.0052$. Furthermore, $iCOH_{\theta}$ and LZC display the lowest inter-clusters difference with $d_{FCM}(iCOH, LZC) = 0.0019$. Both of these values are extremely low. So, as can be seen in the figures, the centroids of the two clusters are quasi overlapping. In addition, the degree of membership value to the *conscious* cluster appear to be around 0.5 for all data points, with a mean value of 0.4979.

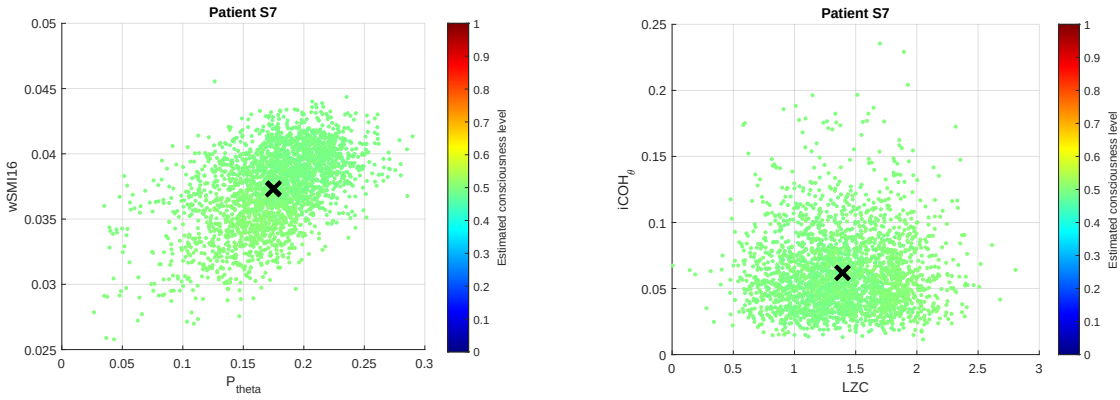

Figure 6.16: FCM clusters plots for patient S7 for the pair of features displaying **(a)** the highest and **(b)** the lowest centroid linkage distance. The barplot on the right side of each figure represents the degree of membership to the *conscious* cluster.

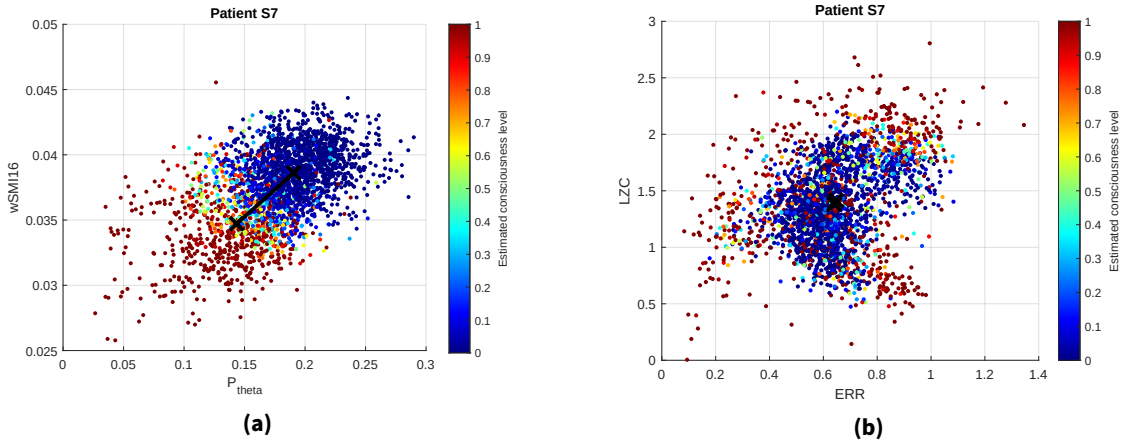

Figure 6.17: GMM clusters plots for patient S7 for the pair of features displaying **(a)** the highest and **(b)** the lowest centroid linkage distance. The barplot on the right side of each figure represents the degree of membership to the *conscious* cluster.

The degrees of membership obtained from the GMM clustering analysis cover more range of values. As previously stated and can be seen in Table 6.3, clustering results of P_{theta} and wSMI contradict those of the other features. It is also illustrated in Fig. 6.17a. Particularly, low values of wSMI and P_{theta} belong to the *conscious* cluster, and inversely. These observations are also contradicting the hypothesis in Section 4.2. wSMI and P_{theta} also display the largest inter-clusters distance with $d_{GMM}(wSMI, P_{theta}) = 0.2662$ for the GMM clustering approach. The lowest distance is observed between LZC and ERR with $d_{GMM}(LZC, ERR) = 0.0125$ (see Fig. 6.17b). The cluster centres are practically overlapping and objects with different degrees of memberships to the *conscious* cluster are all mixed. There is no smooth transition from unconscious to conscious states as in Fig. 6.14a.

Fig. 6.18a shows the results of FCM cluster analysis for patient S7. The estimated level of consciousness is essentially constant, with a mean value of 0.49. All data points are centred to roughly the same point. Indeed, the values of the clusters centres for both *Cluster 1* and *Cluster 2* in Table 6.3 correspond to conscious states. The output of the GMM clustering analysis is presented in Fig. 6.18b. The results suggest that patient S7 was unconscious from 19:48 to 22:30, as well as during night-time from 00:40 to 05:00 in particular. In terms of signal behaviour, the estimated levels of consciousness are conform to the inferences made in Section 6.1.1.4. The values are however inaccurate.

Table 6.4 recapitulates the results of the correlation analysis between all the features and the obtained levels of consciousness using FCM and GMM for MCS patient S7. Consistent to the observations made in Section 6.1.2, P_{theta} and wSMI are highly but negatively correlated with the obtained estimations of the consciousness level. It also revealed that the other features are positively but only moderately correlated with the estimated consciousness levels. This also confirms the inferences made in Section 6.1.1.4. Moreover, LZC and $iCOH_{\theta}$ for FCM, and ERR and LZC are the features that contribute the less to the final estimated consciousness levels.

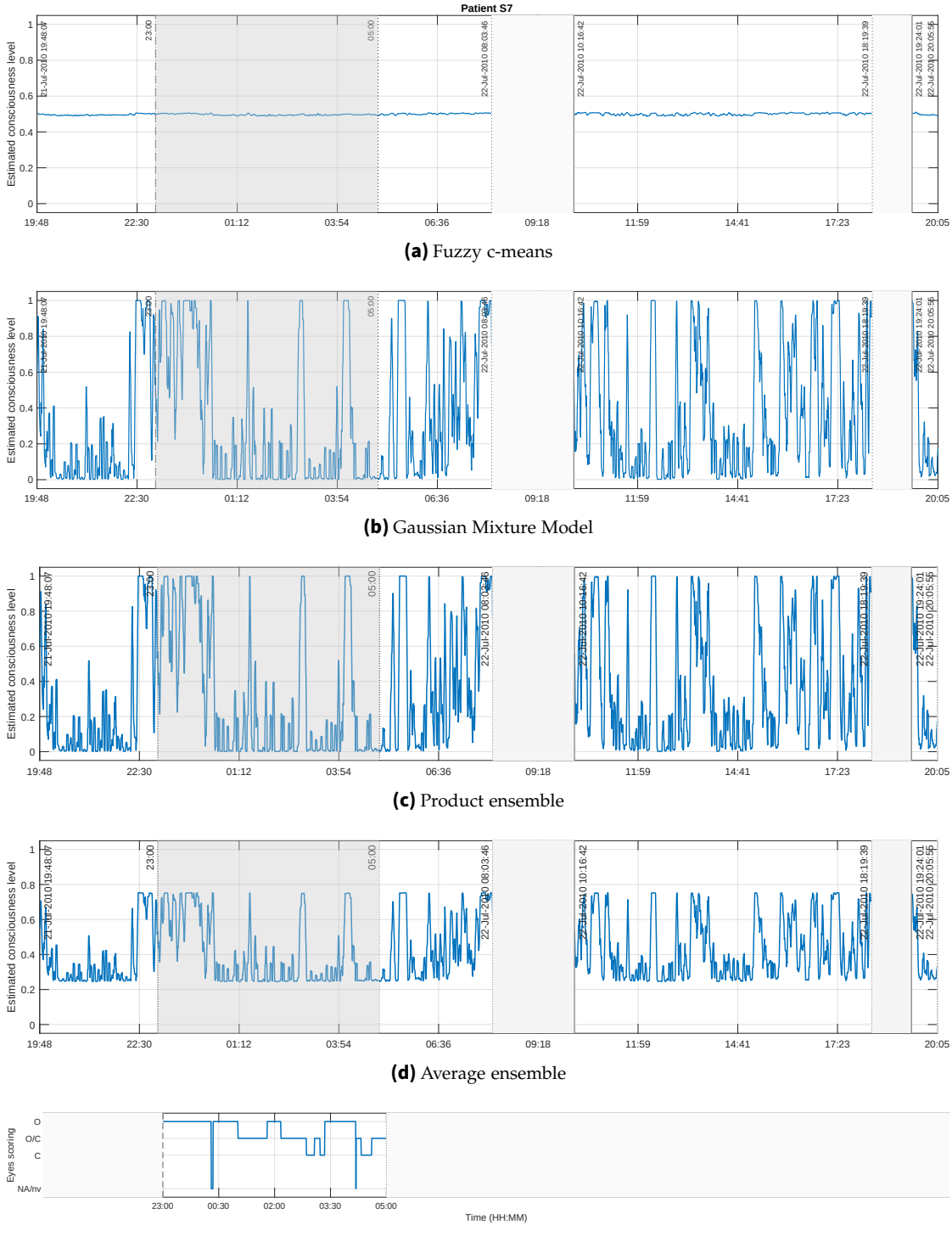

(a) Fuzzy c-means

(b) Gaussian Mixture Model

(c) Product ensemble

(d) Average ensemble

(e) Eyes scoring

Figure 6.18: Estimated consciousness level for MCS patient S7 using **(a)** FCM, and **(b)** GMM, **(c)** product ensemble, and **(d)** average ensemble of FCM and GMM. The closer to 1 the curve is, the higher the probability that the patient is conscious, and inversely.The blank areas represent the times during which no EEG data were recorded ((**a**), (**b**), (**c**) and (**d**)) or no eyes scoring were made **(e)**. Shaded areas between 23:00 and 05:00 delimit the night time.

Those were respectively the pairs of features with the lowest inter-clusters distances for both clustering analysis.

Table 6.4: Spearman correlation coefficients for MCS patient S7 between all features and estimated levels of consciousness. The p-value < 0.05 in all cases.

Features	Spearman correlation			
	FCM	GMM	Product ens.	Average ens.
P_{theta}	-0,5660	-0,7500	-0,7496	-0,7181
P_{beta}	0,3920	0,3223	0,3228	0,3550
SEF95	0,5771	0,4907	0,4915	0,5294
ERR	0,3611	0,1181	0,1195	0,1655
LZC	0,3113	0,0547	0,0558	0,0910
$iCOH_{theta}$	0,1535	0,1283	0,1286	0,1330
wSMI	-0,7443	-0,7511	-0,7515	-0,7432

6.1.2.3 Overview of the results for the remaining of the DoC patients

The median values of the individual features used in this work are generally lower for MCS patients compared to the UWS patients, except for LZC and wSMI. The differences were assessed by the means of a Wilcoxon ranksum test performed on each EEG measure between both group of patients. It revealed that the difference were significant. The p-values are recapped in Table B.2 of Appendix B. These results are a bit surprising since first, the CRS-R of the UWS are mostly lower than those of the MCS patients (cf. Table 5.1). And second, a handful of researches indicated that the levels of consciousness of UWS patients are lower than those with MCS. On the other hand, this is probably due to the fact that average results are used here instead of individual electrodes.

The estimated levels of consciousness of the DoC patients except L1 and S7 (Figs. B.1 to B.15) as well as the clusters centres obtained from the clustering analysis (Tables B.3 to B.17) are reported in Appendix B. In general, analogous to a majority vote, the estimations of consciousness levels from both FCM and GMM are positively correlated with the majority of the individual features. In other words, the approach was able to convey the increases and decreases of the patients' levels of consciousness from them. On the other hand, the accuracy of these estimations depends on the overall inter-clusters differences. First of all, the levels of consciousness values are highly influenced by the features with the largest inter-clusters distance and vice versa. The correlation coefficients between the features and the estimated levels of consciousness for all patients are reported in Appendix B. The results showed that there is no common best or worst feature shared by all patients. Each individual is different, and so are the most and less performant features for each of them. In addition, when the dissimilarities are large enough, the estimated levels of consciousness are remarkably accurate when matched with the outcomes of each individual measure (as is the case of patient L1). However, when it is not the case i.e. the inter-clusters distances are small, the estimations are not correctly conveyed. This latter case was observed for patients L13 and S13 in addition to patient S7 which case was presented in the following section.

Furthermore, the evaluation of night and day differences of the individual features determined that the values at night are lower, except for UWS patient S14 and MCS patients L4, L7 and L16. For all of them, a Wilcoxon rank sum test performed to assess the differences determined that they are significant. The implications of this observation are further discussed in Section 6.1.3.

6.1.3 Performance of the approaches

The primary purpose of recording the DoC patients' EEG signal was to study their sleep patterns and investigate the night and day variations [Wie+18; Wis+17]. Researches show that for DoC patients, eyes opening and closing are manifestation of periods of circadian sleep-wake [Wan+18]. A circadian rhythm can be defined as the innate internal process that regulates the sleep–wake cycle and repeats approximately every 24 hours [BCP16]. For this particular dataset, high-to-low frequency power ratio of the EEG as well as permutation entropy were used, and results showed that their values were significantly higher during the day for MCS patients, but no changes were observed for UWS patients [Wis+17]. In addition, a hierarchical clustering analysis using permutation entropy computed on the EEG signals revealed that MCS patients' sleep behaviour are analogous to that of healthy subjects. Particularly, patterns resembling healthy REM were detected during night-time. However, this complexity difference between night and day value were negligible for UWS patients. This suggests that day-night variations are impaired for these patients. In addition, as opposed to MCS, only small inter-clusters differences were observed for them [Wie+18].

Now in this work, as already mentioned in Section 6.1.2.3, a Wilcoxon ranksum test was performed on the results obtained from the clustering ensemble approaches to assess the night versus day differences. Except for four patients, the dissimilarities are significant at the 5% level with higher values during the day. The p-values for all patients are gathered in Table B.18 in Appendix B. Eyes closed do not necessarily mean unconscious, and vice versa. Nonetheless, taking all of the above into consideration, it is most likely the case during the night. Furthermore, since most eyes scoring were recorded at night, it could be assumed that eyes closed correspond to unconscious state, while open eyes indicate conscious state.

Consequently, the performance of the clustering methods are now evaluated by computing the accuracy between the clustering results using the patients eyes scoring as "ground-truth". Since, it is unlikely that 0.5 represent the bound between *conscious* and *unconscious* states, the cluster membership values were defuzzified by converting them into binary numbers using several threshold ranging from 0.3 to 0.7 with a 0.1 increment. Accordingly, the values below the threshold were appointed to 0 (*low* level of consciousness), and those above threshold were set to 1 (*high* level of consciousness). Likewise, the eyes scoring "O" corresponds to 1, while "C" corresponds to 0. Only the scoring indicating eyes open and eyes closed, and the corresponding data were use for the evaluation [Wie+18]. The performance of the approach is then determined by computing the accuracy as:

$$Accuracy = \frac{TP + TN}{TP + TN + FP + FN} \tag{6.1}$$

where TP: True Positive, TN: True Negative, FP: False Positive, and FN: False Negative.

The accuracy was computed for all threshold values. The obtained values for the 17 DoC patients (8 UWS and 9 MCS) are reported in Table B.19 in Appendix B. The accuracy obtained for both ensemble methods are slightly distinct for the different threshold values, except when its value is 0.5, in which case both ensemble method have the same accuracy.

The best results for the MCS patients are illustrated in Fig. 6.19a. Patient S17 achieved the lowest accuracy with 22.22% ($threshold = 0.6$) and was the only patient with an accuracy below 50%. The highest accuracy for the whole group was achieved by patient S14, with up to 85.2% ($threshold = 0.3$) on the average ensemble. Similarly, the best performance results for UWS/VS patients are presented in Fig. 6.19b. The highest accuracy for this group was achieved by patient L8 with 70.11% for both ensemble methods ($threshold = 0.6$ for the product ensemble and 0.7 for the average ensemble). 5 out of the 8 UWS patients also attained an above 50% accuracy. The performances of almost all MCS patients appear better compared to that of UWS/VS patients.

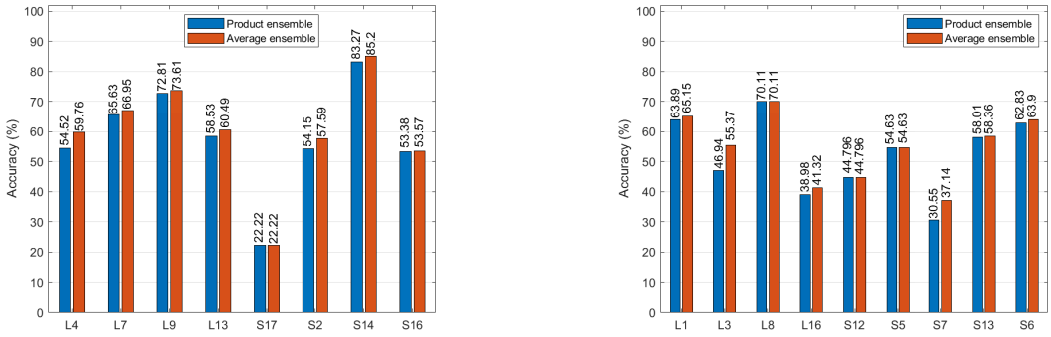

(a) MCS patients

(b) UWS/VS patients

Figure 6.19: Performance of the ensemble clustering methods for **(a)** MCS patients and **(b)** UWS patients. For two MCS patients, accuracy was above 70%. Only one of the UWS patient achieved a 70% accuracy.

Considering the patients' sleep patterns as well as the performance of the clustering analysis using different values of threshold, it can be assumed that the boundary delimiting *conscious* and *unconscious* states depends on the patient. The idea behind this work is to determine patients' consciousness states in order to initiate communication. It is therefore crucial to detect this minimum value at which the level of consciousness is enough for that to happen. An input from the family members or caregiver is therefore necessary.

6.1.4 Discussion I

The different features used in this work were weighted equally and their values were normalised so to not favour any of them for the clustering analysis. Each of the features extracts a particular characteristic of the EEG signal. The hypothesis in Section 4.2 stipulate that conscious states are defined by an increase of each of these signal attributes. However, the features may also contradict each other to some extent. In this group of DoC patients, the results of one or more measures contradict the others, except for patient L1 (UWS).

When the results of the features or somewhat conflicting, a consensus appear to be found by the cluster analysis methods. Moreover, the proposed approach in this work (using FCM and GMM) was able to convey the variations of the levels of consciousness that match the outcomes of the different features. At least, this is the case when the inter-cluster distances between the clusters are important enough as it is the case for patient L1 (cf. Section 6.1.2.1). Otherwise, FCM is monotonous with a value around 0.5, meaning that all the data points belong more or less equally to both clusters (cf. Fig. 6.18a). This can be interpreted as the two clusters representing the same thing as in Fig. 6.16b. GMM on the other hand still reflects the variations observed on the individual features in terms of increase and decrease, but the values of the levels of consciousness are actually invalid. Looking back to the observations made for patient S7 in Section 6.1.2.2, for example, the two resulting clusters both represent a conscious state. Nevertheless, the results of GMM, and consequently those of the ensemble methods, defined the lower values as an *unconscious* and the higher values as a *conscious* states (cf. Fig. 6.18b).

Given these observations, this clustering approach works best when the data is diversified. In other words, the analysed data should cover all the possible states of consciousness of the patient. For a number of reasons, one being the difficulty to record patients data, this is mostly impractical. Consequently, another solution would be to use pre-defined centroids. Since patient L1 displayed high inter-cluster difference, and that all features and cluster centres values verified the conditions defined in Section 4.2, his clustering parameters will be used for the CLIS patients.

6.2 CLIS patients

This part reports the results for the CLIS patients. Those of patient GR are first introduced. The same procedure as for the DoC patients is first followed to determine the consciousness level of the patient. Afterwards, the results of the remaining of the CLIS are presented and discussed.

6.2.1 ECoG data

The data of patient GR consists of a 24-hour ECoG brain recordings from 64 channels. Channels, which signal amplitudes were larger than $\pm 200 \mu V$ were excluded. Consequently, channels

Go08, Go12, Go28, Go34, and Go80 were removed (cf. Fig. 5.2), leaving 59 channels for further analysis.

This patient's data is singular since, to the best of our knowledge, it is the only one in which the experimenters were able to pinpoint one time frame when the CLIS patient was indeed conscious. Besides, he was trained to use BCI since his being diagnosed with ALS. Hence, the experimenter is familiar with his demeanour. The experiment described in Section 5.1.2 was conducted from 14:50 to 17:00. It is delimited by the red lines in Fig. 6.20, which illustrates the results of the ensemble methods regarding the estimated consciousness level. These results were obtained by applying the proposed clustering approach to the features extracted from GR's data without any prerequisite.

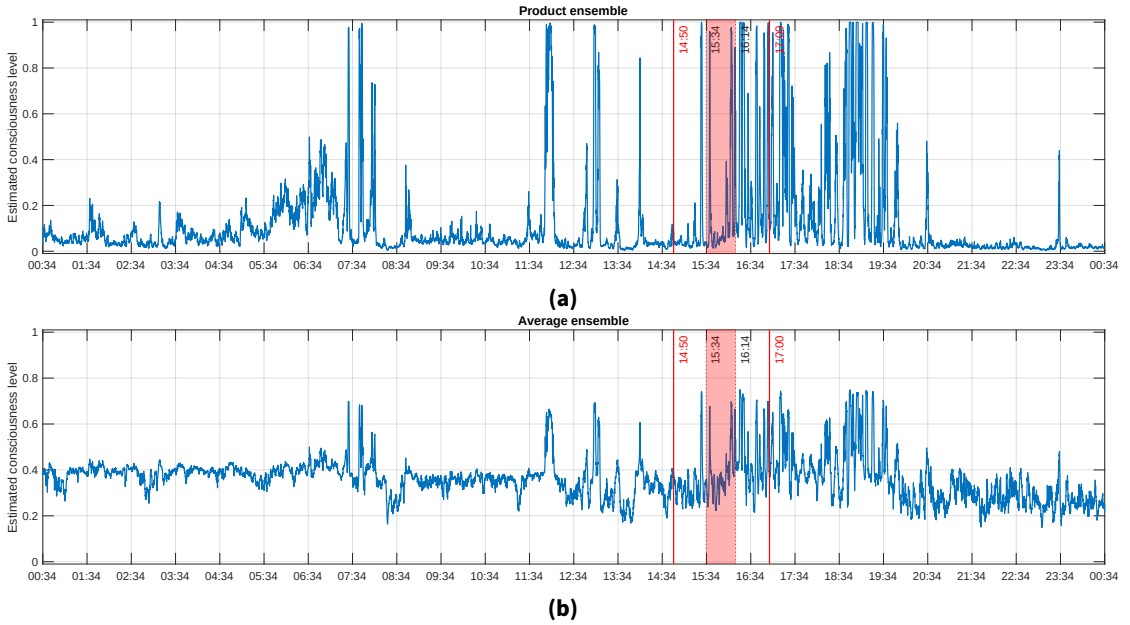

Figure 6.20: Estimated consciousness level for patient GR **(a)** product ensemble, **(b)** average ensemble. The experiment was performed between 14:50 and 17:00 (red vertical lines). The red area from 15:34 to 16:14 represent the time during which the experimenter reported that the patient was correctly answering the questions he was asked. The values of the estimated consciousness level at these times were definitely different than the values the rest of the time.

The experimenter asserts that patient GR was correctly answering the questions in the time frame 15:34 to 16:14. During the experiment, the patient was asked 18 questions. To make sure that the classifier correctly identified his answer, each question was asked in pairs. This means that for each question requiring a positive answer, the same question was reformulated so that the same answer is expressed by a negative answer. The entire course of the interaction between the patient and the experimenter is reported in Table C.2 in Appendix C. Out of the 18 questions, answers for two questions were unclear, but 16 of them were clearly answered by the patient thus correctly determined by the classifier, resulting in a 88.89% correct answer rate.

Table 6.5: Average estimated consciousness level for patient GR during different time frames. The estimated consciousness level were definitely slightly higher during the experiment.

Time	Interval	FCM	GMM	Product ensemble	Average ensemble
all (24h)	00:34 - 00:34^{+1}	0,4978	0,2679	0,2601	0,3829
day time	08:00 - 20:00	0,4756	0,3355	0,3205	0,4055
night time	20:00 - 08:00	0,5200	0,2005	0,1998	0,3603
before experiment	00:34 - 14:50	0,5244	0,2514	0,2481	0,3879
during experiment	14:50 - 17:00	0,4558	0,3598	0,3408	0,4078
after experiment	17:00 - 00:34^{+1}	0,4598	0,2784	0,2598	0,3663
"conscious" time	15:34 - 16:14	0,4574	0,3594	0,3400	0,4084

The degrees of membership obtained from FCM are relatively steady throughout the entire recording, with a average of 0.4978, analogous to the results obtained for DoC patient S7. Some variations are however observed in the results of GMM, notably an increase in the afternoon, and the average score during the entire recording is 0.2679. This then resulted in what can be seen in Fig. 6.20. Table 6.5 summarises the average values of the estimated consciousness level during different time intervals using FCM, GMM and the two ensemble methods. The mean FCM and GMM degrees of membership during the experiment are 0.4574 and 0.3594 respectively. While the values are significantly higher than the average value for the entire recording for GMM, it is the opposite for FCM. Differences were also observed between the average values during day and night times. Times between 08:00 to 20:00 are labelled as day and 20:00 to 08:00 as night [Soe+13]. FCM membership degrees are higher during the night and outside the experiment time. Contrariwise, low values are observed during the night and the highest values occur during the experiment. In case of GMM clustering in particular, other time intervals also depict a higher value of the membership degree, namely between 07:21 and 08:06, and intermittently between 11:51 and 13:16. Additionally, it remains high after the experiment up until 19:42, with an average of 0.49.

Table 6.6: Clusters centroids for CLIS patient GR. Cluster 1 and Cluster 2 represent the two clusters. The cluster corresponding to *conscious* is the one containing the most blue cells. In this case, Cluster 1 for both FCM and GMM. Values are the real values reconverted from the normalised ones. Cells in orange contain high value corresponding to higher consciousness level, but is not in the same cluster as the majority (blue cells).

Features	FCM		GMM	
	Cluster 1	Cluster 2	Cluster 1	Cluster 2
Ptheta	0,1344	0,1263	0,1243	0,135
Pbeta	0,3211	0,3105	0,333	0,3188
SEF95	26,199	25,6050	25,803	26,2035
ERR	0,6441	0,6415	0,6405	0,6474
LZC	0,6767	0,6833	0,6913	0,6754
iCOH_theta	0,0613	0,0614	0,0616	0,0612
wSMI16	0,0311	0,0314	0,0338	0,0308

Table 6.6 presents the values of the clusters centres obtained using FCM and GMM. The inter-clusters distances for FCM is $d_{FCM} = 0.1284$ and equals $d_{GMM} = 0.0797$ for GMM. The values are somewhat low compared to those of patient L1, but are comparable to those of patient S7. For example, akin to patient S7's results, less than 2 Hz separates the SEF95 in both clusters for both clustering approaches. In addition, the complexity values are essentially in the same value range. This is illustrated in Fig. 6.21 that displays the FCM degree of membership to the *conscious* cluster of each data point from SEF95 and LZC. The two centroids are practically overlapping. Most objects are located in the upper right part of the figure corresponding to high LZC and high SEF95, which in turn denote high levels of consciousness [G+21; Tou+19]. No clear clusters are visible although the data points have different degrees of membership. Consequently, the lower limits of the degree of membership in Fig. 6.20 could not be interpreted as *unconscious*, akin to the results of Patient S7 in Section 6.1.1.2.

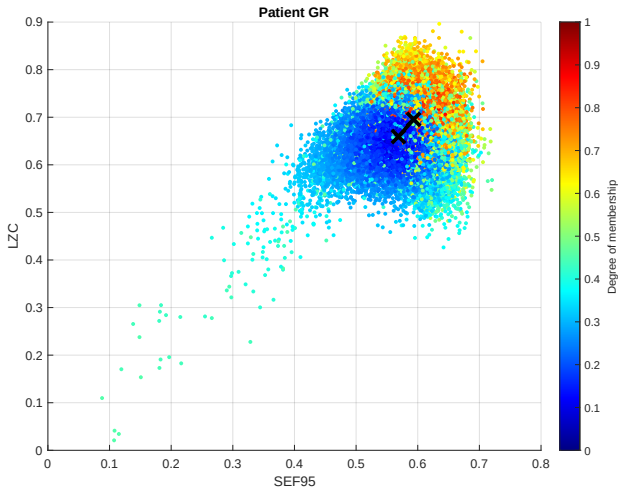

Figure 6.21: Illustration of the clusters using FCM clustering for patient GR with the SEF95 and LZC features. The centroid linkage distance is very low, the centroids are close to each other. The barplot on the right side of the figure represents the degree of membership to the *conscious* cluster. On one hand, the two clusters are basically overlapping; on the other hand, the majority of the data points are located at the upper right of the plot, which means high complexity and high SEF95. This indicates a high level of consciousness.

The data of GR is furthermore partitioned using pre-defined FCM cluster centres and the same Gaussian mixture model as patient L1, as declared in Section 6.1.4. The outcomes of the average ensemble are presented in Fig. 6.22 and Table 6.7 summarises the average values of the estimated consciousness levels during different time intervals using FCM, GMM and the average ensemble methods. The estimated values are high, with an overall mean of 0.9998 and 0.7638 for the product and average ensemble respectively. The values were also slightly higher during and after the experiment. To summarise all of the above, the clustering analysis of GR's ECoG data allowed to determine that the resulting centroids for both clusters are almost undistinguishable and represent high consciousness level. In addition, an undeniable increase of the consciousness level is observed especially in the time of and following the experiment. Moreover, the use of predefined cluster centres determined that patient GR was conscious

during the entire 24-hour recording. Consequently, the patient was assuredly conscious during the whole recording, but also that his level of consciousness increased during the experiment.

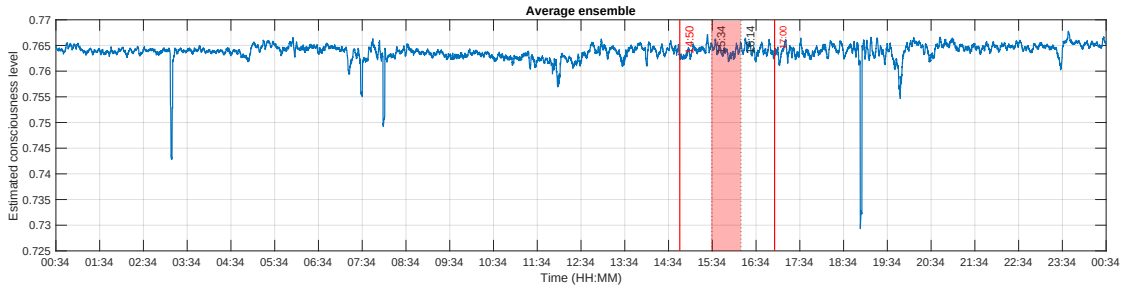

Figure 6.22: Estimated consciousness level for patient GR using the pre-defined cluster centres obtained in Section 6.1.3 (average ensemble). The estimated level of consciousness is constantly high. The experiment was performed between 14:50 and 17:00 (red vertical lines). The red area from 15:34 to 16:14 represent the time during which the experimenter reported that the patient was correctly answering the questions he was asked.

These observations not only confirm the observations of the experimenter regarding the state of consciousness of the patient during part of the experiment, but are also corroborated, at least partly, by the separately obtained results using the imaginary part of coherency, Granger causality and sample entropy in [Ada+19b]. Namely, patterns suggesting a conscious state were observed in the imaginary coherence from 15:15 to 15:30 and from 16:00 to 16:10, in the multi-scale sample entropy between 15:24 and 16:14, and with Granger causality between the frontal and posterior channels from 15:34 until 16:14. A multi-scale approach analysis of patient GR's data involving sample entropy, permutation entropy and Poincaré plots also revealed that the patient was conscious between 16:04 and 16:10 [WNB20].

Table 6.7: Average estimated consciousness level for patient GR during different time frames using pre-defined clustering parameters.

Time	Interval	FCM	GMM	Product ensemble	Average ensemble
all (24h)	00:34 - 00:34^{+1}	0.5277	0.9998	0.9998	0.7638
day time	08:00 - 20:00	0.52689	0.99975	0.99975	0.76332
night time	20:00 - 08:00	0.52858	0.99988	0.99988	0.76423
before experiment	00:34 - 14:50	0.5272	0.99984	0.99984	0.76352
during experiment	14:50 - 17:00	0.52797	1,0000	1,0000	0.76399
after experiment	17:00 - 00:34^{+1}	0.52867	0.99971	0.99971	0.76506
"conscious" time	15:34 - 16:14	0.52772	1,0000	1,0000	0.76386

The clustering analysis employing pre-determined cluster centres argues that there is a high probability that the patient was conscious during these 24 hours, but to a lesser extent than during the experiment. This argument is not inconceivable, since as mentioned in Section 2.1.2, ALS-LIS patients suffer from an increased manifestation of insomnia as the condition evolves [Pos+07]. An investigation of this patient sleep/wake characteristics revealed the pres-

ence of increase SWS fragmentation [Soe+13]. It is therefore highly probable that this day was an instance of such case.

6.2.2 EEG data

The same procedure using pre-defined cluster centres is now applied to the EEG data of the remaining CLIS patients introduced in Section 5.1.2.2. This section reports the results of the product and average ensembles. The mean level of consciousness of all patients is illustrated in Fig. 6.23. The figure shows that as opposed to patients P6, P7 and P10 in particular, who displayed extremely low consciousness levels, patients P1, P2 and P5 exhibited the highest estimated levels of consciousness, with 0.627, 0.764 and 0.587 respectively (product ensemble). The values for patient P6, P7 and P10 were always low during all available recordings.

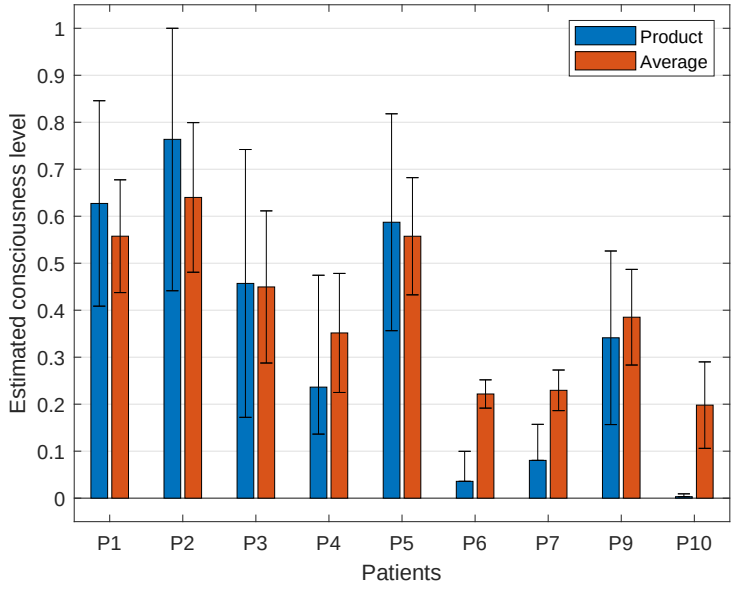

Figure 6.23: Average and standard deviation values of the estimated consciousness level for all sessions and all CLIS patients obtained from the ensemble methods. The obtained estimations of the levels of consciousness were always low for patients P6, P7 and P10.

The patients can therefore be categorised into three groups, depending on the results obtained from the clustering analysis during all recording sessions. First, the estimated consciousness level for patient P1 was consistently high, except for the very last recording. Patient P2 also showed high levels of consciousness, except for one day. The experimenters affirmed that those two patients achieved the highest performance among all the CLIS patients during the experiments. This implies that they were conscious in almost all sessions. Then, there are patients whose estimated consciousness level were highly variable from one session to the other. Patients P3, P4 and P5 belong to this category. Finally, patients P6, P7, P9 and P10 always showed low consciousness levels. The experimenters reported patient P10 as being brain dead, and they observed only a few irregular good sessions with patient P9. Only results with notable

particularities will be presented in details in this section. The results that are not displayed here will be presented in Appendix D.

6.2.2.1 Patient P1

This female patient was diagnosed with sporadic bulbar ALS in May 2007 and as locked-in in 2009. She transitioned into a completely locked-in state in May 2010. The patient died in 2019 (see Appendix D.1).

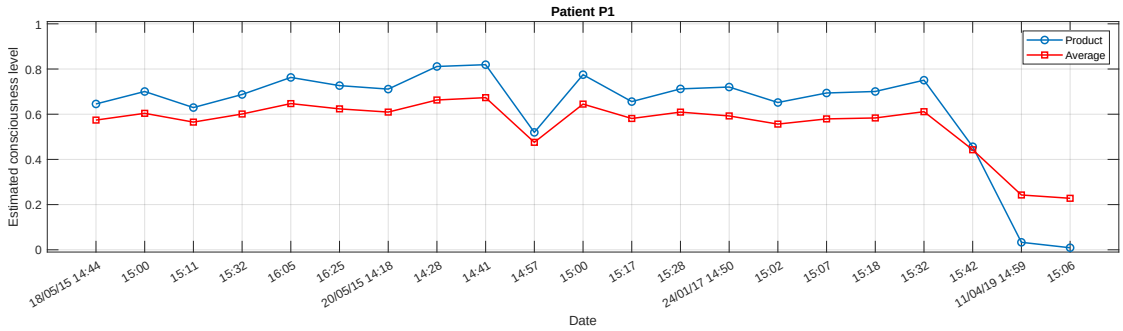

Figure 6.24: Estimated consciousness level for CLIS patient P1. The x-axis represents the dates and times of recording. Estimated levels of consciousness are high enough, except in 2019, to allow communication with the patient.

Three years of EEG recordings from 2015, 2017 and 2019 are available for analysis. The number of sessions is variable, ranging from 2 to 7. The estimated level of consciousness of patient P1 is highly consistent through the years except for the last, as illustrated in Fig. 6.24, with an overall mean exceeding 0.6/0.55 (product / average ensemble). Both methods produce results with the same trend, only their value differ, the average ensemble being lower in general. There are nonetheless changes, particularly on 20/05/2015 during the session starting at 14:57, as can be seen in the figure. Although a sharp drop is observed, the consciousness level remains high to still suggest that the patient was conscious the entire day. Consequently, communication with the patient can be initiated for all these sessions. The above-mentioned findings substantiate the experimenters' report that patient P1 was almost always successful in *yes* and *no* communication, especially using fNRIS. In 2019, the estimated value of the consciousness level dropped considerably, approaching 0 for the product ensemble and around 0.2 for the average ensemble, suggesting that the patient was undoubtedly unconscious. For that reason, all communication attempts will definitely fail.

Let's take a closer look at the first two dates for patient P1: 18/05/2015 and 20/05/2015. The estimated consciousness level for this patient on 18/05/2015 is illustrated in Fig. 6.25a for all sessions. That day's experiment comprises six sessions including five task sessions and one rest session. The patient was instructed not to think of anything during the rest sessions. As described in Section 5.1.2, the tasks consist of *yes* and *no* questions that the patients need to answer using their brain signals. The overall consciousness level during all sessions is high. However, the highest level is observed during the fourth task session (*d1b4*) beginning at

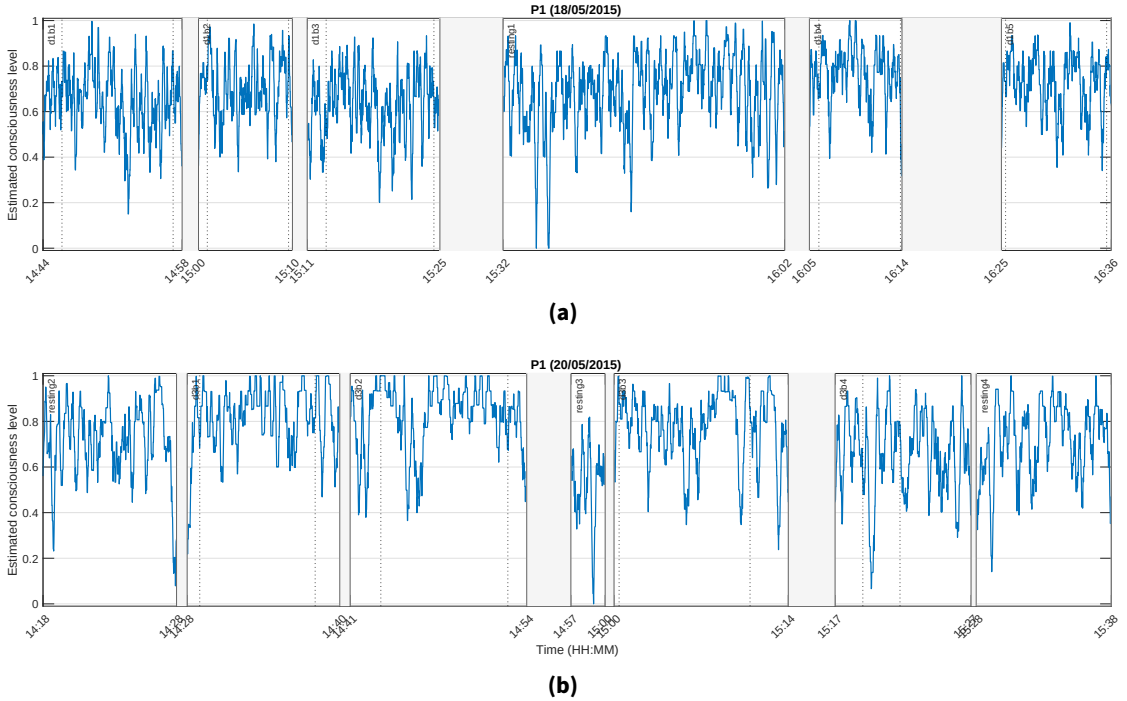

Figure 6.25: Estimated consciousness level for patient P1 (product ensemble) on **(a)** 18/05/2015 (day 1) and **(b)** 20/05/2015 (day 2). Shaded areas represent period during which no data were recorded. The dotted lines delimit the start and end of the experiment. Plain vertical lines mark the start of each session. The name of each of them is marked on the top left of each experiment part.

16:05 with a mean value of 0.7628/0.647 (product/average ensemble). The high values suggest that the patient was conscious overall, but with an increased level during session *d1b4*. The experiments on 20/05/2015 are composed of seven sessions: rest sessions at the beginning and the end, and four task sessions separated by another brief rest session as shown in Fig. 6.25b. The level of consciousness of the patient increased during the first and the second session (*d3b1* and *d3b2*, with an average consciousness level estimate at 0.8112 and 0.8192, respectively). A slight decrease is observed for the remaining sessions, but mostly during the rest session *resting3* with an average of 0.5196. These results are in accordance to those obtained in [AB21b] in which it was established that the levels of consciousness of this patient were highly variable and that it can also happen that during a specific experiment, it consistently decreased. Such decline is probably due to patient's fatigue.

No critical differences across the sessions were observed. Consequently, as already stated previously, the patient's performance in answering the questions should be high. In the study reported in [AB21a], patient P1 achieved the highest accuracy among a group of 4 CLIS patients to classify *yes*/*no* answers. An analysis of her EEG data during these experiments revealed that she was able to achieve an accuracy of 67.94% using Random Forest with the SEF95 feature. This is probably due to the fact that she spent the most time in ALS condition (see Appendix D.1). During the experiment, the patients were asked to "*think*" *yes* or *no* to answer the questions. It

is hypothesised that given these instructions, each patient possibly finds a way to convey their answer. It is then likely that she has the most experience in accurately expressing her answers.

6.2.2.2 Patient P2

This male patient was diagnosed with non-bulbar ALS in May 2011. He first used a speech device in his throat to communicate beginning of December 2011. When this failed, it was replaced by MyTobii eye tracking device from April 2012 until December 2013. The response using this system was variable and communication was no more possible from August 2014 (see Appendix D.1).

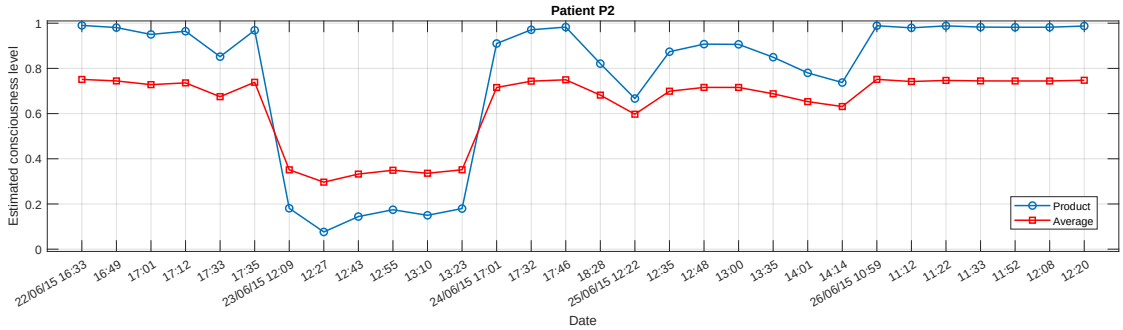

Figure 6.26: Average estimated consciousness level for CLIS patient P2 during the different recording days. The x-axis represents the dates and times of recording.

Fig. 6.26 illustrates the estimated consciousness level obtained from the approach proposed in this thesis. The EEG data consists of 5 days of recordings from 2015 with from 4 to 7 sessions each. Similar to patient P1's results, both ensemble methods follow the same trend. The estimated consciousness levels are also high for patient P2 except on 23/06/2015 (average ensemble: 0.3361, product ensemble: 0.1503). No information about what may have caused such decrease was obtained from the experimenters. In [Van+16] for instance, the decrease of performance and motivation on the patient's part during some days was due to health issues. Since nothing specific was reported that day for this patient, it can be speculated that he was simply not conscious, possibly asleep. This result constitutes an example of unfavourable time to start communication with the patient.

6.2.2.3 Patient P3

This female patient was diagnosed with bulbar ALS in 2010. She lost speech and capability to walk by 2011. Starting February 2013, she started using assistive communication devices using one finger to communicate, until it failed. Afterwards, in early 2014, an attempt has been made to use eye tracking for communication, which was stopped in August 2014. After that, the patient was tried to communicate using subtle twitch of eyelid. Unfortunately, this was not

reliable and the husband and caretakers declared no communication with her since then (see Appendix D.1).

There is only one year of EEG recordings available for this patient, consisting of 4 days in 2017. The number of sessions ranges from 4 to 5. The obtained estimations of her consciousness levels are highly variable from day to day, but also from session to session. This can be seen for example in Fig. 6.27, which illustrates its mean values for each session. The mean value across all sessions is 0.457 (product ensemble). It can be seen however that this comparatively low value is due to the low values on some days. Indeed, the estimated consciousness levels are high on 13/07/2017 and 14/07/2017 attaining up to 0.8356/0.6649 (product/average ensemble). Nevertheless, for the first two sessions on 14/07/2017, the estimated values of the patient's consciousness level is 0.4839/0.4743 (product/average ensemble) and 0.2046/0.3209 (product / average ensemble) respectively. These levels of consciousness are possibly not enough to perform a communication task. Afterwards, the values increased throughout the last 3 sessions, with mean values of 0.7895 and 0.6470 for the product and average ensemble respectively. In this case, communication can be initiated with the patient has high chances of being successful. On the other hand, the estimated levels of consciousness are consistently low on 15/07/2017, indicating that no fruitful communication can be undertaken then.

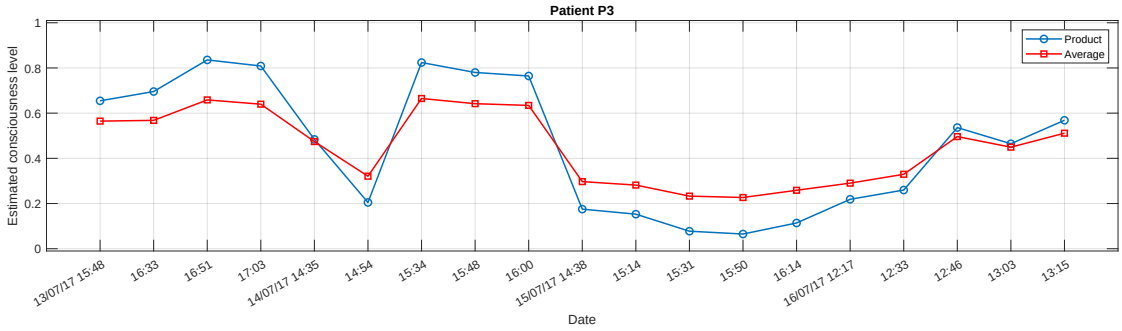

Figure 6.27: Daily average of the estimated consciousness levels for CLIS patient P3. The x-axis represents the dates and times of recording.

Fig. 6.28a presents the estimated level of consciousness for patient P3 throughout the experiments on 14/07/2017. The experiment started with two training sessions during which it can be observed that despite a noticeable surge at the end of the first training session, the level of consciousness remains low, below 0.4. After an half hour break, three feedback sessions (cf. Section 5.1.2.1) were performed during which higher consciousness levels were estimated. Then, on 15/07/2017, the values of the estimated consciousness levels for patient P3 are consistently low, with a mean value of 0.1170/0.2594 (product/average ensemble). The results for this specific day are illustrated in Fig. 6.28b. The low values suggest that it is highly probable that all experiments carried out that day were unsuccessful. This demonstrates the importance of evaluating the level of consciousness of the patients before attempting to communicate with them.

Table 6.8 summarises the mean values of the estimated consciousness levels during each session on 14 and 15/07/2017 for this patient. The rows in green represent the sessions during

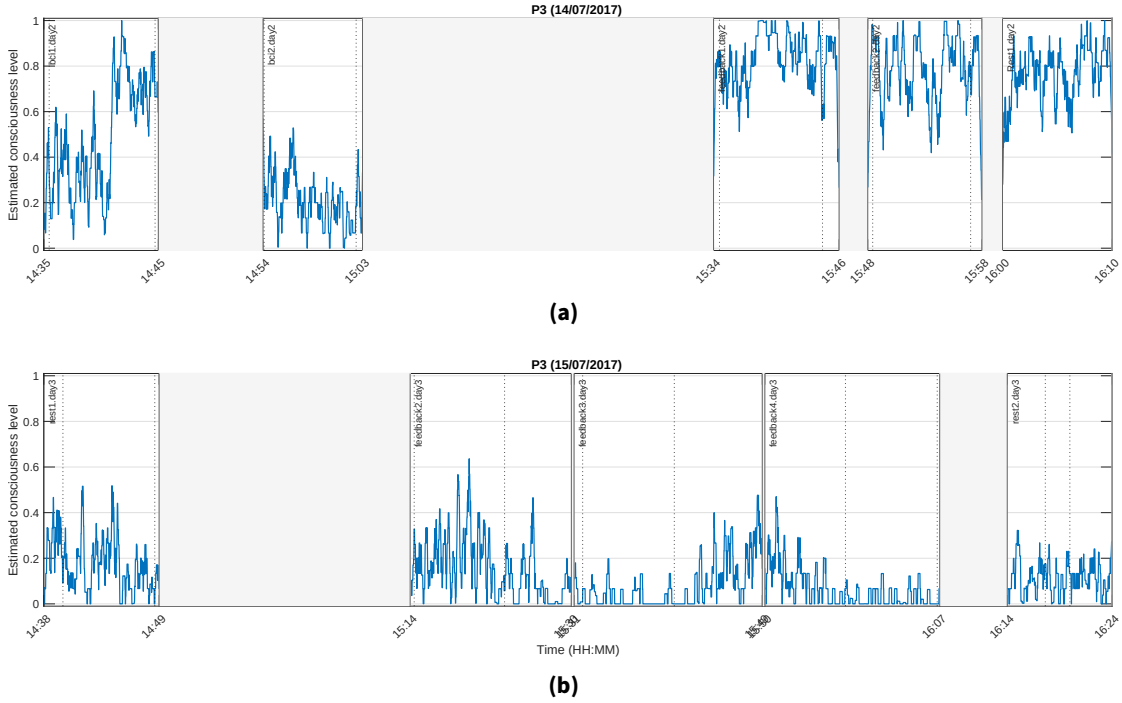

Figure 6.28: Estimated consciousness level for patient P3 (product ensemble) on **(a)** 14/07/2017 (day 2) and **(b)** 15/07/2017 (day 3). Blank areas represent period during which no data were recorded. The dotted lines delimit the start and end of the experiment. Plain vertical lines delimit each session.

which the patient is assessed as being conscious according to the outcomes of the proposed ensemble approach. The values are significantly lower compared to 15 July.

The experimenters declared that this patient was only successful in *yes* and *no* communication using fNRIS from 2014 to 2015, which data were not available, thus not analysed in this research. From the results obtained using the approach presented in this work, it can be concluded that on one hand, patient P3 was mostly conscious on the first two days of experiments (13/07/2017 and 14/07/2017). On the other hand, it can also be inferred that he was possibly unconscious the rest of the time, especially on 15/07/2017.

6.2.2.4 Patient P4

This female patient represents a particular case given the rapid evolution of the condition in addition to her young age. She is 29 years old and was diagnosed with juvenile ALS in December 2012. She was completely paralysed within half a year after diagnosis. She was able to communicate with the eye-tracking device from early 2013 but was unable to use it after she lost some control of her eyes in August 2014. She was also trained to communicate with her family members using eye movements: moving to the right to answer *yes* and to the left to answer *no*. This method was used until the complete loss of eye control in December

Table 6.8: Mean values of the estimated consciousness level per session on 14 and 15 July 2017 for patient P3. The highlighted rows represent the sessions with a high level of consciousness, during which the patient was undoubtedly conscious. The values obtained on 15 July suggest that he was unconscious that day during the experiment.

2017-07-14	Product ensemble	Average ensemble
bci1.day2	0,4839	0,4743
bci2.day2	0,2046	0,3209
feedback1.day2	0,8240	0,6649
feedback2.day2	0,7800	0,6419
Rest1.day2	0,7644	0,6342

2017-07-15	Product ensemble	Average ensemble
rest1.day3	0,1753	0,2970
feedback2.day3	0,1529	0,2816
feedback3.day3	0,0776	0,2328
feedback4.day3	0,0651	0,2267
rest2.day3	0,1139	0,2587

2014. Subsequently, she attempted to twitch the right corner of her mouth to answer *yes*, but this was not reliable, leaving no other alternative for her parents to communicate with her (see Appendix D.1).

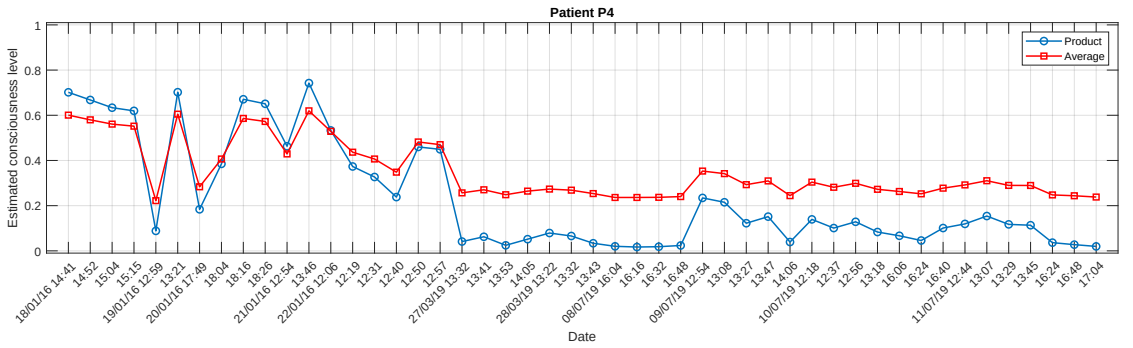

Figure 6.29: Average estimate of the consciousness level of CLIS patient P4. The x-axis represents the dates and times of recording.

The EEG data from patient P4 were recorded in 2016 and 2019. Each day of recording comprises 2 to 7 sessions. Fig. 6.29 illustrates the estimates of her levels of consciousness. At first sight, high values of the consciousness levels are observed on 2016. However, the values decreased in 2019, especially for the product ensemble. Accordingly, it can be deduced that patient P4 was mostly conscious in 2016, but the probability that she was also conscious in 2019 is very low. Communication attempts when the estimated consciousness levels are high would undoubtedly be successful. In point of fact, the experimenters declared that she was only able to communicate using fNRIS from 2014 to 2016. Nonetheless, variations in the estimated consciousness level in 2016, imply that the patient was undoubtedly unconscious during some sessions. For example, on 19/01/2016 and 20/01/2016 both during the first session. Coincidentally, these two sessions are rest sessions. This means that this patient was actually "resting" during these periods.

6.2.2.5 Patient P6

CLIS patient P6 was diagnosed with bulbar ALS in 2009. He lost speech and was unable to move from 2010. He is in home care. No communication with whatever means was possible since 2012. This patient died in 2019 [Mal+19; Sec+21] (also see Appendix D.1).

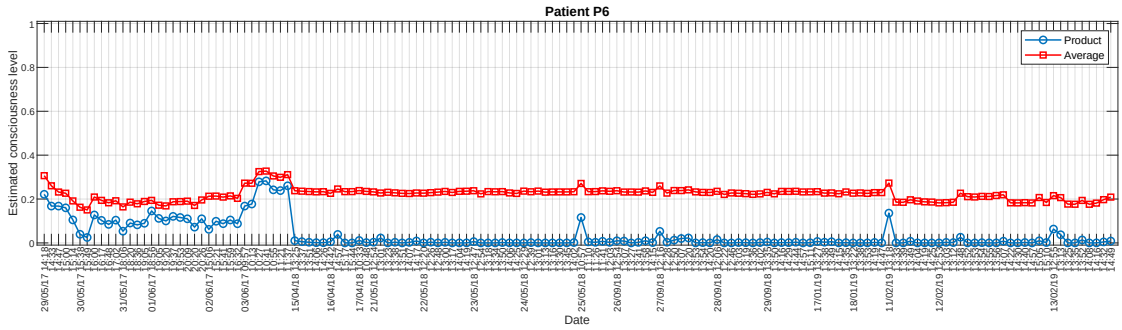

Figure 6.30: Daily average of the estimated consciousness level for CLIS patient P6. The x-axis represents the dates and times of recording.

Three years of recordings were available for this patient, from 2017 to 2019. Fig. 6.30 shows the patient's consciousness level determined as a result of the clustering analysis presented in this thesis. The values are very small for both ensemble methods. Additionally, a substantial drop is observed starting in 2018 with the product ensemble but the changes do not appear so drastic for the average ensemble. Nonetheless, these low values imply that there is a high probability that patient P6 was actually never conscious during these recordings. However, the experimenters reported a successful *yes/no* communication using fNRIS in 2017. The clustering analysis determined mean values of 0.1313 for the product ensemble and 0.2188 for the average ensemble that year. Nevertheless, these seemingly low values may probably be enough for the patient to perform the tasks.

6.2.2.6 Patient P10

This patient is in locked-in state and on the verge of CLIS. He is also the youngest patient in this group (25 years old). Patient P10 was diagnosed with familial juvenile ALS with ALS 6-FUS gene mutation[25] in December 2012. He was completely paralysed within a year after the diagnosis. He used an eye-tracking device to communicate starting at the beginning of 2014 until he lost eye control in August 2016. The patient was unable to communicate afterwards [Mal+19] (also see Appendix D.1).

The daily average of the estimated level of consciousness for patient P10 is illustrated in Fig. 6.31. The analysed data were from 2017 and 2018, with 2 days of recordings comprising 5 to 6 sessions each. Among all the CLIS patients, patient P10 displayed the lowest level of

[25] In 10% of the cases, ALS neurodegenerative disease that is familial. This is caused by a missense mutation in the FUS (Fused in Sarcoma) gene encoding. This mutation causes familial ALS type 6 [Van+09].

consciousness according the method presented in this thesis. These values are extremely low undoubtedly indicating that patient P10 was unconscious during the course of all recordings. It is hypothesised that the patient's performance in answering the questions increases with a higher level of consciousness. Consequently, the results suggest that no successful communication could ever established with this patients. Indeed, the experimenters reported that this patient was brain dead. Unsurprisingly, he was also never successful with the *yes* and *no* communication using fNRIS.

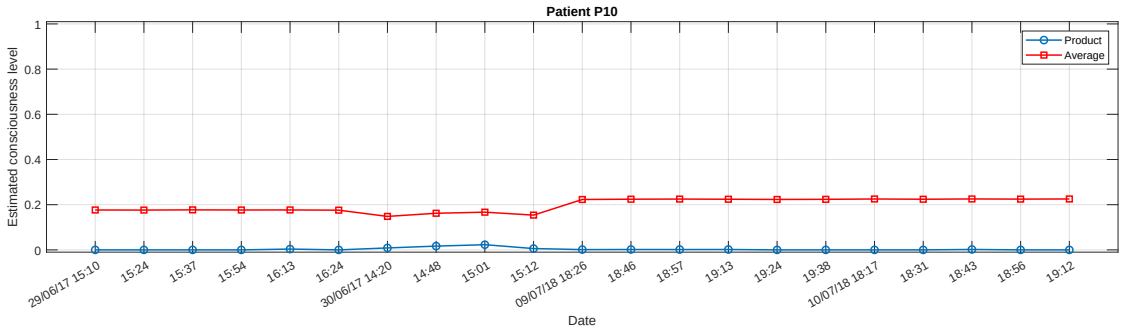

Figure 6.31: Estimated consciousness levels for CLIS patient P10. The x-axis represents the dates and times of recording.

6.2.3 Discussion II

The results obtained by the soft-clustering approach proposed in this thesis were compared to the performances of the patients using fNRIS (reported by the experimenters) when available. While EEG measures the electrical activity of the brain, fNRIS determines the cortical haemodynamic response of the brain to a neural activity [GIM18; Sub19]. An investigation using TMS in the cortex of cats revealed that the fluctuations in oxygen concentration in the brain are correlated with brain electrical activity [Milo7; All+07]. It can be assumed then that this also applied to human brain, justifying the legitimacy of the comparison. Overall, the obtained results are validated by the report of the experimenters regarding the patient's performance with the fNRIS-based BCI. For patient P6 in particular, although the experimenters reported that he was able to communicate using fNRIS until 2017, the obtained estimations of his consciousness levels were less than 0.3. Considering the evaluation of the performance of the clustering approach on data from the DoC patients in Section 6.1.3, either the patient was unconscious or the minimum threshold for him to be able to perform the task was already achieved. This, combined with the previously obtained results from patient GR, consequently prove the effectiveness of the proposed approach and validate the hypothesis introduced in Section 4.2.

Sadly, patients P1 and P7 passed away in 2019, and patients P2 and P6 in 2018. The results of the clustering analysis determined that the consciousness levels of P1, P6 and P7 patients decreased shortly prior their death (cf. Figs. 6.24 and 6.30, and Fig. D.2 in Appendix D). Unfortunately, only data from 2015 was available for the patient P2, so no such finding could be

substantiated. Nonetheless, the quasi similar behaviour of the estimated levels of consciousness of the three patients begs the question whether this decrease could be an indicator of patients' decline and/or predict their death. To get a definite answer, a study in that direction should be extended to a larger number of patients.

On one hand, an increase of consciousness level was detected when feedback are provided to the patients. This was for instance the case for patients P3, P6, P7 and P9. This tendency may be explained by the fact that feedback is among the key factors of a successful experience since it boosts the patient's motivation and engagement [vWL15]. Nevertheless, as the patients transition from locked-in to completely locked-in states, a decrease of the EEG power is observed, shifting it toward the δ and θ bands [Sec+21]. This decrease also apply to other characteristics such as the brain signal complexity [Ada+20]. The more time the patient spends in CLIS, the more important this decline is, although it can be delayed by providing them with means of communication, especially using BCIs [Sec+21]. Subsequently, this stresses the importance of continuously communicating and interacting with the patients.

6.3 Summary

This chapter reported the results of the soft-clustering approaches used to estimate different patients' consciousness level. When applied to the data of DoC patients, the proposed approach was able to convey the characteristics of most of the features, although some of them are contradictory. Some limitations of the method were found, but were overcome using predefined centroids on the CLIS patients' data. The results obtained this time were corroborated by the experimenters' observations and/or the patients' performance using another brain imaging technique (fNRIS). What's more, it also estimated low values indicating the absence of consciousness for one of the patient that was brain dead. In the end, keeping these different results in mind, the proposed approach was able to achieve the aim that was established at the beginning of this thesis. Its limitations, implications as well as possible future works will be briefly introduced in the next chapter before concluding this thesis.

7 Conclusions

> There is no real ending. It's just the place where you stop the story.
>
> *Frank Herbert*

7.1 Summary

In the present work, the task of assessing the levels of consciousness of completely locked-in patients was undertaken. Patients with this condition are entirely paralysed but retain their cognitive abilities. A major problem with this state is that there is no ground-truth relating to the patients' actual states of consciousness. This means that there is no definite way to be sure if they are conscious or not at a given time since on one hand, no behavioural responses can be detected and on the other hand, the patients themselves cannot overtly voice their states. CLIS patients are often misdiagnosed as in a vegetative state, which subsequently leads to inappropriate care. A proper care not only improves their quality of life by allowing them to express themselves, but also enhances their prognosis. The ability to communicate constitutes a crucial factor of this improvement, and is made possible by the use of brain-computer interfaces. Nonetheless, the majority of existing studies attempted communicating with the patients without taking into account if they are conscious and/or willing to do so.

In this thesis, the determination of the consciousness levels comes into play to determine the optimal time to communicate with the patients instead of randomly starting the experiments. In order to maximise the probability of detecting the patients' actual state, a group of diverse signal characteristics including spectral and complexity measures as well as connectivity metrics were used. The idea behind the combined use of these different features was because each of them may extract additional information that can not be obtained from the others. The features were computed for each channel or pair of channels and subsequently averaged across all of them. The obtained results were then input to two soft-clustering methods, Fuzzy c-means and Gaussian mixture models, which outputs were later combined using their product and/or average to obtain a unique outcome. The use of soft-clustering was preferred to hard-clustering since instead of a binary decision regarding the patient's consciousness state, a probability of the patient being conscious was desired.

The proposed approach was first applied to data from DoC patients since according to previous studies, their levels of consciousness are lower than that of LIS and CLIS patients,

which levels are assumed to be comparable to those of healthy subjects. The approach was subsequently evaluated using eyes scoring recorded along the EEG signal of the same DoC patients. It was also applied to data from one CLIS patient which is unique since it is the only one where the experimenter could identify one time frame during which said patient was actually conscious. Consequently, if the method manages to correctly estimate the patients' level of consciousness in these two cases, it is highly probable that it can correctly estimate that of the remaining CLIS patients in this work.

The obtained results revealed that the method proposed in this thesis was able to emulate the collective increases and decreases of the different EEG measures reflecting the patients' consciousness levels. However, this level was accurately determined under the condition that the clusters centroids are distant from each other. This means that there should be enough data so that all possible states (from *unconscious* to *conscious*) are represented. Given the rarity of EEG data acquired from CLIS patients, this condition is certainly difficult to fulfil. So, to remedy to this situation, pre-determined parameters were subsequently employed to cluster the data from the remaining CLIS patients. By comparing these results to informations provided by the experimenters, the proposed approach was again capable of determining the possible levels of consciousness of the patients. Furthermore, the results appear to presage patient's death, in which case a decrease of their levels of consciousness was observed in the months preceding their death. These observations were detected in all except one patient that passed away due to data unavailability. Nonetheless, more data are needed to corroborate these observations.

One major limitation of the presented work is evidently the lack of data from CLIS patients, leading to the use of these pre-defined centroids for the clustering analysis. In addition, no features selection were performed, i.e. all the EEG measures were used regardless if they positively or negatively influence the results. Despite these restrictions however, the proposed approach was able to accurately determine the patients' levels of consciousness for the majority of the DoC patients and all the CLIS patients. This approach can be used as an additional tool to the traditional behavioural tests to help clinicians reduce the misdiagnosis rate of (completely) locked-in patients. Furthermore, given the importance of communication to such patients and to avoid unnecessary fatigue, it can also be used as a preliminary step before initiate communication with the patient. That way, it can be established only when the patient is conscious enough.

The method proposed in this thesis was able to correctly evaluate the levels of consciousness of different group of patients in vegetative and minimally conscious states, but more importantly in completely locked-in patients, using a combination of different EEG signal characteristics. This thesis constitutes a step toward improving the lives of CLIS patients. To the author's knowledge, no such investigation to detect CLIS patients' consciousness levels using the different features used in this work, as well as the soft-clustering analysis exist at this time.

7.2 Outlook

In the approach proposed in this thesis, all features are weighted equally and no selection were performed. However, every patient is different and some features may be more relevant than others for each individual. Future work will primarily focus on tailoring the features to each CLIS patient. The list of features employed in this research are not exhaustive. Additional EEG characteristics can be added in view of gathering more hidden patterns and ameliorate the system. Furthermore, since levels of consciousness are provided as output of the clustering analysis and that in Section 6.1.3, it was reported that the performance of the cluster analysis depended on the value of the threshold chosen to separate *unconscious* and *conscious* states, an automatic and personalised detection of this threshold will be developed. As mentioned in Section 3.1, family members are primarily the ones that first discover that the patient was conscious. They are familiar with them and are consequently more likely to know how they appear when they are conscious. Therefore, all future works will involve and require their contributions. Their input will be used to adaptively select useful features for each patient in the first case, and to determine the optimal threshold in the second case.

Since the principal goal was to assess consciousness of the patients before any attempt to communicate with them, the next step will be an online implementation of the system. This requires of course a continuous recording of the patient's EEG. Since the computation of LZC and wSMI are time consuming, an output of the patient's state can be provided by the system every few minutes to allow time for calculation. A duration of five to ten minutes alike the length of the sessions during the experiments with CLIS patients seems appropriate.

Bibliography

[AB18] V. S. Adama and M. Bogdan. "Stroke Rehabilitation and Parkinson's Disease Tremor Reduction Using BCIs Combined With FES". In: *International Journal of Privacy and Health Information Management (IJPHIM)* 6.1 (2018), pages 20–36. DOI: 10.4018/IJPHIM.2018010102.

[AB21a] S. Adama and M. Bogdan. "Yes/No Classification of EEG data from CLIS patients". In: *43rd Annual International Conference of the IEEE Engineering in Medicine and Biology Society (EMBC)*. 2021, pages 1–6.

[AB21b] V. S. Adama and M. Bogdan. "Consciousness Detection in Complete Locked-in State Patients using Electroencephalogram Coherency and Artificial Neural Networks". In: *Sensor Networks and Signal Processing*. Volume 176. Smart Innovation, Systems and Technologies. Singapore: Springer, 2021, pages 397–409. DOI: 10.1007/978-981-15-4917-5_29.

[Abo+06] M. Aboy, R. Hornero, D. Abasolo, and D. Alvarez. "Interpretation of the Lempel-Ziv Complexity Measure in the Context of Biomedical Signal Analysis". In: *IEEE Transactions on Biomedical Engineering* 53.11 (2006), pages 2282–2288. DOI: 10.1109/TBME.2006.883696.

[Ada+19a] V. S. Adama, A. Blankenburg, C. Ernst, R. Kummer, S. Murugaboopathy, and M. Bogdan. "Motion Detection in Videos of Coherence Matrices in order to detect Consciousness States in CLIS-patients - an Approach". In: *Abstracts of the 10th EUROSIM Congress on Modelling and Simulation*. 2019. ISBN: 978-3-901608-92-6. DOI: 10.11128/arep.58.

[Ada+19b] V. S. Adama, S.-J. Wu, N. Nicolaou, and M. Bogdan. "Extendable Hybrid approach to detect conscious states in a CLIS patient using machine learning". In: *Abstracts of the 10th EUROSIM Congress on Modelling and Simulation*. 2019. ISBN: 978-3-901608-92-6. DOI: 10.11128/arep.58.

[Ada+20] S. Adama, U. Chaudhary, N. Birbaumer, and M. Bogdan. "Longitudinal Analysis of the Connectivity and Complexity of Complete Locked-in Syndrome Patients Electroencephalographic signal". In: *IEEE International Conference on Bioinformatics and Biomedicine, BIBM 2020, Virtual Event, South Korea, December 16-19, 2020*. Edited by Taesung Park, Young-Rae Cho, Xiaohua Hu, Illhoi Yoo, Hyun Goo Woo, Jianxin Wang, Julio C. Facelli, Seungyoon Nam, and Mingon Kang. IEEE, 2020, pages 958–962. DOI: 10.1109/BIBM49941.2020.9313391.

[Ada+21] V. S. Adama, S.-J. Wu, N. Nicolaou, and M. Bogdan. "Extendable Hybrid approach to detect conscious states in a CLIS patient using machine learning". In: *Simulation Notes Europe SNE* 31.4 (2021). In print.

[All+07] E. A. Allen, B. N. Pasley, T. Duong, and R. D. Freeman. "Transcranial Magnetic Stimulation Elicits Coupled Neural and Hemodynamic Consequences". In: *Science* 317.5846 (2007), pages 1918–1921. DOI: 10.1126/science.1146426.

[Alp09] E. Alpaydin. *Introduction to Machine Learning, Second Edition*. Adaptive Computation and Machine Learning series. The MIT Press, 2009. ISBN: 978-0262303262.

[AMK09] V. Abootalebi, M. H. Moradi, and M. A. Khalilzadeh. "A new approach for EEG feature extraction in P300-based lie detection". In: *Computer Methods and Programs in Biomedicine* 94.1 (2009), pages 48–57. DOI: 10.1016/j.cmpb.2008.10.001.

[Ann+20] J. Annen, I. Mertel, R. Xu, C. Chatelle, D. Lesenfants, R. Ortner, E. A. C. Bonin, C. Guger, S. Laureys, and F. Müller. "Auditory and Somatosensory P3 Are Complementary for the Assessment of Patients with Disorders of Consciousness". In: *Brain Sciences* 10.10 (2020). ISSN: 2076-3425. DOI: 10.3390/brainsci10100748. URL: https://www.mdpi.com/2076-3425/10/10/748.

[ANV20] A. S. Assiri, S. Nazir, and S. A. Velastin. "Breast Tumor Classification Using an Ensemble Machine Learning Method". In: *Journal of Imaging* 6.6 (2020). ISSN: 2313-433X. DOI: 10.3390/jimaging6060039.

[aut74] Unknown author(s). "A glossary of terms most commonly used by clinical electroencephalographers". In: *Electroencephalography and clinical neurophysiology* 37.5 (1974), 538—548. ISSN: 0013-4694. DOI: 10.1016/0013-4694(74)90099-6.

[Bau05] G. Bauer. "Coma and Brain Death". In: *Electroencephalography: Basic principles, Clinical applications, and related Fields*. Edited by E. Niedermeyer and F. L. da Silva. Fifth edition. Philadelphia, USA: Lippincott Williams & Wilkins (LWW), 2005, pages 167–192. DOI: 978-0-78-178942-4.

[BCP16] M. F. Bear, B. W. Connors, and M. A. Paradiso. *Neuroscience: Exploring the Brain*. 4th edition. Wolters Kluwer, 2016. ISBN: 978-0-7817-7817-6.

[Ben+07] M. Bensch, A. A. Karim, J. Mellinger, T. Hinterberger, M. Tangermann, M. Bogdan, W. Rosenstiel, and N. Birbaumer. "Nessi: an EEG-controlled web browser for severely paralyzed patients". In: *Computational intelligence and neuroscience* 71863 (2007). DOI: 10.1155/2007/71863.

[Ben+14] M. Bensch, S. Martens, S. Halder, J. Hill, F. Nijboer, A. Ramos, N. Birbaumer, M. Bogdan, B. Kotchoubey, W. Rosenstiel, B. Schölkopf, and A. Gharabaghi. "Assessing attention and cognitive function in completely locked-in state with event-related brain potentials and epidural electrocorticography". In: *Journal of Neural Engineering* 11.2 (Feb. 2014), page 026006. DOI: 10.1088/1741-2560/11/2/026006.

[Bez81] J. C. Bezdek. *Pattern Recognition with Fuzzy Objective Function Algorithms*. 1st edition. Springer, Boston, MA, 1981. ISBN: 978-0-306-40671-3. DOI: 10.1007/978-1-4757-0450-1.

[Bir+00] N. Birbaumer, A. Kubler, N. Ghanayim, T. Hinterberger, J. Perelmouter, J. Kaiser, I. Iversen, B. Kotchoubey, N. Neumann, and H. Flor. "The thought translation device (TTD) for completely paralyzed patients". In: *IEEE Transactions on Rehabilitation Engineering* 8.2 (2000), pages 190–193. DOI: 10.1109/86.847812.

[Bir+99] N. Birbaumer, N. Ghanayim, T. Hinterberger, I. Iversen, B. Kotchoubey, A. Kübler, J. Perelmouter, E. Taub, and H. Flor. "A spelling device for the paralysed". In: *Nature* 398 (1999), 297–298. DOI: 10.1038/18581.

[Bis06] C. Bishop. *Pattern Recognition and Machine Learning*. Springer, Jan. 2006. URL: https://www.microsoft.com/en-us/research/publication/pattern-recognition-machine-learning/.

[Bor+13] J. Borjigin, U. Lee, T. Liu, D. Pal, S. Huff, D. Klarr, J. Sloboda, J. Hernandez, M. M. Wang, and G. A. Mashour. "Surge of neurophysiological coherence and connectivity in the dying brain". In: *Proc Natl Acad Sci USA* 110.35 (2013), pages 14432–7. DOI: 10.1073/pnas.1308285110.

[Bou+20] P. Bourdillon, B. Hermann, M. Guénot, H. Bastuji, J. Isnard, J.-R. King, J. Sitt, and L. Naccache. "Brain-scale cortico-cortical functional connectivity in the delta-theta band is a robust signature of conscious states: an intracranial and scalp EEG study". In: *Scientific Reports* 10.14037 (2020).

[BPL08] M.-A. Bruno, F. Pellas, and S. Laureys. "Quality of Life in Locked-in Syndrome Survivors". In: *Yearbook of Intensive Care and Emergency Medicine*. Edited by J-L. (Ed.) Vincent. Springer-Verlag Berlin Heidelberg, 2008, pages 881–890. DOI: 10.1007/978-3-540-77290-3.

[BR15] T. Burns and R. Ramesh. *Combining complexity measures of EEG data: multiplying measures reveal previously hidden information - Script*. June 2015. DOI: 10.12688/f1000research.6590.1. URL: https://github.com/tfburns/MATLAB-functions-for-complexity-measures-of-one-dimensional-signals. Accessed: 03/12/2020.

[Bru+11] M.-A. Bruno, A. Vanhaudenhuyse, A. Thibaut, G. Moonen, and S. Laureys. "From unresponsive wakefulness to minimally conscious PLUS and functional locked-in syndromes: recent advances in our understanding of disorders of consciousness". In: *Journal of Neurology* 258.7 (2011), pages 1373–84. DOI: 10.1007/s00415-011-6114-x.

[BZ11] K. J. Blinowska and J. Zygierewicz. *Practical Biomedical Signal Analysis Using MATLAB*. 1st edition. CRC Press, Inc., 2011. ISBN: 978-1439812020.

[CF14] G. W. Corder and D. I. Foreman. "Comparing More Than Two Related Samples: The Friedman Test". In: *Nonparametric Statistics: A Step-by-Step Approach, 2nd Edition*. John Wiley & Sons, Inc., 2014. ISBN: 978-1-118-84031-3.

[Cha+17] U. Chaudhary, B. Xia, S. Silvoni, L. G. Cohen, and N. Birbaumer. "Brain–Computer Interface–Based Communication in the Completely Locked-In State". In: *PLOS Biology* 15.1 (Jan. 2017), pages 1–25. DOI: 10.1371/journal.pbio.1002593.

[Cha+18] U. Chaudhary, B. Xia, S. Silvoni, L. G. Cohen, and N. Birbaumer. "Correction: Brain-Computer Interface-Based Communication in the Completely Locked-In State". In: *PLOS Biology* 16.12 (Dec. 2018), pages 1–4. DOI: 10.1371/journal.pbio.3000089.

[Cha+20] U. Chaudhary, I. Vlachos, J. B. Zimmermann, A. Espinosa, A. Tonin, A. Jaramillo-Gonzalez, M. Khalili-Ardali, H. Topka, J. Lehmberg, G. M. Friehs, A. Woodtli, J. P. Donoghue, and N. Birbaumer. "Verbal Communication using Intracortical Signals in a Completely Locked In-Patient". In: *medRxiv* (2020). DOI: 10.1101/2020.06.10.20122408. eprint: https://www.medrxiv.org/content/early/2020/06/25/2020.06.10.20122408.full.pdf.

[Che+17] S. Chennu, J. Annen, S. Wannez, A. Thibaut, C. Chatelle, H. Cassol, G. Martens, C. Schnakers, O. Gosseries, D. Menon, and S. Laureys. "Brain networks predict metabolism, diagnosis and prognosis at the bedside in disorders of consciousness". In: *Brain* 140.8 (June 2017), pages 2120–2132. ISSN: 0006-8950. DOI: 10.1093/brain/awx163.

[Chi94] S. L. Chiu. "Fuzzy Model Identification Based on Cluster Estimation". In: *J. Intell. Fuzzy Syst.* 2.3 (May 1994), 267–278.

[CMKB21] U. Chaudhary, N. Mrachacz-Kersting, and N. Birbaumer. "Neuropsychological and neurophysiological aspects of brain-computer-interface (BCI) control in paralysis". In: *The Journal of Physiology* 599.9 (2021), pages 2351–2359. DOI: 10.1113/JP278775.

[Coh14] M. X. Cohen. *Analyzing neural time series data. Theory and practice*. The MIT Press, 2014. ISBN: 9780262319553. DOI: 10.7551/mitpress/9609.001.0001.

[Com+13] A. Combaz, C. Chatelle, A. Robben, G. Vanhoof, A. Goeleven, V. Thijs, M. M. Van Hulle, and S. Laureys. "A comparison of two spelling Brain-Computer Interfaces based on visual P3 and SSVEP in Locked-In Syndrome". In: *PloS one* 8.9 (2013), e73691. ISSN: 1932-6203. DOI: 10.1371/journal.pone.0073691.

[DHI05] B. Dworetzky, S. Herman, and W. O. Tatum IV. "Artifacts of Recordings". In: *Electroencephalography: Basic principles, Clinical applications, and related Fields*. Edited by E. Niedermeyer and F. L. da Silva. Fifth edition. Philadelphia, USA: Lippincott Williams & Wilkins (LWW), 2005, pages 167–192. DOI: 978-0-78-178942-4.

[Dro06] W. van Drongelen. *Signal Processing for Neuroscientists. An Introduction to the Analysis of Physiological Signals*. 1st edition. Academic Press, 2006. ISBN: 9780080467757.

[Eag+18] S. L. Eagleman, D. A. Vaughn, D. R. Drover, C. M. Drover, M. S. Cohen, N. T. Ouellette, and M. B. MacIver. "Do Complexity Measures of Frontal EEG Distinguish Loss of Consciousness in Geriatric Patients Under Anesthesia?" In: *Frontiers in Neuroscience* 12 (2018), page 645. ISSN: 1662-453X. DOI: 10.3389/fnins.2018.00645.

[Eng+18] D. A. Engemann, F. Raimondo, J.-R. King, B. Rohaut, G. Louppe, F. Faugeras, J. Annen, H. Cassol, O. Gosseries, D. Fernandez-Slezak, S. Laureys, L. Naccache, S. Dehaene, and J. D. Sitt. "Robust EEG-based cross-site and cross-protocol classification of states of consciousness". In: *Brain* 141.11 (Oct. 2018), pages 3179–3192. ISSN: 0006-8950. DOI: 10.1093/brain/awy251.

[FDC13] R. Formisano, M. D'Ippolito, and S. Catani. "Functional locked-in syndrome as recovery phase of vegetative state". In: *Brain Injury* 27.11 (2013), pages 1332–1332. DOI: 10.3109/02699052.2013.809555.

[FG20] M. B. Ferraro and P. Giordani. "Soft clustering". In: *WIREs Computational Statistics* 12.1 (2020), e1480. DOI: 10.1002/wics.1480.

[Fin19] M. Finetti. *Scientific Misconduct: DFG Imposes Sanctions Against Brain Researcher Niels Birbaumer and Research Associate*. Sept. 2019. URL: https://www.dfg.de/en/service/press/press_releases/2019/press_release_no_46/index.html. Accessed: 20/05/2021.

[Fis36] R. A. Fisher. "The use of multiple measurements in taxonomic problems". In: *Annals of Eugenics* 7.2 (1936), 179–188. DOI: 10.1111/j.1469-1809.1936.tb02137.x.

[Fre+19] Z. V. Freudenburg, M. P. Branco, S. Leinders, B. H. van der Vijgh, E. G. M. Pels, T. Denison, L. H. van den Berg, K. J. Miller, E. J. Aarnoutse, N. F. Ramsey, and M. J. Vansteensel. "Sensorimotor ECoG Signal Features for BCI Control: A Comparison Between People With Locked-In Syndrome and Able-Bodied Controls". In: *Frontiers in Neuroscience* 13 (2019), page 1058. ISSN: 1662-453X. DOI: 10.3389/fnins.2019.01058.

[Gór+21] U. Górska, A. Rupp, T. Celikel, and B. Englitz. "Assessing the state of consciousness for individual patients using complex, statistical stimuli". In: *NeuroImage: Clinical* 29 (2021), page 102471. ISSN: 2213-1582. DOI: 10.1016/j.nicl.2020.102471.

[Gao+19] J. Gao, M. Wu, Y. Wu, and P. Liu. "Emotional consciousness preserved in patients with disorders of consciousness?" In: *Neurol Sci* 40.7 (2019), pages 1409–1418. DOI: 10.1007/s10072-019-03848-w.

[Gaz99] M. S. Gazzaniga. *The new Cognitive Neurosciences*. Second Edition. The MIT Press, 1999. ISBN: 978-0262071956.

[GIM18] M. S. Gazzaniga, R. B. Ivry, and G. R. Mangun. *Cognitive Neuroscience: The Biology of the Mind*. 5th Edition. W. W. Norton & Company, 2018. ISBN: 978-0393603170.

[GM08] J. T. Giacino and R. Malone. "The Vegetative and Minimally Conscious States". In: *Disorders of Consciousness*. Edited by Young and Wijdicks. Volume 90. Handbook of Clinical Neurology. Elsevier, 2008, pages 99–111. DOI: https://doi.org/10.1016/S0072-9752(07)01706-X.

[Gol+11] A. M. Goldfine, J. D. Victor, M. M. Conte, J. C. Bardin, and N. D. Schiff. "Determination of awareness in patients with severe brain injury using EEG power spectral analysis". In: *Clinical Neurophysiology* 122.11 (2011), pages 2157–2168. ISSN: 1388-2457. DOI: 10.1016/j.clinph.2011.03.022.

[Gol13] A. K. Golińska. "Poincaré Plots in Analysis of Selected Biomedical Signals". In: *Studies in Logic, Grammar and Rethoric* 35.48 (2013). DOI: 10.2478/slgr-2013-0031.

[Gos+09] O. Gosseries, M.-A. Bruno, A. Vanhaudenhuyse, S. Laureys, and C. Schnakers. "Consciousness in the Locked-in Syndrome". In: *The Neurology of Consciousness*. Edited by S. Laureys and G. Tononi. San Diego: Academic Press, 2009, pages 191–203. ISBN: 978-0-12-374168-4. DOI: 10.1016/B978-0-12-374168-4.00015-0.

[Gos+11] O. Gosseries, A. Vanhaudenhuyse, M.-A. Bruno, A. Demertzi, C. Schnakers, M. M. Boly, A. Maudoux, G. Moonen, and S. Laureys. "Disorders of Consciousness: Coma, Vegetative and Minimally Conscious States". In: *States of Consciousness*. Edited by D. Cvetkovic and I. Cosic. The Frontiers Collection. Berlin, Heidelberg: Springer, 2011, pages 29–55. DOI: 10.1007/978-3-642-18047-7_2.

[Gos+14a] O. Gosseries, H. Di, S. Laureys, and M. Boly. "Measuring consciousness in severely damaged brains." In: *Annu Rev Neurosci.* 37.4 (2014), pages 457–78. DOI: 10.1146/annurev-neuro-062012-170339.

[Gos+14b] O. Gosseries, A. Thibaut, M. Boly, M. Rosanova, M. Massimini, and S. Laureys. "Assessing consciousness in coma and related states using transcranial magnetic stimulation combined with electroencephalography". In: *Annales Françaises d'Anesthésie et de Réanimation* 33.2 (2014), pages 65–71. ISSN: 0750-7658. DOI: 10.1016/j.annfar.2013.11.002.

[Gug+17] C. Guger, R. Spataro, B. Z. Allison, A. Heilinger, R. Ortner, W. Cho, and V. La Bella. "Complete Locked-in and Locked-in Patients: Command Following Assessment and Communication with Vibro-Tactile P300 and Motor Imagery Brain-Computer Interface Tools". In: *Frontiers in Neurology* 251.11 (2017). DOI: 10.3389/fnins.2017.00251.

[Han+19] C.-H. Han, Y.-W. Kim, D. Y. Kim, S. H. Kim, Z. Nenadic, and C.-H. Im. "Electroencephalography-based endogenous brain–computer interface for online communication with a completely locked-in patient". In: *J NeuroEngineering Rehabil* 16.18 (2019). DOI: 10.1186/s12984-019-0493-0.

[Hei+18] A. Heilinger, R. Ortner, V. La Bella, Z. R. Lugo, C. Chatelle, S. Laureys, R. Spataro, and C. Guger. "Performance Differences Using a Vibro-Tactile P300 BCI in LIS-Patients Diagnosed With Stroke and ALS". In: *Frontiers in Neuroscience* 12 (2018), page 514. DOI: 10.3389/fnins.2018.00514.

[Hen+15] T. S. Henriques, S. Mariani, A. Burykin, F. Rodrigues, T. F. Silva, and A. L. Goldberger. "Multiscale Poincaré plots for visualizing the structure of heartbeat time series". In: *BMC Med Inform Decis Mak* 16.17 (2015). DOI: 10.1186/s12911-016-0252-0.

[Hit15] S. Hitziger. "Modeling the variability of electrical activity in the brain". PhD thesis. 2015. URL: https://tel.archives-ouvertes.fr/tel-01175851.

[HMB03] T. Hinterberger, J. Mellinger, and N. Birbaumer. "The Thought Translation Device: structure of a multimodal brain-computer communication system". In: *First International IEEE EMBS Conference on Neural Engineering, 2003. Conference Proceedings.* 2003, pages 603–606. DOI: 10.1109/CNE.2003.1196900.

[HMS14] K. Hayashi, N. Mukai, and T. Sawa. "Poincaré analysis of the electroencephalogram during sevoflurane anesthesia". In: *Clinical Neurophysiology* 126 (2014). DOI: 10.1016/j.clinph.2014.04.019.

[HWC14] M. Hollander, D. A. Wolfe, and E. Chicken. *Nonparametric Statistical Methods*. 2nd edition. John Wiley & Sons, Inc., 2014. ISBN: 978-1-118-55329-9.

[Imp+19] L. S. Imperatori, M. Betta, L. Cecchetti, A. Canales-Johnson, E. Ricciardi, F. Siclari, P. Pietrini, S. Chennu, and G. Bernardi. "EEG functional connectivity metrics wPLI and wSMI account for distinct types of brain functional interactions". In: *Sci Rep* 8894 (9 2019). DOI: 10.1038/s41598-019-45289-7.

[IRV14] S. A. Imtiaz and E. Rodriguez-Villegas. "A Low Computational Cost Algorithm for REM Sleep Detection Using Single Channel EEG". In: *Ann Biomed Eng* 42 (2014), 2344–2359. DOI: 10.1007/s10439-014-1085-6.

[Jam+13] G. James, D. Witten, T. Hastie, and R. Tibshirani. "Unsupervised Learning". In: *An Introduction to Statistical Learning*. Volume 103. Springer Texts in Statistics. New York, NY: Springer, 2013. ISBN: 978-1-4614-7137-0. DOI: 10.1007/978-1-4614-7138-7_10.

[Jas58] H. H. Jasper. "The ten-twenty electrode system of the International Federation". In: *Electroenceph. clin. Neurophysiol.* 10 (1958), pages 371–375. DOI: 10.1371/journal.pone.0190458.

[JR20] R. Jain and A. G. Ramakrishnan. "Electrophysiological and Neuroimaging Studies – During Resting State and Sensory Stimulation in Disorders of Consciousness: A Review". In: *Frontiers in Neuroscience* 14 (2020), page 987. ISSN: 1662-453X. DOI: 10.3389/fnins.2020.555093.

[K+01] A. Kübler, B. Kotchoubey, J. Kaiser, J. R. Wolpaw, and N. Birbaumer. "Brain-computer communication: Unlocking the locked in". In: *Psychological Bulletin* 127.3 (2001), pages 358–375. DOI: 10.1037/0033-2909.127.3.358.

[K+09] A. Kübler, A. Furdea, S. Halder, E. M. Hammer, F. Nijboer, and B. Kotchoubey. "A brain-computer interface controlled auditory event-related potential (p300) spelling system for locked-in patients". In: *Ann N Y Acad Sci.* 1157 (2009), pages 90–100. DOI: 10.1111/j.1749-6632.2008.04122.x.

[Kü20] A. Kübler. "The history of BCI: From a vision for the future to real support for personhood in people with locked-in syndrome". In: *Neuroethics* 13 (2020), 163–180. DOI: 10.1007/s12152-019-09409-4.

[KB08] A. Kübler and N. Birbaumer. "Brain–computer interfaces and communication in paralysis: Extinction of goal directed thinking in completely paralysed patients?" In: *Clinical Neurophysiology* 119.11 (2008), pages 2658–2666. ISSN: 1388-2457. DOI: 10.1016/j.clinph.2008.06.019.

[KC16] S. Kapil and M. Chawla. "Performance evaluation of K-means clustering algorithm with various distance metrics". In: *2016 IEEE 1st International Conference on Power Electronics, Intelligent Control and Energy Systems (ICPEICES)*. 2016, pages 1–4. DOI: 10.1109/ICPEICES.2016.7853264.

[KN05] A. Kübler and N. Neumann. "Brain-computer interfaces–the key for the conscious brain locked into a paralyzed body". In: *Prog Brain Res.* 150 (2005), pages 513–25. DOI: 10.1016/S0079-6123(05)50035-9.

[Koc04] C. Koch. *The Quest for Consciousness: A Neurobiological Approach*. Roberts and Company, 2004. ISBN: 9780974707709.

[KSD09] A. S. Kayser, F. T. Sun, and M. D'Esposito. "A comparison of Granger causality and coherency in fMRI-based analysis of the motor system". In: *Human Brain Mapping* 30.11 (2009), pages 3475–3494. DOI: 10.1002/hbm.20771.

[KSF13] J.-R. King, J. D. Sitt, and S. Faugeras. "Information Sharing in the Brain Indexes Consciousness in Non-communicative Patients". In: *Current Biology* 23.19 (2013), pages 1914–1919. DOI: 10.1016/j.cub.2013.07.075.

[Lau+05] S. Laureys, F. Pellas, P. Van Eeckhout, S. Ghorbel, C. Schnakers, F. Perrin, J. Berré, M.-E. Faymonville, K.-H. Pantke, F. Damas, M. Lamy, G. Moonen, and S. Goldman. "The locked-in syndrome : what is it like to be conscious but paralyzed and voiceless?" In: *Prog Brain Res.* 150 (2005), pages 495–511. DOI: 10.1016/S0079-6123(05)50034-7.

[LBMM15] U. Lee, S. Blain-Moraes, and G. A. Mashour. "Assessing levels of consciousness with symbolic analysis". In: *Phil. Trans. R. Soc. A.* 373.20140117 (2015). DOI: 10.1098/rsta.2014.0117.

[LCERDM02] J. Leon-Carrión, P. van Eeckhout, and M. del Rosario Domínguez-Morales. "Review of subject: The locked-in syndrome: a syndrome looking for a therapy". In: *Brain Injury* 16.7 (2002), pages 555–569. DOI: 10.1080/02699050110119466.

[Les+14] D. Lesenfants, D. Habbal, Z. Lugo, M. Lebeau, P. Horki, E. Amico, C. Pokorny, F. Gómez, A. Soddu, G. Müller-Putz, S. Laureys, and Q. Noirhomme. "An independent SSVEP-based brain–computer interface in locked-in syndrome". In: *Journal of Neural Engineering* 11.3 (May 2014), page 035002. DOI: 10.1088/1741-2560/11/3/035002.

[Les+15] D. Lesenfants, C. Chatelle, S. Laureys, and Q. Noirhomme. "Interfaces cerveau-ordinateur, locked-in syndrome et troubles de la conscience". In: *Med Sci (Paris)* 31.10 (2015), pages 904–911. DOI: 10.1051/medsci/20153110017. URL: https://doi.org/10.1051/medsci/20153110017.

[LMT10] M. Lukowicz, K. Matuszak, and A. D. Talar. "A misdiagnosed patient: 16 years of locked-in syndrome, the influence of rehabilitation". In: *Med Sci Monit* 16.2 (2010), pages 18–23.

[Lug+14] Z. R. Lugo, J. Rodriguez, A. Lechner, R. Ortner, I. S. Gantner, S. Laureys, Q. Noirhomme, and C. Guger. "A vibrotactile p300-based brain-computer interface for consciousness detection and communication." In: *Clin EEG Neurosci.* 45.1 (2014), pages 14–21. DOI: 10.1177/1550059413505533.

[LZ76] A. Lempel and J. Ziv. "On the Complexity of Finite Sequences". In: *IEEE Transactions on Information Theory* 22.1 (1976), pages 75–81. DOI: 10.1109/TIT.1976.1055501.

[Mal+13] U. Malinowska, C. Chatelle, M. A. Bruno, Q. Noirhomme, S. Laureys, and Durka P. J. "Electroencephalographic profiles for differentiation of disorders of consciousness". In: *Biomed Eng Online* 12.109 (2013). DOI: 10.1186/1475-925X-12-109.

[Mal+19] A. Malekshahi, U. Chaudhary, A. Jaramillo-Gonzalez, A. Lucas Luna, A. Rana, A. Tonin, N. Birbaumer, and S. Gais. "Sleep in the completely locked-in state (CLIS) in amyotrophic lateral sclerosis". In: *Sleep* 42.12 (2019), pages 1–8. DOI: 10.1093/sleep/zsz185.

[Mar+21] Y. Maruyama, N. Yoshimura, A. Rana, A. Malekshahi, A. Tonin, A. Jaramillo-Gonzalez, N. Birbaumer, and U. Chaudhary. "Electroencephalography of completely locked-in state patients with amyotrophic lateral sclerosis". In: *Neuroscience Research* 162 (2021), pages 45–51. DOI: 10.1016/j.neures.2020.01.013.

[Mat21] Mathworks. *Cluster Gaussian Mixture Data Using Soft Clustering*. Statistics and Machine Learning Toolbox™User's Guide. The MathWorks, Inc., 2021. URL: https://de.mathworks.com/help/stats/cluster-gaussian-mixture-data-using-soft-clustering.html.

[McC04] J. McCarthy. *What is Artificial Intelligence?* Nov. 2004. URL: https://homes.di.unimi.it/borghese/Teaching/AdvancedIntelligentSystems/Old/IntelligentSystems_2008_2009/Old/IntelligentSystems_2005_2006/Documents/Symbolic/04_McCarthy_whatisai.pdf. Accessed: 17/08/2021.

[Mil07] G. Miller. "Uncovering the Magic in Magnetic Brain Stimulation". In: *Science* 317.5846 (2007), pages 1846–1846. DOI: 10.1126/science.317.5846.1846a.

[MLO10] M. M. Monti, S. Laureys, and A. M. Owen. "The vegetative state". In: *BMJ* 341 (2010). ISSN: 0959-8138. DOI: 10.1136/bmj.c3765.

[MP00] G. McLachlan and D. Peel. *Finite Mixture Models*. John Wiley & Sons, Inc., 2000. ISBN: 9780471006268. DOI: 10.1002/0471721182.

[Mur+11] A. R. Murguialday, J. Hill, M. Bensch, S. Martens, S. Halder, and F. Nijboer. "Transition from the locked in to the completely locked-in state: A physiological analysis". In: *Clinical Neurophysiology* 122.5 (2011), pages 925–933. DOI: 10.1016/j.clinph.2010.08.019.

[Mut13] S. Muthukumaraswamy. "High-frequency brain activity and muscle artifacts in MEG/EEG: A review and recommendations". In: *Frontiers in Human Neuroscience* 7 (2013), page 138. ISSN: 1662-5161. DOI: 10.3389/fnhum.2013.00138.

[Nak+17] T. Nakamura, V. Goverdovsky, M. J. Morrell, and D. P. Mandic. "Automatic Sleep Monitoring Using Ear-EEG". In: *IEEE Journal of Translational Engineering in Health and Medicine* 5 (2017), pages 1–8.

[Nie05] E. Niedermeyer. "The normal EEG of the waking adult". In: *Electroencephalography: Basic principles, Clinical applications, and related Fields*. Edited by E. Niedermeyer and F. L. da Silva. Fifth edition. Philadelphia, USA: Lippincott Williams & Wilkins (LWW), 2005, pages 167–192. DOI: 978-0-78-178942-4.

[NIN13] NINDS. *Amyotrophic Lateral Sclerosis (ALS) Fact Sheet*. June 2013. URL: https://www.ninds.nih.gov/Disorders/Patient-Caregiver-Education/Fact-Sheets/Amyotrophic-Lateral-Sclerosis-ALS-Fact-Sheet. Accessed: 26/06/2021.

[Nol+04] G. Nolte, O. Bai, L. Wheaton, Z. Mari, S. Vorbach, and M. Hallett. "Identifying true brain interaction from EEG data using the imaginary part of coherency". In: *Clinical Neurophysiology* 115.10 (2004), pages 2292–2307. DOI: 10.1016/j.clinph.2004.04.029.

[NS05] K. Najarian and R. Splinter. *Biomedical Signal and Image Processing*. 1st Edition. CRC Press, 2005. ISBN: 978-0849320996.

[NS06] P. L. Nunez and R. Srinivasan. *Electrical Fields of the Brain. The Neurophysics of EEG*. Second Edition. Oxford University Press, 2006. ISBN: 978-0-19-505038-7.

[Nuw+98] M. R. Nuwer, G. Comi, R. Emerson, A. Fuglsang-Frederiksen, J.-M. Guérit, H. Hinrichs, A. Ikeda, F. J. C. Luccas, and P. Rappelsburger. "IFCN standards for digital recording of clinical EEG". In: *Electroencephalography and Clinical Neurophysiology* 106 (3 1998), pages 259–261. DOI: 10.1016/S0013-4694(97)00106-5.

[Oke+14] B S. Oken, U. Orhan, B. Roark, D. Erdogmus, A. Fowler, A. Mooney, B. Peters, M. Miller, and M. B. Fried-Oken. "Brain-computer interface with language model-electroencephalography fusion for locked-in syndrome". English (US). In: *Neurorehabilitation and Neural Repair* 28.4 (May 2014), pages 387–394. ISSN: 1545-9683. DOI: 10.1177/1545968313516867.

[Oos+01] R. Oostenveld, P. Fries, E. Maris, and J.-M. Schoffelen. "FieldTrip: Open Source Software for Advanced Analysis of MEG, EEG and Invasive Electrophysiological Data". In: *Computational Intelligence and Neuroscience* (2001). DOI: 10.1155/2011/156869.

[Pal+15] D. Pal, V. S. Hambrecht-Wiedbusch, B. H. Silverstein, and G. A. Mashour. "Electroencephalographic coherence and cortical acetylcholine during ketamine-induced unconsciousness". In: *British Journal of Anaesthesia* 114.6 (2015), pages 979–989. ISSN: 0007-0912. DOI: 10.1093/bja/aev095.

[Pan+14] J. Pan, Q. Xie, Y. He, F. Wang, H. Di, S. Laureys, R. Yu, and Y. Li. "Detecting awareness in patients with disorders of consciousness using a hybrid brain-computer interface". In: *Journal of Neural Engineering* 11.5 (2014). DOI: 10.1088/1741-2560/11/5/056007.

[Pan+18] J. Pan, Q. Xie, H. Huang, Y. He, Y. Sun, R. Yu, and Y. Li. "Emotion-Related Consciousness Detection in Patients With Disorders of Consciousness Through an EEG-Based BCI System". In: *Frontiers in Human Neuroscience* 12 (2018), page 198. DOI: 10.3389/fnhum.2018.00198.

[Per+06] F. Perrin, C. Schnakers, M. Schabus, C. Degueldre, S. Goldman, S. Brédart, M.-E. Faymonville, M. Lamy, G. Moonen, A. Luxen, P. Maquet, and S. Laureys. "Brain Response to One's Own Name in Vegetative State, Minimally Conscious State, and Locked-in Syndrome". In: *Archives of Neurology* 63.4 (Apr. 2006), pages 562–569. ISSN: 0003-9942. DOI: 10.1001/archneur.63.4.562.

[Pet+13] G. Peters, F. Crespo, P. Lingras, and R. Weber. "Soft clustering – Fuzzy and rough approaches and their extensions and derivatives". In: *International Journal of Approximate Reasoning* 54.2 (2013), pages 307–322. ISSN: 0888-613X. DOI: 10.1016/j.ijar.2012.10.003.

[PN05] G. Pfurtscheller and C. Neuper. "EEG-based Brain-Computer Interfaces". In: *Electroencephalography: Basic principles, Clinical applications, and related Fields*. Edited by E. Niedermeyer and F. L. da Silva. Fifth edition. Philadelphia, USA: Lippincott Williams & Wilkins (LWW), 2005, pages 167–192. DOI: 978-0-78-178942-4.

[Pos+07] J. B. Posner, C. B. Saper, N. Schiff, and F. Plum. *Plum and Posner's Diagnosis of Stupor and Coma.* 4th edition. Oxford University Press, 2007. ISBN: 0195321316.

[PP04] J. N. Parker and P. M. Parker. *The Official Patient's Sourcebook on Locked-In Syndrome: A Revised and Updated Directory for the Internet Age*. Revised, Updated Edition. ICON Health Publications, 2004. ISBN: 978-0597841941.

[Pri81] M. B. Priestley. *Spectral Analysis and Time Series, Two-Volume Set: Volumes I and II*. Both volumes bound together. Elsevier Science, 1981. ISBN: 9780125649223.

[Pul+20] R. M. Pullon, L. Yan, J. W. Sleigh, and C. E. Warnaby. "Granger Causality of the Electroencephalogram Reveals Abrupt Global Loss of Cortical Information Flow during Propofol-induced Loss of Responsiveness". In: *Anesthesiology* 133.4 (Oct. 2020), pages 774–786. ISSN: 0003-3022. DOI: 10.1097/ALN.0000000000003398.

[QN05] L. F. Quesney and E. Niedermeyer. "Electrocorticography". In: *Electroencephalography: Basic principles, Clinical applications, and related Fields*. Edited by E. Niedermeyer and F L. da Silva. Fifth edition. Philadelphia, USA: Lippincott Williams & Wilkins (LWW), 2005, pages 167–192. DOI: 978-0-78-178942-4.

[Ram+80] I. J. Rampil, F. J. Sasse, N. T. Smith, B. H. Hoff, and D. C. Flemming. "SPECTRAL EDGE FREQUENCY - A NEW CORRELATE OF ANESTHETIC DEPTH". In: *Anesthesiology* 53.3 Suppl (Sept. 1980), S12–S12. ISSN: 0003-3022. DOI: 10.1097/00000542-198009001-00012.

[Rei05] E L. Reilly. "EEG recording and operation of the apparatus". In: *Electroencephalography: Basic principles, Clinical applications, and related Fields*. Edited by E. Niedermeyer and F. L. da Silva. Fifth edition. Philadelphia, USA: Lippincott Williams & Wilkins (LWW), 2005, pages 139–160. DOI: 978-0-78-178942-4.

[Rij19] Dr. K. G. Rijkhoek. *Untersuchungskommission stellt wissenschaftliches Fehlverhalten durch Tübinger Hirnforscher fest*. June 2019. URL: https://uni-tuebingen.de/en/university/news-and-publications/press-releases/press-releases/article/untersuchungskommission-stellt-wissenschaftliches-fehlverhalten-durch-tuebinger-hirnforscher-fest/. Accessed: 20/05/2021.

[Roh+17] B. Rohaut, F. Raimondo, D. Galanaud, M. Valente, J. D. Sitt, and L. Naccache. "Probing consciousness in a sensory-disconnected paralyzed patient". In: *Brain Injury* 31.10 (2017), pages 1398–1403. DOI: 10.1080/02699052.2017.1327673.

[Rou+15] M.-C. Rousseau, K. Baumstarck, M. Alessandrini, V. Blandin, T. B. de Villemeur, and P. Auquier. "Quality of life in patients with locked-in syndrome: Evolution over a 6-year period". In: *Orphanet J Rare Dis* 10.88 (2015). DOI: 10.1186/s13023-015-0304-z.

[Sak+16] D. Sakellariou, A. M. Koupparis, V. Kokkinos, M. Koutroumanidis, and G. K. Kostopoulos. "Connectivity Measures in EEG Microstructural Sleep Elements". In: *Frontiers in Neuroinformatics* 10 (Feb. 2016). DOI: 10.3389/fninf.2016.00005.

[Sat+15] D. Sattin, L. Minati, D. Rossi, V. Covelli, A. M. Giovannetti, C. Rosazza, A. Bersano, A. Nigri, and M. Leonardi. "The Coma Recovery Scale Modified Score". In: *International Journal of Rehabilitation Research* 38.4 (2015), pages 350–356. DOI: 10.1097/MRR.0000000000000135.

[Sat+19] R. Satti, N.-U.-H. Abid, M. Bottaro, M. De Rui, M. Garrido, M. R. Raoufy, S. Montagnese, and A. R. Mani. "The Application of the Extended Poincaré Plot in the Analysis of Physiological Variabilities". In: *Frontiers in Physiology* 116.10 (2019). DOI: 10.3389/fphys.2019.00116.

[SB18] R. S. Sutton and A. G. Barto. *Reinforcement Learning: An Introduction, Second edition*. Adaptive Computation and Machine Learning series. Bradford Books, 2018. ISBN: 978-0262039246.

[SBL21] S. W. A. Sherazi, J.-W. Bae, and J. Y. Lee. "A soft voting ensemble classifier for early prediction and diagnosis of occurrences of major adverse cardiovascular events for STEMI and NSTEMI during 2-year follow-up in patients with acute coronary syndrome". In: *PLOS ONE* 16.6 (June 2021), pages 1–20. DOI: 10.1371/journal.pone.0249338.

[SBS18] P. Schober, C. Boer, and L. A. Schwarte. "Correlation Coefficients: Appropriate Use and Interpretation." In: *Anesth Analg.* 126.5 (2018), pages 1763–1768. DOI: 10.1213/ANE.0000000000002864.

[SC13] S. Sanei and J. A. Chambers. *EEG Signal Processing*. Wiley, 2013. ISBN: 9781118691236.

[Sch+09] C. Schnakers, F. Perrin, M. Schabus, R. Hustinx, S. Majerus, G. Moonen, M. Boly, A. Vanhaudenhuyse, M. A. Bruno, and S. Laureys. "Detecting consciousness in a total locked-in syndrome: An active event-related paradigm". English. In: *Neurocase* 15.4 (July 2009), pages 271–277. ISSN: 1355-4794. DOI: 10.1080/13554790902724904.

[Sch+15] M. Schartner, A. Seth, Q. Noirhomme, M. Boly, M.-A. Bruno, S. Laureys, and A. Barrett. "Complexity of Multi-Dimensional Spontaneous EEG Decreases during Propofol Induced General Anaesthesia". In: *PLOS ONE* 10.8 (Aug. 2015), pages 1–21. DOI: 10.1371/journal.pone.0133532.

[Sec+21] A. Secco, A. Tonin, A. Rana, A. Jaramillo-Gonzalez, M. Khalili-Ardali, N. Birbaumer, and U. Chaudhary. "EEG power spectral density in locked-in and completely locked-in state patients: a longitudinal study". In: *Cogn Neurodyn* 15 (2021), pages 473–480. ISSN: 1388-2457. DOI: 10.1007/s11571-020-09639-w.

[Ser+17] C. Sergent, F. Faugeras, B. Rohaut, F. Perrin, M. Valente, C. Tallon-Baudry, L. Cohen, and L. Naccache. "Multidimensional cognitive evaluation of patients with disorders of consciousness using EEG: A proof of concept study". In: *NeuroImage. Clinical* 13 (2017), 455—469. ISSN: 2213-1582. DOI: 10.1016/j.nicl.2016.12.004.

[Sil05] F. L. da Silva. "EEG Analysis: Theory and Practice". In: *Electroencephalography: Basic principles, Clinical applications, and related Fields*. Edited by E. Niedermeyer and F. L. da Silva. Fifth edition. Philadelphia, USA: Lippincott Williams & Wilkins (LWW), 2005, pages 167–192. DOI: 978-0-78-178942-4.

[SM05] P. Stoica and R. L. Moses. *Spectral Analysis of Signals*. Prentice Hall, 2005. ISBN: 0-13-113956-8.

[SM10] G. Schalk and J. Mellinger. *A Practical Guide to Brain-Computer Interfacing with BCI2000*. Springer, 2010. ISBN: 978-1-84996-091-5. DOI: 10.1007/978-1-84996-092-2.

[Soe+13] S. R. Soekadar, J. Born, N. Birbaumer, M. Bensch, S. Halder, and A. R. Murguialday. "Fragmentation of slow wave sleep after onset of complete locked-in state". In: *Journal of clinical sleep medicine* 9.9 (2013), pages 951–953. DOI: 10.5664/jcsm.3002.

[Spu19] M. Spueler. "Questioning the evidence for BCI-based communication in the complete locked-in state". In: *PLOS Biology* 17.4 (Apr. 2019), pages 1–5. DOI: 10.1371/journal.pbio.2004750.

[SS12] D. Stahl and H. Sallis. "Model-based cluster analysis". In: *WIREs Computational Statistics* 4.4 (2012), pages 341–358. DOI: 10.1002/wics.1204.

[Sub19] A. Subasi. "Chapter 2 - Biomedical Signals". In: *Practical Guide for Biomedical Signals Analysis Using Machine Learning Techniques*. Edited by A. Subasi. Academic Press, 2019, pages 27–87. ISBN: 978-0-12-817444-9. DOI: 10.1016/B978-0-12-817444-9.00002-7.

[Tay02] J. G. Taylor. "Neural models of consciousness". In: *The Handbook of brain theory and neural networks*. Edited by M. A. Arbib. Second Edition. The MIT Press, 2002. ISBN: 978-0262011976.

[Ton+16] G. Tononi, M. Boly, O. Gosseries, and S. Laureys. "Chapter 25 - The Neurology of Consciousness: An Overview". In: *The Neurology of Conciousness (Second Edition)*. Edited by S. Laureys, O. Gosseries, and G. Tononi. Second Edition. San Diego: Academic Press, 2016, pages 407–461. ISBN: 978-0-12-800948-2. DOI: 10.1016/B978-0-12-800948-2.00025-X.

[Tou+19] C. Touchard, J. Cartailler, C. Levé, P. Parutto, C. Buxin, L. Garnot, J. Matéo, N. Kubis, A. Mebazaa, E. Gayat, and F. Vallée. "EEG power spectral density under Propofol and its association with burst suppression, a marker of cerebral fragility". In: *Clinical Neurophysiology* 130.8 (2019), pages 1311–1319. ISSN: 18728952. DOI: 10.1016/j.clinph.2019.05.014.

[TR15] B. Thomas and R. Rajan. "Combining complexity measures of EEG data: multiplying measures reveal previously hidden information". In: *F1000Research* 137.4 (June 2015). DOI: 10.12688/f1000research.6590.1.

[Van+09] C. Vance et al. "Mutations in FUS, an RNA processing protein, cause familial amyotrophic lateral sclerosis type 6". English. In: *Science (New York, N.Y.)* 323.5918 (Feb. 2009), pages 1208–1211. ISSN: 0036-8075. DOI: 10.1126/science.1165942.

[Van+16] M. J. Vansteensel, E. G. M. Pels, M. G. Bleichner, M. P. Branco, T. Denison, Z. V. Freudenburg, P. Gosselaar, S. Leinders, T. H. Ottens, M. A. Van Den Boom, P. C. Van Rijen, E. J. Aarnoutse, and N. F. Ramsey. "Fully Implanted Brain–Computer Interface in a Locked-In Patient with ALS". In: *New England Journal of Medicine* 375.21 (2016), pages 2060–2066. DOI: 10.1056/NEJMoa1608085.

[Van+18] A. Vanhaudenhuyse, V. Charland-Verville, A. Thibaut, C. Chatelle, J.-F. L. Tshibanda, and A. Maudoux. "Conscious While Being Considered in an Unresponsive Wakefulness Syndrome for 20 Years". In: *Frontiers in Neurology* 9 (2018), page 671. DOI: 10.3389/fneur.2018.00671.

[vWL15] L. E. H. van Dokkum, T. Ward, and I. Laffont. "Brain computer interfaces for neurorehabilitation – its current status as a rehabilitation strategy post-stroke". In: *Annals of Physical and Rehabilitation Medicine* 58.1 (2015). Brain Computer Interfaces (BCIs) / Coordinated by Jacques Luauté and Isabelle Laffont, pages 3–8. ISSN: 1877-0657. DOI: 10.1016/j.rehab.2014.09.016.

[Wan+13] H. Wang, Y. Yang, H. Wang, and D. Chen. "Soft-Voting Clustering Ensemble". In: *Multiple Classifier Systems. MCS 2013*. Edited by Kittler J. (eds) Zhou Z. H. Roli F. Volume 7872. Lecture Notes in Computer Science. Berlin, Heidelberg: Springer, 2013. DOI: 10.1007/978-3-642-38067-9_27.

[Wan+15] R. Wang, J. Wang, H. Yu, X. Wei, C. Yang, and B. Deng. "Power spectral density and coherence analysis of Alzheimer's EEG". In: *Cogn Neurodyn* 9 (2015), 291–304. DOI: 10.1007/s11571-014-9325-x.

[Wan+18] J. Wang, H. Di, N. Hu, and S. Laureys. "Circadian Rhythm of Patients with Disorders of Consciousness". In: *Open Access J Neurol Neurosurg* 9.3 (2018). DOI: 10.19080/OAJNN.2018.09.555763.

[WB21] S.-J. Wu and M. Bogdan. "Application of Sample Entropy to Analyze Consciousness in CLIS Patients". In: *Sensor Networks and Signal Processing*. Volume 176. Smart Innovation, Systems and Technologies. Singapore: Springer, 2021, pages 521–531. DOI: 10.1007/978-981-15-4917-5_37.

[Wel67] P. Welch. "The use of fast Fourier transform for the estimation of power spectra: A method based on time averaging over short, modified periodograms". In: *IEEE Transactions on Audio and Electroacoustics* 15.2 (1967), pages 70–73. DOI: 10.1109/TAU.1967.1161901.

[WHO12] WHO. *WHOQOL: Measuring Quality of Life*. 2012. URL: https://www.who.int/tools/whoqol. Accessed: 15/05/2021.

[Wie+18] T. Wielek, J. Lechinger, M. Wislowska, C. Blume, P. Ott, S. Wegenkittl, R. del Giudice, D. P. J. Heib, H. A. Mayer, S. Laureys, G. Pichler, and M. Schabus. "Sleep in patients with disorders of consciousness characterized by means of machine learning". In: *PLOS ONE* 13.1 (2018), pages 1–14. DOI: 10.1371/journal.pone.0190458.

[Wis+17] M. Wislowska, R. del Giudice, J. Lechinger, T. Wielek, D. P. J. Heib, A. Pitiot, G. Pichler, G. Michitsch, J. Donis, and M. Schabus. "Night and day variations of sleep in patients with disorders of consciousness". In: *Scientific Reports* 7.266 (2017). DOI: 10.1038/s41598-017-00323-4.

[Wit+17] I. H. Witten, E. Frank, M. A. Hall, and C. J. Pal. *Data Mining: Practical Machine Learning Tools and Techniques*. Fourth edition. Elsevier, 2017. ISBN: 978-0-12-804291-5.

[WNB20] S.-J. Wu, N. Nicolaou, and M. Bogdan. "Consciousness Detection in a Complete Locked-in Syndrome Patient through Multiscale Approach Analysis". In: *Entropy* 22.12 (2020). ISSN: 1099-4300. DOI: 10.3390/e22121411.

[Zha+17] Y. Zhang, R. Li, J. Du, S. Huo, J. Hao, and W. Song. "Coherence in P300 as a predictor for the recovery from disorders of consciousness". In: *Neuroscience Letters* 653 (2017), pages 332–336. ISSN: 0304-3940. DOI: 10.1016/j.neulet.2017.06.013.

[ZK11] T. O. Zander and C. Kothe. "Towards passive brain–computer interfaces: applying brain–computer interface technology to human–machine systems in general". In: *Journal of Neural Engineering* 8.2 (2011), page 025005. DOI: 10.1088/1741-2560/8/2/025005.

A Appendix: K-means++ algorithm

GMM uses the k-means++ algorithm to determine the initial parameters of the clustering analysis [Mat21]. Given a number k of clusters, they are chosen like so:

1. First, the component mixture probability is chosen as the uniform probability $p_i = \frac{1}{k}$, where $i = 1, ..., k$.

2. Then, the covariance matrices are set to be diagonal and identical, where $\sigma_i = diag(a_1, a_2, \ldots, a_k)$ and $a_j = var(X_j)$.

3. Afterwards, the first initial component centre μ_1 is uniformly determined from all data points in X.

4. To obtain centre j:

   a) The Mahalanobis distances from each observation to each centroid is calculated, and each observation is assigned to its closest centroid.

   b) For $m = 1, ..., n$ and $p = 1, ..., j-1$, a centroid j is randomly selected from X with probability

   $$\frac{d^2\left(x_m, \mu_p\right)}{\sum_{h; x_h \in M_p} d^2\left(x_h, \mu_p\right)} \tag{A.1}$$

   where $d(x_h, \mu_p)$ is the distance between observation m and μ_p, and M_p is the set of all observations closest to centroid μ_p and x_m belongs to M_p. i.e., each subsequent centre is selected with a probability proportional to the distance from itself to the closest centre already selected.

5. Step 4 is repeated until the k centroids are chosen.

B Appendix: Additional information about DoC patients

Table B.1: Data and eyes scoring length.

Patient	EEG data length	Eyes scoring length
L1	2891	2170
L3	2881	1920
L13	2881	2150
S12	2691	1229
S13	2665	1620
S14	2536	1559
S16	2622	1700
S17	1865	960
L4	2883	2150
L7	2881	2150
L8	2968	2160
L9	2910	2160
L16	2881	2150
S2	2180	1170
S5	2894	720
S6	2593	1430
S7	2522	720

Table B.2: Results of the Wilcoxon ranskum statistical analysis comparing the values of each feature between MCS and UWS patients.

Features	p-value	zval
Ptheta	0	-56,46
Pbeta	0	-42,96
SEF95	1,80E-206	-30,66
ERR	3,11E-73	-18,1
LZC	1,61E-206	30,67
iCOH	3,48E-06	4,64
wSMI	1,75E-99	21,17

Table B.3: Clustering analysis results UWS patient L3. **(a)**: Clusters centroids. Values displayed here are the normalised values. **(b)**: Spearman correlation coefficients between the features and the estimated levels of consciousness.

Features	FCM		GMM	
	Cluster 1	Cluster 2	Cluster 1	Cluster 2
P_{theta}	0,1234	0,2418	0,2243	0,1132
P_{beta}	0,0112	0,0409	0,0382	0,0071
SEF95	6,1560	11,6325	11,4705	5,1300
ERR	0,5345	0,9378	0,8764	0,5032
LZC	1,0259	1,1774	1,1847	0,9907
$iCOH_{theta}$	0,0631	0,0634	0,0639	0,0646
wSMI	0,0377	0,0370	0,0646	0,0373

(a)

Features	Spearman correlation			
	FCM	GMM	Product ens.	Average ens.
P_{theta}	0,8615	-0,8036	0,8266	0,8627
P_{beta}	0,8299	-0,9717	0,9412	0,8439
SEF95	0,7900	-0,9555	0,9290	0,8059
ERR	0,7780	-0,7568	0,7547	0,7752
LZC	0,3736	-0,4113	0,4386	0,3803
$iCOH_{theta}$	0,0144	0,0064	-0,0043	0,0082
wSMI	-0,0978	-0,0773	0,0334	-0,0866

(b)

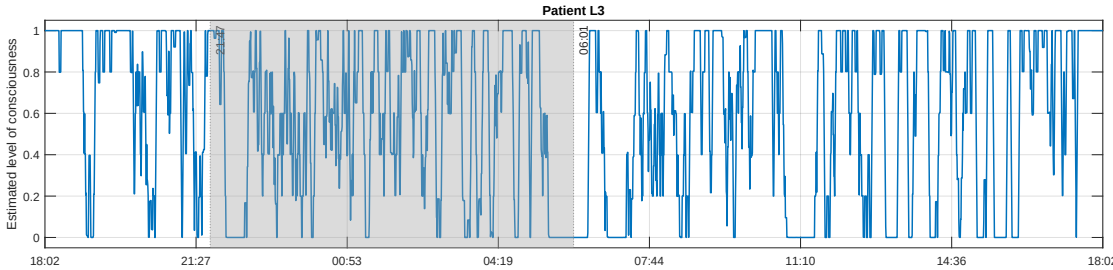

(a) Product ensemble

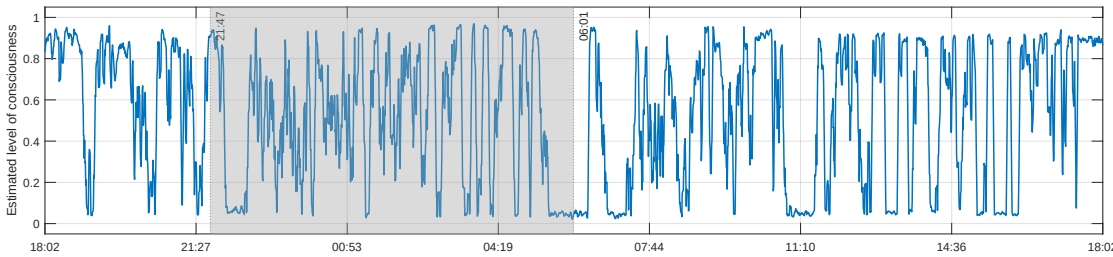

(b) Average ensemble

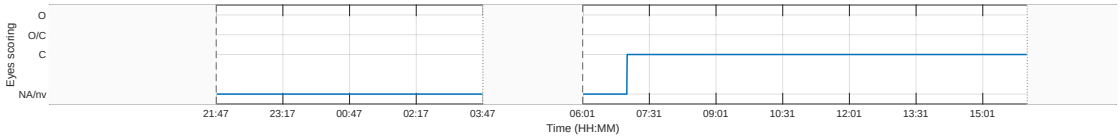

(c) Eyes scoring

Figure B.1: Estimated consciousness level for UWS patient L3 using **(a)** a product of the results obtained from , and **(b)** an average ensemble of FCM and GMM. The blank areas represent the times during which no eyes scoring were made in **(c)**. Shaded area represents night time.

Table B.4: Clustering analysis results UWS patient L13. **(a)**: Clusters centroids. Values displayed here are the normalised values. **(b)**: Spearman correlation coefficients between the features and the estimated levels of consciousness.

Features	FCM		GMM	
	Cluster 1	Cluster 2	Cluster 1	Cluster 2
P_{theta}	0,1016	0,1022	0,1486	0,0708
P_{beta}	0,0085	0,0085	0,0136	0,0051
SEF95	5,4990	5,517	7,3305	4,2930
ERR	0,3639	0,3637	0,3838	0,3504
LZC	0,7742	0,7729	0,8229	0,7408
$iCOH_{theta}$	0,0649	0.0655	0,0676	0,0636
wSMI	0,0473	0,0473	0,0489	0,0462

(a)

Features	Spearman correlation			
	FCM	GMM	Product ens.	Average ens.
P_{theta}	0,4933	-0,5122	0,5123	0,5354
P_{beta}	0,4556	-0,8997	0,8978	0,8270
SEF95	0,5011	-0,9091	0,9081	0,8481
ERR	0,0481	-0,3973	0,3951	0,3046
LZC	-0,2004	-0,2662	0,2630	0,1242
$iCOH_{theta}$	0,5246	-0,0680	0,0718	0,2032
wSMI	0,2718	-0,3499	0,3495	0,3227

(b)

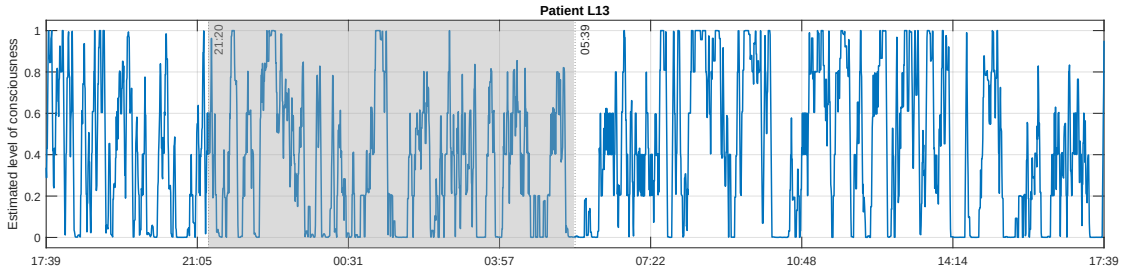

(a) Product ensemble

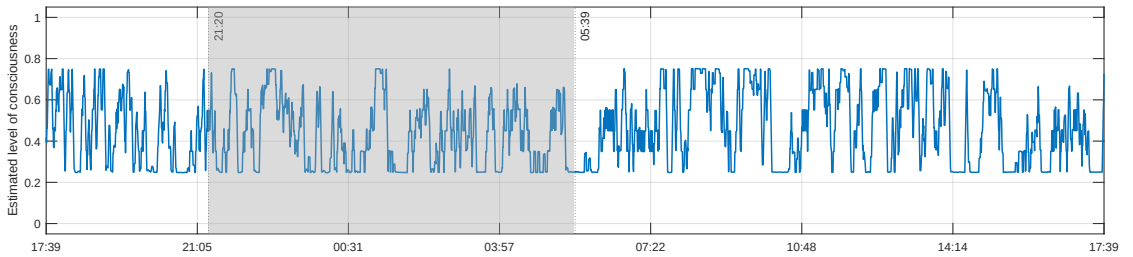

(b) Average ensemble

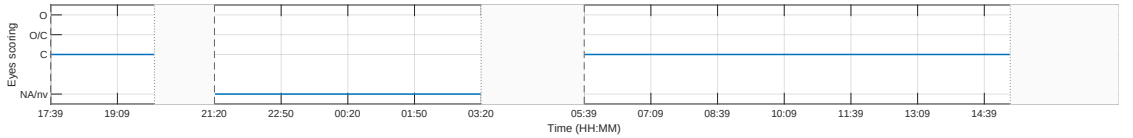

(c) Eyes scoring

Figure B.2: Estimated consciousness level for UWS patient L13 using using **(a)** a product of the results obtained from , and **(b)** an average ensemble of FCM and GMM. The blank areas represent the times during which no eyes scoring were made in **(c)**. Shaded area represents night time.

Table B.5: Clustering analysis results UWS patient S12. **(a)**: Clusters centroids. Values displayed here are the normalised values. **(b)**: Spearman correlation coefficients between the features and the estimated levels of consciousness.

Features	FCM		GMM	
	Cluster 1	Cluster 2	Cluster 1	Cluster 2
P_{theta}	0,4075	0,2682	0,4163	0,2790
P_{beta}	0,0611	0,1367	0,0591	0,1159
SEF95	14,1705	32,2515	13,5405	28,0125
ERR	0,5845	1,8422	0,4762	1,792
LZC	0,2395	1,1007	0,2182	0,8519
$iCOH_{theta}$	0,0625	0,0608	0,0634	0,0610
wSMI	0,0307	0,0547	0,0299	0,0485

(a)

Features	Spearman correlation			
	FCM	GMM	Product ens.	Average ens.
P_{theta}	-0,6193	0,5232	-0,6566	0,4908
P_{beta}	0,4830	0,7516	0,5118	0,6979
SEF95	0,6922	0,8228	0,7371	0,7358
ERR	0,7307	0,4314	0,8068	0,5019
LZC	0,5034	-0,0451	0,4330	-0,0058
$iCOH_{theta}$	-0,0026	0,3858	-0,0309	0,4479
wSMI	0,4503	0,2183	0,3932	0,3042

(b)

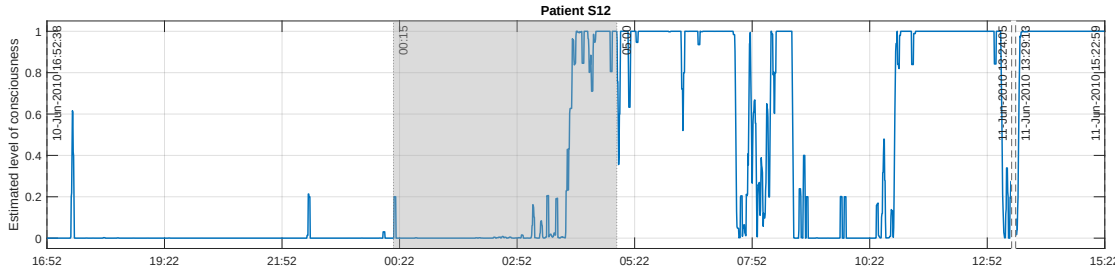

(a) Product ensemble

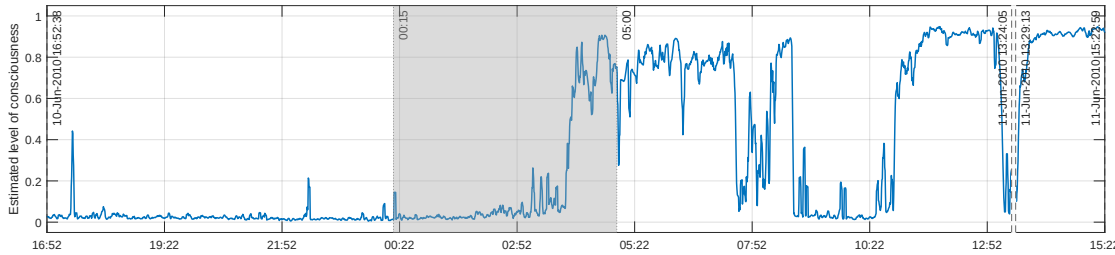

(b) Average ensemble

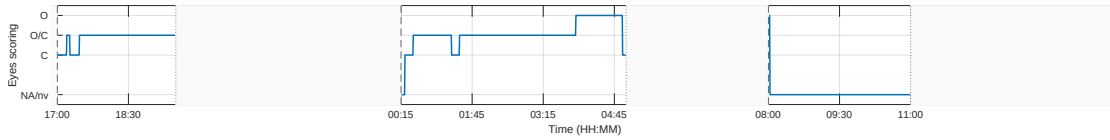

(c) Eyes scoring

Figure B.3: Estimated consciousness level for UWS patient S12 using using **(a)** a product of the results obtained from , and **(b)** an average ensemble of FCM and GMM. The blank areas represent the times during which no eyes scoring were made in **(c)**. Shaded area represents night time.

Table B.6: Clustering analysis results UWS patient S13. **(a)**: Clusters centroids. Values displayed here are the normalised values. **(b)**: Spearman correlation coefficients between the features and the estimated levels of consciousness.

Features	FCM		GMM	
	Cluster 1	Cluster 2	Cluster 1	Cluster 2
P_{theta}	0,1280	0,1283	0,1229	0,1401
P_{beta}	0,0276	0,0277	0,0200	0,0452
SEF95	10,2330	10,26	7,4070	16,7085
ERR	0,1722	0,1724	0,1395	0,2468
LZC	1,0285	1,0273	0,8300	1,4783
$iCOH_{theta}$	0,0590	0,0591	0,0594	0,0583
wSMI	0,0330	0,033	0,0329	0,0333

(a)

Features	Spearman correlation			
	FCM	GMM	Product ens.	Average ens.
P_{theta}	0,4820	0,2183	0,2189	0,3042
P_{beta}	0,5345	0,8942	0,8944	0,8551
SEF95	0,4645	0,9380	0,9381	0,8732
ERR	0,3159	0,8638	0,8637	0,7653
LZC	-0,0988	0,7039	0,7033	0,4809
$iCOH_{theta}$	0,1504	-0,0375	-0,0375	0,0237
wSMI	0,6432	0,0865	0,0877	0,2793

(b)

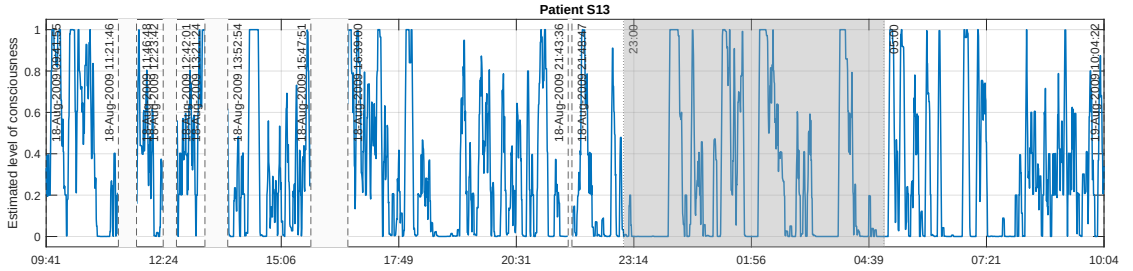

(a) Product ensemble

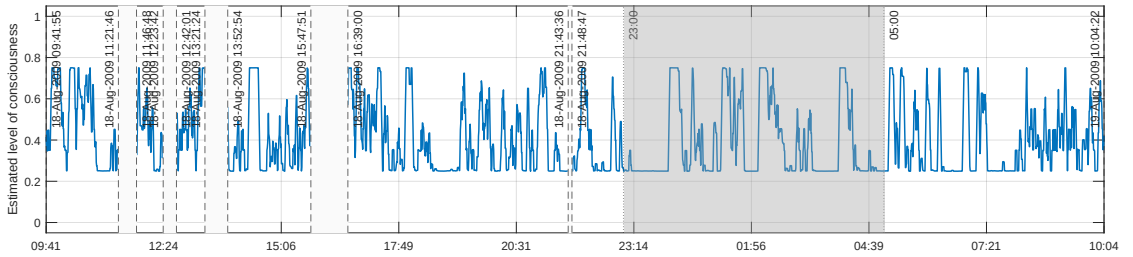

(b) Average ensemble

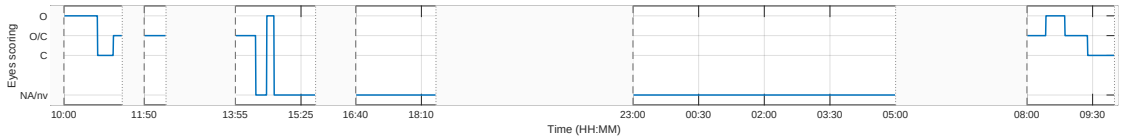

(c) Eyes scoring

Figure B.4: Estimated consciousness level for UWS patient S13 using using **(a)** a product of the results obtained from , and **(b)** an average ensemble of FCM and GMM. The blank areas represent the times during which no data were recorded in **(a)** and **(b)**, or no eyes scoring were made in **(c)**. Shaded area represents night time.

Table B.7: Clustering analysis results UWS patient S14. **(a)**: Clusters centroids. Values displayed here are the normalised values. **(b)**: Spearman correlation coefficients between the features and the estimated levels of consciousness.

Features	FCM		GMM	
	Cluster 1	Cluster 2	Cluster 1	Cluster 2
P_{theta}	0,0608	0,0696	0,0706	0,0628
P_{beta}	0,2017	0,1248	0,1091	0,204
SEF95	36,35	27,01	24,72	36,81
ERR	0,4643	0,2672	0,2278	0,4665
LZC	1,2839	0,7793	0,7776	1,2303
$iCOH_{theta}$	0,0623	0,0600	0,0580	0,0639
wSMI	0,0441	0,0391	0,0384	0,0442

(a)

Features	Spearman correlation			
	FCM	GMM	Product ens.	Average ens.
P_{theta}	-0,0744	-0,0742	0,0609	-0,0307
P_{beta}	0,8034	-0,9272	0,9253	0,8274
SEF95	0,8454	-0,9667	0,9659	0,8713
ERR	0,7785	-0,9244	0,9215	0,8046
LZC	0,4942	-0,3605	0,3809	0,4553
$iCOH_{theta}$	0,0416	-0,0924	0,0901	0,0483
wSMI	0,4954	-0,5486	0,5491	0,4988

(b)

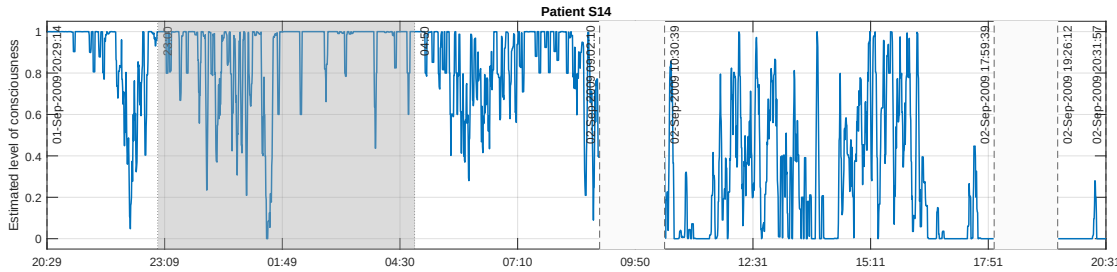

(a) Product ensemble

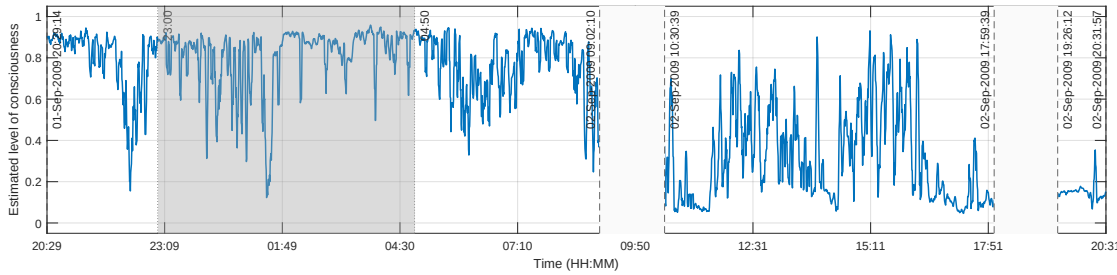

(b) Average ensemble

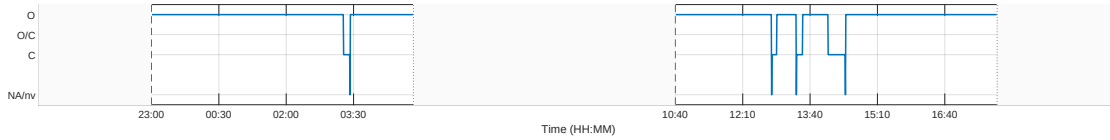

(c) Eyes scoring

Figure B.5: Estimated consciousness level for MCS patient S14 using using **(a)** a product of the results obtained from , and **(b)** an average ensemble of FCM and GMM. The blank areas represent the times during which no eyes scoring were made **(c)**. Shaded area represents night time.

Table B.8: Clustering analysis results UWS patient S16. **(a)**: Clusters centroids. Values displayed here are the normalised values. **(b)**: Spearman correlation coefficients between the features and the estimated levels of consciousness.

Features	FCM		GMM	
	Cluster 1	Cluster 2	Cluster 1	Cluster 2
P_{theta}	0,1105	0,1703	0,1137	0,1780
P_{beta}	0,1044	0,0154	0,0853	0,0116
SEF95	25,2495	6,4800	21,582	5,4990
ERR	0,6927	0,5659	0,6717	0,5639
LZC	1,5211	0,8293	1,4122	0,7754
$iCOH_{theta}$	0,0594	0,0575	0,06	0,0578
wSMI	0,0267	0,0302	0,0267	0,0307

(a)

Features	Spearman correlation			
	FCM	GMM	Product ens.	Average ens.
P_{theta}	-0,4848	-0,7251	-0,7236	-0,4893
P_{beta}	0,8016	0,8008	0,8074	0,8273
SEF95	0,8004	0,7701	0,7747	0,8269
ERR	0,3968	0,3170	0,3274	0,3861
LZC	0,6407	0,7669	0,7555	0,6729
$iCOH_{theta}$	0,0738	0,0423	0,0483	0,0719
wSMI	-0,4714	-0,7052	-0,6993	-0,4821

(b)

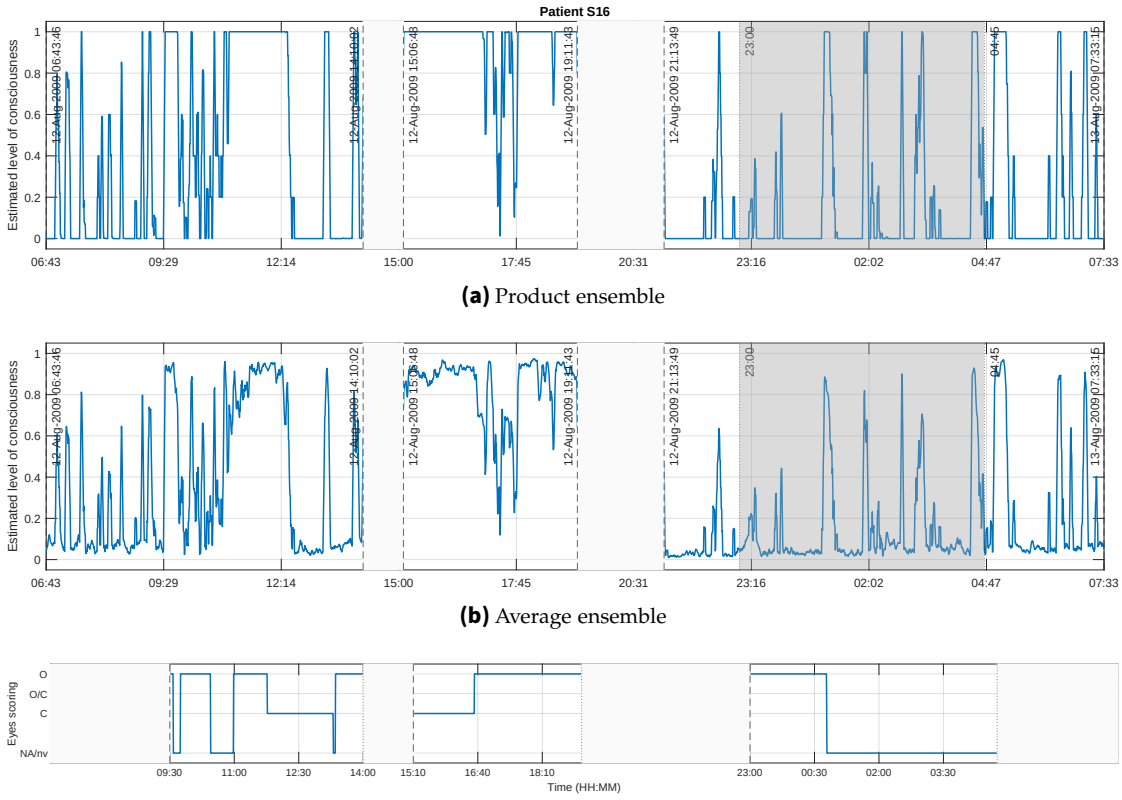

(a) Product ensemble

(b) Average ensemble

(c) Eyes scoring

Figure B.6: Estimated consciousness level for UWS patient S16 using using **(a)** a product of the results obtained from , and **(b)** an average ensemble of FCM and GMM. The blank areas represent the times during which no data were recorded in **(a)** and **(b)**, or no eyes scoring were made in **(c)**. Shaded area represents night time.

Table B.9: Clustering analysis results UWS patient S17. **(a)**: Clusters centroids. Values displayed here are the normalised values. **(b)**: Spearman correlation coefficients between the features and the estimated levels of consciousness.

Features	FCM		GMM	
	Cluster 1	Cluster 2	Cluster 1	Cluster 2
P_{theta}	0,1674	0,0672	0,0682	0,1571
P_{beta}	0,0687	0,1043	0,1116	0,0645
SEF95	13,9590	24,741	25,614	13,7250
ERR	0,3036	0,4422	0,4517	0,2999
LZC	0,7619	1,8324	1,804	0,8143
$iCOH_{theta}$	0,0621	0,0603	0,0602	0,0632
wSMI	0,0346	0,0271	0,0270	0,0343

(a)

Features	Spearman correlation			
	FCM	GMM	Product ens.	Average ens.
P_{theta}	-0,6990	0,7421	-0,7495	-0,6779
P_{beta}	0,5480	-0,6529	0,6464	0,5850
SEF95	0,8449	-0,8931	0,8925	0,8583
ERR	0,5551	-0,6222	0,6239	0,5681
LZC	0,7808	-0,7316	0,7390	0,7612
$iCOH_{theta}$	-0,0219	0,0338	-0,0336	-0,0205
wSMI	-0,7970	0,7950	-0,7972	-0,7971

(b)

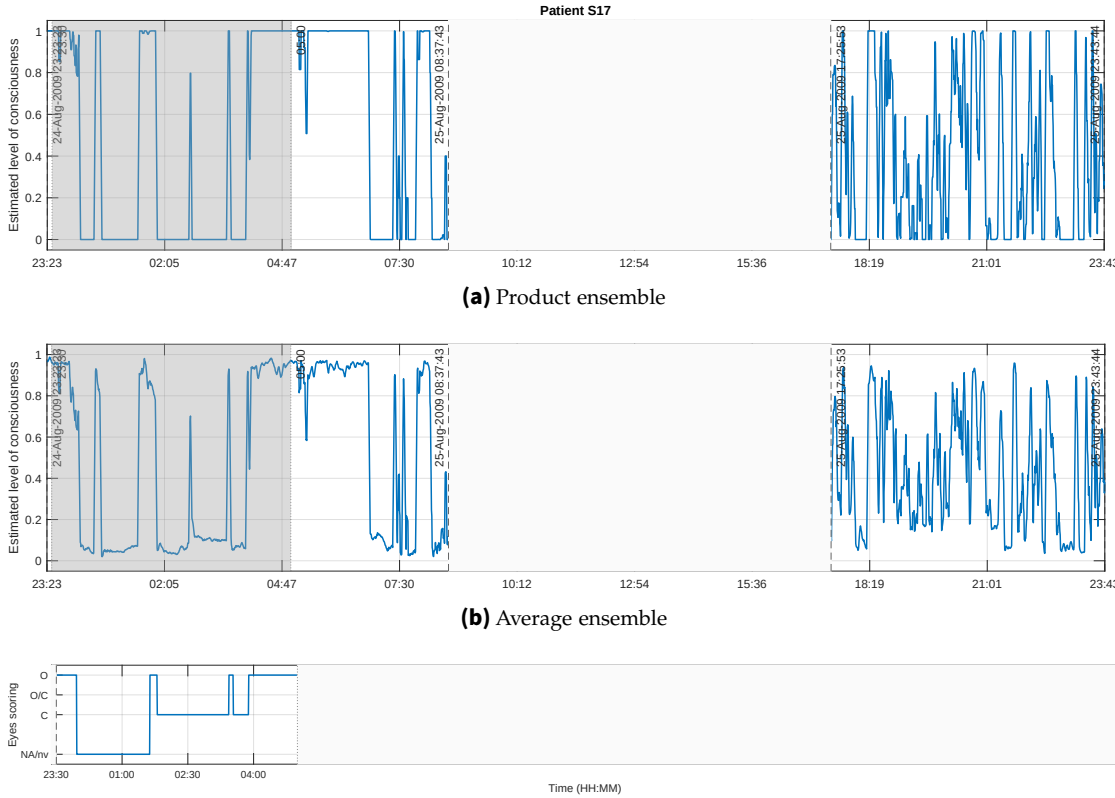

(a) Product ensemble

(b) Average ensemble

(c) Eyes scoring

Figure B.7: Estimated consciousness level for UWS patient S17 using using **(a)** a product of the results obtained from , and **(b)** an average ensemble of FCM and GMM. The blank areas represent the times during which no data were recorded in **(a)** and **(b)**, or no eyes scoring were made in **(c)**. Shaded area represents night time.

Table B.10: Clustering analysis results MCS patient L4. **(a)**: Clusters centroids. Values displayed here are the normalised values. **(b)**: Spearman correlation coefficients between the features and the estimated levels of consciousness.

Features	FCM		GMM	
	Cluster 1	Cluster 2	Cluster 1	Cluster 2
P_{theta}	0,1289	0,1821	0,1401	0,1789
P_{beta}	0,0230	0,0503	0,0237	0,0591
SEF95	8,3880	15,93	8,4015	18,729
ERR	0,4063	0,4918	0,4273	0,4862
LZC	1,1144	1,6139	1,1279	1,7756
$iCOH_{theta}$	0,0603	0,0591	0,0614	0,0586
wSMI	0,0383	0,0414	0,0586	0,0448

(a)

Features	Spearman correlation			
	FCM	GMM	Product ens.	Average ens.
P_{theta}	0,6894	0,5700	0,5967	0,6204
P_{beta}	0,8503	0,9447	0,9470	0,8673
SEF95	0,8212	0,9506	0,9501	0,8519
ERR	0,4857	0,4242	0,4510	0,4528
LZC	0,7665	0,9396	0,9302	0,8038
$iCOH_{theta}$	-0,0261	-0,0589	-0,0512	-0,0282
wSMI	0,1958	0,3729	0,3620	0,2592

(b)

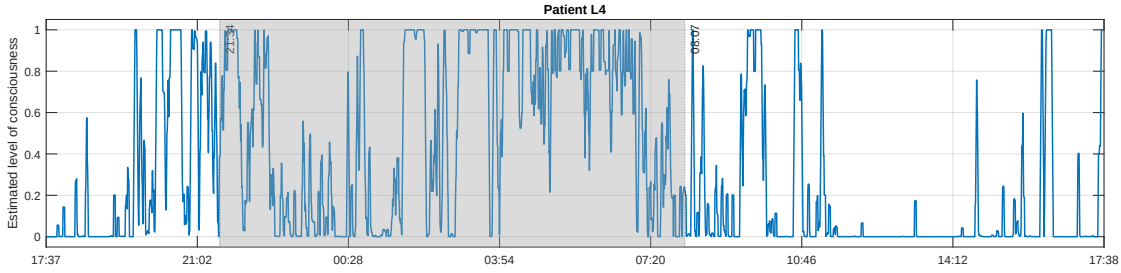

(a) Product ensemble

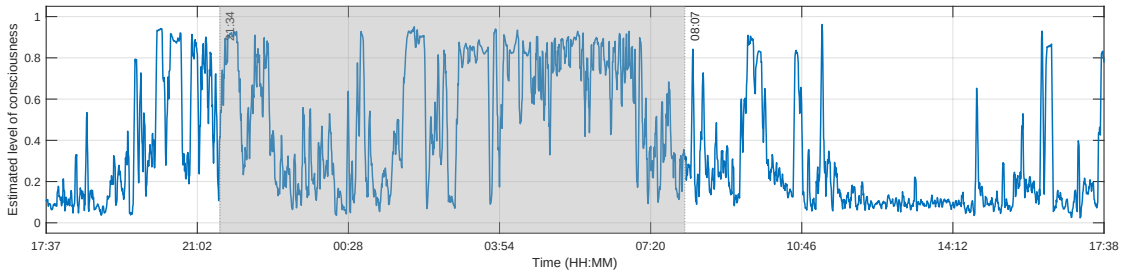

(b) Average ensemble

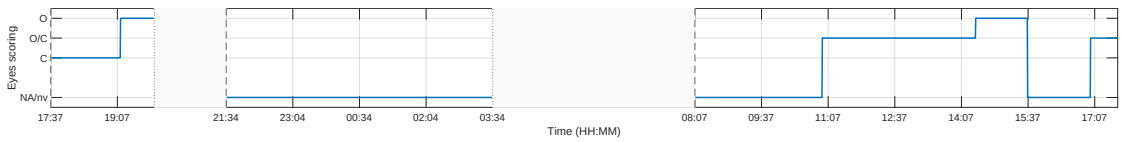

(c) Eyes scoring

Figure B.8: Estimated consciousness level for MCS patient L4 using using **(a)** a product of the results obtained from , and **(b)** an average ensemble of FCM and GMM. The blank areas represent the times during which no data were recorded in **(a)** and **(b)**, or no eyes scoring were made in **(c)**. Shaded area represents night time.

Table B.11: Clustering analysis results MCS patient L7. **(a)**: Clusters centroids. Values displayed here are the normalised values. **(b)**: Spearman correlation coefficients between the features and the estimated levels of consciousness.

Features	FCM		GMM	
	Cluster 1	Cluster 2	Cluster 1	Cluster 2
P_{theta}	0,1638	0,1323	0,1311	0,1645
P_{beta}	0,0387	0,0921	0,0951	0,0391
SEF95	15,4485	33,93	34,866	16,0020
ERR	0,6047	0,5710	0,5639	0,6093
LZC	1,2622	1,97	1,9987	1,2648
$iCOH_{theta}$	0,0591	0,0571	0,0571	0,0603
wSMI	0,0472	0,0659	0,667	0,0474

Features	Spearman correlation			
	FCM	GMM	Product ens.	Average ens.
P_{theta}	-0,2871	0,2455	-0,2466	-0,2858
P_{beta}	0,8024	-0,9249	0,9255	0,8042
SEF95	0,8626	-0,9847	0,9844	0,8638
ERR	0,0587	0,0849	-0,0827	0,0585
LZC	0,7572	-0,9060	0,9054	0,7583
$iCOH_{theta}$	-0,0283	0,0630	-0,0615	-0,0282
wSMI	0,7688	-0,8472	0,8490	0,7685

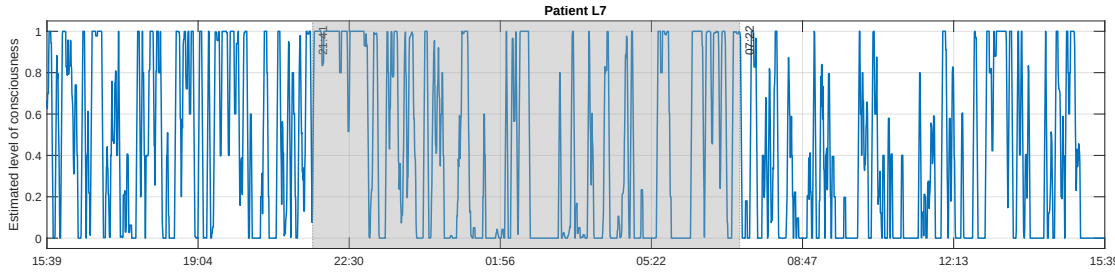

(a) Product ensemble

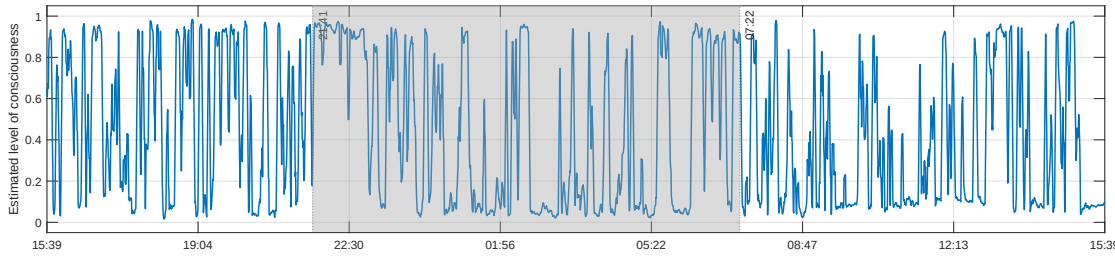

(b) Average ensemble

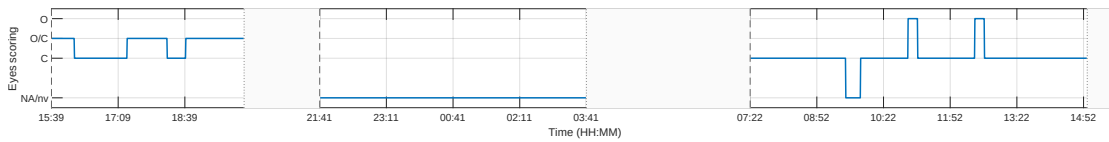

(c) Eyes scoring

Figure B.9: Estimated consciousness level for MCS patient L7 using using **(a)** a product of the results obtained from , and **(b)** an average ensemble of FCM and GMM. The blank areas represent the times during which no eyes scoring were made in **(c)**. Shaded area represents night time.

Table B.12: Clustering analysis results MCS patient L8. **(a)**: Clusters centroids. Values displayed here are the normalised values. **(b)**: Spearman correlation coefficients between the features and the estimated levels of consciousness.

Features	FCM		GMM	
	Cluster 1	Cluster 2	Cluster 1	Cluster 2
P_{theta}	0,0753	0,0850	0,0887	0,0748
P_{beta}	0,0748	0,0189	0,0150	0,0646
SEF95	22,49	7,34	6,04	20,14
ERR	0,3297	0,1150	0,0986	0,2906
LZC	1,5441	0,6743	0,6045	1,3941
$iCOH_{theta}$	0,0577	0,0568	0,0578	0,0587
wSMI	0,0437	0,0418	0,0417	0,0433

Features	Spearman correlation			
	FCM	GMM	Product ens.	Average ens.
P_{theta}	-0,1053	0,2060	-0,2199	-0,1166
P_{beta}	0,8685	-0,9443	0,9275	0,8758
SEF95	0,8782	-0,9440	0,9291	0,8866
ERR	0,8664	-0,9556	0,9417	0,8773
LZC	0,8440	-0,9398	0,9252	0,8553
$iCOH_{theta}$	0,0566	-0,0348	0,0446	0,0504
wSMI	0,1601	-0,2636	0,2469	0,1621

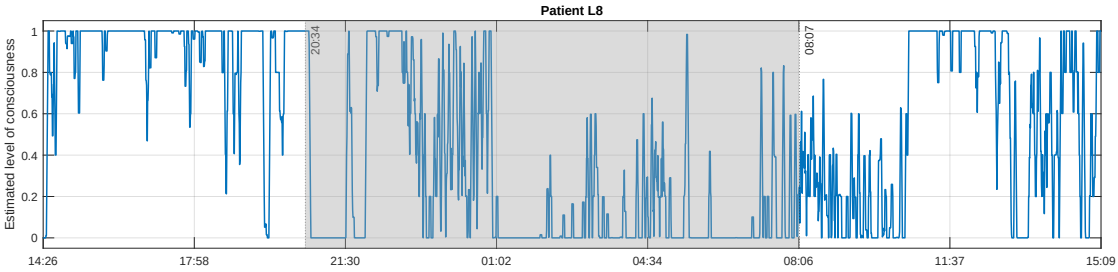

(a) Product ensemble

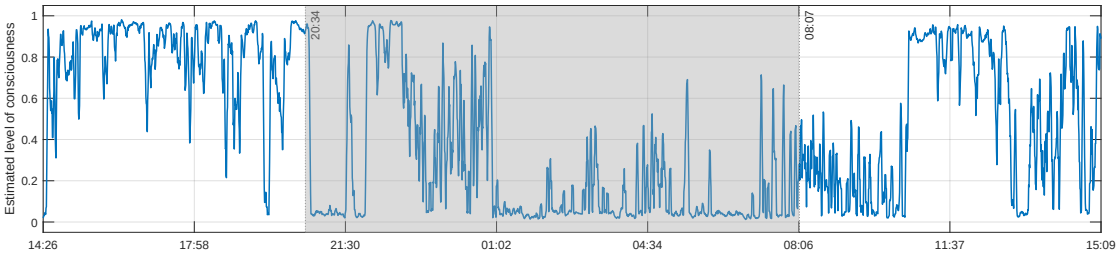

(b) Average ensemble

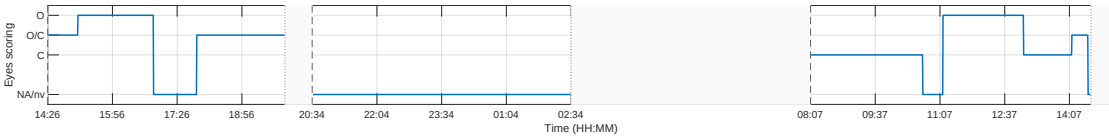

(c) Eyes scoring

Figure B.10: Estimated consciousness level for MCS patient L8 using using **(a)** a product of the results obtained from , and **(b)** an average ensemble of FCM and GMM. The blank areas represent the times during which no eyes scoring were made in **(c)**. Shaded area represents night time.

Table B.13: Clustering analysis results MCS patient L9. **(a)**: Clusters centroids. Values displayed here are the normalised values. **(b)**: Spearman correlation coefficients between the features and the estimated levels of consciousness.

Features	FCM		GMM	
	Cluster 1	Cluster 2	Cluster 1	Cluster 2
P_{theta}	0,0891	0,0769	0,0901	0,0748
P_{beta}	0,0461	0,0211	0,0476	0,0157
SEF95	15,6825	7,7670	15,831	6,1830
ERR	0,3699	0,3322	0,372	0,3239
LZC	1,3687	0,9533	1,3739	0,8724
$iCOH_{theta}$	0,0557	0,0575	0,0561	0,0594
wSMI	0,0555	0,0494	0,055	0,0491

(a)

Features	Spearman correlation			
	FCM	GMM	Product ens.	Average ens.
P_{theta}	0,3046	0,3232	0,3206	0,3032
P_{beta}	0,8251	0,9502	0,9439	0,8546
SEF95	0,8565	0,9599	0,9544	0,8855
ERR	0,3153	0,3876	0,3790	0,3142
LZC	0,7810	0,8463	0,8398	0,8053
$iCOH_{theta}$	-0,0385	-0,0733	-0,0663	-0,0447
wSMI	0,4238	0,3470	0,3494	0,4008

(b)

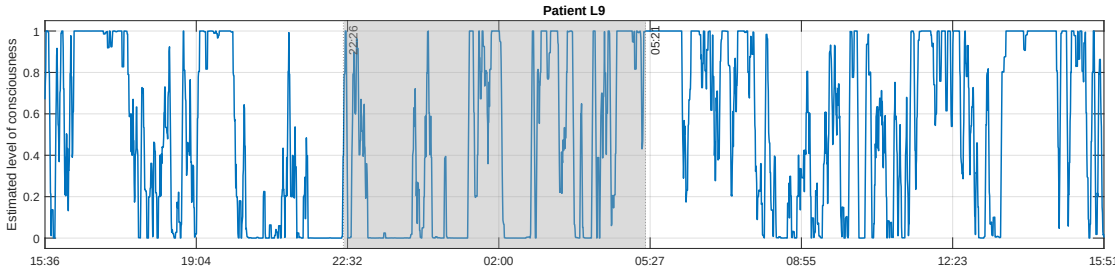

(a) Product ensemble

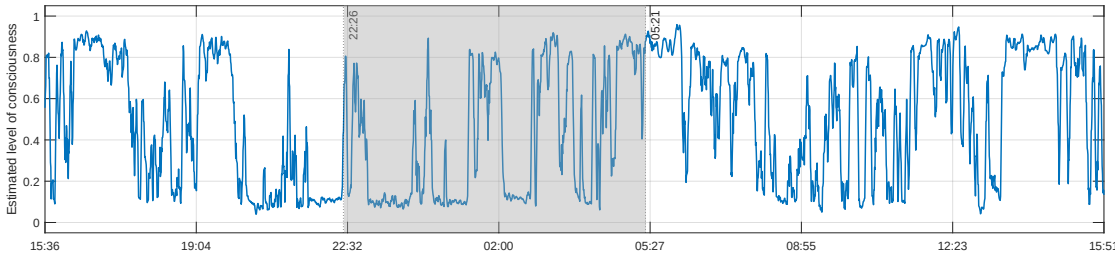

(b) Average ensemble

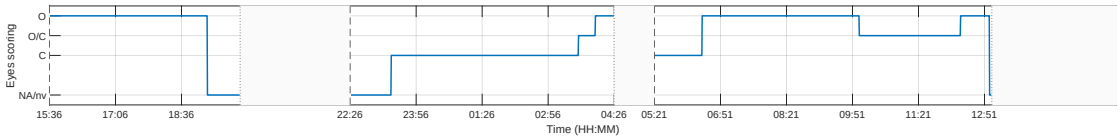

(c) Eyes scoring

Figure B.11: Estimated consciousness level for MCS patient L9 using using **(a)** a product of the results obtained from , and **(b)** an average ensemble of FCM and GMM. The blank areas represent the times during which no eyes scoring were made in **(c)**. Shaded area represents night time.

Table B.14: Clustering analysis results MCS patient L16. **(a)**: Clusters centroids. Values displayed here are the normalised values. **(b)**: Spearman correlation coefficients between the features and the estimated levels of consciousness.

Features	FCM		GMM	
	Cluster 1	Cluster 2	Cluster 1	Cluster 2
P_{theta}	0,1834	0,1840	0,1829	0,1834
P_{beta}	0,1283	0,0577	0,1257	0,0483
SEF95	30,897	18,1800	30,7935	16,2855
ERR	0,6242	0,5798	0,62	0,5701
LZC	1,8859	1,2149	1,8601	1,1312
$iCOH_{theta}$	0,0665	0,0659	0,0677	0,0661
wSMI	0,0505	0,0440	0,0501	0,0440

(a)

Features	Spearman correlation			
	FCM	GMM	Product ens.	Average ens.
P_{theta}	-0,0147	0,0305	0,0305	-0,0143
P_{beta}	0,8654	0,9810	0,9800	0,8722
SEF95	0,8661	0,9584	0,9589	0,8705
ERR	0,1263	0,2056	0,2052	0,1275
LZC	0,8244	0,9042	0,9051	0,8294
$iCOH_{theta}$	0,0120	0,0253	0,0246	0,0119
wSMI	0,5141	0,4868	0,4900	0,5077

(b)

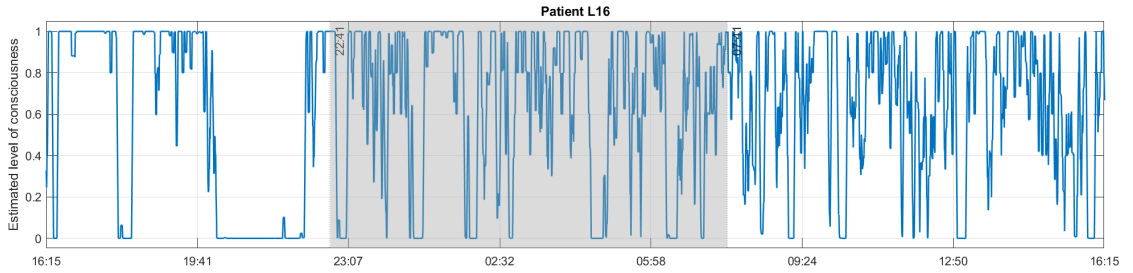

(a) Product ensemble

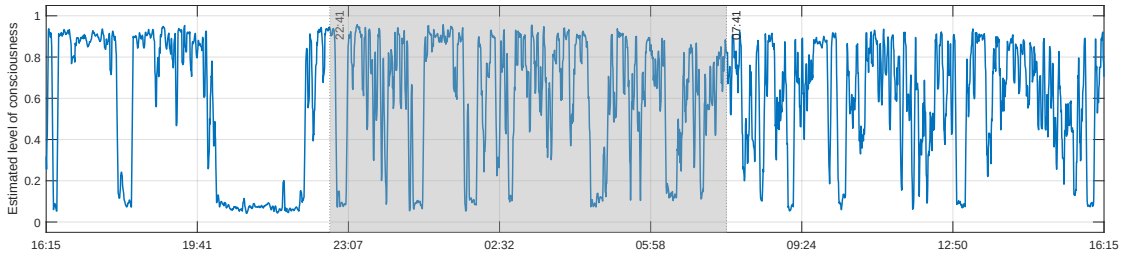

(b) Average ensemble

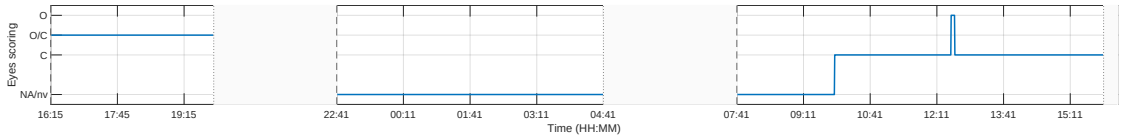

(c) Eyes scoring

Figure B.12: Estimated consciousness level for MCS patient L16 using using **(a)** a product of the results obtained from , and **(b)** an average ensemble of FCM and GMM. The blank areas represent the times during which no eyes scoring were made in **(c)**. Shaded area represents night time.

Table B.15: Clustering analysis results MCS patient S2. **(a)**: Clusters centroids. Values displayed here are the normalised values. **(b)**: Spearman correlation coefficients between the features and the estimated levels of consciousness.

Features	FCM		GMM	
	Cluster 1	Cluster 2	Cluster 1	Cluster 2
P_{theta}	0,1122	0,1254	0,0972	0,1518
P_{beta}	0,0468	0,0220	0,0444	0,0168
SEF95	18,522	9,2430	18,315	6,9975
ERR	0,4533	0,3456	0,4441	0,3267
LZC	1,2811	0,9875	1,2479	0,9265
$iCOH_{theta}$	0,0602	0,0597	0,0582	0,0628
wSMI	0,0340	0,0361	0,0329	0,0384

(a)

Features	Spearman correlation			
	FCM	GMM	Product ens.	Average ens.
P_{theta}	-0,0914	-0,4109	-0,4149	-0,1643
P_{beta}	0,6822	0,6946	0,6936	0,7423
SEF95	0,7918	0,8513	0,8505	0,8359
ERR	0,4830	0,2671	0,2695	0,4760
LZC	0,4236	0,3742	0,3807	0,4545
$iCOH_{theta}$	0,0025	-0,0740	-0,0696	-0,0088
wSMI	-0,3249	-0,5361	-0,5450	-0,4002

(b)

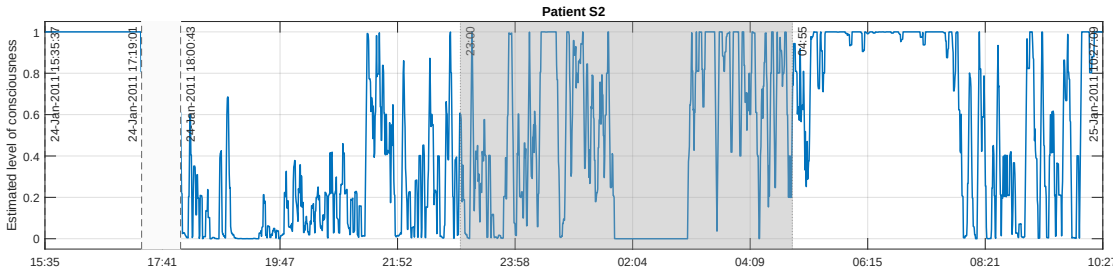

(a) Product ensemble

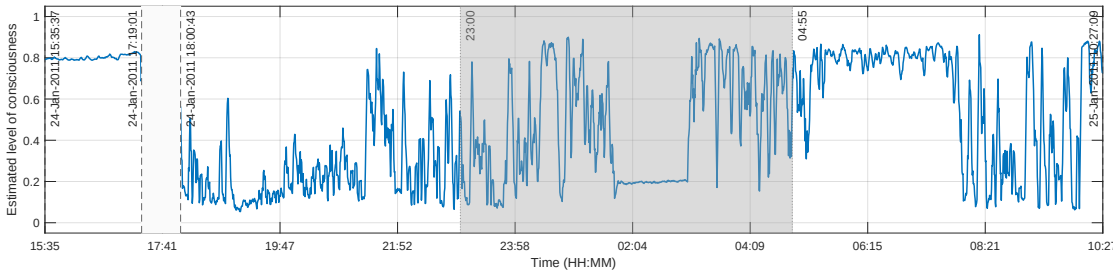

(b) Average ensemble

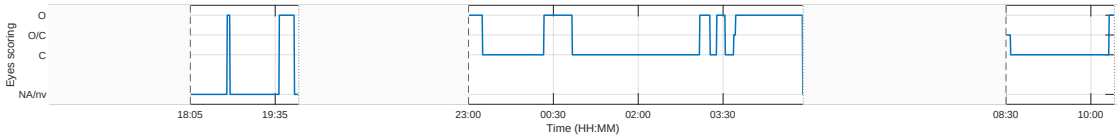

(c) Eyes scoring

Figure B.13: Estimated consciousness level for MCS patient S2 using using **(a)** a product of the results obtained from , and **(b)** an average ensemble of FCM and GMM. The blank areas represent the times during which no data were recorded in **(a)** and **(b)**, or no eyes scoring were made in **(c)**. Shaded area represents night time.

Table B.16: Clustering analysis results MCS patient S5. **(a)**: Clusters centroids. Values displayed here are the normalised values. **(b)**: Spearman correlation coefficients between the features and the estimated levels of consciousness.

Features	FCM		GMM	
	Cluster 1	Cluster 2	Cluster 1	Cluster 2
P_{theta}	0,2131	0,1927	0,0728	0,2221
P_{beta}	0,1751	0,1323	0,0261	0,1733
SEF95	30,69	22,84	8,54	29,61
ERR	0,64	0,6162	0,3050	0,6721
LZC	1,2261	0,6025	0,5785	0,9983
$iCOH_{theta}$	0,0644	0,0624	0,0587	0,0646
wSMI	0,0340	0,0368	0,0386	0,0347

(a)

Features	Spearman correlation			
	FCM	GMM	Product ens.	Average ens.
P_{theta}	0,1436	-0,5158	0,5587	0,2113
P_{beta}	0,4884	-0,9269	0,8335	0,5399
SEF95	0,8262	-0,6649	0,6630	0,8544
ERR	0,0440	-0,6656	0,5917	0,1264
LZC	0,7650	-0,1689	0,2199	0,7277
$iCOH_{theta}$	0,0573	-0,0629	0,0695	0,0631
wSMI	-0,4952	0,3101	-0,2706	-0,4814

(b)

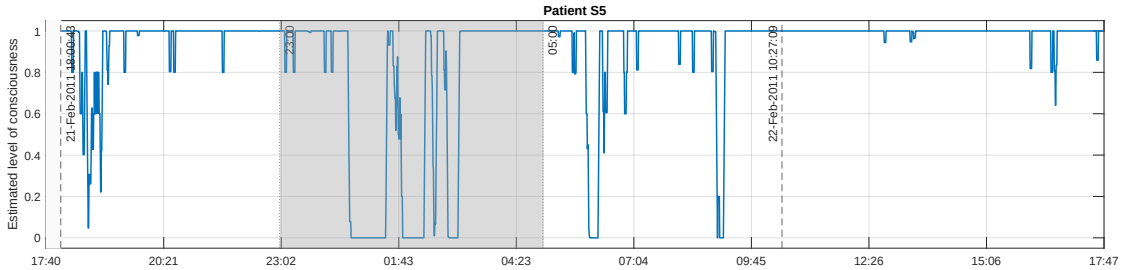

(a) Product ensemble

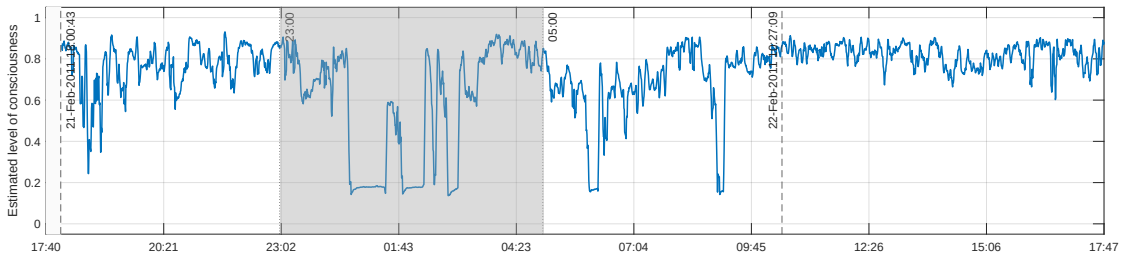

(b) Average ensemble

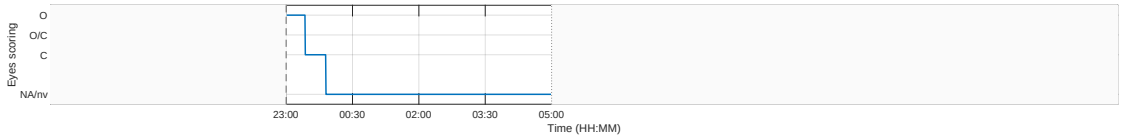

(c) Eyes scoring

Figure B.14: Estimated consciousness level for MCS patient S5 using using **(a)** a product of the results obtained from , and **(b)** an average ensemble of FCM and GMM. The blank areas represent the times during which no eyes scoring were made in **(c)**. Shaded area represents night time.

Table B.17: Clustering analysis results MCS patient S6. **(a)**: Clusters centroids. Values displayed here are the normalised values. **(b)**: Spearman correlation coefficients between the features and the estimated levels of consciousness.

Features	FCM		GMM	
	Cluster 1	Cluster 2	Cluster 1	Cluster 2
P_{theta}	0,1357	0,0921	0,0890	0,1299
P_{beta}	0,1079	0,0482	0,0392	0,1044
SEF95	22,06	12,66	11,12	21,70
ERR	0,3384	0,1629	0,1435	0,3208
LZC	0,3984	0,3851	0,3375	0,4462
$iCOH_{theta}$	0,0594	0,0614	0,0627	0,0595
wSMI	0,0301	0,0306	0,0309	0,0300

(a)

Features	Spearman correlation			
	FCM	GMM	Product ens.	Average ens.
P_{theta}	0,4876	-0,4458	0,4546	0,4740
P_{beta}	0,8475	-0,9155	0,9174	0,8595
SEF95	0,8241	-0,8996	0,9011	0,8379
ERR	0,7944	-0,8146	0,8195	0,7930
LZC	-0,1260	0,0128	-0,0214	-0,1033
$iCOH_{theta}$	-0,0385	0,0537	-0,0525	-0,0458
wSMI	-0,1309	0,1367	-0,1360	-0,1457

(b)

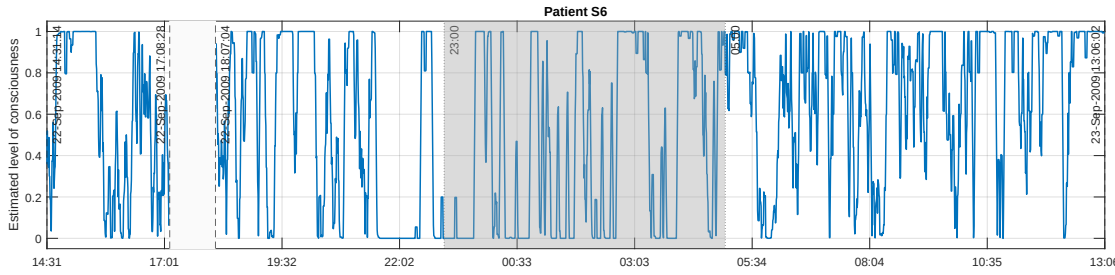

(a) Product ensemble

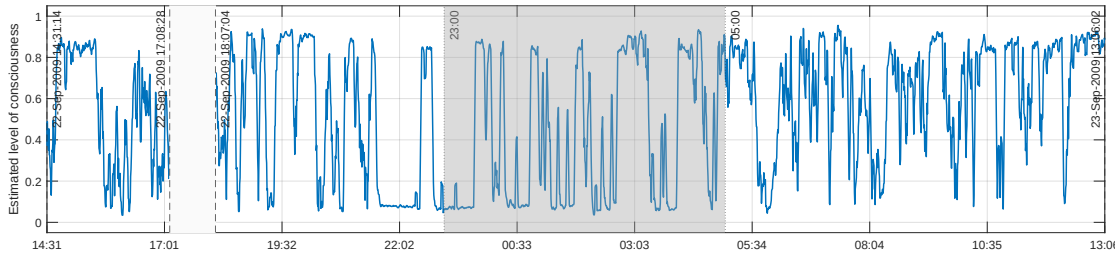

(b) Average ensemble

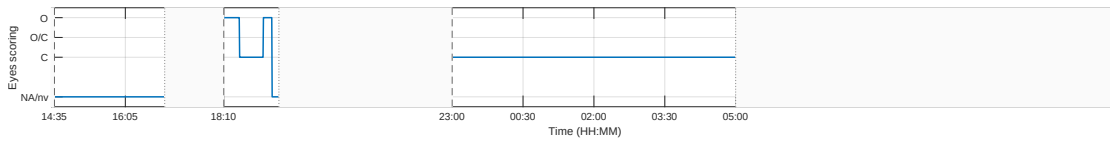

(c) Eyes scoring

Figure B.15: Estimated consciousness level for MCS patient S6 using using **(a)** a product of the results obtained from , and **(b)** an average ensemble of FCM and GMM. The blank areas represent the times during which no data were recorded in **(a)** and **(b)**, or no eyes scoring were made in **(c)**. Shaded area represents night time.

Table B.18: *p*-values of the Wilcoxon ranksum tests comparing night and day values of the different features as well as the estimated consciousness level for all DoC patients. The cells in red represent the cases when the differences are not significant at the 5% level.

Patient	Diagnosis	Ptheta	Pbeta	SEF95	ERR	LZC	iCOH	wSMI	FCM	GMM	Average ens.	Product ens.
L1	UWS	8,37E-10	1,04E-20	4,22E-34	1,60E-94	1,47E-14	0,55	3,16E-48	1,40E-48	6,31E-37	4,08E-47	4,47E-38
L3	UWS	3,33E-03	1,13E-07	2,35E-05	6,91E-43	7,01E-21	0,32	3,05E-05	3,07E-02	4,50E-07	3,63E-02	1,97E-07
L13	UWS	8,72E-03	0,0852	4,69E-02	1,79E-13	2,12E-05	0,25	2,31E-05	2,63E-09	1,57E-03	1,52E-06	1,46E-03
S12	UWS	0,0692	1,01E-24	2,59E-06	6,05E-13	9,53E-25	0,42	9,31E-168	4,52E-07	0,48	1,15E-06	0,92
S13	UWS	0,01	6,29E-22	6,79E-30	0,83	3,89E-16	0,26	6,49E-55	9,12E-13	4,41E-19	1,19E-09	4,30E-09
S14	UWS	0,0172	1,23E-106	1,91E-108	2,66E-91	1,32E-21	5,03E-06	6,09E-19	4,80E-82	9,79E-104	1,45E-83	7,51E-104
S16	UWS	7,83E-32	1,36E-51	3,18E-56	3,37E-26	3,93E-21	0,11	0,1	2,75E-54	1,01E-28	1,01E-54	2,20E-29
S17	MCS/VS	2,80E-77	0,74	8,47E-05	2,20E-03	1,49E-04	8,55E-03	7,54E-10	7,33E-13	2,78E-19	3,84E-12	1,28E-19
L4	MCS	9,26E-80	1,65E-135	2,36E-129	2,63E-06	7,61E-143	0,19	0,29	8,04E-108	9,54E-129	1,93E-105	1,60E-127
L7	MCS	5,04E-123	1,85E-30	7,84E-09	9,24E-06	2,42E-34	0,76	0,23	0,53	1,41E-10	0,58	3,57E-10
L8	MCS	0,28	3,82E-177	1,06E-171	1,50E-171	1,30E-198	0,17	2,42E-04	2,58E-136	1,93E-174	3,14E-139	4,10E-172
L9	MCS	6,50E-04	4,51E-24	5,75E-23	4,45E-07	6,37E-28	0,95	3,95E-17	7,82E-12	3,62E-16	1,16E-14	8,28E-15
L16	MCS	4,46E-07	0,16	0,83	4,71E-28	2,70E-02	0,68	0,29	1,13E-05	0,14	1,08E-05	0,1
S2	MCS	2,51E-56	0,13	4,61E-02	1,42E-22	9,06E-03	3,18E-29	2,28E-29	3,21E-03	2,66E-18	0,66	8,12E-18
S5	MCS	6,48E-24	7,92E-20	1,38E-33	3,33E-20	7,19E-52	2,70E-04	2,18E-05	2,76E-33	9,03E-30	1,04E-44	2,34E-32
S6	MCS	3,84E-126	3,72E-47	5,97E-36	9,71E-08	0,73	3,20E-03	7,18E-128	3,15E-16	2,78E-16	8,52E-20	8,34E-16
S7	MCS	4,20E-20	0,01	2,40E-03	0,89	3,01E-21	0,61	5,28E-55	1,03E-28	1,49E-15	6,33E-14	1,55E-15

Table B.19: Performance of the cluster analysis for different threshold values for the binarisation of the degrees of membership (cf. Section 6.1.3). The cells in green represent the values of the threshold corresponding to the highest accuracy.

Patient	Threshold	Average ensemble	Product ensemble
L1	0,3	63,89%	65,15%
	0,4	62,55%	63,89%
	0,5	61,88%	61,88%
	0,6	61,06%	59,72%
	0,7	60,09%	56,52%
L3	0,3	44,91%	44,26%
	0,4	45,46%	44,81%
	0,5	46,11%	46,11%
	0,6	46,39%	49,17%
	0,7	46,94%	55,37%
L13	0,3	55,66%	52,52%
	0,4	56,36%	55,66%
	0,5	57,20%	57,20%
	0,6	57,48%	58,53%
	0,7	58,53%	60,49%
S12	0,3	44,80%	44,34%
	0,4	44,80%	44,80%
	0,5	44,80%	44,80%
	0,6	44,80%	44,80%
	0,7	44,80%	44,80%
S13	0,3	56,23%	56,23%
	0,4	57,30%	56,23%
	0,5	57,65%	57,65%
	0,6	57,30%	58,01%
	0,7	58,01%	58,36%
S14	0,3	83,27%	85,20%
	0,4	82,63%	83,27%
	0,5	82,24%	82,24%
	0,6	81,66%	80,57%
	0,7	80,76%	78,64%
S16	0,3	53,38%	53,57%
	0,4	53,20%	53,29%
	0,5	53,20%	53,20%
	0,6	53,20%	53,20%
	0,7	53,10%	51,88%
S17	0,3	21,79%	21,57%
	0,4	22,00%	21,79%
	0,5	22,00%	22,00%
	0,6	22,22%	22,22%
	0,7	22,22%	22,00%

Patient	Threshold	Average ensemble	Product ensemble
L4	0,3	54,52%	59,76%
	0,4	54,05%	54,52%
	0,5	53,33%	53,33%
	0,6	52,38%	51,90%
	0,7	51,90%	51,19%
L7	0,3	63,56%	62,05%
	0,4	64,03%	63,47%
	0,5	64,50%	64,50%
	0,6	65,16%	65,63%
	0,7	65,63%	66,95%
L8	0,3	69,77%	69,89%
	0,4	69,89%	69,89%
	0,5	69,77%	69,77%
	0,6	70,11%	69,66%
	0,7	69,89%	70,11%
L9	0,3	72,81%	73,60%
	0,4	72,44%	72,87%
	0,5	71,76%	71,76%
	0,6	71,70%	70,96%
	0,7	71,15%	68,32%
L16	0,3	34,57%	32,64%
	0,4	35,26%	34,57%
	0,5	36,64%	36,64%
	0,6	37,47%	39,12%
	0,7	38,98%	41,32%
S2	0,3	52,08%	50,94%
	0,4	53,12%	52,08%
	0,5	53,43%	53,43%
	0,6	53,85%	54,78%
	0,7	54,16%	57,59%
S5	0,3	54,63%	54,63%
	0,4	54,63%	54,63%
	0,5	54,63%	54,63%
	0,6	54,63%	52,78%
	0,7	54,63%	50,93%
S6	0,3	60,81%	59,62%
	0,4	61,64%	60,69%
	0,5	62,00%	62,00%
	0,6	62,23%	62,83%
	0,7	62,83%	63,90%
S7	0,3	30,55%	37,14%
	0,4	29,67%	30,55%
	0,5	28,79%	28,79%
	0,6	27,69%	26,15%
	0,7	26,15%	23,30%

C Appendix: Additional information about CLIS patient GR

C.1 Recording channels

Table C.1 lists all recording channels numbers corresponding to the labels of the ECoG grid illustrated in Fig. 5.2

Table C.1: ECoG channels list and labels for CLIS patient GR.

Channel #	Label
1	G034
2	G035
3	G036
4	G037
5	G038
6	G042
7	G043
8	G044
9	G045
10	G049
11	G050
12	G051
13	G052
14	G053
15	G057
16	G058

Channel #	Label
17	G059
18	G060
19	G064
20	G065
21	G066
22	G067
23	G068
24	G072
25	G073
26	G074
27	G075
28	G080
29	G081
30	G082
31	G083
32	G088

Channel #	Label
49	G089
50	G090
51	G096
52	G097
53	G098
54	G099
55	G100
56	G105
57	G107
58	G108
59	G109
60	S007
61	S008
62	S014
63	S015
64	S016

C.2 Experimental setup

Table C.2 presents the questions that were asked during the experiment as well as the answers. It is reported as it was written by the experimenter. The experiment started at 14:50 and ended at 17:00. This is the first and only successful communication attempt out of 170. 18 questions were asked. 16 of them were correctly answered. One question was not correctly answered

(Question) and the answer for Question 13 is unclear. In the answer column, + means that the patient's answer was classified as "yes", and - means that it has been identified as a "no".

Table C.2: Experimental setup for patient GR.

No.	Paired questions	Answer
Date: 2008-03-16 Session: Present: Femke Arrive: 14.50 Leave: Time: Heart rate: 98 Oxygen saturation: 97 Lying on side: back/left Respiration BPM: 15 Ground: S032 Reference: G102		
Initial eye movement looked much stronger than previous days. I asked him questions (without video).		
0.1	You feel good today? You feel bad today?	+ -
0.2	Are you happy that I'm here? Would you prefer to be alone and to watch TV?	+ -
The responses were so strong that I though a conversations was possible. I turned on the video. The following questions were asked. Someone should check the video to check me.		
1	You feel good today? You feel bad today?	+ -
2	Are you German? Are you Dutch?	+ -
3	Do you feel pain? Are you free of pain?	- +
4	Are you satisfied by the health care at BS (city in Germany)? Are you unsatisfied by the health care at BS? Are you unsatisfied by the health care at BS? Are you satisfied by the health care at BS?	+ - - +
5	Are you still happy to have decided for the operation? Are you sorry for having decided to do the operation?	+ -
6	Do you think, you have feedback control over sound? Do you think the feedback is not controllable?	+ -
7	Are the sounds loud enough for you? Should we turn the speaker louder? Should we turn down the speaker? Are the speakers o.k.?	+ - +

Continued on next page

Table C.2 – continued from previous page

No.	Paired questions	Answer
"We would like to know about your psychological status. We want to know how your mood is."		
8	Are you positive regarding the future? Do you not know exactly what future will bring for you, so, are you neutral for your future? Are you negative for the future?	+ - -
"I will ask you now a question, that have to be asked to you somewhen."		
9	Do you wish sometimes, you were dead? You never wished to be dead?	- +##
10	Can you enjoy your life under these circumstances? You don't enjoy your life any more?	+ -
11	Was it a good decision to bring you to BS? Do you prefer to go back to Vohenstrauss (his home town)? Do you prefer to go back to Vohenstrauss?	+ + & - (not clear) -
12	Do you want to stay at BS in the future? Do you want to stay at BS in the future? Do you prefer to go into another nursing home? Do you prefer to go into another nursing home?	- - + +
13	You want to go back to Vohenstrauss in some later period? Do I understand you correctly? You want in another nursing home than Vohenstrauss?	+ (no clear answer) + (no clear answer)
"I have been informed, that our political contacts we have engaged to convince the health insurance regarding your care costs will publish a report about you in the SPEIGEL (very renown German journal). Unfortunately, I don't know more than that, neither about the content of the article. I will inform myself to tell you."		
14	Shouldn't we go to public with the heath insurance? Shouldn't we fight we the health insurance? Should we fight with the health insurance?	- - -
15	For long term schedule: You want to go to Vohenstrauss? For long term schedule: You want to stay at BS?	+ +
"It's not clear to me what you want to say, GR."		
16	You don't care where you will be in future?	-
"I ask you a different way now."		
17	For long term schedule, are you Prefer Vohenstrauss before BS?	-
I see a NO in your eyes, is this correct? +, including corner of the mouth, I tried letting him repeat the mouth twitch but it didn't always work. Instructed him to use whatever he could or both		
17	Do you prefer, for long term, to stay at BS before Vohenstrauss? You want another nursing home than those 2?	-
	You want to spell something?	
GR then spelled the word "AMBERG".		

Continued on next page

Table C.2 – continued from previous page

No.	Paired questions	Answer
This was a long process where I repeatedly double checked (verified "correct?" and "wrong?") if I got all letters correct. I also asked him for confirmation or declination of the final word "AMBERG". Someone should CHECK the video and check me. I, then suspected that he wanted to go to Amberg instead of staying in BS or going back to Vehenstrauss.		
18	You mean, you want to go to Amberg in the future? Did I understood you wrong, that you want to go to Amberg in the future?	-
VIDEO lost power. We take a break and I type up this conversation.		
Time: 17.00 Heart rate: 94 Oxygen saturation: 98 Lying on side: back/left Respiration BPM: 15 Ground: ? Reference: ?		

D Appendix: Additional information about the CLIS patients

D.1 Detailed description of the CLIS patients (except GR)

The following descriptions of the patients were obtained directly from the experimenters. None of them showed any brain disease unrelated to ALS. Descriptions of patients P5, P6, P7, P9 and P10 can also be found in [Mar+21] and [Mal+19]. In addition to EEG, fNRIS were also recorded. All patients were in home care.

Patient P1 P1 is a female CLIS patient that was diagnosed with sporadic bulbar ALS in May 2007 and as locked-in patient in 2009. She transitioned into a completely locked-in state in May 2010 according to the diagnosis of experienced neurologists. The patient has been artificially ventilated since September 2007 and fed through a percutaneous endoscopic gastrostomy tube since October 2007. No communication with eye movements, other muscles, nor assistive devices was possible with this patient. She was however successful in communicating using fNRIS. She passed away in 2019 at the age of 75.

Patient P2 P2 is a male CLIS patient diagnosed with non-bulbar ALS in May 2011. He has been artificially ventilated since August 2011 and fed through a percutaneous endoscopic gastrostomy tube since October 2011. He started communicating with a speech device in his throat from December 2011 which ultimately failed. He then started using a MyTobii eye-tracking device in April 2012 and was successful until December 2013. Subsequently, the family members attempted to communicate by training him to use eyes movements: to the right for *yes* and to the left to answer *no*. The response was variable and no communication was possible since August 2014. Nonetheless, he was able to use a binary communication using fNRIS from 2014 to 2016. The patient passed away in 2018 at the age of 65.

Patient P3 P3 is a 80 years old female CLIS patient diagnosed with bulbar ALS in 2010. She lost speech and capability to walk by 2011. She has been fed through a percutaneous endoscopic gastrostomy tube since September 2011 and artificially ventilated since March 2012. She started using assistive communication devices using one finger to communicate in February 2013 until it failed. Later, in September 2013, she was diagnosed with degeneration of vision due to cornea defects. Afterwards, an attempt was made to communicate with her using eye tracking from

early 2014 until August 2014. No communication was possible with her since then according to the husband and caretakers. She was then introduced to BCI and the experimenters reported successful *Yes/No* communication from 2014 to 2015 using fNRIS.

Patient P4 P4 is a 29 years old female CLIS patient diagnosed with juvenile ALS in December 2012. She was completely paralysed within half a year after diagnosis. She has been artificially ventilated since March 2013 and fed through a percutaneous endoscopic gastrostomy tube since April 2013. She was able to communicate with the eye-tracking device from early 2013 until August 2014 when she lost some eye control. Her family members also trained her to use eye movements to communicate: to the right to answer *yes* to questions and to the left for *no*. This was possible until December 2014. So when the patient completely lost the control of her eyes in January 2015, she attempted to answer *yes* by twitching the right corner of her mouth. That too varied considerably so the parents lost reliable communication contact since. She was however able to successfully communicate using fNRIS from 2014 to 2016.

Patient P5 P5 is a 58 years old male CLIS patient diagnosed with bulbar sporadic ALS in May 2008 and as locked-in in 2009. According to the diagnosis of neurologists and to the recordings of the experimenters, he transitioned into a completely locked-in state in May 2010. He has been artificially ventilated since September 2009 and fed through a percutaneous endoscopic gastrostomy tube since October 2009. No communication with eye movements, other muscles, or assistive devices was possible since 2010. Moreover, the patient was also never successful with fNRIS.

Patient P6 P6 is a male CLIS patient diagnosed with bulbar ALS in 2009. He lost speech and capability to move by 2010 and has been artificially ventilated since September 2010. No communication with eye movements, other muscles, or assistive devices was possible since 2012. However, the patient was able to communicate successfully using fNRIS in 2017. He died in 2019 at 38.

Patient P7 P7 is a female CLIS patient diagnosed with Mills' syndrome[26] of ALS with atypical progression at the beginning of 2010. She lost speech and capability to walk in 2011. She has been fed through a percutaneous endoscopic gastrostomy tube since June 2010 and artificially ventilated since June 2010. The patient started using assistive communication devices using eye movement in 2011 which ultimately failed at the beginning of 2015. She then used thumb-movements to communicate with her family and caretakers since the middle of 2015, and this became unreliable after a year. She was also never successful in using binary communication with the fNRIS and passed away in 2019 at the age of 56.

[26] an idiopathic, slowly progressive, spastic hemiparesis.

Patient P9 P9 is a 23 years old male CLIS patient diagnosed with juvenile ALS with FUS mutation heterozygote on Exon 14: c.1504delG in 2013. He has been artificially ventilated since August 2014. He started communication using MyTobii eye-tracking device from January 2015 and was able to do so until December 2015. Afterwards, the family members attempted to communicate by training him to move his facial muscles near the nose to answer *yes* but the response was unreliable. No communication was possible since June 2016. Moreover, only few irregular good sessions were observed using fNRIS.

Patient P10 P10 is a 25 years old male LIS patient on the verge of CLIS. He was diagnosed with familial juvenile ALS with ALS 6-FUS gene mutation in December 2012. He was completely paralysed within a year of the diagnosis. The patient has been artificially ventilated since November 2013. He was able to communicate with eye-tracking from early 2014 to August 2016 but was unable to use the eye-tracking device after he lost eye control in August 2016. No communication with eye movements, other muscles, or assistive devices was possible since 2016. In addition, no successful communication using fNRIS was ever recorded.

D.2 Estimated consciousness levels for CLIS patients

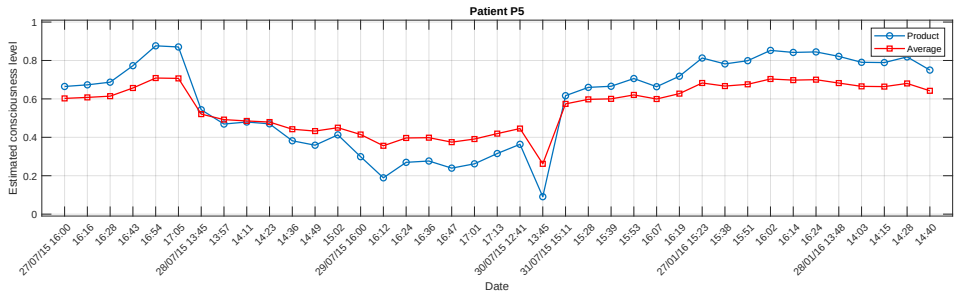

Figure D.1: Average values of the estimated consciousness level for CLIS patient P5. The x-axis represents the dates and times of recording.

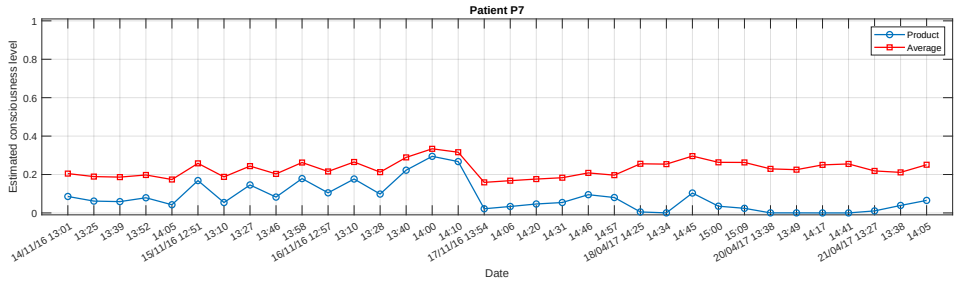

Figure D.2: Average values of the estimated consciousness level for CLIS patient P7. The x-axis represents the dates and times of recording.

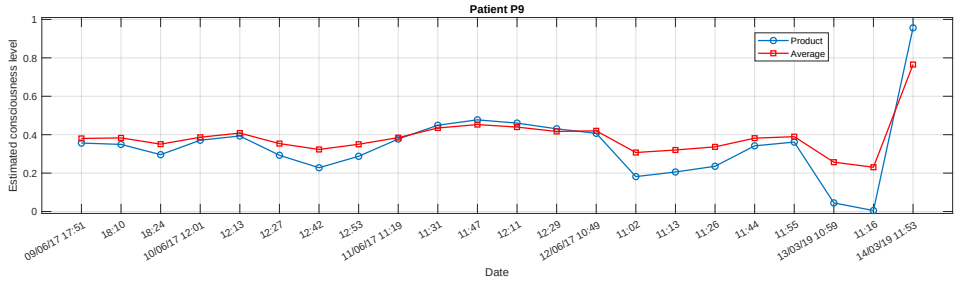

Figure D.3: Average values of the estimated consciousness level for CLIS patient P9. The x-axis represents the dates and times of recording.

Bibliographic details

Adama, VS. (2021). *Consciousness level assessment of Completely Locked-in Syndrome patients using Soft-Clustering*. [Doctoral dissertation]. Department of Neuromorphe Information Processing, Leipzig University.

Selbständigkeitserklärung

Hiermit erkläre ich, die vorliegende Dissertation selbständig und ohne unzulässige fremde Hilfe angefertigt zu haben. Ich habe keine anderen als die angeführten Quellen und Hilfsmittel benutzt und sämtliche Textstellen, die wörtlich oder sinngemäß aus veröffentlichten oder unveröffentlichten Schriften entnommen wurden, und alle Angaben, die auf mündlichen Auskünften beruhen, als solche kenntlich gemacht. Ebenfalls sind alle von anderen Personen bereitgestellten Materialen oder erbrachten Dienstleistungen als solche gekennzeichnet.

Leipzig, den 5. November 2021